HYBRID EXOSKELETONS FOR REHABILITATION: A NONLINEAR CONTROL
APPROACH

By

CHRISTIAN ABRAHAM COUSIN

A DISSERTATION PRESENTED TO THE GRADUATE SCHOOL
OF THE UNIVERSITY OF FLORIDA IN PARTIAL FULFILLMENT
OF THE REQUIREMENTS FOR THE DEGREE OF
DOCTOR OF PHILOSOPHY

UNIVERSITY OF FLORIDA

2019

To my parents, *Tammy* and *Harry*, and to my brother, *Robert*, who have provided invaluable support, encouragement, and love throughout my life. And to God, for His countless blessings and empowerment.

ACKNOWLEDGMENTS

I would like to acknowledge my advisor and mentor, Dr. Warren Dixon, who has driven me to learn and accomplish more than I ever thought possible. His constant guidance, encouragement, and mentorship have not only allowed me to grow intellectually, but also as an individual. I would also like to acknowledge Drs. Carl Crane, Chris Hass, and Scott Banks for their oversight and recommendations throughout the completion of this dissertation. I would also like to extend a special thank you to Dr. Emily Fox and the Motion Analysis Center at Brooks Rehabilitation Hospital for their willingness to collaborate and their belief in my research throughout my time at the University of Florida. I am grateful to the past and present members of the Nonlinear Controls and Robotics Laboratory for their time, intuition, and brilliance in tackling challenging, meaningful problems alongside me. I would also like to thank the National Science Foundation for their generous and overwhelming financial support. Thank you to my friends and my family for your endless encouragement.

TABLE OF CONTENTS

LIST OF TABLES

LIST OF FIGURES

Abstract of Dissertation Presented to the Graduate School
of the University of Florida in Partial Fulfillment of the
Requirements for the Degree of Doctor of Philosophy

HYBRID EXOSKELETONS FOR REHABILITATION: A NONLINEAR CONTROL
APPROACH

By

Christian Abraham Cousin

May 2019

Chair: Warren E. Dixon
Major: Mechanical Engineering

Neuromuscular disorders can arise from disease (e.g., Parkinson's, transverse myelitis), disorders (e.g., cerebral palsy, spina bifida), or injury (e.g., spinal cord injury, stroke, traumatic brain injury) and leave millions of people permanently disabled each year. In an effort to mitigate the severity of such disorders and improve the overall quality of life of those affected, several methods of rehabilitation are available. This dissertation focuses on functional electrical stimulation (FES) and rehabilitation robotics. FES results when neuromuscular electrical stimulation is used to induce an electric field potential across the motor neurons of a muscle and artificially induce an involuntary muscle contraction causing limb motion for some functional task. Because FES has been shown to impart a number of health benefits including increasing muscular strength, motor control, bone mineral density, cardiovascular parameters and others, it is widely employed as a method of rehabilitation. However, FES has numerous challenges including the nonlinear activation dynamics of the muscle and dynamically changing muscle characteristics such as fatigue. Furthermore, because intense, coordinated, repetitive exercise is encouraged in rehabilitation, a combination of robotic technology and therapist interaction is motivated. However, challenges for using rehabilitation robots include selecting the appropriate control scheme and ensuring participant safety. Control schemes such as position, torque, and impedance control have been widely used over the past decade, all of which require a rigorous stability analysis to enforce

the desired behavior of the system and ensure the safety for a person interacting with the robot. Furthermore, when FES is used on multiple muscles, and the robot switches between tracking objectives or is periodically activated, a switched systems stability analysis must be performed to ensure stability of the entire switched system. When FES is combined with rehabilitation robots, hybrid exoskeletons arise and blend the advantages of the two therapies while mitigating their respective drawbacks.

In Chapter 1, motivation for the use of technologies such as FES, rehabilitation robots, and hybrid exoskeletons in rehabilitation settings is presented. A survey of the literature on various control techniques for interfacing with these technologies is provided, establishing a framework for this dissertation. Chapter 2 introduces the hybrid exoskeleton used through this dissertation, an FES cycle, along with the corresponding nonlinear, uncertain, time-varying, switched system dynamics and various properties employed throughout the subsequent chapters. Autonomous state-dependent switching is necessary because multiple muscle groups receive stimulation at different angles throughout the crank cycle to produce positive torque about the crank and propel the cycle forward. The nonlinear and adaptive controllers designed in subsequent chapters are designed to interface with the FES cycle to accomplish various control objectives such as position, cadence, and admittance tracking for the purposes of improving rehabilitation options for people with neuromuscular disorders.

In Chapter 3, two nonlinear controllers are developed to accomplish simultaneous cadence and power (i.e., torque) tracking; one to activate the rider's muscle groups through FES and one for the activation of the cycle's electric motor. The cycle's motor utilizes a robust sliding-mode controller to regulate the cycle's position and cadence for all time. The rider's muscles are activated using a similar robust sliding-mode controller to regulate instantaneous power. To prevent backpedaling and the early onset of fatigue, the rider's muscles are not stimulated when kinematically inefficient and the power tracking objective must be periodically relinquished because of the

lack of control authority available. Hence, incomplete control authority exists and a switched systems dwell-time analysis must be completed to demonstrate stability of the instantaneous power tracking objective. A Lyapunov-like switched systems stability analysis is completed for both controllers and error systems proving global exponential stability of the cadence objective and uniform ultimate boundedness of the power objective. To prove the efficacy of the developed controllers, experiments are conducted on seven able-bodied participants and six participants with neuromuscular disorders. The controller is then compared to two previous developed FES cycling controllers for simultaneous cadence and power tracking. The results indicate the controller developed in this chapter is ideal for simultaneous cadence and power tracking compared to the two previously developed controllers.

In Chapter 4, two new controllers are developed for the FES cycle to accomplish simultaneous cadence and admittance tracking. The controllers are designed to overcome challenges of Chapter 3; namely, selecting the appropriate desired torque trajectory and preserving the rider's safety. Compared to Chapter 3, the admittance controller implemented on the cycle's motor is capable of indirect torque tracking, accomplished by injecting artificial desired dynamics between the rider and the cycle. The rider's muscles are now electrically stimulated using a cadence controller to actuate the cycle. Using the admittance controller, the cycle assumes an assist-as-needed control paradigm and assists the rider in maintaining a desired cadence if the FES is unable to elicit muscle contractions powerful enough to overcome the passive torques of the combined cycle-rider system. Correspondingly, the admittance controller resists the rider if volitional pedaling exceeds the desired cadence. The admittance controller uses a passivity-based stability analysis and is shown to be strictly passive with respect to the rider and globally exponentially stable in isolation (i.e., when the rider is not coupled to the cycle). The cadence controller is shown to be globally exponentially stable in the FES regions. Experiments are conducted on three able-bodied participants and four

13

participants with neuromuscular disorders to demonstrate controller efficacy as well as investigate the effects of selecting various admittance parameters. Results indicate the admittance controller is a promising method to simultaneously elicit torque from the rider's muscles while introducing a degree of compliance to the system.

Chapter 5 seeks to improve upon the controllers presented in Chapter 4 by adding adaptation to the admittance controller implemented on the cycle's motor. Additionally, to accommodate for asymmetric rider capabilities (as in post-stroke hemiparesis), two cranks (one for each leg) are used to eliminate the mechanical coupling between the left and right legs. Consequently, the cycle is instrumented with an additional motor, encoder, powermeter, and chain to establish feedback and control authority on both sides of the cycle. The muscles of each leg of the rider are tasked with maintaining the cycle's cadence on their respective sides and each motor is controlled using a separate admittance controller. A Lyapunov-like stability analysis is conducted to prove the admittance controllers globally asymptotically regulate the admittance error systems and the cadence controller is passive with respect to the motor. When implemented, the admitted trajectory is generated online by averaging the output torques between the two sides such that the pedals are kept at a desired offset. If the rider demonstrates hemiparesis, the stronger leg will experience resistance and the weaker leg will experience assistance such that the two pedals are held in the desired relative phase. Experiments are conducted on one able-bodied participant and three participants with neuromuscular disorders to compare the effect of adding adaptation to the cycle. Results indicate significant improvement in various performance metrics with the use of adaptation.

In Chapter 6, the adaptive admittance controller in Chapter 5 is further modified with the addition of a neural network to estimate the control effectiveness of the rider's muscles and more accurately track the admitted trajectory. The neural network is shaped according to the anticipated rider output torque curve. As in Chapter 5, the

rider's muscles are assigned to regulate the cycle's cadence. A stability analysis is conducted and proves the admittance controller globally asymptotically regulates the admittance error system and the cadence controller is passive with respect to the motor. Experiments are conducted using the single-crank FES cycle on one able-bodied participant and four participants with neuromuscular disorders. Results indicate improvements of performance metrics in three of five participants when adaptation is enabled.

Chapter 7 concludes the dissertation by highlighting the contributions of the developed controllers and discussing future extensions.

CHAPTER 1
INTRODUCTION

1.1 Background

Within the United States (US), there are an estimated 2.5 million new cases of traumatic brain injury (TBI) [1], 800,000 cases of stroke [2], and nearly 18,000 cases of spinal cord injury (SCI) [3] every year. Additionally, it is reported that there are 3.17 million people within the US with permanent disability from TBI [1] and 285,000 people with a spinal cord injury [3]. Neuromuscular injuries such as these, as well as diseases (e.g., Parkinson's, etc.) and other congenital disorders (e.g., cerebral palsy, spina bifida, etc.) can severely impact a person's neuromuscular system by damaging the brain, spinal cord, or nerves. Because neuromuscular disorders (NDs) can arise from injury, disease, and other disorders, they can manifest themselves in incredibly complex ways. Oftentimes NDs compromise a person's ability to properly utilize and accurately control their own neuromuscular system, causing partial/total paresis/paralysis, and significantly affecting their activities of daily living [1–3]. Consequently, these individuals are at an increased risk of negative secondary health effects such as obesity, heart disease, muscle atrophy, diabetes, and others, due to sedentary lifestyles [4]. Moreover, as the average age of the global population increases, people are becoming increasingly susceptible to neurological disorders and injuries.

In an effort to reduce the negative secondary consequences of neuromuscular disorders, promote rehabilitation, and improve the overall quality of life of individuals affected by NDs, therapies such as neuromuscular electrical stimulation (NMES) may be employed. NMES has been shown to impart a number of health benefits, including improved bone mineral density [5], muscular strength [6], motor control [7], range of motion [8], and cardiovascular parameters [9]. NMES works by applying an electric field across the motor neurons of a muscle to induce an artificial, involuntary contraction. When NMES is used to complete functional and assistive actions, it is termed functional

electrical stimulation (FES). FES, however, possesses a number of inherent challenges, including, but not limited to, the nonlinear activation dynamics exhibited by muscles and dynamically changing muscle characteristics such as fatigue [10, 11]. Hence, closed-loop control of FES is motivated to produce accurate regulation of generated movements [12].

In addition to FES, another common method of rehabilitation is the use rehabilitation robots [13, 14]. Rehabilitation robots assist people in performing rehabilitative tasks and have been shown to improve sensory perception and motor function [14–16]. In some studies, robotic rehabilitation has demonstrated improved clinical and biomechanical measures compared to intervention by physical therapists [17]. It has also been shown that robot aided rehabilitation does not have negative effects, patients are amenable to it, and it may influence brain recovery [14]. Numerous upper-limb rehabilitation robots have been developed, namely, MIME, MULOS, MIT-MANUS, GENTLE/s, and lower-limb robots such as the commercially available LOKOMAT, Gait Trainer, and Autoambulator, and research robots such as ALEX, Haptic Walker, PAM, and the LOPES exoskeleton [18]. Traditionally in robotic therapy, the robot is physically coupled to the human (including all the aforementioned robots), and results in physical human-robot interaction. Hence, human safety must be prioritized and incorporated into the robot's control structure, especially when the human is in a compromised, unpredictable, and unreliable state to avoid further injury [19, 20].

Because every ND is unique, rehabilitation robots should be able to accommodate each individual instead of tasking each individual to conform with identical rehabilitation tasks (i.e., identical position, cadence, or torque trajectories) [21]. Previous studies have developed various control strategies including assistive controllers, which aid rehabilitative movements [22, 23], and challenge-based controllers, which resist movements [15]. Both classes of controllers impart rehabilitative benefits, with assistive controllers promoting somatosensory stimulation [24, 25] and challenge-based controllers improving

motor function [16, 26–29]. Additionally, muscle effort is thought to be essential for eliciting motor plasticity [30, 31], which promotes the use of challenge-based control strategies on rehabilitation robots. In creating rehabilitation-based controllers for robots, strategies such as torque control (cf., [32, 33]), hybrid control (combining position and force tracking) (cf., [34, 35]), and admittance control (cf., [36–40]) are typically employed.

Admittance control, established by Hogan [41], provides an intuitive method for rehabilitation robots to safely interact with humans without unduly forcing them to adhere to predefined trajectories [20]. It is a control strategy capable of modifying robot behavior based on force-feedback and artificial injected dynamics, offering a method to promote safety over explicit tracking performance by resolving conflicts in motion between the robot and human [42]. Admittance control allows force feedback to modify desired position/velocity trajectories, and based on the admittance parameters selected, can modify it to various degrees to assist or resist a person [43], creating an *assist-as-needed* or *resist-as needed* control paradigm.

Numerous studies have investigated various control strategies, including [44] which utilized invariance control to enforce dynamic constraints and keep the robot in a safe configuration. Other studies have implemented a number of control modes for the robot to operate under, such as the *assist-as-needed* control paradigm for upper-limb rehabilitation robots [42, 45], *human-in-charge/force control mode* for use with series elastic actuators [46], and *patient-in-charge/robot-in-charge* modes for elbow rehabilitation [47]. Alternatively, [48] provides a framework where a therapist can be injected into the control loop with the use of haptics-enabled telerobotic rehabilitation to provide resistive/assistive motor therapy remotely to stabilize nonpassive, nonlinear, and nonautonomous behavior. However, among the available control strategies, admittance control provides an intuitive solution to many of the challenges arising from human-robot interaction [10, 49–52] because it modulates behavior instead of explicit force or position trajectories [53, 54].

Admittance control is amenable to adaptive control methods and previous results have integrated adaptation in the outer-loop of force-feedback to modify the admittance parameters [55, 56] or within the inner-loop to modify the position controller using techniques such as neural networks [43]. While admittance control has been implemented on a number of rehabilitation robots [43, 57, 58], subsets of admittance control such as stiffness control [59], and extensions such as dissipative control [60] (i.e., admittance control with a minimum guarantee of passivity) have also been used to accomplish safe, stable human-robot interaction. While admittance control is traditionally viewed as a safer alternative than robust position/torque control in terms of physical human-robot interaction [61], a stability analysis remains necessary to demonstrate safe interaction between the human and robot [62]. Of note, when dealing with admittance controllers, a passivity analysis is commonly performed to prove stability. Passive systems are capable of dissipating energy [63, 64] and are a common metric to prove safety in physical human-robot interaction [46].

When a rehabilitation robot is utilized in conjunction with FES, a hybrid exoskeleton arises and attempts to blend the advantages of rehabilitation robots and FES while mitigating the drawbacks of each [43, 62, 65, 66]. However, like FES and rehabilitation robots, hybrid exoskeletons are inherently challenging to implement due to the nonlinear, uncertain, time-varying dynamics of both muscle and robotic systems [67]. While hybrid exoskeletons can be controlled similarly to rehabilitation robots, the studies in [10, 62] specifically utilize admittance control. An example of a hybrid exoskeleton (and the focus of this dissertation) is a motorized recumbent FES tricycle. FES cycles utilize the application of FES across a person's (i.e., rider's) leg muscles (i.e., the quadriceps, hamstring, and gluteal muscle groups) to cause elicit contractions and cooperatively pedal the cycle alongside an electric motor attached to the cycle [67].

FES cycling combines the benefits of FES and rehabilitation robots and has been shown to yield improvements in musculoskeletal and cardiorespiratory fitness as well as

19

other neurological, physiological, and psychological measures [68–70]. FES cycling is a popular rehabilitative therapy because the fall risks associated with other therapies are mitigated, it can provide sufficient intensity and repetitive practice of coordinated limb movements critical for facilitating nervous system reorganization, and promote potential beneficial changes in the neuromuscular system [71, 72].

Although FES cycling is a convenient rehabilitation option for many people, when applied in practice, it is commonly applied open-loop without regard of the rider's performance. However, the metabolic efficiency of FES cycling is significantly lower than volitional cycling [73] due to poor control of the muscle groups, unfavorable biomechanics and nonphysiological muscle recruitment [74], non-optimal stimulation parameters [75, 76], fatigue [77–79], and other factors (cf. [80–82]). Furthermore, because the sensation from FES can be uncomfortable [77] and the benefits from FES are reported to culminate over long time periods (cf. [77, 79]), improved FES cycles (and controllers) are needed to accelerate the benefits and reduce the discomforts.

To best promote rehabilitation, the increase of efficiency and power output (PO) of FES cycling is desirable because it can reverse muscle atrophy and cultivate fatigue-resistant muscle fibers [77]. Multiple strategies have been employed to increase the PO of FES cycling such as the use of cadence control [74, 81], creating the optimal pedal path [75], releasing the ankle joint [80], using a fixed gear cycle [83], using higher stimulation currents [77], and modifying the stimulation frequency and pattern [76]. Furthermore, when power (i.e., torque[1]) is tracked directly, it is unclear how to best coordinate the FES and motor contributions and if power should be tracked instantaneously or averaged over a period of time (i.e., discretized tracking). Based on the idea that the limited bandwidth of electrically stimulated muscle groups inhibits instantaneous torque tracking, few torque/power tracking results are available for

---

[1] Within the scope of this work, power tracking and torque tracking are synonymous.

instantaneous torque tracking (cf. [84–86]), discretized torque tracking (cf. [87, 88]) (which periodically updates the controller based on a power reading averaged over a region of the crank), or track power only when kinematically efficient (cf. [89]), and instead analyze power output (PO) outside the control loop (cf. [82, 90, 91]).

Although FES cycles are an invaluable research and rehabilitation tool for movement disorders, when dealing with hemiparesis, FES cycles can often mask asymmetries in the rider due to coupled pedals and a single torque sensor. Previous works have thus derived methods for isolating the torque contributions of each leg by instrumenting cycles with torque sensors on each pedal [88, 91], decoupling the pedals (i.e., split-crank cycling) [92, 93], or pedaling with one leg at a time [94]. Because FES cycling has been shown to improve symmetry in hemiplegic individuals [91], further research into asymmetric rehabilitation is warranted. For example, asymmetric rehabilitation is supported by studies such as [95] which indicated that children with unilateral brain injury have separate control circuits for each leg and these circuits can be adapted independently to improve symmetry; [96] which found that split-belt treadmills and individual limb-weighting can improve spatiotemporal symmetry in post-stroke adults; and [97] which demonstrated that decreases in asymmetry were observed in people with Parkinson's disease in cycling when average workload increased. As a whole, literature suggests that within various NDs resulting in hemiparesis, symmetry can be improved, at least in the short-term, by targeted rehabilitation of the affected and non-affected side of the body. Moreover, motivation exists to have individuals participate in rehabilitation to the greatest extent possible in an effort to reduce neuromuscular impairment [58].

FES cycling offers a method for neuromuscular rehabilitation, but because it involves physically coupling a rehabilitation robot to the human rider, the aforementioned challenges (e.g., safety, closed-loop control, nonlinearities) must be addressed. Furthermore, FES cycling has the added challenge of discretely switching muscle stimulation

21

on/off with continuously evolving state-dynamics, resulting in a switched system. Split-crank cycling is also highly susceptible to periodic torques (e.g., due to gravity) which are no longer balanced about the cycle's crankshaft due to decoupled pedals. Because people have unique capabilities and every movement disorder is subtly different, adaptive control of FES cycling is warranted to not only account for cycle dynamics, but also produce a customized experience for each rider while avoiding high frequency switching in the control effort, typically found in robust control methods (e.g., sliding-mode control).

From a control systems perspective, FES cycling is an example of a switched system in the sense that there are continuous physical dynamics of the limbs and the cycle, yet there are discrete logical jumps necessary to engage different muscle groups of the legs, potentially engage a motor for assistance, or discretely turn on/off the control inputs (motivated by different stimulation schemes or the desire to allow the rider to contribute all the torque). Furthermore, because not all muscles can contribute to the forward motion of the crank at all times due to kinematic efficiency, switching between muscles is necessary and a switched systems analysis is required to prove stability [98]. However, few results consider the fact that such switching could yield degraded performance or even destabilizing effects. Although past FES cycling studies have been produced which control FES cycles using open-loop methods [91], or closed-loop methods using linear control techniques [84] or nonlinear control techniques (e.g., fuzzy logic, sliding mode) [85], generally, the FES-cycling community has only addressed the ramifications of having a switched input by examining different regions to activate the muscle if at all (cf. [74, 91, 99–101]). Few control developments include a nonlinear stability analysis that considers the impacts of switching during FES cycling (cf. [67, 102–107]). Moreover, a stability analysis is crucial because it is well known that people with NDs possess a weakened/impaired musculoskeletal system and the utmost care must be taken to avoid destabilizing behavior.

While the majority of objectives of FES cycling include cadence [67, 76, 102, 105, 108] and torque tracking [86, 89, 109], admittance control strikes a balance between the two, prioritizing safety over performance, and has only been implemented on FES cycles in the author's preliminary works (cf. [107, 110, 111]). Because each ND is unique, not only is the need to utilize closed-loop control motivated, but the use of adaptive control as well. While past results such as [67, 86, 102] have utilized robust closed-loop methods, others have utilized learning-based methods such as neural networks (NN), fuzzy logic, and repetitive learning controllers to improve cadence/torque tracking of FES cycling, but few conduct or include a rigorous stability analysis (cf. exceptions in [67, 86, 89, 102, 105, 112]).

1.2   Outline of the Dissertation

Chapter 2 describes the uncertain, nonlinear, time-varying dynamic model of the hybrid exoskeleton used in the context of this dissertation, a motorized recumbent FES cycle. A rider is seated on the cycle and FES is implemented on his/her quadriceps femoris, hamstrings, and gluteal muscle groups to elicit artificial, involuntary muscle contractions to pedal the cycle alongside an electric motor coupled to the drive chain. By discretely switching between muscle groups to control continuous dynamics, an autonomous state-dependent switched system is created. Properties and assumptions for the switched dynamic system are introduced which are employed in subsequent chapters.

Chapter 3 presents the dual-objective of cadence and power tracking using the FES cycle introduced in Chapter 2. While, simultaneous cadence and power tracking are common objectives in FES cycling, it is unclear how to best coordinate the FES and motor contributions and if power should be tracked instantaneously or averaged over a period of time. This chapter develops a new FES cycling controller which has the cycle's motor regulate the system's cadence and the rider's muscles regulate instantaneous power. Using a switched systems Lyapunov-like dwell-time analysis, it is proven that

the developed controllers achieve global exponential cadence tracking and uniformly ultimately bounded power tracking. To evaluate the performance of the developed controller, comparisons are made with two previously developed FES cycling controllers (cf. [86, 87]) through experiments on seven able-bodied participants and six participants with neuromuscular disorders. For a desired cadence of 50 RPM and a desired power of 10 W, the developed controller in this chapter demonstrated the smallest tracking errors with an average cadence and power error of 0.01 ± 1.03 RPM and 0.00 ± 0.94 W, respectively, in the able-bodied population and an average cadence and power error of 0.02 ± 1.87 RPM and 0.00 ± 2.46 W, respectively, in the population with neuromuscular disorders. Results suggest that the electric motor should be used to track cadence and the FES induced muscle torques should be used to track instantaneous power.

Chapter 4 seeks to improve upon the results in Chapter 3 by utilizing an admittance controller on the cycle's motor to preserve rider safety while indirectly tracking torque. While the muscle controller is proven to globally exponentially track cadence in the FES regions, the admittance controller is proven to be passive with respect to the rider's applied torque. Experiments are conducted on three able-bodied participants and four participants with neuromuscular disorders to demonstrate the efficacy of the developed controllers and investigate the effect of manipulating individual admittance parameters. Results demonstrate an average admittance cadence error of -0.06 ± 1.47 RPM for able bodied participants and -0.02 ± 0.93 RPM for participants with NDs.

Chapter 5 improves upon the results presented in Chapter 4 by adding adaptation to the admittance controller implemented on a now decoupled split-crank FES cycle capable of measuring and addressing rider asymmetries. Unlike Chapter 4, the cadence controller used to stimulate the rider's muscles is now passive with respect to the motor's applied torque. Theoretical development of the controllers is based on a Lyapunov-based switched systems stability analysis where the admittance controller is proven to globally asymptotically regulate the admittance error systems. Experiments

were conducted on one able-bodied participant and three participants with various neuromuscular disorders, resulting in an average admittance tracking error of -0.13$\pm$1.77 RPM with adaptation and -0.03$\pm$4.05 RPM without adaptation between the two sides of the cycle.

Chapter 6 seek to further improve upon the performance of the FES cycle over Chapter 5 by adding a neural network on top of the adaptive controller. The neural network is used to estimate and compensate for the rider's muscle control effectiveness. Through a Lyapunov-like switched systems stability analysis, global asymptotic stability of the admittance controller is guaranteed and the cadence controller is proven to be passive with respect to the cycle's motor. Experiments on one able-bodied participant and four participants with NDs were conducted to validate the control design with an average admittance error of -0.09$\pm$1.14 RPM at 50 RPM.

Chapter 7 concludes the dissertation. A summary of the contributions is provided along with a discussion on potential extensions and future research directions. The experimental results presented in this dissertation quantify the FES cycling performance using position, cadence, torque, and admittance control. A key contribution of this dissertation is the development of various nonlinear and adaptive controllers for hybrid exoskeletons, validated through experiments in people with NDs such as stroke, spinal cord injury, spina bifida, and traumatic brain injury.

CHAPTER 2
DYNAMIC MODEL

2.1 FES Cycling

In this chapter, the hybrid exoskeleton utilized in the subsequent chapters is introduced, a motorized recumbent FES cycle. The dynamic model of a person riding the motorized FES cycle is adopted from [67, 102]. While the human (i.e., rider) is seated on the cycle, FES is implemented on the rider's quadriceps femoris, hamstring, and gluteal muscle groups to elicit muscle contractions, actuate the legs, and pedal the cycle. Muscle contractions from FES must be coordinated in an appropriate manner to produce forward motion of the cycle. Moreover, based on the position of the cycle (e.g., the crank angle), it becomes more kinematically efficient to stimulate certain muscles over others [113]. In limb configurations where all the muscle groups are unable to efficiently contribute torque to pedal the cycle (e.g., kinematic deadzones), no FES is applied. Therefore, any controller designed to implement FES on a cycle must switch between multiple inputs (i.e., six muscle groups and a motor) to continuously pedal the cycle and achieve desired behavior. Although continuous state dynamics exist (i.e., position, cadence, etc.), discontinuous inputs result in the development of an autonomous state-dependent switched system.

2.1.1 FES Cycle

For Chapters 3, 4, and 6 the experimental testbed consists of a stationary TerraTrike Rover recumbent tricycle mounted on a Kinetic Bike Trainer. A 250 W, 24 V DC brushed motor, by Unite Motor Co. Ltd., is mounted under the frame of the cycle and coupled to the drive chain to allow for motor assistance/resistance. The motor is interfaced with an ADVANCED Motion Controls (AMC) PS300W24 power supply and an AMC AB25A100 motor driver. An AMC FC15030 filter card is wired between the motor and power supply to reduce electrical noise. The crank angle is measured using a US Digital H5 optical encoder coupled to the crank through spur gears. Brackets attached

to commercially available bike pedals allow for the mounting of orthotic boots to fix the rider's feet to the pedals and prevent dorsiflexion/plantarflexion of the ankles, maintaining sagittal alignment of the legs. Torque applied about the crank is measured using an SRM Science Road Wireless Powermeter mounted to the bike crank. A Quanser QPIDe DAQ is used to interface with the encoder, motor driver, and powermeter. Controllers are implemented on a computer using Matlab/Simulink, Quarc, and Windows 7 at a sample rate of 500 Hz. A Hasomed Rehastim 1 current-controlled stimulator delivers biphasic, symmetric, rectangular pulses to the rider's muscle groups via bipolar, self-adhesive, PALS® electrodes. For all experiments, the stimulation is applied at 60 Hz and amplitudes are fixed at 90, 80, and 70 mA for the quadriceps, hamstrings, and gluteals, respectively. The stimulation pulsewidth for each muscle group is determined by the subsequently designed controllers and commanded to the stimulator by the control software. An emergency stop button is fastened to the tricycle that enabled the participant to immediately stop the experiment if desired. A rider seated on the motorized FES cycle is depicted in Figure 2-1.

For Chapter 5, the experimental testbed is modified by severing the crank shaft connecting the two pedals, decoupling them. Consequently, a second encoder, powermeter, motor, and chain are mounted on both sides of the cycle for full feedback and actuation. This cycle is referred to as the split-crank FES cycle.

2.1.2 Notation

$$\equiv \quad \text{indentically equal}$$

$$\approx \quad \text{approximately equal}$$

$$\neq \quad \text{not equal}$$

$$\triangleq \quad \text{defined as}$$

$$< \ (>) \quad \text{less (greater) than}$$

Figure 2-1. Motorized FES cycle: (A) Encoder (B) Power Meter (C) Electrodes (D) E-Stop (E) Filter Card (F) Stimulator.

$\leq$ ($\geq$)	less (greater) than or equal to
$\times$	cross product
$\forall$	for all
∞	infinity
$\in$	belongs to
$\subset$ ($\subseteq$)	subset (strict) of
$\cup$	union
$\cap$	intersection
$\rightarrow$	tends to
$\Longleftrightarrow$	equivalent to, if and only if
$\sum$	summation
$\lvert \cdot \rvert$	absolute value
$\lVert \cdot \rVert$	the norm of a vector
$\max$	maximum
$\min$	minimum
$\sup$	supremum, the least upper bound
$\inf$	infimum, the greatest lower bound
$\mathbb{N}$	the set of natural numbers
$\mathbb{R}^n$	the n-dimensional Euclidean space
$f : S_1 \rightarrow S_2$	a function f mapping a set S_1 into a set S_2
∇f	the gradient vector
∂f	the Clarke generalized gradient
$\dot{y}$	the first derivative of y with respect to time
$\ddot{y}$	the second derivative of y with respect to time

$$\text{diag}\,[a_1, ..., a_n] \qquad \text{a diagonal matrix with diagonal elements } a_1 \text{ to } a_n$$

$$A^T \; (x^T) \qquad \text{the transpose of matrix } A \text{ (of a vector } x)$$

$$\mathcal{L}_\infty \qquad \text{the space of all essentially bounded functions}$$

$$\text{sgn}\,(\cdot) \qquad \text{the signum function}$$

$$\ln\,(\cdot) \qquad \text{the natural logarithm}$$

$$\text{a.e.} \qquad \text{almost everywhere}$$

$$\mathcal{O}^2 \qquad \text{higher order terms of a Talyor series expansion}$$

$$\square \qquad \text{designation of end of proofs}$$

2.1.3 Dynamics

The combined cycle-rider dynamics can be modeled as [67][1]

$$\tau_m\,(q, \dot{q}, t) + \tau_e\,(t) \;\; = \;\; M\,(q)\,\ddot{q} + V\,(q, \dot{q})\,\dot{q} + G\,(q) + P\,(q, \dot{q}) + b_c\dot{q} + d\,(t), \qquad (2\text{--}1)$$

where $q \; : \; \mathbb{R}_{\geq 0} \to \mathcal{Q}$, $\dot{q} \; : \; \mathbb{R}_{\geq 0} \to \mathbb{R}$, and $\ddot{q} \; : \; \mathbb{R}_{\geq 0} \to \mathbb{R}$ denote the measurable crank angle, measurable velocity (cadence), and unknown acceleration, respectively. Time is represented as a member of the set of positive reals, $t \in \mathbb{R}_{\geq 0}$, where $\mathbb{R}_{\geq 0} \equiv [0, \infty)$. The set of $\mathcal{Q} \subseteq \mathbb{R}$ denotes the possible angles of the crank. The torque applied by the rider's muscles is denoted as $\tau_m \; : \; \mathcal{Q} \times \mathbb{R} \times \mathbb{R}_{\geq 0} \to \mathbb{R}$, and defined as

$$\tau_m\,(q, \dot{q}, t) \;\; \triangleq \;\; \sum_{m \in \mathcal{M}} b_m\,(q, \dot{q})\,u_{FES}\,(q, t), \qquad (2\text{--}2)$$

where $b_m \; : \; \mathcal{Q} \times \mathbb{R} \to \mathbb{R}_{>0}$ denotes the individual uncertain, nonlinear muscle control effectiveness and $u_{FES} \; : \; \mathcal{Q} \times \mathbb{R}_{\geq 0} \to \mathbb{R}$ denotes the subsequently designed FES muscle control current input. The subscript $m \in \mathcal{M} = \{RQ, \; RG, \; RH, \; LQ, \; LG, \; LH\}$ indicates

---

[1] For notational brevity, all explicit dependence on time, t, within the terms $q(t), \; \dot{q}(t), \; \ddot{q}(t)$ is suppressed.

the right (R) and left (L) quadriceps femoris (Q), gluteal (G), and hamstring (H) muscle group, respectively, which denote the stimulated muscle groups. The torque applied by the cycle's electric motor is denoted as $\tau_e : \mathbb{R}_{\geq 0} \to \mathbb{R}$ and defined as

$$\tau_e(t) \triangleq b_e u_{MOT}(t), \tag{2–3}$$

where $b_e \in \mathbb{R}_{>0}$ denotes the known motor control constant and $u_{MOT} : \mathbb{R}_{\geq 0} \to \mathbb{R}$ denotes the subsequently designed motor control current input. The torques applied about the crank axis by the combined inertial, centripetal-Coriolis, and gravitational effects are denoted by $M : \mathcal{Q} \to \mathbb{R}_{>0}, V : \mathcal{Q} \times \mathbb{R} \to \mathbb{R}$, and $G : \mathcal{Q} \to \mathbb{R}$, respectively, and the torques applied about the crank by the rider's passive viscoelastic tissue forces are denoted by $P : \mathcal{Q} \times \mathbb{R} \to \mathbb{R}$. The viscous damping effects applied by the cycle are denoted by $b_c : \mathbb{R}_{\geq 0} \to \mathbb{R}$ and unmodeled disturbances (e.g., dynamic fatigue, electromechanical delays [114]) are denoted by $d : \mathbb{R}_{\geq 0} \to \mathbb{R}$.

Although the parameters in (2–1) capture the torques affecting the dynamics of the combined cycle-rider system, the exact value of these parameters are unknown for each rider. However, several subsequently designed controllers only require known bounds on the aforementioned parameters. Specifically, the following properties [67] are provided for the dynamic system in (2–1):

Property 2.1. The inertia parameter is upper- and lower-bounded by $c_m \leq M(q) \leq c_M$, where $c_m, c_M \in \mathbb{R}_{>0}$ are known constants.

Property 2.2. The centripetal-Coriolis parameter is upper-bounded by $|V(q,\dot{q})| \leq c_V |\dot{q}|$, where $c_V \in \mathbb{R}_{>0}$ is a known constant.

Property 2.3. The torque generated by gravity is upper-bounded by $|G(q)| \leq c_G$, where $c_G \in \mathbb{R}_{>0}$ is a known constant.

Property 2.4. The torque generated by the rider's viscoelastic tissues is upper-bounded by $|P(q,\dot{q})| \leq c_{P1} + c_{P2}|\dot{q}|$, where $c_{P1}, c_{P2} \in \mathbb{R}_{>0}$ are known constants.

Property 2.5. The torque generated by the cycle's friction is upper-bounded by $b \leq c_b$, where $c_b \in \mathbb{R}_{>0}$ is a known constant.

Property 2.6. The torques generated by system disturbances are upper-bounded by $|d(t)| \leq c_d$, where $c_d \in \mathbb{R}_{>0}$ is a known constant.

Property 2.7. The system is skew-symmetric by the relation $\dot{M}(q) - 2V(q, \dot{q}) = 0$.

2.1.4 Switched System Dynamics

As in results such as [67, 102, 115, 116], FES-cycling is accomplished by switching the stimulation input to different muscle groups based on the region of the crank cycle designed a priori based on the kinematic effectiveness of the torque transferred to the crank axis from the muscle (i.e., FES regions). In regions of the crank where it is inefficient to stimulate muscle, a kinematic deadzone (KDZ) region exists and no muscle stimulation is applied. The stimulation regions are based on the work in [67], denoted by $\mathcal{Q}_m \subset \mathcal{Q}$, and defined as

$$\mathcal{Q}_m \triangleq \{q \in \mathcal{Q} \mid T_m(q) > \varepsilon_m\}, \tag{2-4}$$

$\forall m \in \mathcal{M}$, where $T_m : \mathcal{Q} \rightarrow \mathbb{R}$ denotes the torque transfer ratio of each muscle group about the cycle's crank. The selectable torque transfer threshold is denoted by $\varepsilon_m \in \left(0, \max\left(T_m(q)\right)\right]$ and dictates the angles at which each muscle group is stimulated based on its respective kinematic effectiveness. Because the torque transfer ratios are dependent on each rider's leg geometry, they are calculated independently for each rider. The torque transfer threshold is selected such that backpedaling is prevented, stimulation is only applied when each muscle group can positively contribute to the motion of the crank (i.e., $\varepsilon_m > 0$, $\forall m \in \mathcal{M}$), and muscle fatigue is delayed by only stimulating muscles in kinematically efficient regions (i.e., $\tau_m(q) > \varepsilon_m$, $\forall m \in \mathcal{M}$). The union of all muscle stimulation regions establishes the combined FES region of the crank cycle, defined as $\mathcal{Q}_{FES} \triangleq \bigcup_{m \in \mathcal{M}} \{\mathcal{Q}_m\}$, and the kinematic deadzone (KDZ) region as the remainder $\mathcal{Q}_{KDZ} \triangleq \mathcal{Q} \backslash \mathcal{Q}_{FES}$. By discretely switching between muscle groups to control continuous dynamics, an autonomous state-dependent switched system is created. The FES and KDZ regions are depicted in Figure 2-2.
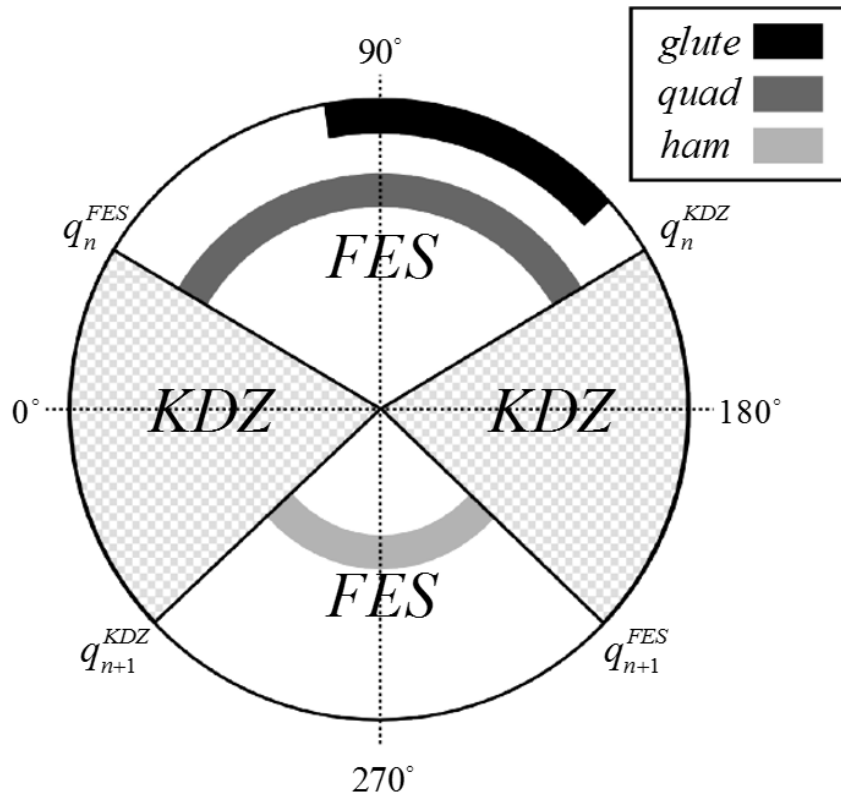
Figure 2-2. Sample crank cycle illustrating the FES and KDZ regions. The crank positions q_n^{FES} and q_n^{KDZ} denote the points at which the crank enters the FES and KDZ regions of cycle n, respectively. Cycle n refers to the nth time the crank enters the FES/KDZ region.

The stimulation input to the muscle groups and the current input to the electric motor are defined as

$$u_{FES}(q, t) \triangleq k_m \sigma_m(q) u_M(t), \tag{2–5}$$

$$u_{MOT}(t) \triangleq k_e u_e(t), \tag{2–6}$$

$\forall m \in \mathcal{M}$, where k_m, $k_e \in \mathbb{R}_{>0}$ are positive selectable control gains, u_M, $u_e : \mathbb{R}_{\geq 0} \to \mathbb{R}$ denote the subsequently designed control inputs for the muscle and motor, respectively, and $\sigma_m : Q \to \{0, 1\}$ denotes the switching signal for each muscle group, defined as

$$\sigma_m(q) \triangleq \begin{cases} 1 & q \in \mathcal{Q}_m \\ 0 & q \notin \mathcal{Q}_m \end{cases}, \tag{2–7}$$

$\forall m \in \mathcal{M}$. Substituting (2–5) and (2–3) into (2–1) and rearranging terms yields the switched system

$$B_M(q, \dot{q}) u_M(t) + B_e u_e(t) = M(q)\ddot{q} + V(q, \dot{q})\dot{q} + G(q) + P(q, \dot{q}) + b_c \dot{q} + d(t), \tag{2–8}$$

where $B_M : \mathcal{Q} \times \mathbb{R} \to \mathbb{R}$ is the combined, uncertain, nonlinear switched muscle control effectiveness, and $B_e \in \mathbb{R}_{>0}$, is the motor control effectiveness, respectively defined as

$$B_M(q, \dot{q}) \triangleq \sum_{m \in \mathcal{M}} b_m(q, \dot{q}) k_m \sigma_m(q), \tag{2–9}$$

$$B_e \triangleq b_e k_e. \tag{2–10}$$

Property 2.8. The uncertain individual muscle control effectiveness, $b_m(q, \dot{q})$, is subject to nonlinear activation dynamics and a muscle fiber recruitment curve (commonly represented by sigmoidal function) [117, 118]. However, based on [114], the function relating the stimulation input current to output torque is bounded by $b_{\underline{m}} \leq b_m(q, \dot{q}) \leq b_{\overline{m}}$, $\forall m \in \mathcal{M}$, where $b_{\underline{m}}$, $b_{\overline{m}} \in \mathbb{R}_{>0}$ are known constants. Hence, in the FES regions

(i.e., $q \in \mathcal{Q}_{FES}$) the lumped switched control effectiveness term is also bounded by $B_{\underline{M}} \leq B_M(q, \dot{q}) \leq B_{\overline{M}}$, where $B_{\underline{M}}, B_{\overline{M}} \in \mathbb{R}_{>0}$ are known constants.

2.1.5 Torque Dynamics

To allow for torque tracking, the dynamics in (2–1) can be rewritten as

$$\tau_m(q, \dot{q}, t) + \tau_e(t) = \tau_p(q, \dot{q}, \ddot{q}, t) + \tau_c(q, \dot{q}, \ddot{q}, t), \tag{2–11}$$

where the torques applied about the crank axis by the rider's muscles, the electric motor, the rider's passive effects, and the cycle are denoted by $\tau_m : \mathcal{Q} \times \mathbb{R} \times \mathbb{R}_{\geq 0} \to \mathbb{R}$, $\tau_e : \mathbb{R}_{\geq 0} \to \mathbb{R}$, $\tau_p : \mathcal{Q} \times \mathbb{R}^2 \times \mathbb{R}_{\geq 0} \to \mathbb{R}$, and $\tau_c : \mathcal{Q} \times \mathbb{R}^2 \times \mathbb{R}_{\geq 0} \to \mathbb{R}$, respectively. Motivated by the need to separate the torque contribution of the motor and muscles, when no stimulation is applied, $\tau_m(q, \dot{q}, t) \equiv 0$. Hence, (2–11) simplifies to

$$\tau_{est}(t) = \tau_p(q, \dot{q}, \ddot{q}, t) + \tau_c(q, \dot{q}, \ddot{q}, t), \tag{2–12}$$

where $\tau_{est} : \mathbb{R}_{\geq 0} \to \mathbb{R}$ is an auxiliary term defined as $\tau_{est}(t) \triangleq \tau_e(t)$ when no stimulation is applied. The structure of (2–12) is motivated by the fact that $\tau_p(q, \dot{q}, \ddot{q}, t)$ and $\tau_c(q, \dot{q}, \ddot{q}, t)$ represent the passive rider and cycle dynamics, respectively, which are amenable to pre-trial estimation. Based on the structure of (2–12), the following assumptions are made.

Assumption 2.1. The disturbances and auxiliary terms are sufficiently smooth in the sense that $\dot{d}(t), \tau_{est}(t), \dot{\tau}_{est}(t) \in \mathcal{L}_\infty$.

Assumption 2.2. A continuously differentiable estimate of $\tau_{est}(t)$, denoted by $\hat{\tau}_{est} : \mathbb{R}_{\geq 0} \to \mathbb{R}$, can be generated during preliminary testing such that the estimate error, $\tilde{\tau}_{est} : \mathbb{R}_{\geq 0} \to \mathbb{R}$ defined as

$$\tilde{\tau}_{est}(t) \triangleq \hat{\tau}_{est}(t) - \tau_{est}(t), \tag{2–13}$$

is bounded by $|\tilde{\tau}_{est}(t)| \leq c_{est}$, where $c_{est} \in \mathbb{R}_{\geq 0}$ is a known constant. This assumption is reasonable provided no stimulation is applied during preliminary testing (i.e. $\tau_m(q, \dot{q}, t) = $

0), the disturbances are sufficiently small when $\tau_{est}(t)$ is generated, and the desired trajectory is the same during the generation of $\tau_{est}(t)$ and the actual experimental trial.

The muscle torque can be rewritten by subtracting $\hat{\tau}_{est}(t)$ from (2–11) and using (2–13) as

$$\tau_m(q, \dot{q}, t) = \hat{\tau}_{est}(t) - \tau_e(t) + \tilde{\tau}_{est}(t). \tag{2–14}$$

Defining the estimate of the muscle torque, denoted by $\hat{\tau}_m : \mathbb{R}_{\geq 0} \to \mathbb{R}$, and defined as

$$\hat{\tau}_m(t) \triangleq \hat{\tau}_{est}(t) - \tau_e(t), \tag{2–15}$$

and subtracting (2–15) from (2–14) yields the muscle torque estimation error, denoted by $\tilde{\tau}_m : \mathcal{Q} \times \mathbb{R} \times \mathbb{R}_{\geq 0} \to \mathbb{R}$, defined as

$$\tilde{\tau}_m(q, \dot{q}, t) \triangleq \hat{\tau}_m(t) - \tau_m(q, \dot{q}, t), \tag{2–16}$$

which can be bounded by $|\tilde{\tau}_m(q, \dot{q}, t)| \leq c_{est}$, where c_{est} was defined in Assumption 2.2.

CHAPTER 3
CLOSED-LOOP CADENCE AND INSTANTANEOUS POWER CONTROL ON A MOTORIZED FUNCTIONAL ELECTRICAL STIMULATION CYCLE

Compared to the recent work in [105], which utilizes a repetitive learning controller to track a time-periodic cadence trajectory, this chapter and the associated precursory results in [86] and [87], examine simultaneous cadence and power tracking for the FES cycle introduced in Chapter 2 using Lyapunov-based and switched systems analysis tools, including a dwell-time analysis. Building on the development in [86], a running integral is employed to allow for instantaneous power tracking. Additionally, the effect of switching between different actuators is considered for both cadence and power tracking objectives using a novel Lyapunov-like switched system stability analysis, which yields global exponential cadence tracking and uniform ultimately bounded (UUB) power tracking. The controller in this chapter updates the power tracking error instantaneously, compared to once per crank cycle as in [87], and heuristically is better able to accommodate for rider asymmetries because each leg receives a unique stimulation pattern, compared to each leg receiving the same pattern, as in [87]. Furthermore, the electric motor is used for cadence tracking, which is the opposite strategy of the development in [86].

To evaluate the performance of the developed controller, comparisons are made with two previously developed FES cycling controllers through experiments on seven able-bodied participants and six participants with neuromuscular disorders. For a desired cadence of 50 RPM and a desired power of 10 W, the developed controller demonstrated the smallest tracking errors with an average cadence and power error of 0.01 ± 1.03 RPM and 0.00 ± 0.94 W, respectively, in the able-bodied population and an average cadence and power error of 0.02 ± 1.87 RPM and 0.00 ± 2.46 W, respectively, in the population with neuromuscular disorders. Results suggest that the electric motor should be used to track cadence and the FES induced muscle torques should be used to track instantaneous power.

3.1 Control Development

3.1.1 Robust Cadence Control

The position tracking objective is quantified by $e_1 : \mathbb{R}_{\geq 0} \to \mathbb{R}$, defined as

$$e_1 \triangleq q_d - q, \tag{3–1}$$

where $q_d : \mathbb{R}_{\geq 0} \to \mathbb{R}$ denotes the desired angular trajectory which is sufficiently smooth (i.e., $\dot{q}_d, \ddot{q}_d \in \mathcal{L}_\infty$) and bounded by $q_d \leq c_{q0}$, $\dot{q}_d \leq c_{q1}$, and $\ddot{q}_d \leq c_{q2}$. To facilitate the control development and stability analysis, an auxiliary tracking error $e_2 : \mathbb{R}_{\geq 0} \to \mathbb{R}$ is defined as

$$e_2 \triangleq \dot{e}_1 + \alpha e_1, \tag{3–2}$$

where $\alpha \in \mathbb{R}_{>0}$ is a constant control gain. Taking the derivative of (3–2), multiplying it by M, adding and subtracting e_1, then substituting (2–8), (3–1), and (3–2) yields the open-loop cadence error system

$$M\dot{e}_2 = \chi_1 - e_1 - Ve_2 - B_e u_e - B_M u_M. \tag{3–3}$$

The lumped auxiliary term, $\chi_1 : \mathcal{Q} \times \mathbb{R} \times \mathbb{R}_{\geq 0} \to \mathbb{R}$, defined as $\chi_1 \triangleq M(\ddot{q}_d + \alpha \dot{e}_1) + V(\dot{q}_d + \alpha e_1) + G + P + b_c(\dot{q}_d + \alpha e_1 - e_2) + d + e_1$ can be upper bounded as $|\chi_1| \leq c_1 + c_2 \|z\| + c_3 \|z\|^2$ by Properties 2.1-2.6, where $c_1, c_2, c_3 \in \mathbb{R}_{>0}$ are known constants, defined as

$$c_1 \triangleq c_M c_{q2} + c_V c_{q1}^2 + c_G + c_{P1} + c_{P2} c_{q1} + c_b c_{q1} + c_d, \tag{3–4}$$

$$c_2 \triangleq (c_M \alpha + c_{P2} + c_b)(\alpha + 1) + c_V c_{q1}(2\alpha + 1) + 1, \tag{3–5}$$

$$c_3 \triangleq c_V \alpha (\alpha + 1), \tag{3–6}$$

where the error vector $z \in \mathbb{R}^2$ is defined as $z \triangleq [e_1 \ e_2]^T$. Based on (3–3) and the subsequent stability analysis, the motor controller is designed as

$$u_e \;=\; \frac{1}{B_e}\Big[\Big(k_2 + k_3\,\|z\| + k_4\,\|z\|^2 + k_5\,|u_M|\Big)\mathsf{sgn}(e_2) + k_1 e_2\Big],\qquad(3\text{–}7)$$

where $k_i \in \mathbb{R}_{\geq 0}\ \forall i = 1,\,2\,,...,5$ denote constant control gains. Substituting (3–7) into (3–3) yields the closed-loop error system

$$M\dot{e}_2 \;=\; \chi_1 - e_1 - Ve_2 - B_M u_M - \Big[\Big(k_2 + k_3\,\|z\| + k_4\,\|z\|^2 + k_5\,|u_M|\Big)\mathsf{sgn}(e_2) + k_1 e_2\Big].$$
$$(3\text{–}8)$$

3.1.2 Robust Torque Control

Compared to discrete torque (i.e., power) tracking, instantaneous torque tracking offers numerous benefits. With discretized tracking, because the error system is updated once per crank cycle, the control input is updated once per crank cycle, resulting in both legs receiving identical stimulation. Such an approach fails to isolate the capabilities of either leg as the control input is based on the error generated from the contribution of both the legs as a whole. Additionally, because the error is updated at the same point every cycle, the initially (i.e., soon after the error update) stimulated muscle groups receive a control input that reflects the error with little delay, but other muscle groups receive a considerably delayed error. Over the course of an experiment, this effect can culminate in one-sided fatigue and could potentially mitigate rehabilitation outcomes. For this reason, the torque tracking objective in this chapter is to prove that the estimated muscle torque instantaneously tracks the desired muscle torque (i.e., $\hat{\tau}_m \to \tau_{m,d}$), where $\tau_{m,d} : \mathbb{R}_{\geq 0} \to \mathbb{R}$ denotes the sufficiently smooth (i.e., $\tau_{m,d},\ \dot{\tau}_{m,d} \in \mathcal{L}_\infty$) desired torque trajectory which is bounded by $\tau_{m,d} \leq c_{\tau 0}$ and $\dot{\tau}_{m,d} \leq c_{\tau 1}$. To facilitate the subsequent analysis, the torque tracking objective is represented as a integral, denoted by $e_3 : \mathbb{R}_{\geq 0} \to \mathbb{R}$, and defined as [119]

$$e_3 \triangleq \int_{t_0}^{t} \big(\tau_{m,d}(\psi) - \hat{\tau}_m(\psi)\big)\,d\psi,\qquad(3\text{–}9)$$

where $t_0 \in \mathbb{R}_{\geq 0}$ represents the initial time, and the derivative of (3–9), given by

$$\dot{e}_3 = \tau_{m,d}(t) - \hat{\tau}_m(t), \qquad (3\text{--}10)$$

represents the true torque tracking error. Motivated by the result in [119] and the subsequent stability analysis, the form of the tracking error in (3–9) was designed such that the subsequently designed torque controller is able to directly influence the derivative in (3–10), and hence, the closed-loop error system. Substituting (2–15) into (3–9) and taking its derivative, then inserting (2–5), (2–9), (2–11), and (2–12) yields the open-loop torque error system

$$\dot{e}_3 = \chi_2 - B_M u_M. \qquad (3\text{--}11)$$

The lumped auxiliary term, $\chi_2 : \mathcal{Q} \times \mathbb{R}^2 \times \mathbb{R}_{\geq 0}$, defined as $\chi_2 \triangleq \tilde{\tau}_{est} + \tau_{m,d}$, can be upper bounded as $|\chi_2| \leq c_4$, by Assumption 2.2, where $c_4 \in \mathbb{R}_{>0}$ is a known constant defined as

$$c_4 \triangleq c_{est} + c_{\tau 0}. \qquad (3\text{--}12)$$

Based on (3–11) and the subsequent stability analysis, the muscle controller is designed as

$$u_M \;=\; \frac{1}{B_{\underline{\sigma}}} \left[k_6 e_3 + k_7 \mathsf{sgn}(e_3) \right], \qquad (3\text{--}13)$$

where $k_6, \; k_7 \in \mathbb{R}_{\geq 0}$ denote constant control gains. Substituting (3–13) into (3–11), respectively, yields the closed-loop error systems

$$\dot{e}_3 \;=\; \chi_2 - \frac{B_{\sigma}}{B_{\underline{\sigma}}} \left[k_6 e_3 + k_7 \mathsf{sgn}(e_3) \right]. \qquad (3\text{--}14)$$

Figure 3-1 displays the combined closed-loop systems.
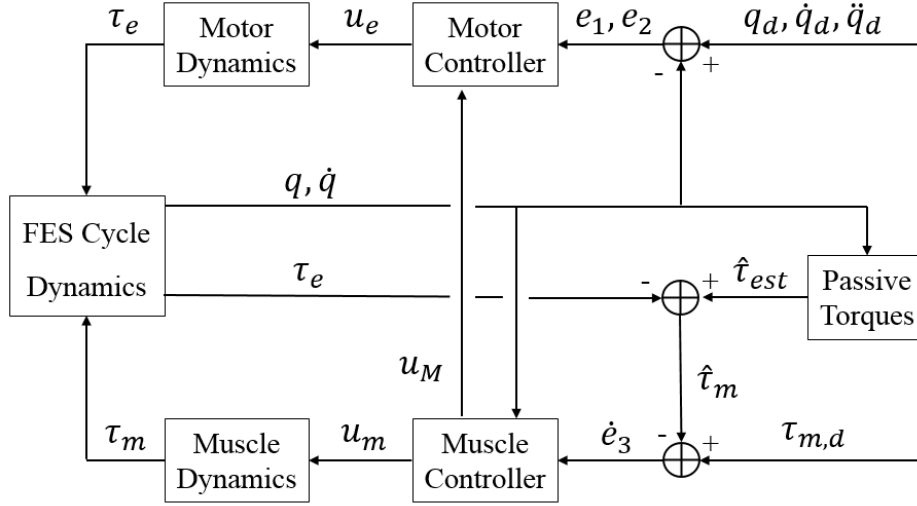
Figure 3-1. Block diagram representing the closed-loop feedback structure of combined cycle-rider system.

3.2 Stability Analysis

To ensure overall system stability, both the cadence and torque error systems must be analyzed in the FES and KDZ regions along with analyzing the effect of switching between the subsystems. Because cadence is regulated with the electric motor throughout the entire crank cycle, switching occurs between stabilizable subsystems. Therefore, Theorem 3.1 includes a common Lyapunov function to demonstrate exponential cadence tracking for all time. Torque, however, is only regulated in the FES region using the rider's muscles; this leads to incomplete control authority and opportunities for error growth in the KDZ region. Theorems 3.2-3.4 include an additional candidate Lyapunov function that not only establishes an ultimate bound on the torque error system, but also its derivative (i.e., the true torque objective). For the following analysis, let $V_1 : \mathbb{R}^2 \rightarrow \mathbb{R}$ and $V_2 : \mathbb{R} \rightarrow \mathbb{R}$ denote continuously differentiable, positive definite candidate Lyapunov functions respectively defined as

$$V_1 \triangleq \frac{1}{2}e_1^2 + \frac{1}{2}Me_2^2, \tag{3-15}$$

$$V_2 \triangleq \frac{1}{2}e_3^2. \tag{3-16}$$

The candidate Lyapunov function V_1 satisfies the following inequalities:

$$\underline{\lambda} \left\| z \right\|^2 \leq V_1 \leq \overline{\lambda} \left\| z \right\|^2, \tag{3–17}$$

where $\underline{\lambda}, \overline{\lambda} \in \mathbb{R}_{>0}$ are known constants defined as $\underline{\lambda} \triangleq \min \left(\frac{1}{2}, \frac{c_m}{2} \right), \overline{\lambda} \triangleq \max \left(\frac{1}{2}, \frac{c_M}{2} \right)$.

Theorem 3.1. *For $q \in \mathcal{Q}$, the closed-loop error system in (3–8) yields global exponential position and cadence tracking in the sense that*

$$\left\| z(t) \right\| \leq \sqrt{\frac{\overline{\lambda}}{\underline{\lambda}}} \left\| z(t_n) \right\| \exp \left[-\frac{1}{2} \Lambda (t - t_n) \right], \tag{3–18}$$

$\forall t \in [t_0, \infty)$, $\forall n$, where $n \in \mathbb{N}$ represents the nth iteration the crank enters/exits an FES region, and consequently, the nth iteration the crank enters/exits a KDZ, and $\Lambda \in \mathbb{R}_{>0}$ is defined as

$$\Lambda = \frac{1}{\overline{\lambda}} min \left(\alpha, \ k_1 \right), \tag{3–19}$$

provided the following gain conditions are satisfied

$$k_2 \geq c_1, \ k_3 \geq c_2, \ k_4 \geq c_3, \tag{3–20}$$

and $k_5 \geq B_{\overline{M}}$ if $q \in \mathcal{Q}_{FES}$, $k_5 = 0$ if $q \in \mathcal{Q}_{KDZ}$, where c_1, c_2, c_3 and $B_{\overline{M}}$ are defined in (3–4)-(3–6), and Property 2.8, respectively.

Proof. Let $z(t)$ be a Filippov solution to the differential inclusion $\dot{z} \in K[h_1](z)$, where $K[\cdot]$ is defined as in [120], and where $h_1 : \mathbb{R}^2 \to \mathbb{R}^2$ is defined using (3–2) and (3–8), as

$$h_1 \triangleq \begin{bmatrix} \dot{e}_1 \\ \dot{e}_2 \end{bmatrix}. \tag{3–21}$$

The time derivative of (3–15) exists almost everywhere (i.e., for almost all $t \in [t_0, \infty)$), and $\dot{V}_1(z) \overset{a.e.}{\in} \dot{\tilde{V}}_1(z)$, where $\dot{\tilde{V}}_1$ is the generalized time derivative of (3–15) along the Filippov trajectories of $\dot{z} = h_1(z)$ and is defined as [121] $\dot{\tilde{V}}_1 \triangleq \underset{\xi \in \partial V_1(z)}{\cap} \xi^T K \begin{bmatrix} h_1(z) & 1 \end{bmatrix}^T$,

where ∂V_1 is the Clarke generalized gradient of V_1. Since V_1 is continuously differentiable in z, $\partial V_1 = \{\nabla V_1\}$; thus, $\dot{\tilde{V}}_1 \subseteq \begin{bmatrix} e_1 & Me_2 & \frac{1}{2}\dot{M}e_2^2 \end{bmatrix} K \begin{bmatrix} h_1(z) & 1 \end{bmatrix}^T$. Using the calculus of $K[\cdot]$ from [121], substituting (3–2), (3–13), (3–8), and (3–21) into the result yields

$$
\begin{aligned}
\dot{\tilde{V}}_1 \subseteq \; & -\alpha e_1^2 + e_2\chi_1 + \left(\frac{1}{2}\dot{M} - V\right)e_2^2 - k_1 e_2^2 - \left(k_2 + k_3\|z\| + k_4\|z\|^2\right)K[\mathsf{sgn}(e_2)]e_2 \\
& -\frac{k_5}{B_{\underline{M}}}\left(k_6\,|e_3| + k_7 K\left[|\mathsf{sgn}(e_3)|\right]\right)K\left[\mathsf{sgn}(e_2)\right]e_2 - e_2\frac{K[B_M]}{B_{\underline{M}}}\left(k_6 e_3 + k_7 K[\mathsf{sgn}(e_3)]\right).
\end{aligned}
$$

(3–22)

where, $K[\mathsf{sgn}(\cdot)] = \mathsf{SGN}(\cdot)$ such that $\mathsf{SGN}(\cdot) = \{1\}$ if $(\cdot) > 0$, $[-1, 1]$ if $(\cdot) = 0$, and $\{-1\}$ if $(\cdot) < 0$; and $K[|\mathsf{sgn}(\cdot)|] = |\mathsf{SGN}(\cdot)|$ such that $|\mathsf{SGN}(\cdot)| = \{1\}$ if $(\cdot) \neq 0$, and $[0, 1]$ if $(\cdot) = 0$. To illustrate convergence for all time, the expression in (3–22) must be evaluated when $q \in \mathcal{Q}_{FES}$ and $q \in \mathcal{Q}_{KDZ}$.

For $q \in \mathcal{Q}_{FES}$, $K[B_M]$ can be upper bounded by $B_{\overline{M}}$, hence by Properties 2.7 and 2.8, and since $\dot{V}_1(z) \overset{\text{a.e.}}{\in} \dot{\tilde{V}}_1(z)$, (3–22) can be bounded as

$$
\dot{V}_1 \overset{\text{a.e.}}{\leq} -\alpha e_1^2 + |e_2\chi_1| - k_1 e_2^2 - |e_2|\left(k_2 + k_3\|z\| + k_4\|z\|^2\right) - \frac{(k_5 - B_{\overline{M}})}{B_{\underline{M}}}|e_2|\left(k_6\,|e_3| + k_7\right)
$$

(3–23)

Using Properties 2.1-2.6 allows (3–23) to be further upper bounded as

$$
\dot{V}_1 \overset{\text{a.e.}}{\leq} -\alpha e_1^2 - k_1 e_2^2 - \lambda_1\,|e_2| - \lambda_2\,|e_2|\,\|z\| - \lambda_3\,|e_2|\,\|z\|^2 - \frac{\lambda_4}{B_{\underline{M}}}|e_2|\left(k_6\,|e_3| + k_7\right),
$$

(3–24)

where $\lambda_i \in \mathbb{R}$, $\forall i \in \mathcal{I} = \{1,\, 2,\, 3,\, 4\}$ are known constants defined as $\lambda_1 \triangleq k_2 - c_1$, $\lambda_2 \triangleq k_3 - c_2$, $\lambda_3 \triangleq k_4 - c_3$, $\lambda_4 \triangleq k_5 - B_{\overline{M}}$. By Property 2.8, (3–24) holds for all B_M; hence, (3–15) is verified as a common Lyapunov function across the controlled regions. Provided the gain conditions in (3–20) are satisfied, $\lambda_i \geq 0\ \forall i \in \mathcal{I}$, and (3–24) can be upper bounded as

$$\dot{V}_1 \overset{\text{a.e.}}{\leq} -\Lambda V_1, \tag{3–25}$$

where Λ was defined in (3–19). Solving the differential inequality yields

$$V_1 \overset{\text{a.e.}}{\leq} V_1 \left(t_n^{FES} \right) \exp \left(-\Lambda \left(t - t_n^{FES} \right) \right). \tag{3–26}$$

When evaluating (3–22) for $q \in \mathcal{Q}_{KDZ}$, Property 2.7, and the fact that $k_5 = 0$ if $q \in \mathcal{Q}_{KDZ}$, allows (3–22) to be bounded as

$$\dot{V}_1 \overset{\text{a.e.}}{\leq} -\alpha e_1^2 + |e_2 \chi_1| - k_1 e_2^2 - |e_2| \left(k_2 + k_3 \|z\| + k_4 \|z\|^2 \right). \tag{3–27}$$

Properties 2.1-2.6 allow (3–27) to be further upper bounded as

$$\dot{V}_1 \overset{\text{a.e.}}{\leq} -\alpha e_1^2 - k_1 e_2^2 - \lambda_1 |e_2| - \lambda_2 |e_2| \|z\| - \lambda_3 |e_2| \|z\|^2, \tag{3–28}$$

which can further be upper bounded as (3–25) provided the gain conditions in (3–20) are satisfied. Hence, (3–15) is a common Lyapunov function for all time. Based on (3–17) and (3–25), the result in (3–18) can be obtained, and from the closed-loop error systems, the controller in (3–7) is bounded. Hence, the first control objective is satisfied (i.e., cadence). □

Because incomplete control authority exists over the torque tracking objective (i.e., the rider's muscles are stimulated in the FES region, but not in the KDZ region), the following theorem is employed to establish a decay rate on the torque error system in the FES region and a growth rate in the KDZ region.

Theorem 3.2. *For $q \in \mathcal{Q}_{FES}$, the closed-loop error system in (3–14) yields exponential torque tracking in the sense that*

$$|e_3(t)| \leq \left| e_3(t_n^{FES}) \right| \exp \left[-k_6 (t - t_n^{FES}) \right], \tag{3–29}$$

$\forall t \in \left[t_n^{FES},\, t_n^{KDZ}\right)$ and $\forall n$, where $t_n^{FES} \in \mathbb{R}_{\geq 0}$ is the time the crank enters $\mathcal{Q}_{FES}$ of cycle n, provided the gain conditions in (3–20) and the following constant gain condition is satisfied:

$$k_7 \geq c_4, \tag{3–30}$$

where c_4 was introduced in (3–12). Additionally, for $q \in \mathcal{Q}_{KDZ}$, the torque tracking error can be bounded as

$$|e_3(t)| \;\leq\; \begin{cases} \sqrt{|e_3(t_n^{KDZ})|^2 + c_4\sqrt{8}\,(t - t_n^{KDZ})} & \text{for } |e_3| \leq \sqrt{2} \\[2mm] |e_3(t_n^{KDZ})| \exp\left(\frac{c_4}{\sqrt{2}}\left(t - t_n^{KDZ}\right)\right) & \text{for } |e_3| > \sqrt{2} \end{cases} \tag{3–31}$$

$\forall t \in \left[t_n^{KDZ},\, t_{n+1}^{FES}\right)$, and $\forall n$, where $t_n^{KDZ} \in \mathbb{R}_{\geq 0}$ is the time the crank enters $\mathcal{Q}_{KDZ}$ (i.e., exits $\mathcal{Q}_{FES}$) of cycle n.

Proof. Let $e_3(t)$ for $t \in [t_0, \infty)$ be a Filippov solution to the differential inclusion $\dot{e}_3 \in K[h_2](e_3)$, where $h_2 : \mathbb{R} \to \mathbb{R}$ is defined using (3–14) as

$$h_2 \triangleq \dot{e}_3. \tag{3–32}$$

The time derivative of (3–16) exists almost everywhere and $\dot{V}_2(e_3) \overset{\text{a.e.}}{\in} \dot{\tilde{V}}_2(e_3)$, where $\dot{\tilde{V}}_2$ is the generalized time derivative of (3–15) along the Filippov trajectories of $\dot{e}_3 = h_2(e_3)$, defined as [121] $\dot{\tilde{V}}_2 \triangleq \underset{\xi \in \partial V_2(e_3)}{\cap} \xi^T K\left[\, h_2(e_3)\, \right]$, where ∂V_2 is the Clarke generalized gradient of V_2. Since V_2 is continuously differentiable in e_3, $\partial V_2 = \{\nabla V_2\}$; thus, $\dot{\tilde{V}}_2 \subseteq e_3\, K\left[\, h_2(e_3)\, \right]$. Using the calculus of $K[\cdot]$ from [121], (3–14), and (3–32), yields

$$\dot{\tilde{V}}_2 \subseteq e_3\chi_2 - \frac{B_M}{B_{\underline{M}}}\left(k_6 e_3^2 + k_7 K\left[\text{sgn}(e_3)\right] e_3\right), \tag{3–33}$$

where $K[B_M] = B_M$ within the FES regions. By Property 2.8, and since $\dot{V}_2(e_3) \overset{\text{a.e.}}{\in} \dot{\tilde{V}}_2(e_3)$, (3–33) can be bounded as

$$\dot{V}_2 \overset{\text{a.e.}}{\leq} |e_3\chi_2| - k_6 e_3^2 - k_7 |e_3|. \tag{3–34}$$

45

Assumption 2.2 allows (3–34) to be further upper bounded as

$$\dot{V}_2 \overset{\text{a.e.}}{\leq} - k_6 e_3^2 - \lambda_5 |e_3|, \tag{3–35}$$

where $\lambda_5 \in \mathbb{R}$ is a known constant defined as $\lambda_5 \triangleq k_7 - c_4$. By Property 2.8, (3–16) is verified as a common Lyapunov function across the controlled regions. Provided the gain condition in (3–30) is satisfied, (3–35) can be upper bounded as

$$\dot{V}_2 \overset{\text{a.e.}}{\leq} -2k_6 V_2. \tag{3–36}$$

Solving the differential inequality in (3–36) yields

$$V_2 \overset{\text{a.e.}}{\leq} V_2 \left(t_n^{FES} \right) \exp \left(-2k_6 \left(t - t_n^{FES} \right) \right). \tag{3–37}$$

Hence, by (3–16) the result in (3–29) can be obtained.

When $q \in \mathcal{Q}_{KDZ}$, the control input term $u_M = 0$, and the expression in (3–33) can be written as

$$\dot{\tilde{V}}_2 \subseteq e_3 \chi_2, \tag{3–38}$$

because $B_M = 0$. Using (3–16), and since $\dot{V}_2(e_3) \overset{\text{a.e.}}{\in} \dot{\tilde{V}}_2(e_3)$, (3–38) can be upper bounded as

$$\dot{V}_2 \overset{\text{a.e.}}{\leq} c_4 \sqrt{2V_2}. \tag{3–39}$$

From (3–39),

$$\dot{V}_2 \overset{\text{a.e.}}{\leq} \begin{cases} c_4 \sqrt{2} & \text{if } V_2 \leq 1 \\ c_4 \sqrt{2} V_2 & \text{if } V_2 > 1 \end{cases}. \tag{3–40}$$

By invoking the Comparison Lemma [63, Lemma 3.4] for each case,

$$V_2 \overset{\text{a.e.}}{\leq} \begin{cases} V_2\left(t_n^{KDZ}\right) + c_4\sqrt{2}\left(t - t_n^{KDZ}\right) & \text{if } V_2 \leq 1 \\ V_2\left(t_n^{KDZ}\right)\exp\left(c_4\sqrt{2}\left(t - t_n^{KDZ}\right)\right) & \text{if } V_2 > 1 \end{cases}. \tag{3–41}$$

Using (3–16) provides the result in (3–31), and from the closed-loop error systems, the controller in (3–13) is bounded. $\square$

Despite the growth of the torque error system in the KDZ region, the following theorem leverages the results of Theorem 3.2 to guarantee convergence to an ultimate bound through dwell-time conditions which manifest themselves as a minimum and maximum allowable cadence.

Theorem 3.3. *For $q \in \mathcal{Q}$, the closed-loop error system in (3–14) yields a uniformly ultimately bounded torque tracking error in the sense that*

$$|e_3(t)| \leq 4\sqrt{\exp\left(-2k_6\Delta t_{min}^{FES}\right) + c_4\sqrt{2}\Delta t_{max}^{KDZ}} \leq \sqrt{2}, \tag{3–42}$$

$\forall t \in [t_0, \infty)$ when (3–30) and the following gain condition is satisfied

$$k_6 \geq \max\left(\frac{c_4\sqrt{2}\Delta t_{max}^{KDZ}}{2\Delta t_{min}^{FES}}, \frac{\ln\left(1 - c_4\sqrt{2}\Delta t_{max}^{KDZ}\right)}{2\Delta t_{min}^{FES}}\right),$$

$$\Delta t_{max}^{KDZ} < \frac{1}{c_4\sqrt{2}},$$

where $\Delta t_{min}^{FES}, \Delta t_{max}^{KDZ} \in \mathbb{R}_{>0}$ are known constants defined as

$$\Delta t_{min}^{FES} \triangleq \min\left(t_n^{KDZ} - t_n^{FES}\right), \tag{3–43}$$

$$\Delta t_{max}^{KDZ} \triangleq \max\left(t_{n+1}^{FES} - t_n^{KDZ}\right), \tag{3–44}$$

which denote the minimum allowable dwell-time in the FES region and the maximum allowable dwell-time in the KDZ region, $\forall n$, as dictated by (2–4) and the selectable minimum and maximum allowable cadences, respectively.

Proof. By evaluating V_2 at the switching instances (i.e., $V_2\left(t_n^{FES}\right)$) and enforcing

$$V_2\left(t_{n+1}^{FES}\right) \leq V_2\left(t_n^{FES}\right), \tag{3-45}$$

an ultimate bound is guaranteed to exist. Specifically, using (3–37) and (3–41), (3–45) can be rewritten as

$$V_2\left(t_{n+1}^{FES}\right) \leq \begin{cases} V_2\left(t_n^{FES}\right)\exp\left(-2k_6\left(t_n^{KDZ}-t_n^{FES}\right)\right)+c_4\sqrt{2}\left(t_{n+1}^{FES}-t_n^{KDZ}\right) & \text{if } V_2 \leq 1 \\ V_2\left(t_n^{FES}\right)\exp\left(-2k_6\left(t_n^{KDZ}-t_n^{FES}\right)+c_4\sqrt{2}\left(t_{n+1}^{FES}-t_n^{KDZ}\right)\right) & \text{if } V_2 > 1 \end{cases}. \tag{3-46}$$

By examining the worst case scenario (i.e., inserting the minimum and maximum allowable dwell-times), (3–46) can be bounded as

$$V_2\left(t_{n+1}^{FES}\right) \leq \begin{cases} V_2\left(t_n^{FES}\right)\exp\left(-2k_6\Delta t_{min}^{FES}\right)+c_4\sqrt{2}\Delta t_{max}^{KDZ} & \text{if } V_2 \leq 1 \\ V_2\left(t_n^{FES}\right)\exp\left(c_4\sqrt{2}\Delta t_{max}^{KDZ}-2k_6\Delta t_{min}^{FES}\right) & \text{if } V_2 > 1 \end{cases}. \tag{3-47}$$

Examining (3–47), when $V_2 \leq 1$, and inserting the largest possible initial condition (i.e., $V_2\left(t_n^{FES}\right)=1$), (3–47) simplifies to

$$V_2\left(t_{n+1}^{FES}\right) \leq \exp\left(-2k_6\Delta t_{min}^{FES}\right)+c_4\sqrt{2}\Delta t_{max}^{KDZ}. \tag{3-48}$$

To enforce overall decay, $V_2\left(t_{n+1}^{FES}\right)$ needs to be less than the initial condition (i.e., $V_2\left(t_{n+1}^{FES}\right) < 1$), and (3–48) becomes

$$1 \geq \exp\left(-2k_6\Delta t_{min}^{FES}\right)+c_4\sqrt{2}\Delta t_{max}^{KDZ},$$

which can be solved for the gain condition

$$k_6 \geq \frac{\ln(1-c_4\sqrt{2}\Delta t_{max}^{KDZ})}{2\Delta t_{min}^{FES}}. \tag{3-49}$$

Hence, for $V_2 \leq 1$, the ultimate bound is

$$V_2 \leq \exp\left(-2k_6\Delta t_{min}^{FES}\right)+c_4\sqrt{2}\Delta t_{max}^{KDZ} \leq 1. \tag{3-50}$$

Examining (3–47) when $V_2 > 1$ and imposing the following gain condition will result in overall exponential decay to the smallest possible bound (i.e., $\lim_{t\to\infty} V_2 = 1$),

$$k_6 \geq \frac{c_4\sqrt{2}\Delta t_{max}^{KDZ}}{2\Delta t_{min}^{FES}}. \tag{3–51}$$

Because overall decay is enforced for both of the above conditions (i.e., $V_2 \leq 1$ and $V_2 > 1$), the overall ultimate bound is given by (3–50) provided the gain conditions in (3–49) and (3–51) are satisfied. Figure 3-2 provides an example decay to the ultimate bound using (3–37) and (3–41). Bounding (3–50) with (3–16) provides the result in (3–42). □

Theorem 3.3 establishes an ultimate bound for the integral torque tracking error (i.e., e_3). Theorem 3.4 provides a bound on the instantaneous torque tracking error (i.e., $\dot{e}_3$).

Theorem 3.4. *For $q \in \mathcal{Q}$, the closed-loop error system in (3–14) yields a uniformly ultimately bounded instantaneous torque tracking error in the sense that*

$$|\dot{e}_3| \overset{a.e.}{\leq} c_4 + \frac{B_{\overline{M}}}{B_{\underline{M}}}\left(k_7 + 4k_6\sqrt{\exp\left(-2k_6\Delta t_{min}^{FES}\right) + c_4\sqrt{2}\Delta t_{max}^{KDZ}}\right). \tag{3–52}$$

Proof. To establish an ultimate bound on $\dot{e}_3$, the result in (3–33) is evaluated for $q \in \mathcal{Q}_{FES}$ and $q \in \mathcal{Q}_{KDZ}$ as

$$\dot{\tilde{V}}_2 \subseteq \begin{cases} e_3\chi_2 - \frac{B_M}{B_{\underline{M}}}\left(k_6 e_3^2 + k_7 K\left[\text{sgn}\left(e_3\right)\right] e_3\right) & \text{if } q \in \mathcal{Q}_{FES} \\ e_3\chi_2 & \text{if } q \in \mathcal{Q}_{KDZ} \end{cases}. \tag{3–53}$$

Using (3–16), and since $\dot{V}_2(e_3) \overset{a.e.}{\in} \dot{\tilde{V}}_2(e_3)$, (3–53) can be rewritten as

$$\dot{e}_3 \overset{a.e.}{=} \begin{cases} \chi_2 - \frac{B_M}{B_{\underline{M}}}\left(k_6 e_3 + k_7 K\left[\text{sgn}\left(e_3\right)\right]\right) & \text{if } q \in \mathcal{Q}_{FES} \\ \chi_2 & \text{if } q \in \mathcal{Q}_{KDZ} \end{cases}. \tag{3–54}$$

Establishing the most aggressive decay and growth rate for the FES and KDZ regions, respectively, will provide an ultimate bound on $\dot{e}_3$. For $q \in \mathcal{Q}_{FES}$, (3–54) must be lower
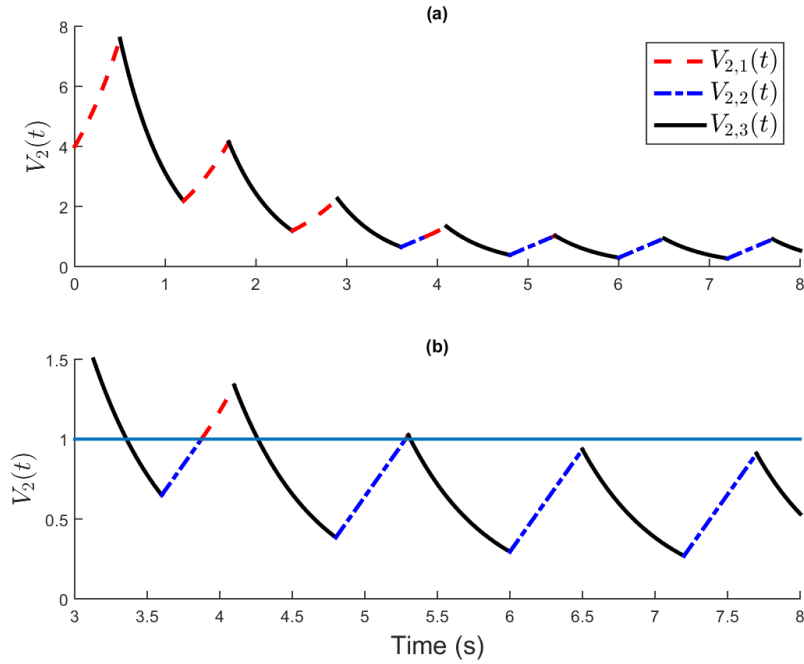
Figure 3-2. Sample Lyapunov function evolution over $n = 8$ cycles with parameters $V_2(t_0) = 4$, $c_4\sqrt{2} = 1.28$, $k_6 = 3.56$, $\Delta t^{KDZ} = 0.5$s, $\Delta t^{FES} = 0.7$s (i.e., constant 50 RPM with the FES regions representing 58% of the crank cycle and KDZs representing 42%). The Lyapunov function $V_{2,1}$ represents the exponential growth bound for $V_2 > 1$ in the KDZ, $V_{2,2}$ represents the linear growth bound for $V_2 \leq 1$ in the KDZ, and $V_{2,3}$ represents the exponential decay bound in the FES regions. (b) The same sequence of Lyapunov functions, with an emphasis on the ultimate bound being less than 1, obtained by adhering to the gain conditions in (3–49) and (3–51).

bounded. Using Property 2.8, and bounding yields

$$\dot{e}_3 \overset{\text{a.e.}}{\geq} -c_4 - \frac{B_{\bar{M}}}{B_{\underline{M}}}\left(k_6\left|e_3\right| + k_7\right). \tag{3--55}$$

For $q \in \mathcal{Q}_{KDZ}$, (3–54) must be upper bounded, which when combined with (3–12) yields the most aggressive growth rate in the KDZ regions given by

$$\dot{e}_3 \overset{\text{a.e.}}{\leq} c_4. \tag{3--56}$$

After combining the bounds in both the FES and KDZ regions (i.e., (3–55) and (3–56)) with the ultimate bound on e_3 given in (3–42), the maximum of the two is taken to obtain the ultimate bound on $\dot{e}_3$ in (3–52). □

Table 3-1. Controller operational details for FES and KDZ regions for Controllers A, B, and C

Controller	Region	Motor Objective	Muscle Objective
A	FES	Cadence	Instantaneous Power
	KDZ	Cadence	None
B* [86]	FES	Instantaneous Power	Cadence
	KDZ	Cadence	None
C* [87]	FES	Cadence	Discretized Power
	KDZ	Cadence	None

3.3   Experiments

Experiments were conducted to validate the performance of the developed controller, henceforth labeled Controller A, in both an able-bodied population and a population with varied neurological conditions. To further examine the performance compared to alternate methods of cadence and power control, two other controllers were implemented, labeled Controller B and Controller C, whose development and stability analyses are available in [86] and [87], respectively. While the forms of the three controllers are different, all have the same objective of cadence and power tracking. Though the tracking objectives in the FES regions vary, all three controllers utilize the motor to track cadence in the KDZ regions because no muscles are activated; see Table 3-1 for details. Although the error systems and controllers take different forms, a side-by-side comparison is made because all controllers possess the same desired cadence and power trajectories for a given participant. By comparing the three controllers, insights are provided to determine which actuator (i.e., muscle or motor) results in better tracking performance of the objectives (i.e., cadence or power) and which is the better method to track power (i.e., instantaneously or discretely).

3.3.1   Experimental Testbed

The experimental testbed used in this chapter is introduced in Chapter 2.

3.3.2   Experimental Methods

Seven able-bodied participants (five male and two female) with ages ranging from 21 to 43 years old, and six participants with neurological impairments (four male and

two female) with ages ranging from 20 to 48 years old participated in the experimental protocol. Participants were either recruited through the University of Florida (UF) Health Integrated Data Repository (UF Consent2Share project) and completed the FES-cycling protocol at UF or were enrolled at Brooks Rehabilitation Hospital in Jacksonville, FL. All participants gave written informed consent approved by the UF Institutional Review Board. Able-bodied participants were blind to the desired trajectories, and asked to remain passive for the duration of the experiment unless otherwise noted. Removing volitional contribution simulates a worst case scenario where the participant's muscles provide no contribution to the trajectory. Although, some contribution is still possible, any voluntary contribution was only partially informed by stimulation cues as participants were unaware of the desired trajectories. As is common in active therapy, participants with a neurological condition were asked to volitionally pedal with stimulation added as needed. These participants were shown a graph of the tracking performance of e_3, exclusively, and asked to contribute to the control objective to the greatest extent possible. In the able-bodied population, all three controllers were implemented in random order. In the population possessing neurological disorders, Controllers A and C were implemented in random order.

In preparation for experimentation, electrodes were placed on the quadriceps femoris, hamstrings, and gluteal muscle groups of a person who was seated with their feet inserted securely into the orthotic pedals attached to the cycle. The tricycle's seat position was adjusted for the person's comfort while ensuring that full extension of the knees could not be achieved (i.e., maintaining a minimum bend of 15° at the knee) while cycling. Measurements including the person's thigh and shank length, as well as distance from the person's greater trochanter to the crank in both the horizontal and vertical directions, were made to calculate the torque transfer ratios and determine the stimulation pattern based on (2–4). Prior to stimulation, the participant's range of motion and comfort was verified by running the cycle at 30, 40, and 50 RPM, sequentially.

Upon reaching 50 RPM, open-loop stimulation was applied and modulated until muscle contractions were visible. For comfort, if the person's threshold was reached during calibration, the stimulation value was saved by the controller and the stimulation was saturated at this level for the duration of the experiment.

The estimate of the rider's passive dynamics, $\hat{\tau}_{est}$, was generated by simultaneously running the cycle at the desired cadence (50 RPM) while recording the torque from the powermeter; the rider was instructed to provide no volitional effort. Subsequently, an eighth-order Fourier fit was applied to the recorded torque measurements to satisfy Assumption 2.2. Afterward, a 180 second experimental protocol was performed on the participant, which began with an exponential ramp to the desired cadence using only the motor. Upon reaching the desired cadence, the power trajectory then began increasing along an exponential ramp until the desired power was obtained, at which point stimulation was applied. The cadence controller given in (3–7) was active during and after the cadence ramp, where the torque controller given in (3–13) was only active after the desired cadence had been reached because large muscle forces are required to move the crank at low speeds [81]. While there is no clear consensus for the optimal cadence of FES cycles for rehabilitation, it has been suggested that lower cadences may be more ideal for torque production, while higher cadences may be better for power production [81]. For feasibility purposes, however, the desired cadence was set to 50 RPM [84, 122] for both the able-bodied population and the population with neurological impairments.

The desired power is denoted by $P_d : \mathbb{R}_{\geq 0} \to \mathbb{R}$ and defined as the product of the desired torque and desired cadence (i.e., $P_d \triangleq \tau_{m,d}\dot{q}_d$), and varied based on participant capability. Although the muscles are stimulated with the controller in (3–13) utilizing a torque-based error system, in the following, results are displayed in terms of measured power, denoted by $P : \mathbb{R}_{\geq 0} \to \mathbb{R}$, defined as the product of the estimated rider torque and measured cadence (i.e., $P \triangleq \hat{\tau}_m\dot{q}$). To account for the

electromechanical delay present in the rider's muscles, the stimulation pattern was advanced as a function of the cadence (i.e., $q_{stim} \triangleq q + 0.1\dot{q}$), where $q_{stim} : \mathcal{Q} \times \mathbb{R} \to \mathcal{Q}$ was substituted for q in (2–7). Although the aforementioned gain conditions (i.e.,

$$k_2 \geq c_1, \; k_3 \geq c_2, \; k_4 \geq c_3, \; k_5 \geq B_{\overline{M}}, \; k_6 \geq \max\left(\frac{c_4\sqrt{2}\Delta t_{max}^{KDZ}}{2\Delta t_{min}^{FES}}, \; \frac{\ln\left(1 - c_4\sqrt{2}\Delta t_{max}^{KDZ}\right)}{2\Delta t_{min}^{FES}}\right), \; k_7 \geq c_4$$

in (3–20), (3–30), (3–49), and (3–51)) are sufficient to achieve stability for the largest uncertainties on the system parameters, they represent conservative gains required by the controllers in (3–7) and (3–13). Therefore, the gain conditions provide guidelines for the initial gain selection and the gains can be subsequently adjusted to achieve desirable performance. Although the listed gains were adjusted using an empirical-based method, the gains could have been adjusted using more methodical approaches. For example, the nonlinear system in [123] was linearized at several operating points and a linear controller was designed for each point, and the gains were chosen by interpolating, or scheduling the linear controllers. In [124], a neural network is used to tune the gains of a PID controller. In [125] a genetic algorithm was used to fine tune the gains after initial guess were made by the controller designer. The authors in [126] provide an extensive discussion on the use of extremum seeking for tuning the gains of a PID controller. Additionally, in [127], the tuning of a PID controller for robot manipulators is discussed.For Controller A, the controller gains in (3–2), (3–7), and (3–13) were selected as $k_1 \in [5, \; 9]$, $k_2 \in [0.08, \; 0.10]$, $k_3 \in [0.02, \; 0.05]$, $k_4 \in [0.02, \; 0.05]$, $k_5 = 0.01$, $k_6 \in [15, \; 60]$, $k_7 \in [0.75, \; 4.0]$, $\alpha = 6$; for Controller B, the controller gains were selected as $k_1 = 0.75$, $k_2 = 0.1$, $k_3 = 0.05$, $k_4 = 0.05$, $k_5 = 1.5$, $k_6 = 0.85$, $k_7 = 0.35$, $\alpha = 6$; and for Controller C, the controller gains were selected as $k_1 = 15$, $k_2 = 1.5$, $k_3 = 7.5$, $k_4 \in [35, \; 50]$, $k_5 = 6$, $k_6 \in [30, \; 35]$, $\alpha \in [1, \; 6]$ across all trials.

3.3.3 Results from Able-Bodied Population

To validate the proposed controller, experiments were conducting using Controllers A, B, and C on able-bodied participants. The able-bodied population's cadence and

power results are displayed in Table 3-2; each controller was implemented on each participant for a single trial.

The developed controller (i.e., Controller A) demonstrated average cadence and power tracking errors of 0.01±1.03 RPM and 0.00±0.94 W, respectively; Controller B demonstrated average cadence and power tracking errors of -0.10±5.35 RPM and -0.01±1.72 W, respectively; and Controller C demonstrated average cadence and power tracking errors of 0.01±0.96 RPM and -0.06±1.70 W, respectively. For Participant C (as a typical result), plots of Controller A's cadence and power performance, and stimulation input are provided in Figures 3-3-3-5; plots of Controller B's cadence and power performance, and stimulation input are provided in Figures 3-6-3-7, respectively; and plots of Controller C's cadence and power performance, and stimulation input are provided in Figures 3-8-3-9, respectively. To compare the current sent to the cycle's motor for each controller, Figure 3-10 displays the motor control input for Controllers A, B, and C. For Participant C, compared to Controller C, Controller A drew 27% more current on average and Controller B drew 58% more current on average.

To determine if the controller significantly affected the results, a Friedman test was conducted on the average cadence error, cadence standard deviations, average power error, and power standard deviations of Controllers A, B, and C. The Friedman test used only the data from the participants who were used for all three controllers. Post-hoc comparisons between the three controllers were developed using Fisher's Least Significant Difference (LSD) method to determine statistical significant differences. The first Friedman test was performed on the average cadence error, $\overline{\tilde{e}_1}$, and determined that the choice of controller significantly affected the error ($P = 0.0062$). From the post-test, it was determined that Controller A was significantly different from Controller B ($P = 0.0026$), as was Controller B from C ($P = 0.0159$). Noting the average cadence errors in Table 3-2, it is then concluded that Controllers A and C are both significantly superior than Controller B, but not from each other. The second Friedman test was conducted on

the cadence standard deviations, $\text{STD}(\dot{e}_1)$, and indicated that the controller significantly affected the result ($P = 0.0094$). The post-test determined that Controllers A and B are significantly different ($P = 0.0039$) and so are Controllers B and C ($P = 0.0209$), with Controllers A and C superior to B. The third Friedman test was run on the average power errors, $\overline{\overline{e}}_3$, and indicated that the choice of controller did not significantly affect the result ($P = 0.1146$). However, the post-test found only Controllers A and C were significantly different ($P = 0.0433$) from each other, with A being superior. The final Friedman test, ran on the power standard deviations, $\text{STD}(\dot{e}_3)$, again determined significant differences among the controllers ($P = 0.0057$). The post-test determined Controllers A and B were significantly different ($P = 0.0015$) and Controllers A and C were significantly different ($P = 0.0433$), with Controller A being superior in both cases. Hence, experimental results from the able-bodied population, indicate that Controllers A and C outperform B in both cadence and power tracking. These results indicate that the motor should control cadence for all time and the muscle should track power in the FES regions. Having the motor control cadence resulted in a reduction in the cadence standard deviation and a more comfortable participant experience due to less oscillatory pedaling performance.

Regardless of the controller, it can be observed in Figures 3-3, 3-6, and 3-8 that the measured cadence and power values fluctuate around the desired values throughout the experiment. The cause of these fluctuations can arise from system disturbances such as chain links, the rider, or inaccurate modeling. Because each controller is designed to account for these disturbances, when the disturbance occurs, the controller is capable of compensating for it and correcting the measured trajectory. The degree of these fluctuations can be quantified using the standard deviation of cadence, displayed in Table 3-2.

Across all trials (i.e., controllers), the participant begins to show signs of fatigue, evidenced by the increasing amount of stimulation required to complete the tracking
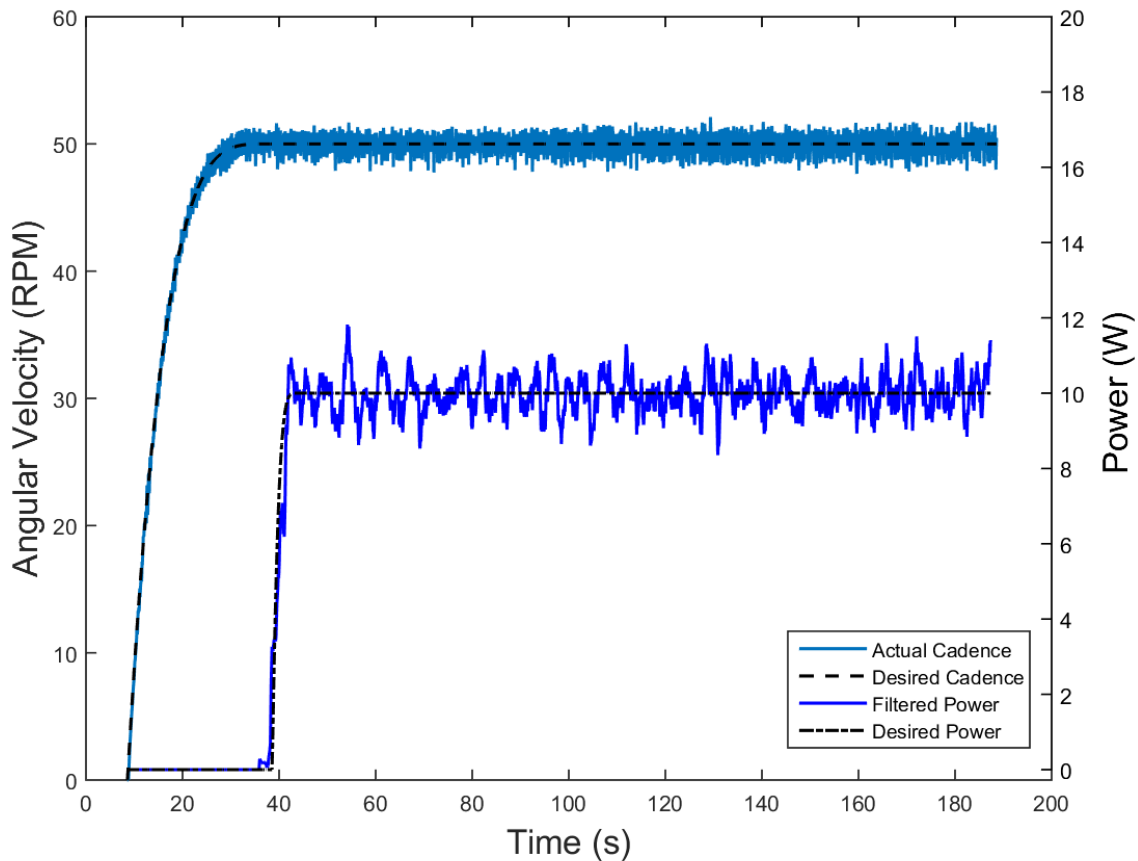
Figure 3-3. Controller A, Participant C: Desired vs. actual cadence and power. The mean cadence is 50.01±0.70 RPM and mean power is 10.00±0.50 W.

objective (e.g., see Figures 3-4, 3-7, and 3-9). Because FES nonselectively recruits muscle fibers, closed-loop control offers one solution to compensate for the effect of fatigue, but the rapid degree to which fatigue occurs remains an outstanding challenge in the use of FES [117]; however strategies such as [128–130] provide inroads to this problem. Furthermore, although the effect of input delay was captured as a system disturbance [114], future works should consider this factor in the control design, as in [131].

3.3.4 Results from Population with Neuromuscular Disorders

Since Controllers A and C had comparable performance on the control population and superior performance over Controller B, only they were implemented on the
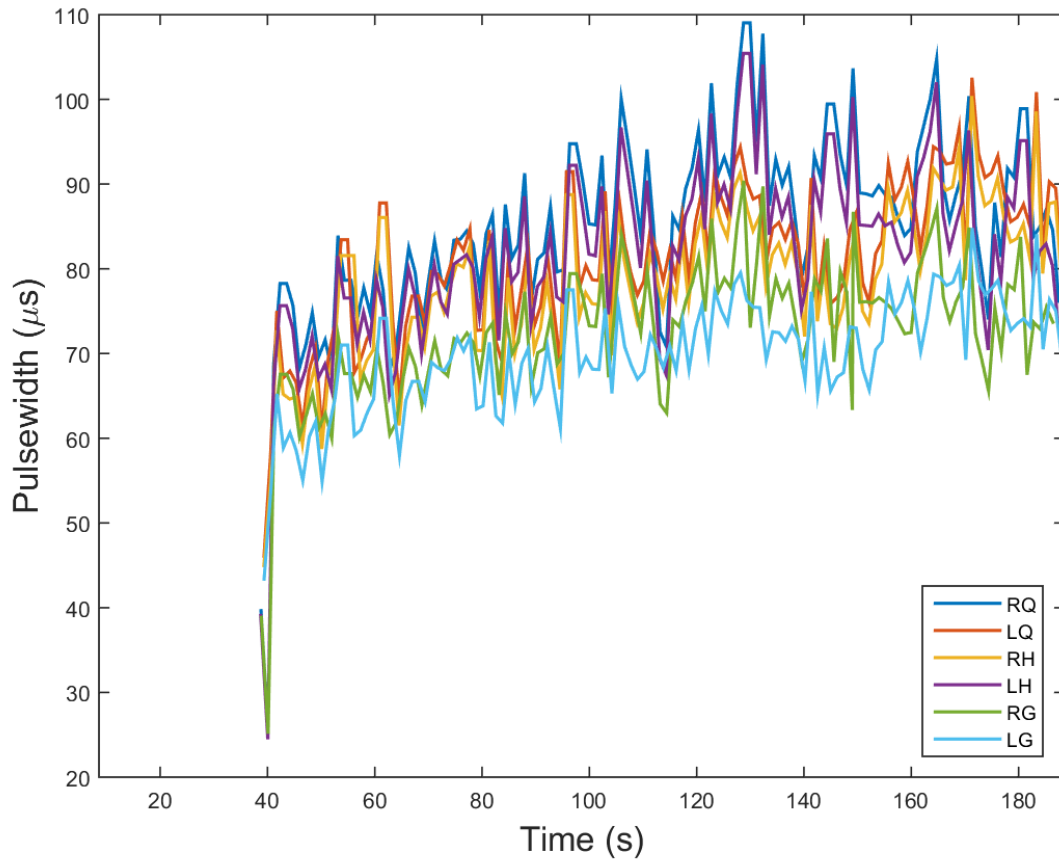
Figure 3-4. Controller A, Participant C: Stimulation input to the participant's six muscle groups. Muscle groups are indicated by RQ, LQ, RH, LH, RG, LG which represent right and left quadriceps, right and left hamstrings, and right and left gluteals, respectively. The stimulation input is displayed as the maximum stimulation for each muscle group in each FES region, at the corresponding time.
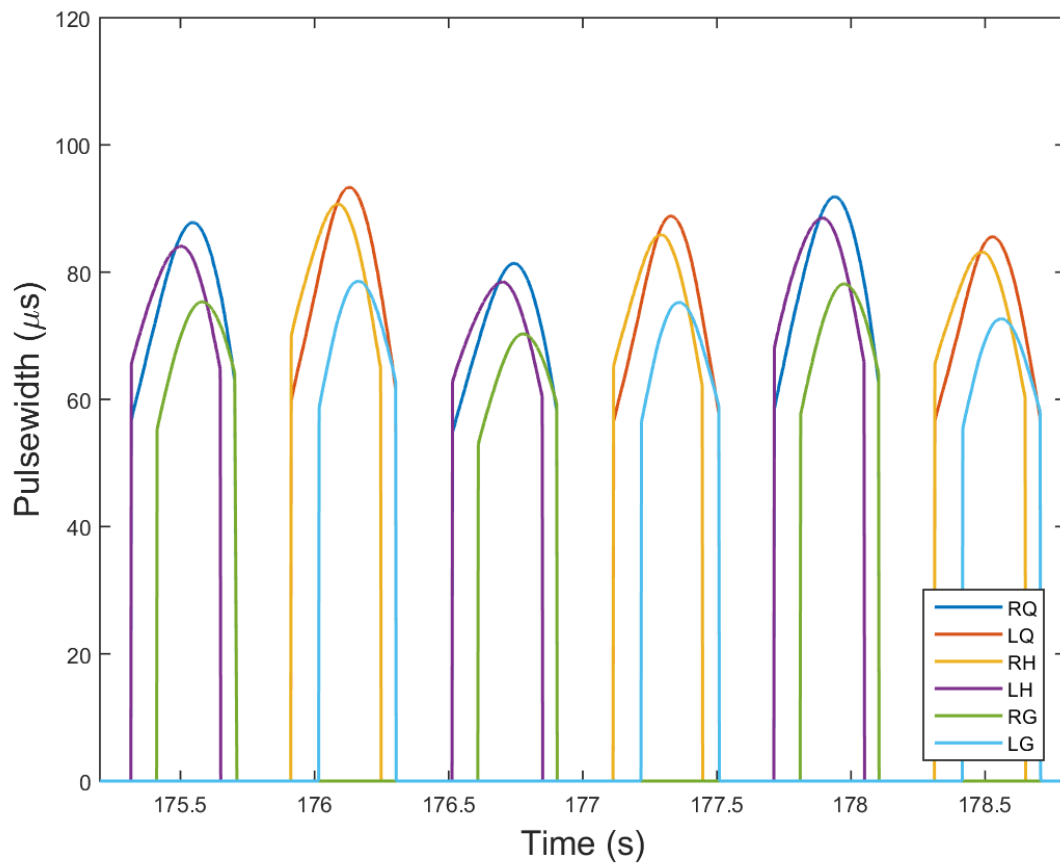
Figure 3-5. Controller A, Participant C: Stimulation input over three revolutions.
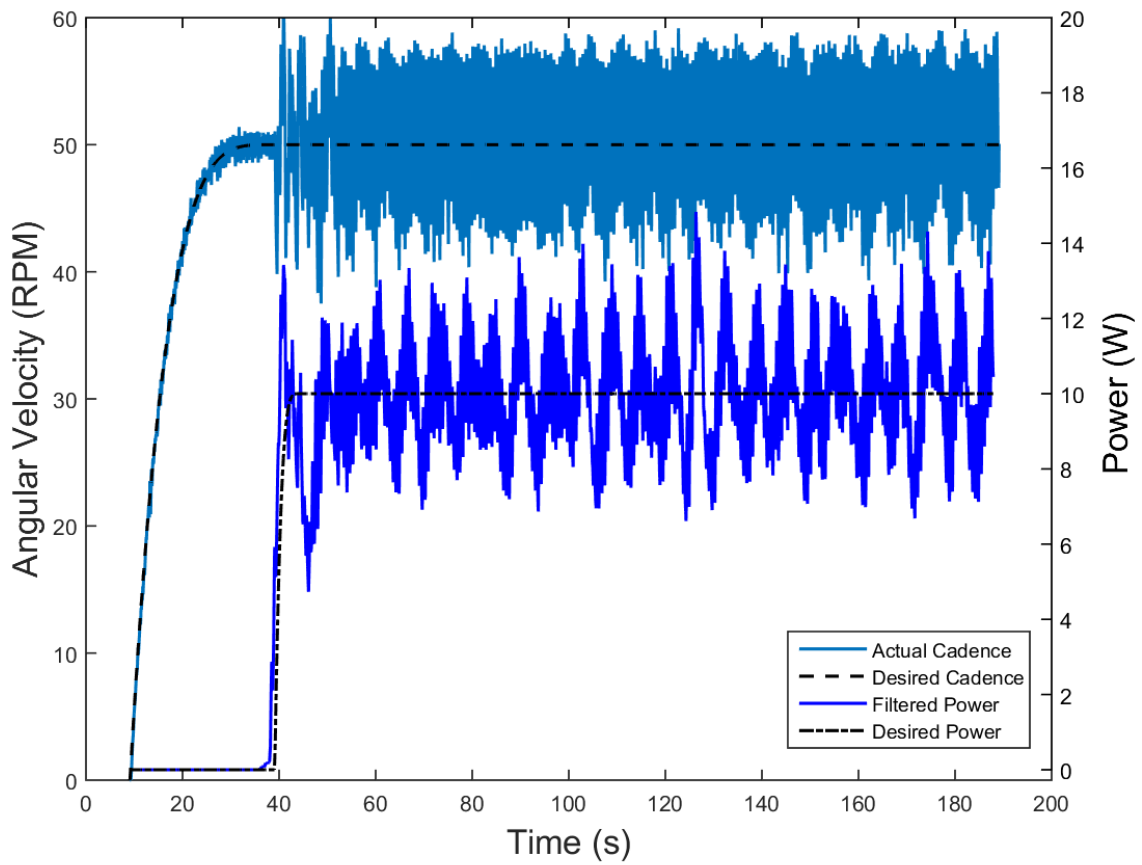
Figure 3-6. Controller B, Participant C: Desired vs. actual cadence and power. The mean cadence is 49.96±4.84 RPM and mean power is 9.98±1.46 W .
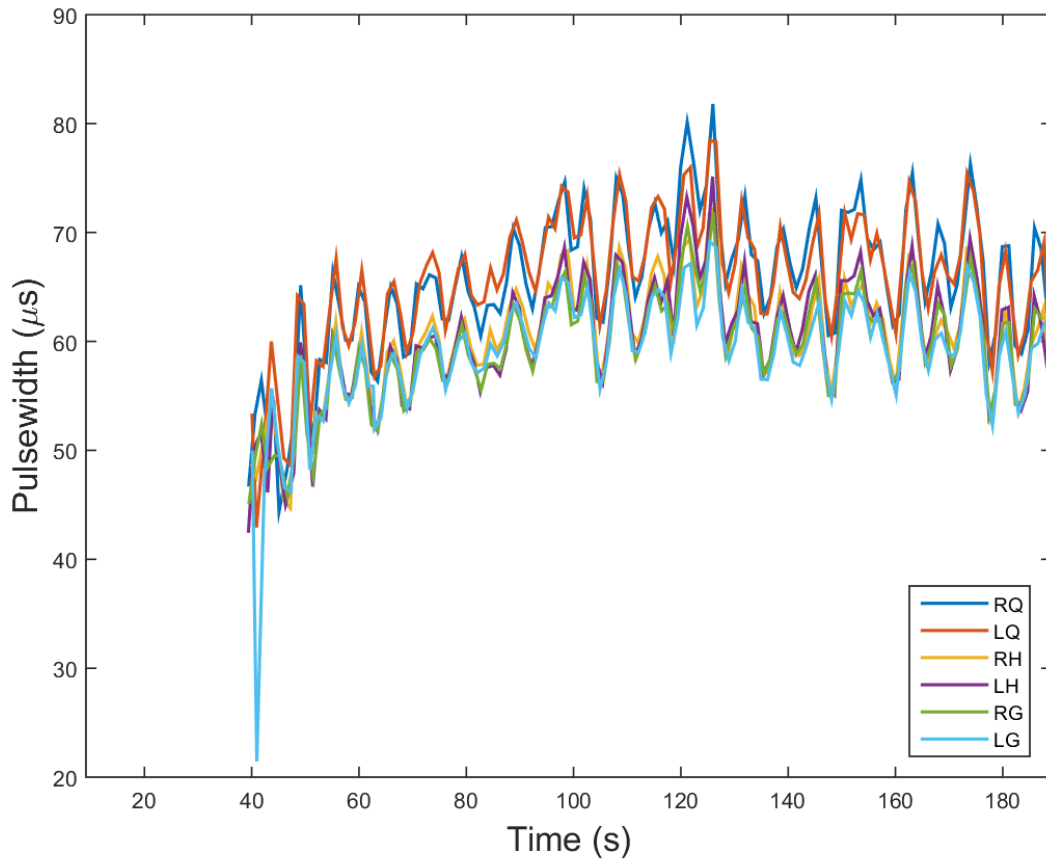
Figure 3-7. Controller B, Participant C: Stimulation input to the participant's six muscle groups.
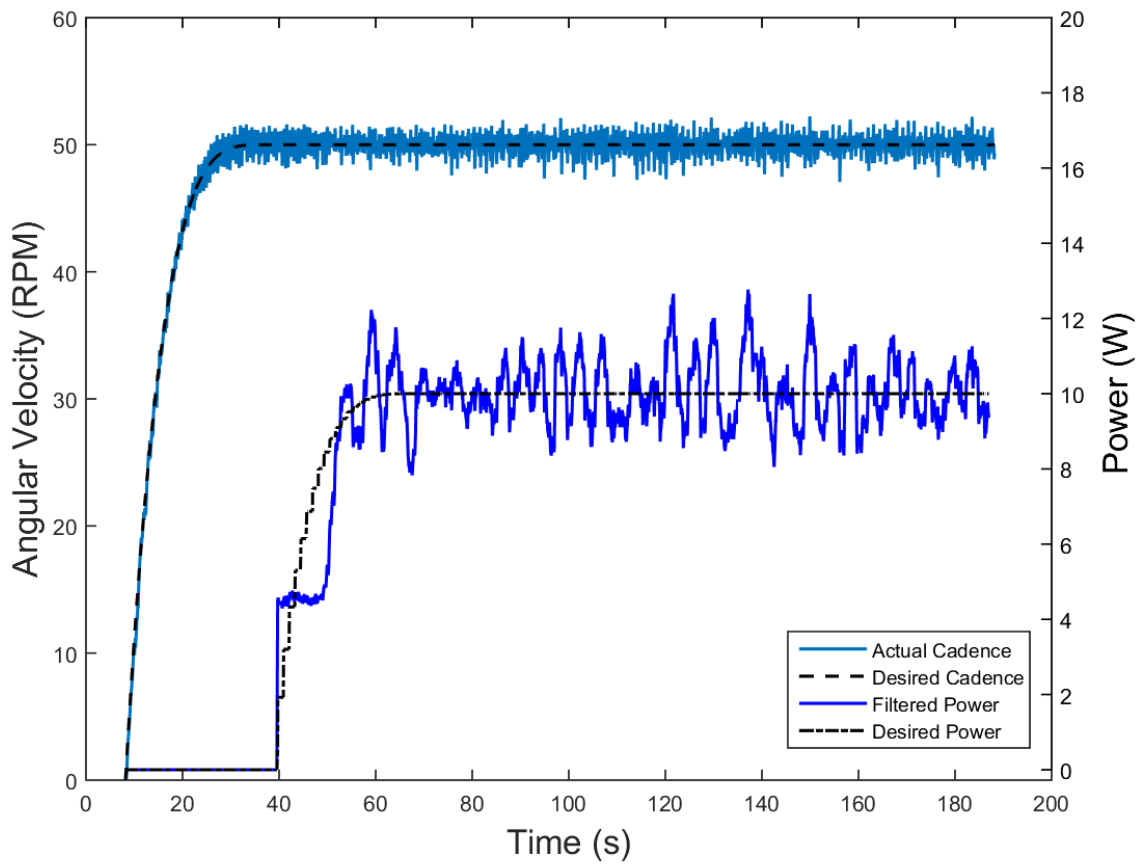
Figure 3-8. Controller C, Participant C: Desired vs. actual cadence and power. The mean cadence is 50.00±0.66 RPM and mean power is 9.70±0.98 W.
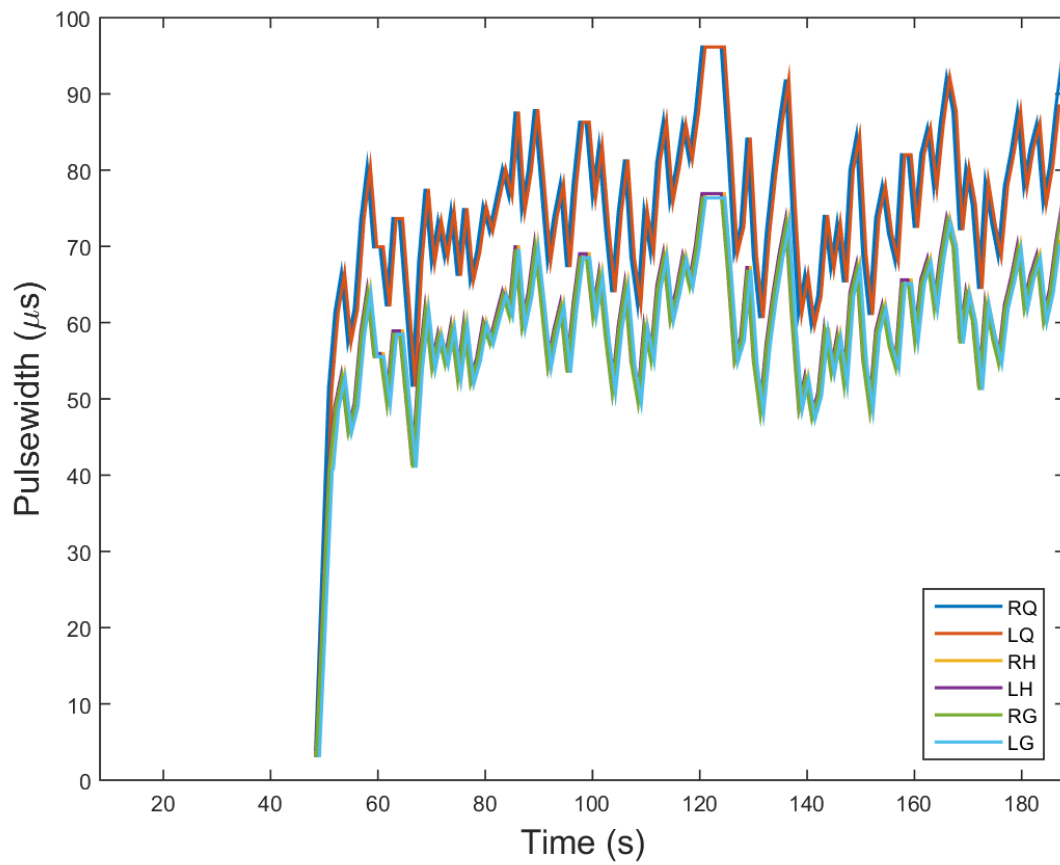
Figure 3-9. Controller C, Participant C: Stimulation input to the participant's six muscle groups. Stimulation is identical for the right and left leg.
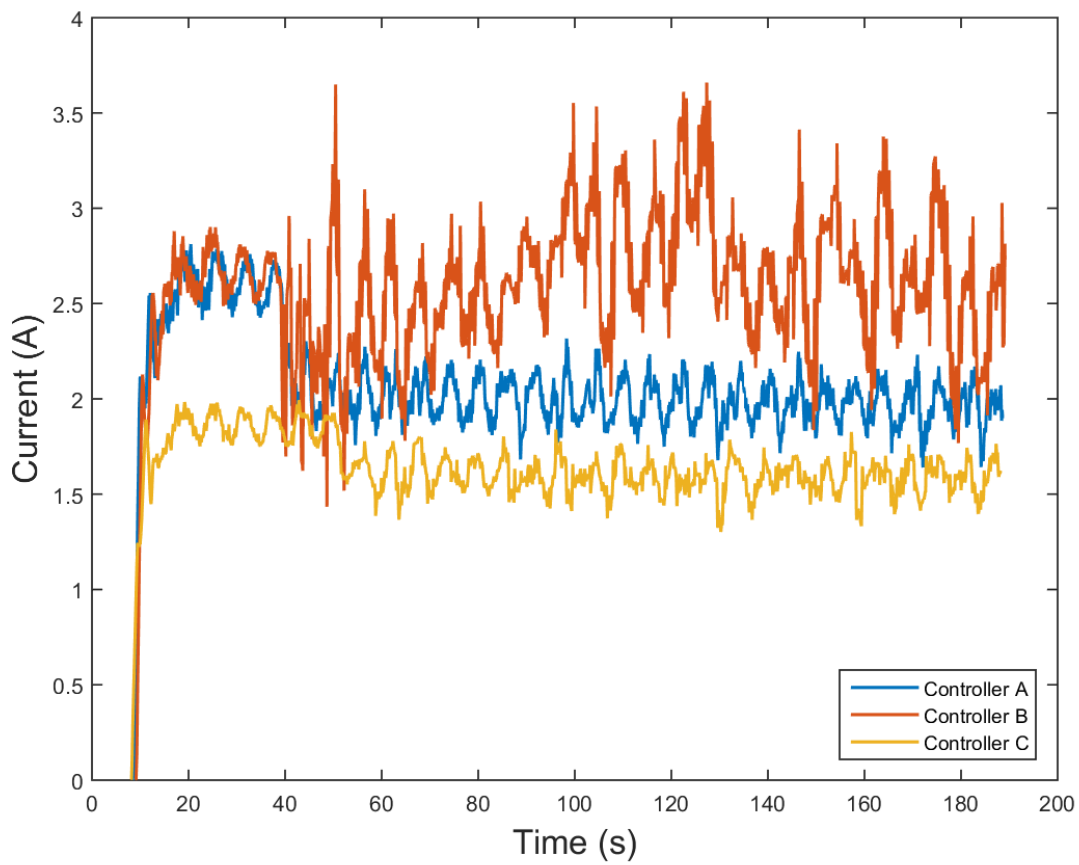
Figure 3-10. Controllers A, B, and C, Participant C: Current input to the cycle's electric motor, filtered with a 1.2 s moving average for visual clarity.

population with neurological impairments to draw further conclusions. The population with neurological impairments is labeled numerically. These participants possess neurological conditions such as hemorrhagic and ischemic stroke, spinal cord injury (SCI), spina bifida, and traumatic brain injury (TBI). They also had varying degrees of exposure to FES; those who had prior experience were typically quicker to acclimate to the stimulation and had higher stimulation thresholds. To evaluate a participant's level of activity (i.e., how often they regularly perform exercise) and capabilities, they were asked to self-report if they regularly participate in physical or occupational therapy (PT/OT) and if they used any physical aid in ambulation. The participants' self-reported demographics are provided in Table 3-3. Of the six participants, three suffered a stroke, all of which had hypersensitivity to electrical stimulation due to hemiparesis, resulting in lower stimulation thresholds. Stroke participants also had asymmetric motor impairments which, to varying degrees, affected limb coordination. Participant 3 lacks any sensation below the injury location, and was unable to volitionally contribute to the task due to a SCI (AIS A). Controller A was implemented on all six participants and Controller C was implemented on five of the six. Experimental results are displayed in Table 3-4.

Controller A demonstrated average cadence and power tracking errors of 0.02 ± 1.87 RPM and 0.00 ± 2.46 W, respectively, and Controller C demonstrated average cadence and power tracking errors of 0.01 ± 1.82 RPM and -0.54 ± 3.96 W, respectively. To highlight the efficacy of the designed controllers, Participant 3's results are displayed in Figures 3-11-3-15. Participant 3's results are depicted because he is paraplegic and unable to volitionally contribute to the forward motion of the crank; hence, any torque produced by the leg muscles is only caused by the controllers. Using Controller A, plots of his cadence and power performance and stimulation input are provided in Figures 3-11-3-13. Using Controller C, plots of his cadence and power performance and stimulation input are provided in Figures 3-14 and 3-15, respectively. To compare the current
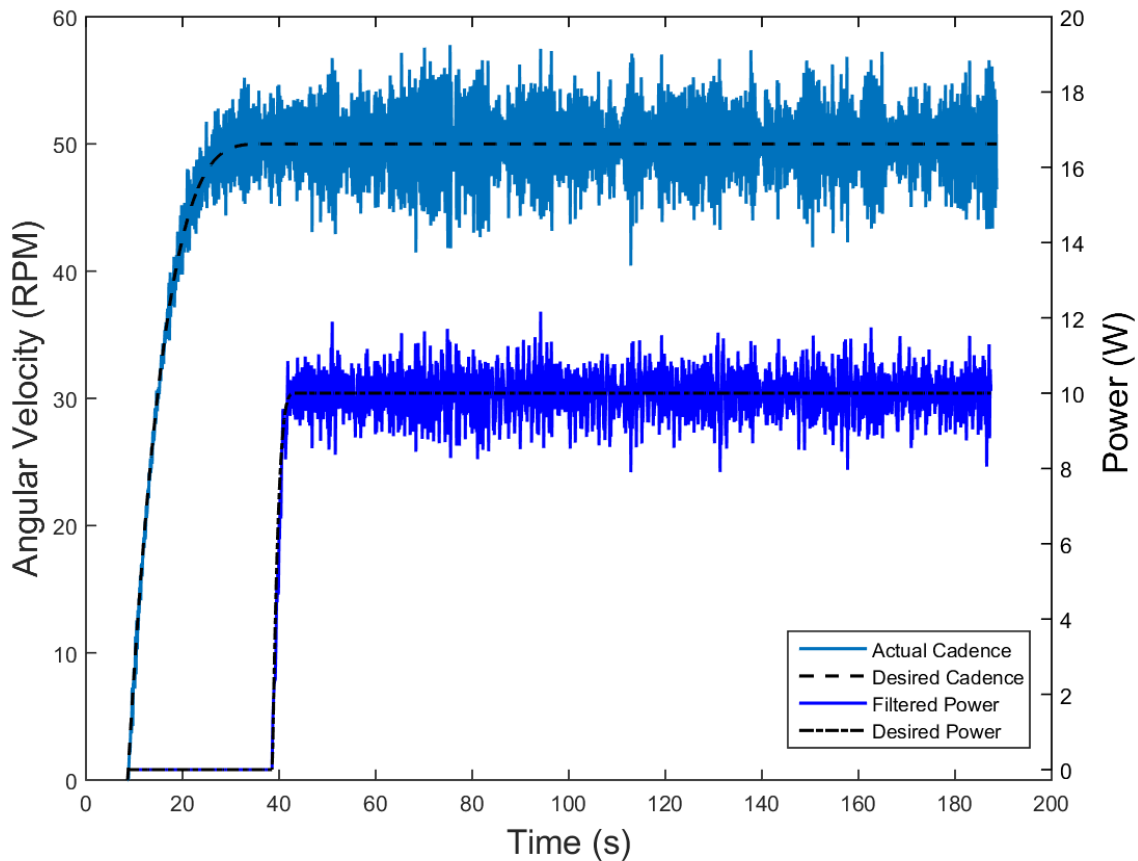
Figure 3-11. Controller A, Participant 3: Desired vs. actual cadence and power. The mean cadence is 50.02±2.35 RPM and mean power is 9.98±0.52 W.

sent to the cycle's motor for each controller, Figure 3-16 displays the motor control input for Controllers A and C. For Participant 3, Controller A drew an average of 33% more current than Controller C.

While the cadence error and standard deviation are comparable for the two controllers, the average power error and standard deviation are smaller for Controller A than Controller C, though not statistically significant, i.e., $\alpha = 0.05$ (using the available paired data sets, i.e., Participants 1-5). It should be noted, however, because Controller C tracks power discretely, it potentially masks asymmetries in the rider. That is, because it updates the error and control input only once per cycle, Controller C delivers identical stimulation to both the right and left leg. Controller A uses a running integral to track

66
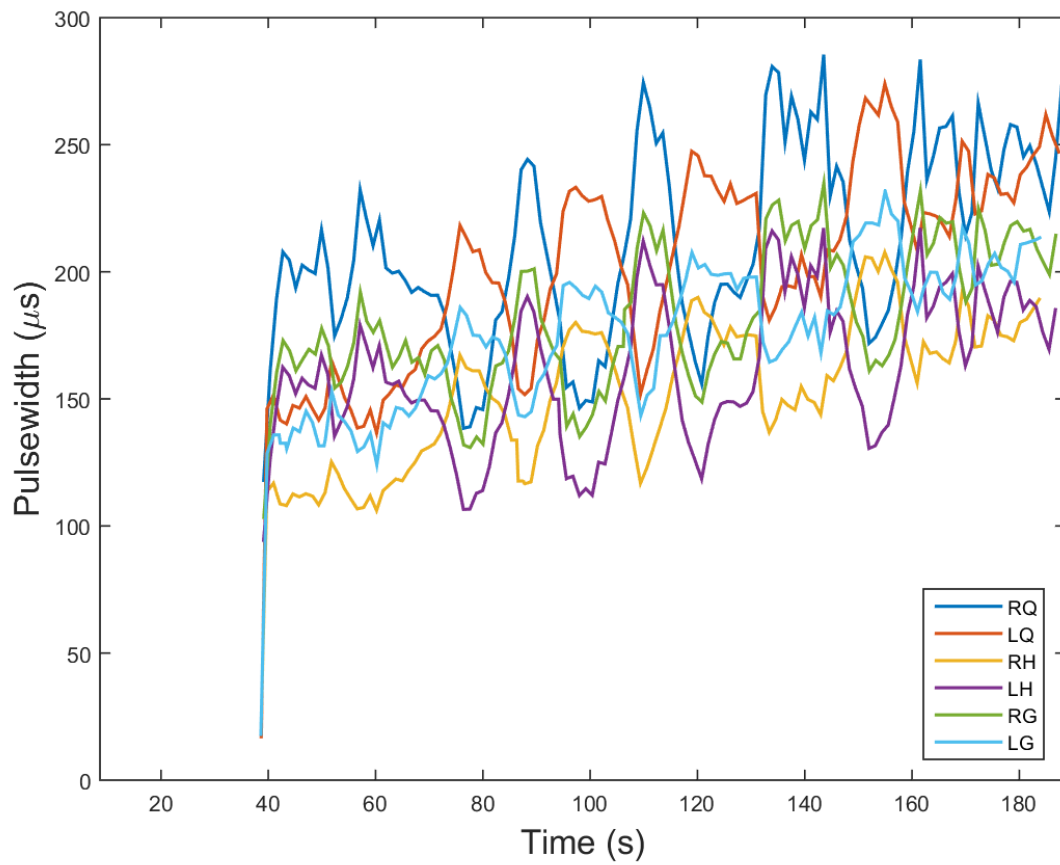
Figure 3-12. Controller A, Participant 3: Stimulation input to the participant's six muscle groups.
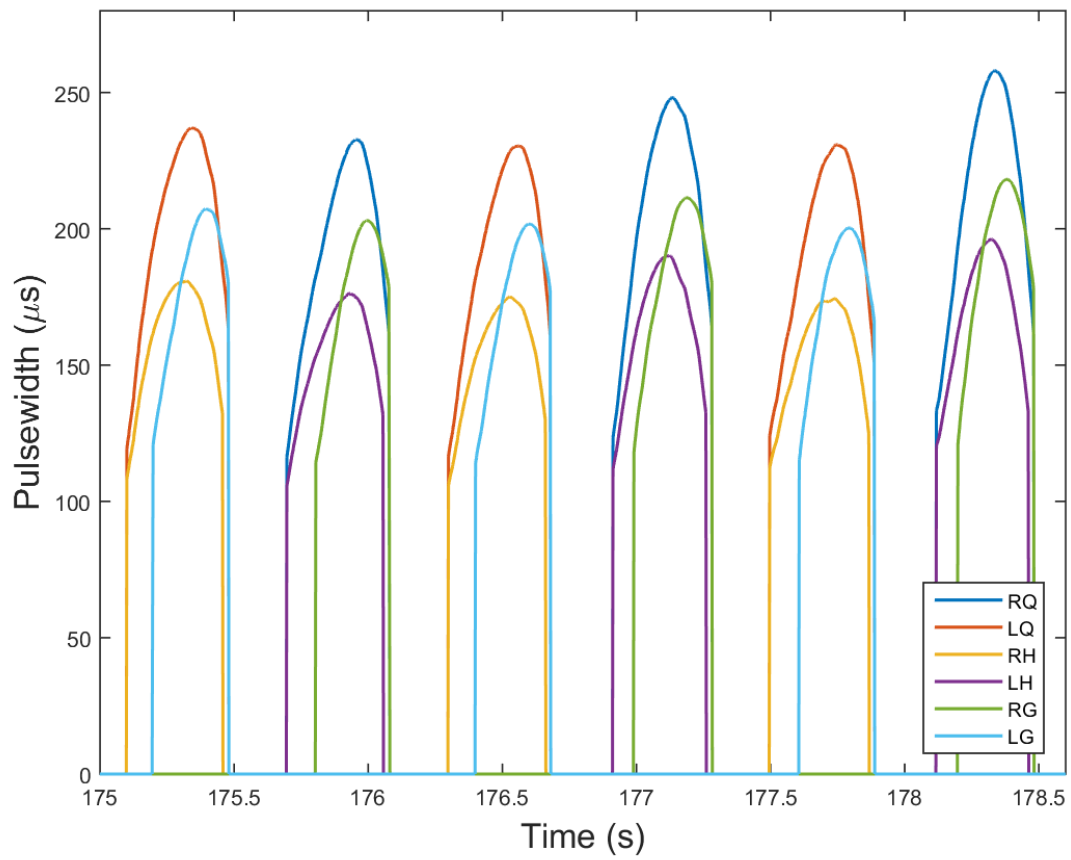
Figure 3-13. Controller A, Participant 3: Stimulation input over three revolutions.
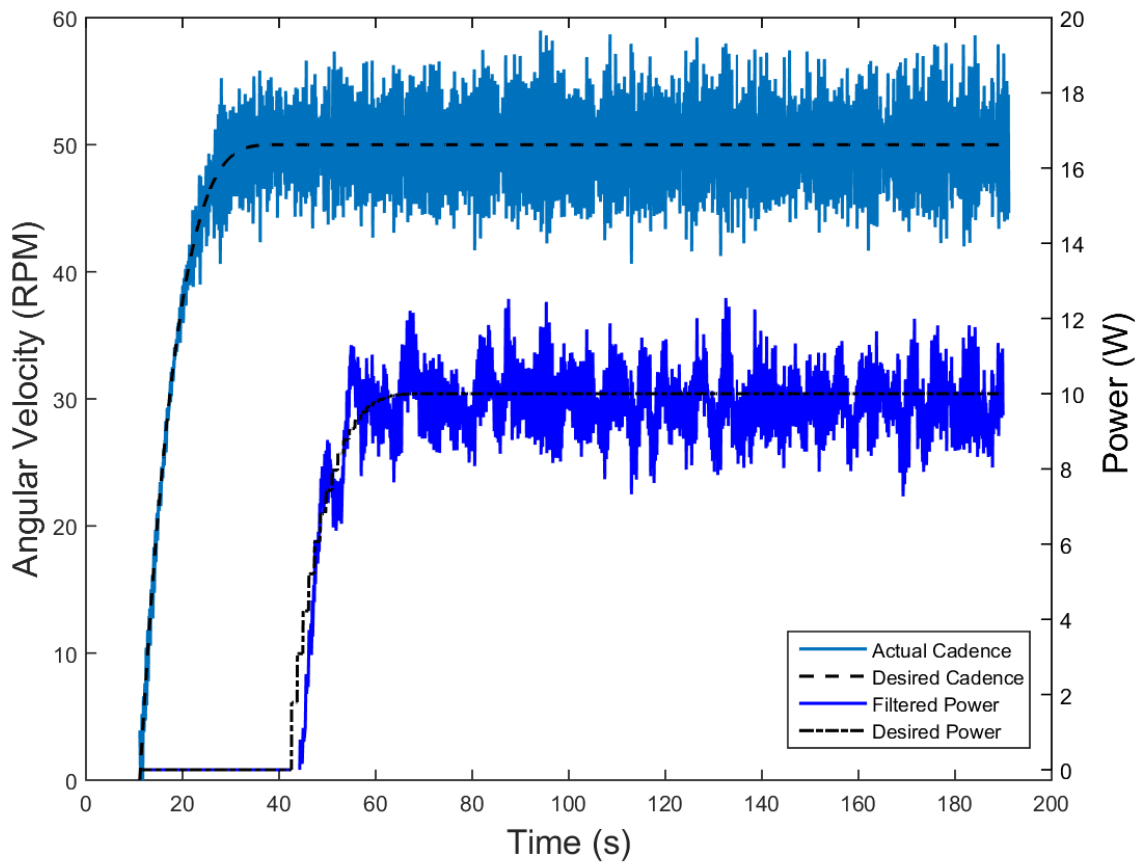
Figure 3-14. Controller C, Participant 3: Desired vs. actual cadence and power. The mean cadence is 50.02±2.79 RPM and mean power is 9.80±0.74 W.
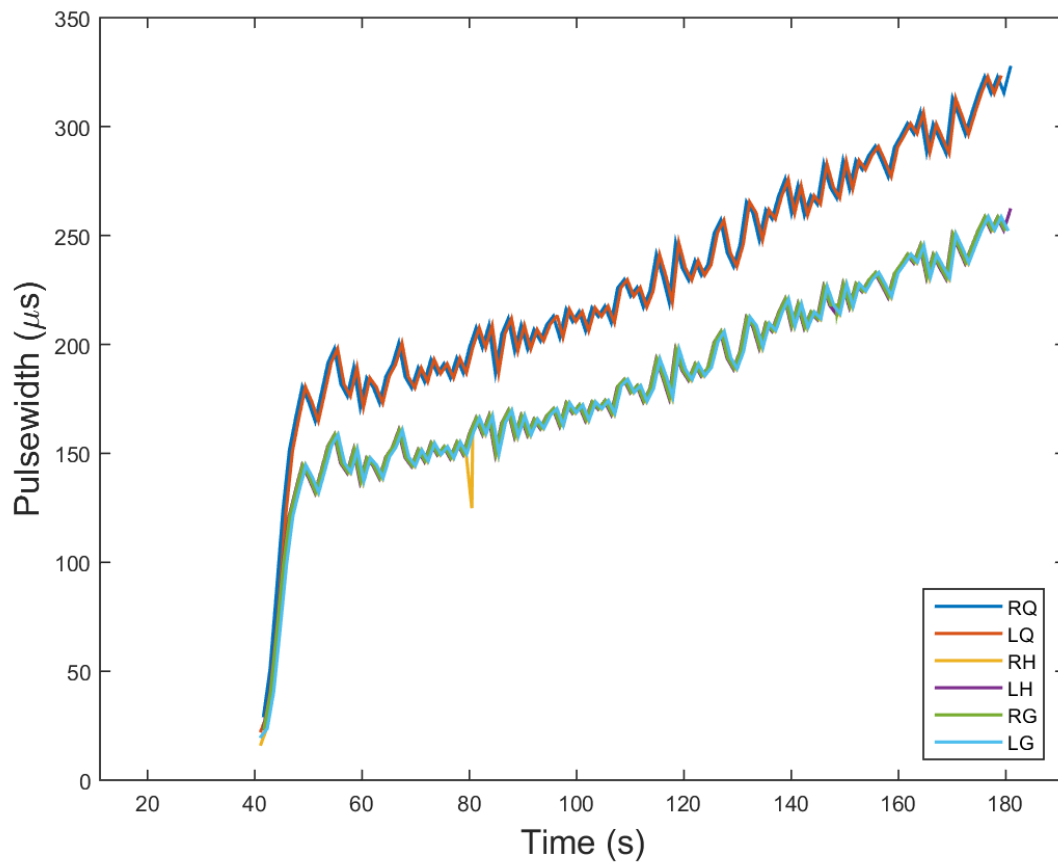
Figure 3-15. Controller C, Participant 3: Stimulation input to the participant's six muscle groups.
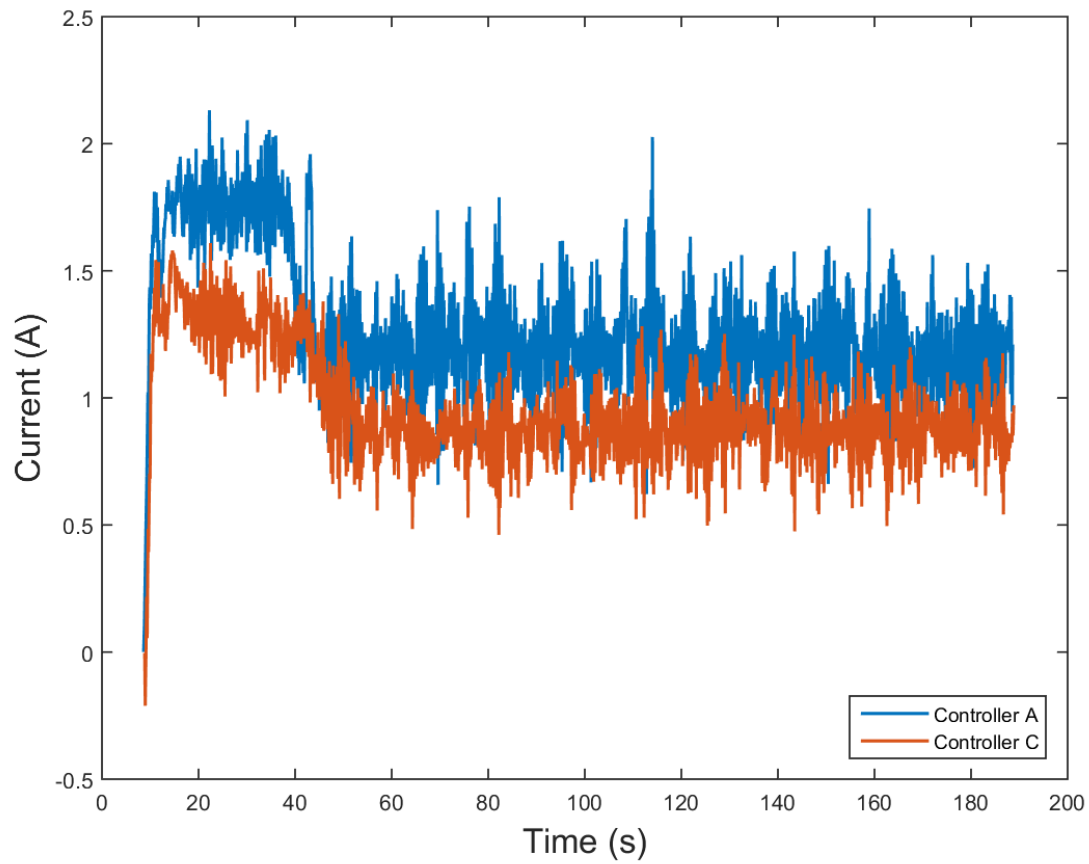
Figure 3-16. Controllers A and C, Participant C: Current input to the cycle's electric motor for Controllers A, and C. Filtered with a 1.2 s moving average for visual clarity.

power, updates continuously, and can potentially better accommodate asymmetries. As in the able-bodied population, the measured cadence and power values fluctuated around the desired values due to unmodeled disturbances, shown in Figures 3-11 and 3-14. Future tests on a split-crank cycle could further explore differences for such asymmetries. Controller A outperformed C in terms of power tracking and power standard deviation, but had a larger cadence standard deviation. Accounting for the errors, standard deviations, and potential masking of asymmetric characteristics, it is determined that Controller A should be used for the population with neurological impairments, and power should be tracked instantaneously, not discretely. Controllers A and C were able to achieve power results comparable to those reported in other experiments involving people with SCIs (e.g., an average PO of 8.0 ± 2.1 W with one leg at 25 RPM [75], an average steady state PO of 16.0 ± 3.6 W ranged 8.5-29.5 W in five participants after one year of training [78], and an improvement from 8.4 ± 1.0 W to 18.4 ± 2.6 W in 11 participants after one year of training [79]).

3.4   Concluding Remarks

In this chapter, an FES cycling controller is developed to track both cadence and instantaneous torque. The torque error system uses a running integral to update the torque error in real-time, compared to once per cycle in discretized tracking prevalent in other cycling methods. Using the proposed controller, a Lyapunov-like switched system stability analysis is conducted which guarantees global exponential cadence tracking and uniform ultimate boundedness of the power objective. Experiments were conducted on seven able-bodied participants and six participants with neurological impairments to evaluate the performance of the proposed controller. A comparison is then made to two previously developed FES-cycling controllers using experimental results. While the controllers varied in their control authority and their method of tracking torque, all controllers demonstrated the ability to accomplish the dual-objective of cadence and power tracking; however, the developed controller exhibited favorable performance and

characteristics. These results indicate that cadence should be controlled by the electric motor for all time (i.e., within the FES and KDZ regions) and power should be tracked instantaneously using the large muscle groups of the legs in the FES regions.

A difficulty observed throughout experiments was selecting the desired torque trajectory for each rider. If the torque trajectory was too difficult, the rider's muscles soon saturated and experienced undue fatigue. Consequently, the experiment needed to be restarted and/or gain tuning performed. Chapter 4 seeks to improve upon this result by transitioning from direct torque tracking to indirect tracking while adding a degree of compliance to the system.

Table 3-2. Comparative results for able-bodied population: mean error of tracking objectives given as $\bar{e} \pm \mathrm{STD}(\dot{e})$, and percent error of $\bar{e}$ during steady state operation for cadence and power[*]

Controller	Participant	$\bar{\dot{e}_1}$ (RPM)	$\bar{\dot{e}_1}$ (% Error)	$\bar{\dot{e}_3}/\overline{e_\tau}$ (W)[†,‡]	$\bar{\dot{e}_3}/\overline{e_\tau}$ (% Error)[†]
A	A	0.01±0.88	0.02	-0.08±0.33	0.76
	B	0.03±0.72	0.05	-0.04±0.38	0.38
	C	0.01±0.70	0.03	-0.00±0.50	0.02
	D	0.02±0.93	0.03	-0.05±0.69	0.48
	E	0.01±1.03	0.03	0.01±0.70	0.06
	F (6W)[∥]	0.02±0.99	0.04	0.16±0.69	2.60
	G (15W)[#]	0.00±1.65	0.00	0.02±2.05	0.11
	Mean	0.01±1.03	0.03	0.00±0.94	0.63
B	A	-0.19±5.38	0.39	-0.03±1.48	0.28
	B	-0.15±5.46	0.30	-0.05±1.43	0.51
	C	-0.04±4.84	0.07	-0.02±1.46	0.18
	D	-0.03±5.24	0.05	0.07±1.47	0.68
	E	-0.10±6.16	0.19	-0.03±2.76	0.30
	F (6W)	-0.11±4.90	0.21	-0.02±1.26	0.32
	G (15W)[△]	-	-	-	-
	Mean	-0.10±5.35	0.21	-0.01±1.72	0.38
C	A	0.01±1.10	0.01	-0.10±0.69	1.00
	B	0.02±0.90	0.04	-0.10±0.76	0.99
	C	0.00±0.66	0.00	-0.30±0.98	0.27
	D	0.03±0.96	0.06	0.02±1.70	0.24
	E	0.00±1.21	0.00	-0.21±1.50	2.13
	F (6W)	0.02±0.89	0.04	-0.00±0.74	0.01
	G (15W)[#]	0.02±0.90	0.04	0.24±3.54	1.61
	Mean	0.01±0.96	0.03	-0.06±1.70	0.89

[*]Unless otherwise noted, all participants provided no volitional contribution; the desired cadence and power are 50 RPM and 10 W, respectively.

[†]The notation $\dot{e}_3$ is valid for the error systems of Controllers A and B. For Controller C in [87], it is analogous to $e_\tau(k)$, which represents the average torque error $e_\tau : \mathbb{N} \to \mathbb{R}$ per crank cycle, k.

[‡]For post-processing, a two crank cycle (a moving window of approximately 2.4 seconds) averaging filter was applied on $\dot{e}_3/e_\tau$.

[∥]Due to participant comfort, this trial ended at two minutes.

[#]The participant provided volitional contribution.

[△]Due to time constraints by the participant, this experiment was not performed, and therefore, this participant was excluded from the statistical analysis.

Table 3-3. Demographics of population with neuromuscular disorders

Participant	Age	Sex	Injury*	Physical Aid[‡]	TSI[†]
1	45	M	Ischemic Stroke (L)	AFO	3yr 9mo
2	48	F	Hemorrhagic Stroke (L)	AFO, Cane	9mo
3	20	M	SCI T8-9 Complete, T9-10 Fusion	Wheelchair	8mo
4	25	M	Spina Bifida (L5-S1), Arnold Chiari Malformation	AFO, Wheelchair	25yr
5	37	M	Traumatic Brain Injury	AFO, Wheelchair	9yr 11mo
6	29	F	Ischemic Stroke (R)	Wheelchair	1mo

*L = Left Hemiparesis, R = Right Hemiparesis
[†]Time since injury (TSI)
[‡]AFO = Ankle Foot Orthosis

Table 3-4. Comparative tracking results for population with neuromuscular disorders: average error of tracking objectives given as $\bar{e} \pm \text{STD}(\dot{e})$, and percent error of $\bar{e}$ during steady state operation for cadence and power*

Controller	Participant	$\bar{\dot{e}_1}$ (RPM)	$\bar{\dot{e}_1}$ (% Error)	$\bar{\dot{e}_3}/\bar{e_\tau}$ (W)[†,‡]	$\bar{\dot{e}_3}/\bar{e_\tau}$ (% Error)[†]
A	1 (8W)	0.01±1.69	0.03	0.09±3.08	1.11
	2 (10W)	0.02±1.85	0.05	-0.18±2.80	1.78
	3 (10W)[‖]	0.02±2.35	0.04	-0.02±0.52	0.16
	4 (5W)[#]	0.03±0.66	0.05	-0.24±0.50	4.76
	4 (5W)[‖]	0.01±0.56	0.02	0.01±0.41	0.21
	5 (10W)	0.02±1.50	0.05	0.29±4.12	2.90
	6 (5W)[#]	0.02±1.54	0.03	0.02±2.72	0.40
	Mean	0.02±1.87	0.04	0.00±2.46	1.47
C	1 (8W)	0.02±1.69	0.04	-2.31±3.61	-28.91
	2 (10W)	0.01±1.68	0.02	-0.81±3.10	-8.05
	3 (10W)[‖]	0.02±2.79	0.05	-0.20±0.74	-2.01
	4 (5W)[‖]	0.00±0.73	0.00	0.02±0.19	0.36
	5 (10W)	0.01±1.59	0.02	0.58±7.44	5.81
	Mean	0.01±1.82	0.03	-0.54±3.96	9.03

*Unless otherwise noted, all participants provided volitional contribution; the desired cadence and power are 50 RPM and 10 W, respectively.
[†]The notation $\dot{e}_3$ is valid for the error systems of Controllers A and B. For Controller C in [87], it is analogous to e_τ.
[‡]A two crank cycle filter was applied on $\dot{e}_3/e_\tau$.
[‖]Participant did not provide any volitional contribution.
[#]Due to time constraints by the participant, the Controller C counterpart was not run, therefore this result was excluded from the signed-rank test.

CHAPTER 4
CONTROLLING THE CADENCE AND ADMITTANCE OF A FUNCTIONAL ELECTRICAL STIMULATION CYCLE

The motorized FES cycle in this chapter utilizes a combined admittance/cadence controller to simultaneously pedal the FES cycle and stimulate the rider's muscles while preserving rider comfort and safety. The admittance controller is implemented on the cycle's motor and a robust sliding-mode cadence controller is applied to the rider's muscle groups. The FES delivered to the rider's muscle groups is saturated for comfort, and due to the admittance controller, the cycle responds appropriately by assisting the rider if the delivered stimulation is insufficient to produce the desired torque at the desired cadence. Heuristically, the cycle strikes a balance between rider safety (which addresses muscle/joint spasticity by allowing the rider to deviate from the desired cadence) and capability. Using a Lyapunov-like switched systems stability analysis, the cadence controller is proven to be globally exponentially stable and the admittance controller is proven to be passive with respect to the rider. By selectively modifying the admittance parameters (i.e., the injected inertia and damping), the admittance controller is capable of emulating a cadence controller (by increasing the inertia and damping) or admitting to the rider significantly (by decreasing the inertia and damping). Hence, by appropriately selecting the admittance parameters, the cycle can be made increasingly stiff or compliant by activating the cycle's motor accordingly. By merging an admittance controller with a cadence controller, an assist-as-needed control methodology is realized; i.e., if the rider's muscles are unable to meet the desired interaction torque requirement as dictated by admittance filter, the admittance controller assists in keeping the rider held to the desired cadence trajectory through injected artificial dynamics. Conversely, if the rider surpasses the desired interaction torque (as is possible in volitional cycling) the cycle will resist-as-needed and challenge the rider. In other words, admittance control is more concerned about the dynamic behavior of the system instead

of explicit position or torque tracking as in Chapter 3. This chapter demonstrates the first use of admittance control on an FES cycle.

Experiments were conducted on four participants with various NDs (i.e., spina bifida, spinal cord injury, post-stroke hemiparesis, and Parkinson's disease) and three able-bodied participants to demonstrate feasibility and desired performance metrics. Admittance parameters were varied across all protocols and the admittance controller achieved an average admittance cadence error of -0.06±1.47 RPM for able bodied participants and -0.02±0.93 RPM for participants with NDs. The developed controllers hold promise for a new person-specific cycling experience to promote rehabilitation while ensuring safety and comfort.

4.1   Control Development

The following section includes the development of an admittance controller for the cycle's motor and cadence controller for the rider's muscles. The admittance controller is designed to be passive with respect to the rider to ensure safety and used to indirectly track a desired torque to assist the rider in maintaining cycle cadence. The cadence controller is used to directly regulate cycle cadence in the FES regions by rejecting the torque from the admittance controller.

4.1.1   Robust Admittance Control

While the rider's muscles regulate cadence in the FES regions (i.e., while $q \in \mathcal{Q}_{FES}$), the cycle's controller is designed such that it will resist the rider if the cadence is too high (i.e., $\dot{q} > \dot{q}_d$) or assist the rider if the cadence is too low (i.e., $\dot{q} < \dot{q}_d$) in both the FES and KDZ regions (i.e., $q \in \mathcal{Q}$) , where $\dot{q}_d : \mathbb{R}_{\geq 0} \to \mathbb{R}$ denotes the desired cadence. The assistance modality is vital because the rider's muscles only contribute torque about the crank in the FES regions; therefore when the rider's muscles are inactive in the KDZ regions, the cycle is expected to decelerate. Admittance control is commonly used as a method of indirect torque tracking, and therefore, employs an interaction torque error,

77

quantified by $e_\tau \ : \ \mathbb{R}_{\geq 0} \to \mathbb{R}$, and defined as

$$e_\tau \triangleq \tau_{int} - \tau_d, \tag{4–1}$$

where the desired interaction torque is denoted by $\tau_d \ : \ \mathbb{R}_{\geq 0} \to \mathbb{R}$, and $\tau_{int} \ : \ \mathbb{R}_{\geq 0} \to \mathbb{R}$ denotes the measurable bounded interaction torque between the cycle and rider (i.e., $\tau_{int} \in \mathcal{L}_\infty$) [56, 132]. By subsequently implementing an admittance filter, the interaction torque error can be transformed into an admitted trajectory, which can be tracked using an inner-loop position controller. The admittance filter is designed as

$$e_\tau \ \triangleq \ M_d \ddot{q}_a + B_d \dot{q}_a, \tag{4–2}$$

where $q_a, \ \dot{q}_a, \ \ddot{q}_a \ : \ \mathbb{R}_{\geq 0} \to \mathbb{R}$ denote the admitted position, velocity, and acceleration, respectively; and $M_d, \$ and $B_d \in \mathbb{R}_{>0}$ denote the desired inertia and damping. To ensure boundedness of the admitted trajectory, the parameters in (4–2) are selected such that the transfer function of (4–2) is passive [63, Lemma 6.4]. After the admitted trajectory is generated by (4–2), an inner-loop position controller is designed to track the admittance error system, quantified by $\xi \ : \ \mathbb{R}_{\geq 0} \to \mathbb{R}$ and $\psi \ : \ \mathbb{R}_{\geq 0} \to \mathbb{R}$, defined as

$$\xi \ \triangleq \ q_a + q_d - q, \tag{4–3}$$

$$\psi \ \triangleq \ \dot{\xi} + \beta \xi, \tag{4–4}$$

where $q_d \ : \ \mathbb{R}_{\geq 0} \to \mathbb{R}$ denotes the desired position, designed to be sufficiently smooth (i.e., $q_d, \ \dot{q}_d, \ \ddot{q}_d \in \mathcal{L}_\infty$). Hence, if the position controller can regulate the errors in (4–3) and (4–4), the controller will preserve the admitted dynamics of the filter in (4–2) and accomplish its indirect torque tracking objective. The open-loop admittance error system is generated by taking the time derivative of (4–4), multiplying by M, adding and subtracting ξ, and substituting (2–8), (4–3), and (4–4) to yield

$$M \dot{\psi} = \chi_1 - B_e u_e - \tau_m - V \psi - \xi, \tag{4–5}$$

78

where the lumped auxiliary signal χ_1 : $\mathcal{Q} \times \mathbb{R} \times \mathbb{R}_{\geq 0} \rightarrow \mathbb{R}$ is defined as $\chi_1 \triangleq$ $M(\ddot{q}_a + \ddot{q}_d + \beta\psi - \beta^2\xi) + V(\dot{q}_d + \beta\xi + \dot{q}_a) + G + P + b_c(\dot{q}_a + \dot{q}_d - \psi + \beta\xi) + d + \xi$ and is bounded by Properties 2.1-2.6 as $|\chi_1| \leq c_1 + c_2||\phi|| + c_3||\phi||^2$, where c_1, c_2, $c_3 \in \mathbb{R}_{>0}$ are known constants, and the error vectors $\phi \in \mathbb{R}^4$ and $\zeta \in \mathbb{R}^2$ are defined as $\phi \triangleq$ $\left[\zeta^T, \dot{q}_a, \ddot{q}_a\right]^T$ and $\zeta \triangleq [\xi, \psi]^T$, respectively. Based on (4–5) and the subsequent stability analysis, the admittance controller is designed as

$$u_e \triangleq \frac{1}{B_e}\left[k_1\psi + \left(k_2 + k_3\|\phi\| + k_4\|\phi\|^2\right)\text{sgn}(\psi)\right], \qquad (4\text{–}6)$$

where sgn($\cdot$) is included to provide robustness to the uncertainty in χ_1, and $k_i \in$ $\mathbb{R}_{>0} \ \forall i = 1, 2, 3, 4$ denote constant control gains. Substituting (4–6) into (4–5) yields the closed-loop admittance error system

$$M\dot{\psi} = \chi_1 - \tau_m - V\psi - \xi - \left[k_1\psi + \left(k_2 + k_3\|\phi\| + k_4\|\phi\|^2\right)\text{sgn}(\psi)\right]. \qquad (4\text{–}7)$$

4.1.2 Robust Cadence Control

While the cycle is assigned to regulate the admitted error system throughout the entire crank cycle (i.e., $q \in \mathcal{Q}$), the cycle's cadence is regulated using the rider's muscles in the FES regions (i.e., $q \in \mathcal{Q}_{FES}$). The cadence tracking objective is quantified by $e : \mathbb{R}_{\geq 0} \rightarrow \mathbb{R}$ and $r : \mathbb{R}_{\geq 0} \rightarrow \mathbb{R}$, each defined as

$$e \triangleq q_d - q, \qquad (4\text{–}8)$$

$$r \triangleq \dot{e} + \alpha e, \qquad (4\text{–}9)$$

where $\alpha \in \mathbb{R}_{>0}$ denotes a constant control gain. The open-loop cadence error system is obtained by taking the derivative of (4–9), multiplying by M, adding and subtracting e, and substituting (2–8), (4–8), and (4–9) to yield

$$M\dot{r} = \chi_2 - B_M u_M - B_e u_e - Vr - e, \qquad (4\text{–}10)$$

where the lumped auxiliary signal χ_2 : $\mathcal{Q} \times \mathbb{R} \times \mathbb{R}_{\geq 0} \to \mathbb{R}$ is defined as $\chi_2 \triangleq$ $M(\ddot{q}_d + \alpha r - \alpha^2 e) + V(\dot{q}_d + \alpha e) + G + P + b_c(\dot{q}_d - r + \alpha e) + d + e$ and bounded by Properties 2.1-2.6 as $|\chi_2| \leq c_4 + c_5 \|z\| + c_6 \|z\|^2$, where $c_4, c_5 \; c_6 \in \mathbb{R}_{>0}$ are known constants, and the error vector $z \in \mathbb{R}^2$ is defined as $z \triangleq [e, \; r]^T$. Based on (4–10) and the subsequent stability analysis, the cadence controller is designed as

$$u_M = \frac{1}{B_{\underline{M}}} \left[k_5 r + \left(k_6 + k_7 \|z\| + k_8 \|z\|^2 + k_9 |u_e| \right) \mathsf{sgn}(r) \right], \qquad (4\text{--}11)$$

where $\mathsf{sgn}(\cdot)$ is included to provide robustness to the uncertainty in χ_2, $k_i \in \mathbb{R}_{>0} \; \forall i = 5, \; 6, \; ..., 9$ denote constant control gains, $B_{\underline{M}}$ is introduced in Property 2.8, and u_e is included to overcome the torque supplied by the motor. Substituting (4–11) into (4–10) yields the closed-loop cadence error system

$$M\dot{r} = \chi_2 - B_e u_e - Vr - e - \frac{B_M}{B_{\underline{M}}} \left[k_5 r + \left(k_6 + k_7 \|z\| + k_8 \|z\|^2 + k_9 |u_e| \right) \mathsf{sgn}(r) \right]. \qquad (4\text{--}12)$$

4.2 Stability Analysis

For the following theorems, let V_1 : $\mathbb{R}^2 \to \mathbb{R}$ denote a continuously differentiable, positive definite storage function defined as

$$V_1 \triangleq \frac{1}{2} M \psi^2 + \frac{1}{2} \xi^2, \qquad (4\text{--}13)$$

which satisfies the following inequalities: $\underline{\gamma} \|\zeta\|^2 \leq V_1 \leq \overline{\gamma} \|\zeta\|^2$, where $\underline{\gamma}, \; \overline{\gamma} \in \mathbb{R}_{>0}$ are known constants defined as $\underline{\gamma} \triangleq \frac{1}{2} \min(c_m, \; 1)$, and $\overline{\gamma} \triangleq \frac{1}{2} \max(c_M, \; 1)$. Let V_2 : $\mathbb{R}^2 \to \mathbb{R}$ denote a continuously differentiable, positive definite Lyapunov function candidate defined as

$$V_2 \triangleq \frac{1}{2} M r^2 + \frac{1}{2} e^2, \qquad (4\text{--}14)$$

which satisfies the following inequalities: $\underline{\gamma} \|z\|^2 \leq V_2 \leq \overline{\gamma} \|z\|^2$.

Theorem 4.1. *Given the closed-loop admittance error system in (4–7) and the admittance relation in (4–2), the admittance controller in (4–6) is passive from input $|\tau_m|$ to output $|\psi|$, provided the constant gain conditions are satisfied: $k_2 \geq c_1$, $k_3 \geq c_2$, $k_4 \geq c_3$. Furthermore, when in isolation (i.e., decoupled from the rider and $\tau_m = 0$) the admittance error system is globally exponentially stable in the sense that*

$$\|\zeta\| \overset{a.e.}{\leq} \sqrt{\frac{\overline{\gamma}}{\underline{\gamma}}} \|\zeta(t_0)\| \exp\left[-\frac{\delta}{2\overline{\gamma}}(t - t_0)\right], \tag{4–15}$$

$\forall t \in [t_0, \infty)$, *where $\delta \triangleq min(k_6, \beta)$.*

Proof. Let $\zeta(t)$ for $t \in [t_0, \infty)$ be a Filippov solution to the differential inclusion $\dot{\zeta} \in K[h_1](\zeta)$, where $K[\cdot]$ is defined as in [120], and where $h_1 : \mathbb{R}^2 \to \mathbb{R}^2$ is defined as $h_1 \triangleq \begin{bmatrix} \dot{\xi} & \dot{\psi} \end{bmatrix}^T$. Because of the discontinuity in the motor controller in (4–6), the time derivative of V_1 exists almost everywhere (a.e.) (i.e., for almost all $t \in [t_0, \infty)$), and $\dot{V}_1(\zeta) \overset{a.e.}{\in} \dot{\tilde{V}}_1(\zeta)$, where $\dot{\tilde{V}}_1$ is the generalized time derivative of V_1 along the Filippov trajectories of $\dot{\zeta} = h_1(\zeta)$ [121]. Using the calculus of $K[\cdot]$ from [121], and substituting (4–4) and (4–5) into $\dot{\tilde{V}}_1$ yields

$$\dot{\tilde{V}}_1 \subseteq -\beta\xi^2 + \psi\chi_1 + \left(\frac{1}{2}\dot{M} - V\right)\psi^2 - k_1\psi^2 - \psi\tau_m - \left(k_2 + k_3\|\phi\| + k_4\|\phi\|^2\right)K[\text{sgn}(\psi)]\psi. \tag{4–16}$$

Hence, by Properties 2.1-2.6, and since $\dot{V}_1(\zeta) \overset{a.e.}{\in} \dot{\tilde{V}}_1(\zeta)$, (4–16) can bounded above as

$$\dot{V}_1 \overset{a.e.}{\leq} |\psi| |\tau_m| - \beta\xi^2 - k_1\psi^2 - |\psi|\left(\lambda_1 + \lambda_2\|\phi\| + \lambda_3\|\phi\|^2\right), \tag{4–17}$$

where $\lambda_1, \lambda_2, \lambda_3 \in \mathbb{R}$ are defined as $\lambda_1 \triangleq k_2 - c_1$, $\lambda_2 \triangleq k_3 - c_2$, $\lambda_3 \triangleq k_4 - c_3$. Provided the gain conditions listed above are satisfied, $\lambda_1, \lambda_2, \lambda_3 \geq 0$, thus (4–17) can be upper bounded as

$$\dot{V}_1 \overset{a.e.}{\leq} |\psi| |\tau_m| - \delta\|\zeta\|^2, \tag{4–18}$$

where δ was defined previously. Hence, by [63, Definition 6.3] the robot system is output strictly passive with input $|\tau_m|$, output $|\psi|$, and storage function V_1. When the robot acts in isolation (i.e., the human is decoupled from the robot), $\tau_m = 0$, and (4–18) can be rewritten using (4–13) as

$$\dot{V}_1 \overset{\text{a.e.}}{\leq} -\frac{\delta}{\overline{\gamma}}V_1. \qquad (4\text{–}19)$$

Hence, the storage function qualifies as a radially unbounded positive definite Lyapunov function per the zero-state observability condition [63, Definition 6.5] and results in global exponential stability when $\tau_m = 0$. Using (4–13) with (4–19) provides the result in (4–15). Because the interaction torque is bounded, from the perspective of the robot, the physically applied rider torque is similarly bounded. Hence, from the closed-loop error system in (4–7), the admittance relation in (4–2), and the passivity result in (4–18), the robot admittance controller in (4–6) is bounded. $\qquad\square$

Remark 4.1. The rider's stimulation-elicited torque contribution is defined as $\tau_m \triangleq B_M u_M$, however, τ_m can be redefined to include the riders volitional torque contribution, $\tau_{vol} : \mathbb{R}_{\geq 0} \to \mathbb{R}$, as $\tau_m \triangleq B_M u_M + \tau_{vol}$ [133] and the conclusion of Theorem 4.1 still holds. Hence, if the rider volitionally contributes to pedaling the cycle in addition to the stimulation, the admittance controller is still passive.

For the following theorem, let $t_n^{FES} \in \mathbb{R}_{\geq 0}$ denote the time the crank enters $\mathcal{Q}_{FES}$ of cycle n, and $t_n^{KDZ} \in \mathbb{R}_{\geq 0}$ as the time the crank enters $\mathcal{Q}_{KDZ}$ (i.e., exits $\mathcal{Q}_{FES}$) of cycle n.

Theorem 4.2. *Given the closed-loop cadence error system in (4–12), for* $q \in \mathcal{Q}_{FES}$, *global exponential tracking is guaranteed in the sense that*

$$\|z\| \overset{\text{a.e.}}{\leq} \sqrt{\frac{\overline{\gamma}}{\underline{\gamma}}} \, \|z(t_n^{FES})\| \exp\left[-\frac{\rho}{2\overline{\gamma}}(t - t_n^{FES})\right], \qquad (4\text{–}20)$$

$\forall t \in \left[t_n^{FES}, t_n^{KDZ}\right)$, $\forall n$, *where* $\underline{\gamma}$, $\overline{\gamma} \in \mathbb{R}_{>0}$ *maintain their definitions from above, and* $\rho \triangleq \min\left(k_5, \alpha\right)$, *provided the constant gain conditions are satisfied:* $k_6 \geq c_4$, $k_7 \geq c_5$, $k_8 \geq c_6$, $k_9 \geq B_e$.

Proof. Similar to the proof of Theorem 4.1, let $z(t)$ for $t \in [t_0, \infty)$ be a Filippov solution to the differential inclusion $\dot{z} \in K[h_2](z)$ and let $h_2 : \mathbb{R}^2 \to \mathbb{R}^2$ be defined as $h_2 \triangleq \begin{bmatrix} \dot{e} & \dot{r} \end{bmatrix}^T$. Using Property 2.7, and substituting (4–9) and (4–10) into $\dot{V}_2(z)$ yields

$$\dot{V}_2 \subseteq -\alpha e^2 - \frac{K[B_M]}{B_M} k_5 r^2 - r B_e K[u_e] - \frac{K[B_M]}{B_M}\Big(k_6$$
$$+ k_7 \|z\| + k_8 \|z\|^2 + k_9 K[|u_e|]\Big) K[\text{sgn}(r)]r + r\chi_2, \tag{4–21}$$

where $K[|\text{sgn}(\cdot)|] = |\text{SGN}(\cdot)|$ such that $|\text{SGN}(\cdot)| = \{1\}$ if $(\cdot) \neq 0$, $[0,1]$ if $(\cdot) = 0$. Note $K[B_M]$ can be lower bounded by $K[\underline{B_M}]$ by Property 2.8 and in the FES regions, B_M is continuous; therefore $K[\underline{B_M}]$ can be replaced with $\underline{B_M}$. This fact, along with Properties 2.1-2.6, and the fact that $\dot{V}_2(z) \overset{\text{a.e.}}{\in} \dot{\tilde{V}}_2(z)$, allows (4–21) to be evaluated in the FES regions and upper bounded as

$$\dot{V}_2 \overset{\text{a.e.}}{\leq} -\alpha e^2 - k_5 r^2 - |r|\left(\lambda_4 + \lambda_5 \|z\| + \lambda_6 \|z\|^2 + \lambda_7 K[|u_e|]\right), \tag{4–22}$$

where $\lambda_i \in \mathbb{R}_{>0}$ $\forall i = 4, 5, ..., 7$ are defined as $\lambda_4 \triangleq k_6 - c_4$, $\lambda_5 \triangleq k_7 - c_5$, $\lambda_6 \triangleq k_8 - c_6$, and $\lambda_7 \triangleq k_9 - B_e$. Provided the aforementioned gain conditions are satisfied, $\lambda_i \geq 0$ $\forall i$; thus, (4–22) can be upper bounded using (4–14) as

$$\dot{V}_2 \overset{\text{a.e.}}{\leq} -\frac{\rho}{\overline{\gamma}} V_2, \tag{4–23}$$

where ρ was introduced in (4–20). Based on (4–14) and (4–23) the result in (4–20) can be obtained. From the result of Theorem 4.1, and from the closed-loop error systems, the cadence controller in (4–11) is bounded. $\qquad\square$

Remark 4.2. Redefining the rider's torque contribution as $\tau_m \triangleq B_M u_M + \tau_{vol}$ no longer guarantees exponential tracking; instead, by assuming the rider is contributing positive

torque about the crank, it guarantees the actual cadence will be at least the desired cadence (i.e., $\dot{q} \geq \dot{q}_d$).

<h2 style="text-align:center">4.3   Experiments</h2>

4.3.1   Experimental Testbed

The experimental testbed used in this chapter is introduced in Chapter 2.

4.3.2   Experimental Methods

Four experimental protocols (i.e., Protocols A, B, C, and D) were conducted on three able-bodied participants and four participants with NCs, whose demographics are listed in Table 4-1. Each protocol had a duration of two minutes with the first twenty seconds consisting of a smooth motor-only ramp to the desired cadence of 50 RPM. Subsequently, the controllers in (4–6) and (4–11) were activated for the remaining duration of the experiment. Across all protocols, the desired inertia parameter was held constant at $M_d = 2 \frac{Nm \cdot s^2}{rad}$ and the damping parameter was selected to be a low $\left(1 \frac{Nm \cdot s}{rad}\right)$, medium $\left(2.5 \frac{Nm \cdot s}{rad}\right)$, or high value $\left(5 \frac{Nm \cdot s}{rad}\right)$ (i.e., Protocols A, B, and C, respectively) to investigate the effects of modifying the parameter. For Protocols A, B, and C, all participants were asked to remain passive, contribute no volitional torque, and were blind to the desired trajectory for the duration of the experiment. An additional protocol was conducted with the medium damping parameter, but with added volition (i.e., Protocol D) where the participants were shown a running plot of the measured and desired cadences. For Participants 1-3, the interaction torque was selected as $\tau_d = 0.5$ Nm for Protocols A-C, and as $\tau_d = 2.0$ Nm for Protocol D. For Participants 4-7, the interaction torque was selected as $\tau_d = 0.0$ Nm for Protocols A-D, unless otherwise noted.

The stimulation input in (4–11) was saturated based on individual participant comfort and was determined prior to experimentation. The experimental protocols were approved by the Institutional Review Board at the University of Florida. Participants are referred to by the letter "P" followed by their participant number. Unique trials

Table 4-1. Demographics of participants with and without neuromuscular disorders

Participant	Age	Sex	Condition	Physical Aid†	TSI‡
P1	25	M	None	- -	- -
P2	25	M	None	- -	- -
P3	24	F	None	- -	- -
P4	25	M	Spina Bifida (L5-S1), Arnold Chiari Malformation	AFO, Wheelchair	25yr
P5	28	F	Spinal Cord Injury (T8-T9)	Wheelchair	12yr
P6	50	F	Hemorrhagic Stroke	Wheelchair	4yr
P7	64	M	Parkinson's Disease	- -	19yr

†AFO: ankle-foot orthosis
‡TSI: Time since injury

are referred to by the participant number followed by the protocol letter; for example, Participant 3 Protocol B is referred to as P3B.

4.3.3 Results and Discussion

To estimate the power generated by the rider, an average passive torque reading, denoted by $\tau_p \ : \ \mathbb{R}_{\geq 0} \to \mathbb{R}$, was collected during each trial for 4.8 seconds prior to controller activation (i.e., approximately four crank cycles at 50 RPM) to provide a baseline estimate for the passive torque required to actuate the combined rider-cycle system at the desired cadence. Subsequently, an average estimate of the power generated by the rider, denoted by $P \ : \ \mathbb{R}_{\geq 0} \to \mathbb{R}$, was obtained through the relation, $P = \text{mean}\,(\dot{q})\,(\text{mean}\,(\tau_{int}) - \tau_p)$. Results from the three able-bodied participants are provided in Table 4-2 and from the participants with neurological disorders in Table 4-3, with details on the average and standard deviation of the measured cadence, admitted cadence, admitted cadence error, measured interaction torque, measured passive torque, and generated power. The controller gains in (4–4), (4–6), (4–9), and (4–11) were selected as $k_1 = 6$, $k_2 = k_3 = k_4 = 0.01$, $k_5 \in [2, \, 4]$, $k_6 = k_7 = k_8 = 0.1$, $k_9 = 0.5$, $\alpha \in [1, \, 8]$, $\beta \in [0.8, \, 1.2]$ across all trials. The aforementioned gain conditions are sufficient to achieve stability based on conservative bounds on the uncertain parameters in the dynamics. Therefore, the sufficient gain conditions provide guidelines for the initial gain selection and the gains can be subsequently adjusted to achieve desirable performance. Although the listed gains were adjusted using an empirical-based method,

the gains could have been adjusted using more methodical approaches. For example, the nonlinear system in [123] was linearized at several operating points and a linear controller was designed for each point, and the gains were chosen by interpolating, or scheduling the linear controllers. In [124], a neural network is used to adjust the gains of a PID controller. In [125] a genetic algorithm was used to adjust the gains after an initial guess. The authors in [126] provide an extensive discussion on the use of extremum seeking for tuning the gains of a PID controller. Additionally, in [127], the tuning of a PID controller for robot manipulators is discussed.

Table 4-2. Experimental results for able-bodied population, reported as average±standard deviation

Participant	Protocol	$\dot{q}$ (RPM)	$\dot{q}_a$ (RPM)	$\dot{\xi}$ (RPM)	τ_{int} (Nm)*	τ_p (Nm)△	P (W)	u_e (A)	u_m (μs)□
P1	A	47.19±1.95	-2.95±1.48	-0.14±1.53	0.15±0.57	-0.61±0.51	3.80±2.84	2.19±1.00	134.51±26.98
	B	48.48±1.64	-1.63±0.91	-0.12±1.56	0.04±0.59	-0.63±0.50	3.44±3.00	2.33±1.01	110.99±29.60
	C	49.23±1.57	-0.90±0.65	-0.14±1.55	0.00±0.65	-0.57±0.49	2.93±3.38	2.16±1.04	83.19±20.87
	D	49.88±1.68	-0.26±0.76	-0.15±1.84	1.87±0.84	-0.58±0.51	12.84±4.39	0.24±1.24	43.48±04.58
P2	A	48.38±2.05	-1.62±1.38	-0.01±1.65	0.29±0.63	-0.58±0.59	4.47±3.20	1.94±1.13	103.65±20.26
	B	48.53±1.93	-1.48±1.16	-0.02±1.63	0.07±0.73	-0.69±0.58	3.91±3.72	2.27±1.15	106.79±25.18
	C	48.74±1.55	-1.30±0.57	-0.04±1.47	-0.21±0.57	-0.74±0.55	2.70±2.91	2.57±1.03	88.45±25.14
	D	49.54±1.70	-0.52±0.67	-0.06±1.72	1.79±0.84	-0.66±0.67	12.79±4.36	0.34±1.23	48.63±07.07
P3	A	49.19±2.20	-0.83±1.87	-0.03±1.26	0.38±0.45	-0.43±0.33	4.26±2.34	1.93±0.87	90.61±11.52
	B	49.22±1.76	-0.79±1.14	-0.01±1.36	0.28±0.51	-0.38±0.31	3.47±2.65	2.02±1.10	87.14±16.57
	C	49.25±1.41	-0.78±0.68	-0.04±1.24	0.06±0.50	-0.45±0.31	2.72±2.59	2.14±0.91	72.39±17.36
	D	50.01±1.44	-0.05±0.55	-0.07±1.43	1.93±0.60	-0.27±0.30	11.60±3.16	0.37±1.02	32.23±03.56
Mean	A	48.25±2.06	-1.80±1.59	-0.06±1.48	0.20±0.55	- -	4.17±2.81	2.02±1.00	109.59±20.58
Mean	B	48.74±1.78	-1.30±1.07	-0.05±1.52	0.13±0.61	- -	3.60±3.15	2.20±1.08	101.64±24.39
Mean	C	49.07±1.65	-0.99±0.86	-0.07±1.42	-0.05±0.57	- -	2.78±2.95	2.29±0.99	81.34±21.36

*A positive interaction torque signifies the participant was able to overcome the torque deficit required to passively actuate their legs.

△The average passive torque is participant-dependent and was not averaged.

□The average and standard deviation of the applied stimulation was calculated using the maximum stimulation delivered to each muscle group for each FES region.

Table 4-3. Experimental results for population with neuromuscular disorders, reported as average±standard deviation

Participant	Protocol	$\dot{q}$ (RPM)	$\dot{q}_a$ (RPM)	$\dot{\xi}$ (RPM)	τ_{int} (Nm)*	τ_p (Nm)$^\triangle$	P (W)	u_e (A)	u_m (μs)$^\square$
P4	A	46.23±1.20	-3.79±0.92	-0.02±0.87	-0.41±0.22	-0.46±0.25	0.22±1.08	2.56±0.60	60.38±10.69
	B	48.46±1.00	-1.56±0.41	-0.03±0.96	-0.42±0.23	-0.47±0.27	0.25±1.19	2.67±0.65	55.64±12.90
	C	49.29±0.97	-0.72±0.23	-0.02±0.96	-0.39±0.23	-0.46±0.27	0.37±1.22	2.55±0.65	46.10±11.95
	D†	49.53±1.61	-0.51±0.86	-0.05±1.46	0.82±0.72	-0.47±0.26	6.75±3.75	1.31±1.02	45.62±06.70
P5	A	44.42±1.27	-5.60±1.12	-0.03±0.73	-0.61±0.18	-0.56±0.22	-0.20±0.84	2.44±0.50	356.76±182.84
	B	47.86±0.87	-2.17±0.40	-0.03±0.81	-0.58±0.19	-0.53±0.27	-0.26±0.96	2.39±0.55	233.13±162.57
	C	48.95±0.86	-1.04±0.20	0.00±0.85	-0.56±0.20	-0.51±0.27	-0.24±1.03	2.46±0.58	172.88±109.94
	D$^\|$	- -	- -	- -	- -	- -	- -	- -	- -
P6	A	45.52±1.05	-4.51±0.89	-0.03±0.64	-0.49±0.16	-0.61±0.15	0.56±0.77	2.22±0.44	56.01±09.90
	B	47.60±0.92	-2.42±0.50	-0.03±0.83	-0.65±0.26	-0.54±0.22	-0.54±1.29	2.38±0.57	53.31±11.58
	C	48.98±0.84	-1.04±0.30	-0.02±0.80	-0.55±0.26	-0.45±0.17	-0.52±1.38	2.30±0.56	42.51±12.72
	D	49.53±1.12	-0.48±0.65	-0.02±0.97	-0.13±0.42	-0.15±0.27	0.1±2.18	1.82±0.68	29.27±06.09
P7	A‡	44.80±1.82	-5.25±1.37	-0.05±1.47	1.39±0.92	-0.13±0.21	7.19±4.31	0.20±1.03	86.87±12.58
	B‡	48.29±1.30	-1.75±0.74	-0.04±1.16	0.51±0.55	-0.31±0.15	4.16±2.79	1.16±0.81	84.06±16.33
	C	50.04±0.87	0.01±0.26	-0.02±0.86	0.00±0.31	-0.19±0.18	1.06±1.62	1.66±0.60	29.38±03.45
	D†	49.94±1.23	-0.09±0.44	-0.03±1.27	0.94±0.67	-0.19±0.21	5.97±3.51	0.72±0.88	30.67±03.40
Mean	A	45.24±1.36	-4.78±1.09	-0.03±0.98	-0.03±0.48	- -	1.94±2.29	1.85±0.68	140.00±91.92
Mean	B	48.05±1.03	-1.97±0.53	-0.03±0.95	-0.28±0.33	- -	0.90±1.71	2.15±0.65	106.53±82.15
Mean	C	49.31±0.90	-0.55±0.25	-0.01±0.86	-0.37±0.25	- -	0.16±2.03	2.24±0.59	72.71±55.68

*A positive interaction torque signifies the participant was able to overcome the torque deficit required to passively actuate their legs.

†Due to volitional ability, the desired interaction torque was lowered to $\tau_d = 1.0$ Nm.

‡Due to minor volitional contributions by P7, the interaction torque was increased to $\tau_d = 2.0$ Nm for Protocol A and $\tau_d = 1.0$ for Protocol B.

$^\|$This run was not performed because the participant was unable to contribute volitionally.

$^\triangle$The average passive torque is participant-dependent and was not averaged.

$^\square$The average and standard deviation of the applied stimulation was calculated using the maximum stimulation delivered to each muscle group for each FES region.

By varying the damping parameter in the admittance filter in (4–2), various behaviors can be obtained from the cycle without changing any other aspect of the control system. For example, a high damping parameter results in a stiffer, less compliant cycle that admits less to any rider-applied torque. Based on Tables 4-2 and 4-3, it can be seen that increasing the damping parameter results in better cadence tracking, but less torque production (e.g., compare P1A to P1C). This is due to less position error accumulating in the cadence controller (because the cycle admits less) and consequently, less stimulation and torque production over time. With a low damping parameter, the admitted trajectory (i.e., $\dot{q}_a$) is allowed to deviate more than with a high damping parameter (see Column 4 of Tables 4-2 and 4-3), and the position error accumulates more quickly, resulting in more stimulation and torque production. Regardless of the cadence tracking error, the admittance tracking error is small in comparison across all experiments and participants (see Column 5 of Tables 4-2 and 4-3), indicating the motor is able to emulate the dynamics dictated by the admittance filter in (4–1) and (4–2). As the rider is stimulated, their muscles produce an interaction torque about the crank (i.e,. τ_{int}); if this torque is greater than the passive amount it takes to actuate their body (i.e., τ_p), the interaction torque will be positive. Any torque reading greater than τ_p is assumed to be the result of torque generated by the rider's muscles and the difference is multiplied by the measured cadence to get an estimate of the power generated by the rider.

To facilitate the following discussion, let $\dot{q}_\alpha : \mathbb{R}_{\geq 0} \to \mathbb{R}$ denote the *admitted cadence trajectory*, defined as $\dot{q}_\alpha \triangleq \dot{q}_d + \dot{q}_a$, in contrast to the *admitted trajectory* denoted by $\dot{q}_a$. Note that although admittance error system is passive with respect to the rider, the admittance controller tracks the admitted trajectory closely. The cadence error system is proven to be exponentially stable, and Figure 4-1[1] indicates that when the participant is

---

[1] For visual clarity, a one-second moving average filter was applied to all cadence/torque plots.

below their saturation level of 110 μs, the measured cadence converges to the desired cadence. Figure 4-1 also illustrates P3B's torque production, which over time, reaches the desired value of 0.5 Nm and demonstrates indirect regulation of the torque tracking error e_τ. Upon reaching the desired torque, the stimulation begins to plateau, as shown in Figure 4-2[2] . With the desired torque reached, the admitted cadence trajectory begins to align with the desired cadence trajectory, and the participant is able to achieve the desired cadence at the desired torque. An estimate of the power produced by P3B is displayed in Figure 4-1 alongside the torque produced. Taken together, Figures 4-1 and 4-2 indicate that as the participant's stimulation increases, her muscles produce stronger contractions. Correspondingly, she is able to offset a portion of the torque required by the motor because it needs to assist the rider less. This results in a decrease of the amount of current required to actuate the motor. Of note, by offsetting a portion of the motor current needed to actuate the cycle with FES, smaller motors can be utilized, resulting in lighter, less powerful, and less expensive FES cycles.

To highlight the performance of a participant with a ND, Figures 4-3 and 4-4 display the tracking results and control inputs for P4B, respectively. As shown in Tables 4-2 and 4-3, the admittance tracking error is small as in the other participants, demonstrating convergence of the admittance error system. However, unlike P3, P4 had a low tolerance to the electrical stimulation. Consequently, only low levels of torques were able to be evoked, and the desired interaction torque was reduced from 0.5 Nm to 0 Nm. Note that due to the passive torque required to actuate P4's legs (i.e., approximately 0.46 Nm), an interaction torque of 0 Nm would still require P4's leg muscle to produce an average torque of 0.46 Nm. As illustrated in Figure 4-3, P4

---

[2] For visual clarity, a half-second moving average filter was applied to the motor current input and the stimulation input is represented as the maximum stimulation for each FES region at the corresponding time.
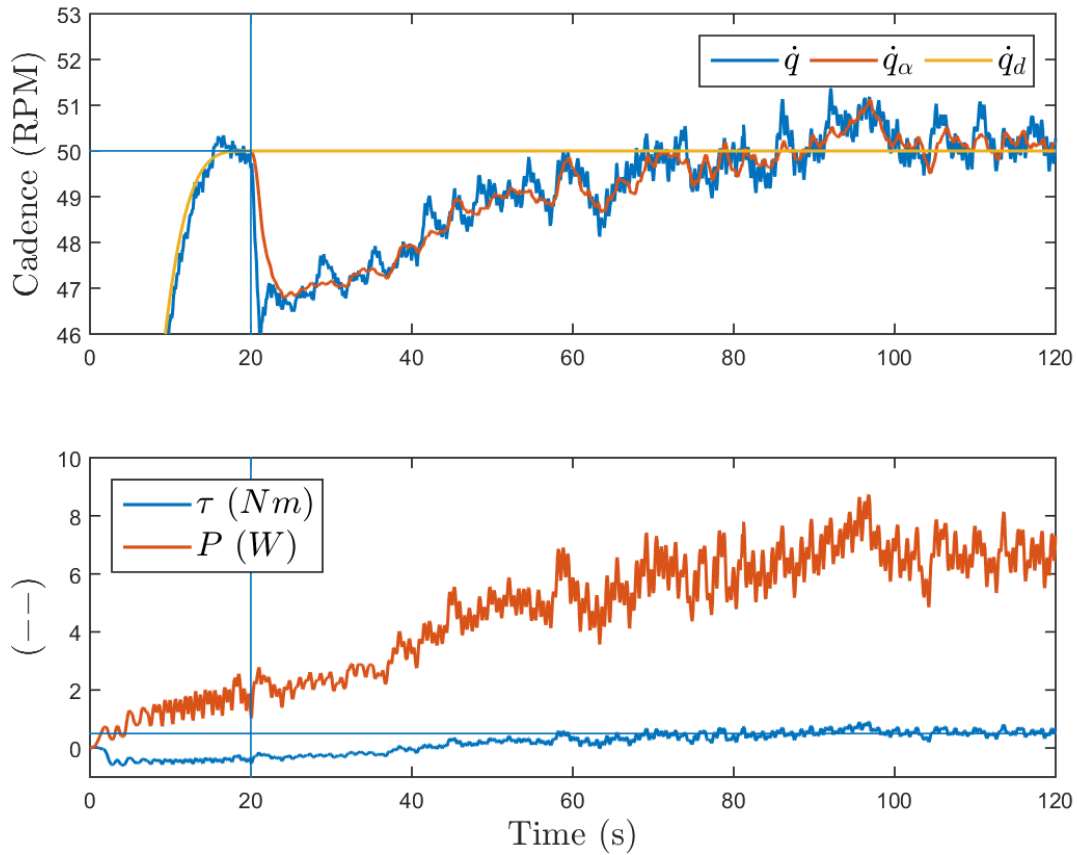
Figure 4-1. P3B: (Top) Measured ($\dot{q}$), admitted ($\dot{q}_a$), and desired cadences ($\dot{q}_d$); (Bottom) Measured torque (τ) and estimated power (P) produced by the rider. Vertical lines represent time of controller activation, horizontal lines represent desired values (for cadence and torque).
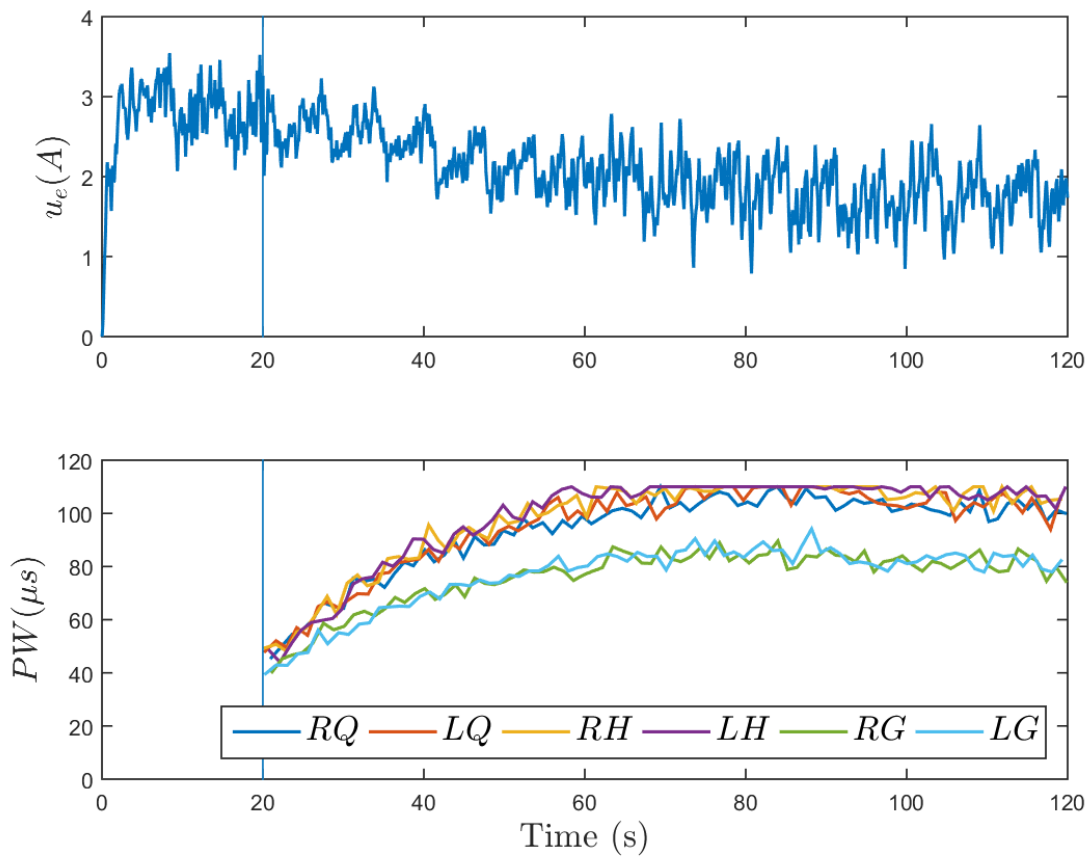
Figure 4-2. P3B: (Top) Control effort sent to motor (Bottom) Control effort sent to rider's right (R) and left (L) quadriceps (Q), hamstring (H), and gluteal (G), respectively. Stimulation was saturated at 110 μs for rider comfort.

was unable to achieve the desired torque production; hence, the admitted cadence trajectory consistently lagged the desired cadence trajectory. However, P4 was able to produce a small amount of torque, as indicated in Figure 4-3. As the experiment progresses, the participant begins to show signs of fatigue and his torque begins to decline (at approximately $t = 55 \ s$). As mentioned in [117], the early onset of fatigue remains an outstanding challenge in the use of FES. Despite the participant not achieving the desired cadence or desired torque (due to stimulation limitations, or actuator saturation), the admittance controller was still able to achieve stable operation and ensure participant safety and comfort. As seen in Tables 4-2 and 4-3, the average cadence achieved is directly related to the selected damping parameter, regardless of stimulation saturation.

To testify to the admittance controller's capabilities to handle participant variability and ability, all participants were asked to repeat Protocol B, but with added volition (Protocol D). Figures 4-5 and 4-6 display the tracking results and control inputs for P4D, respectively. Compared to Figure 4-3, which displays P4's performance when he was asked to remain passive and not contribute to the pedaling task, Figure 4-5 shows notably improved tracking performance. When P4 was instructed to pedal, he not only was able to keep his stimulation levels below his saturation level, but also produce the desired torque (without modifying any gains). This trial more closely reflects the results displayed in Figures 4-1 and 4-2 for P3B. Meaning, if a participant is able to tolerate the required stimulation to produce the desired amount of torque, their performance will be similar to that as when they volitionally pedal (in the sense that they will be able to achieve the desired cadence at the desired torque). Therefore, the controller is capable of being applied to an individual with a complete spinal cord injury or an able-bodied individual that is volitionally pedaling, without any adjustment to the controller.

Figures 4-7 and 4-8 are provided to highlight the performance of P5, the participant with a spinal cord injury. Because she was unable to contribute volitionally to the
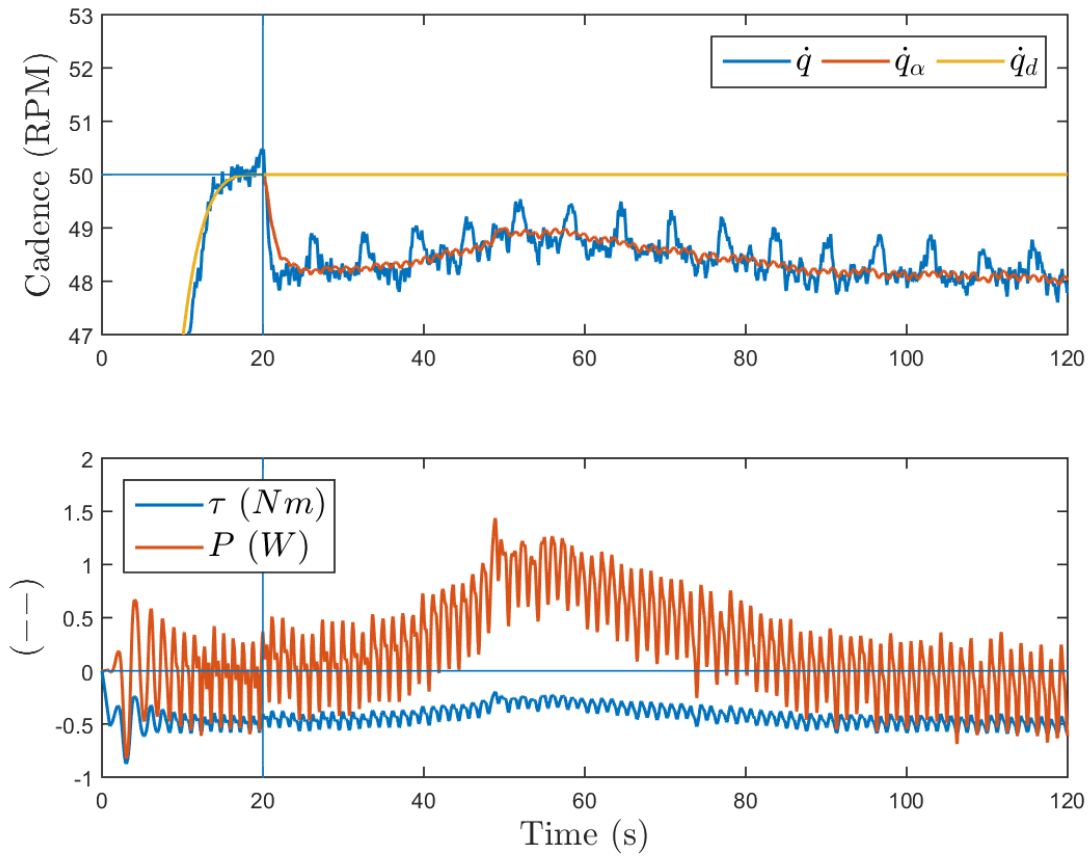
Figure 4-3. P4B: (Top) Measured ($\dot{q}$), admitted ($\dot{q}_a$), and desired cadences ($\dot{q}_d$); (Bottom) Measured torque (τ) and estimated power (P) produced by the rider.
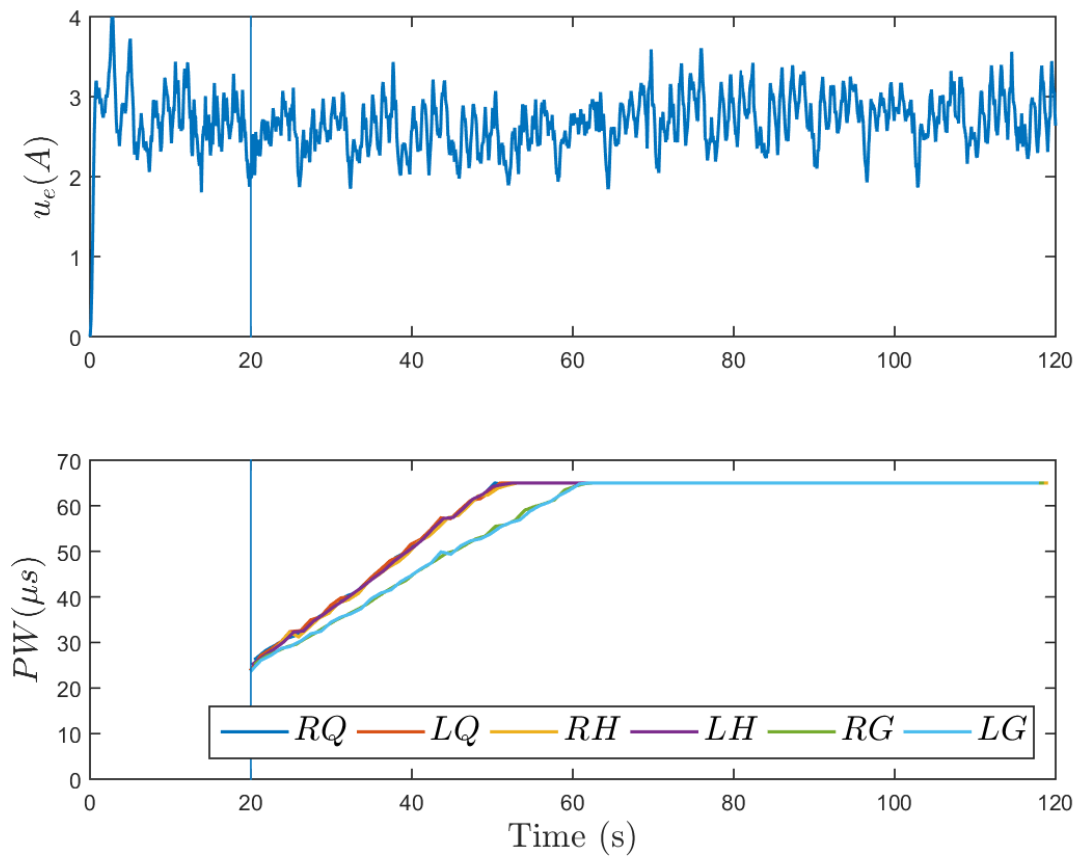
Figure 4-4. P4B: (Top) Control effort sent to motor (Bottom) Control effort sent to rider's right (R) and left (L) quadriceps (Q), hamstring (H), and gluteal (G), respectively. Stimulation was saturated at 65 μs for rider comfort.
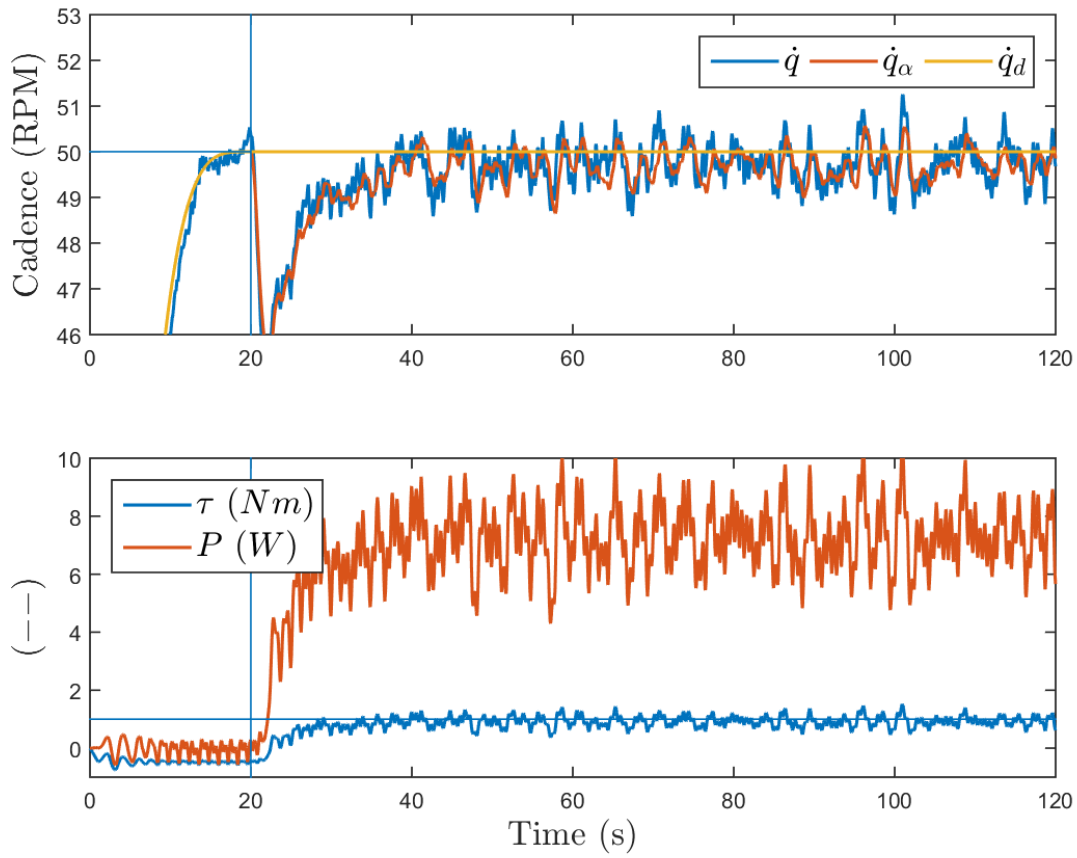
Figure 4-5. P4D: (Top) Measured ($\dot{q}$), admitted ($\dot{q}_a$), and desired cadences ($\dot{q}_d$); (Bottom) Measured torque (τ) and estimated power (P) produced by the rider.
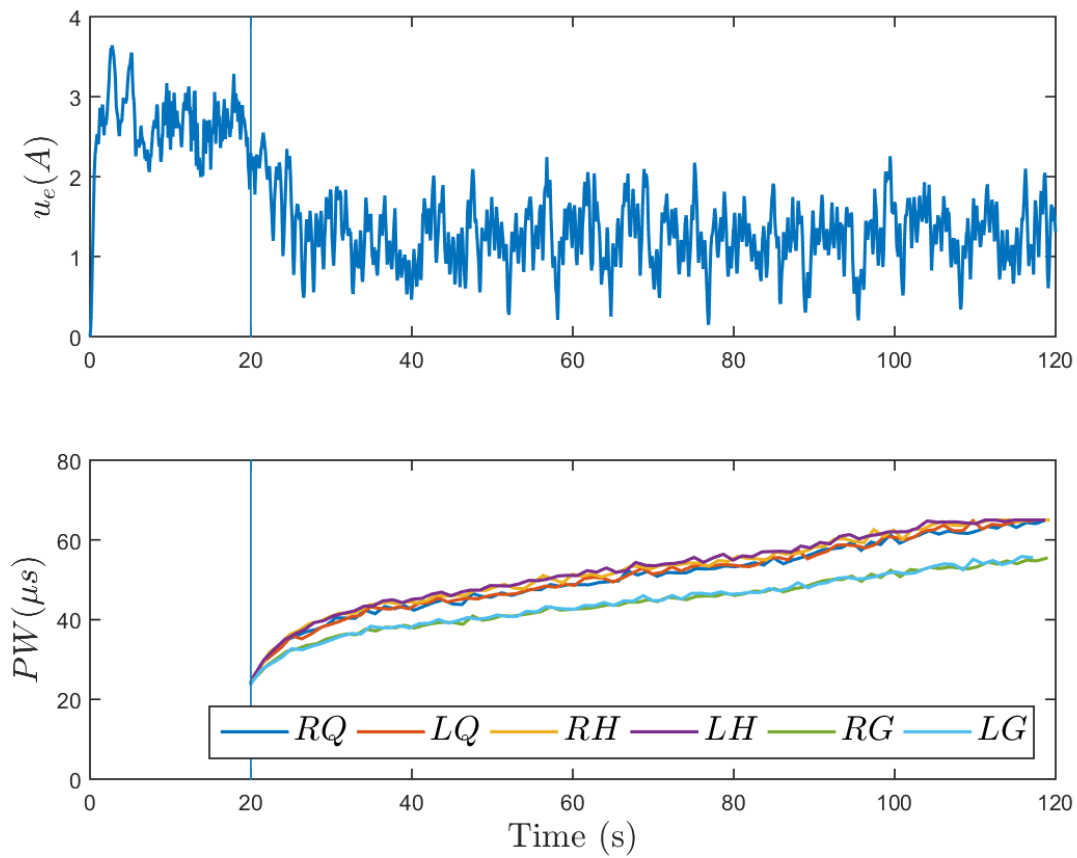
Figure 4-6. P4D: (Top) Control effort sent to motor (Bottom) Control effort sent to rider's right (R) and left (L) quadriceps (Q), hamstring (H), and gluteal (G), respectively. Stimulation was saturated at 65 μs for rider comfort.
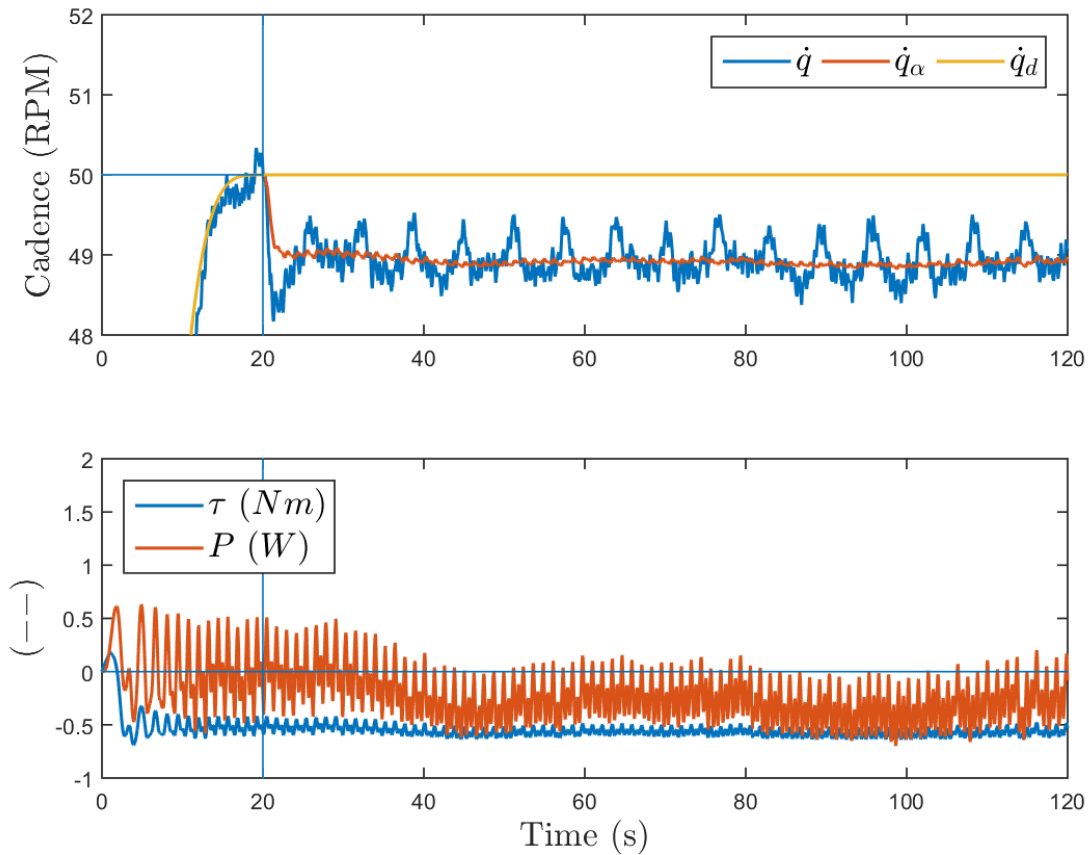
Figure 4-7. P5C: (Top) Measured ($\dot{q}$), admitted ($\dot{q}_a$), and desired cadences ($\dot{q}_d$); (Bottom) Measured torque (τ) and estimated power (P) produced by the rider.

cycling task, Protocol D was not completed. As illustrated in Figure 4-7, there was no improvement in the cadence tracking error over the course of the experiment. Correspondingly, this is attributed to the near-zero torque production elicited by the stimulation. It is hypothesized that because P5 experienced a spinal cord injury 12 year prior, her muscles had atrophied significantly and were small in comparison to other tissues present. According to [134], this can prevent the electricity from penetrating sufficiently deep into the leg to recruit muscle fibers for contraction. Consequently, despite reaching the maximum amount of stimulation deliverable by the stimulator (i.e., 500 μs) as shown in Figure 4-8, P5 is likely not receiving the full benefits of FES, but only of participating in range-of-motion exercises.
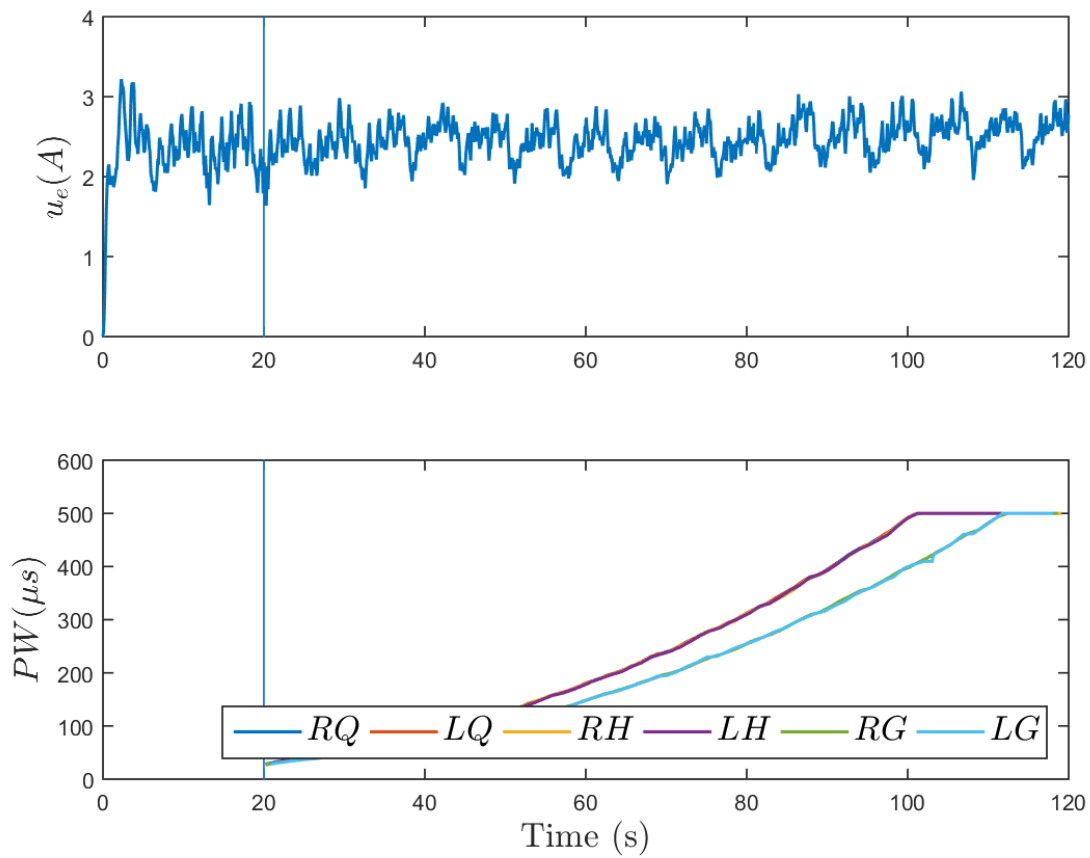
Figure 4-8. P5C: (Top) Control effort sent to motor (Bottom) Control effort sent to rider's right (R) and left (L) quadriceps (Q), hamstring (H), and gluteal (G), respectively. Stimulation was saturated at 500 μs.
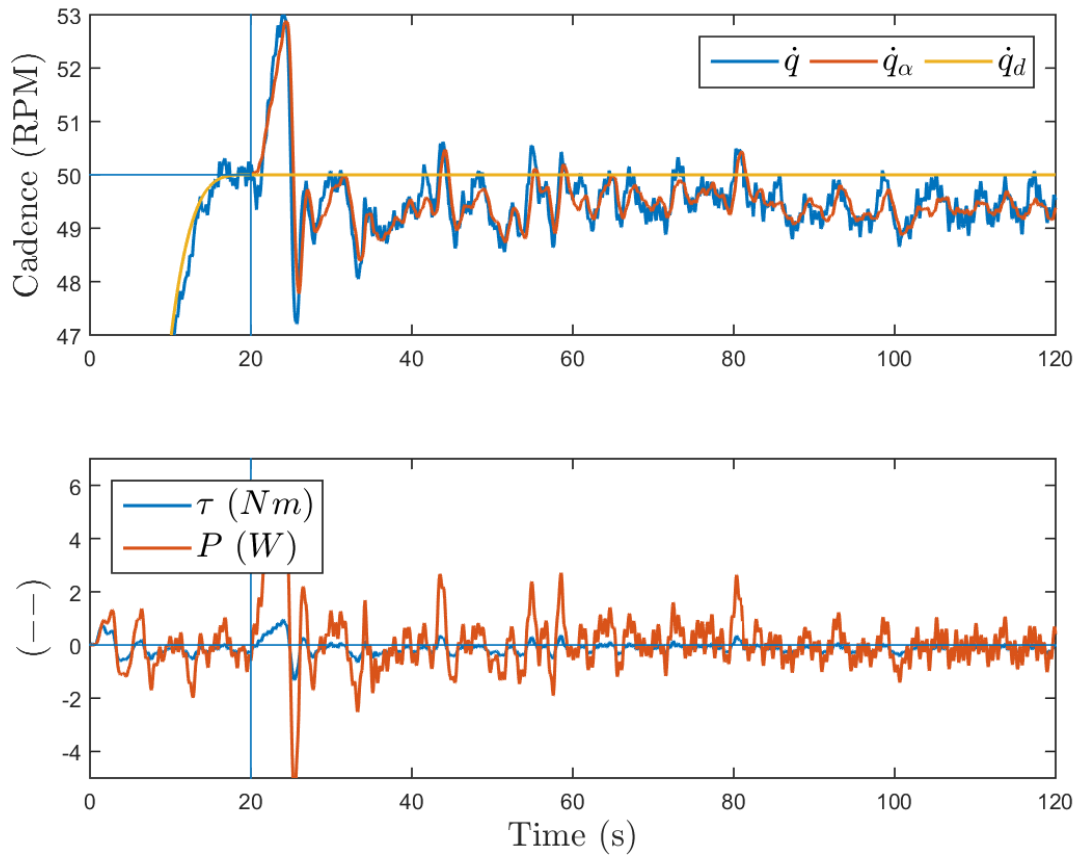
Figure 4-9. P6D: (Top) Measured ($\dot{q}$), admitted ($\dot{q}_a$), and desired cadences ($\dot{q}_d$); (Bottom) Measured torque (τ) and estimated power (P) produced by the rider.

Despite P6 suffering a hemorrhagic stroke four years prior to her involvement in the study, she had regained some functional ability in the affected right arm and leg. Figure 4-9 displays the tracking results for P6D, when she was tasked with volitionally contributing to the cycling objective. Because P6 was able to pedal the cycle near the desired cadence, but with slight undershoot, she accumulated position and cadence error and correspondingly received an increasing amount of stimulation over the course of the experiment, as displayed in Figure 4-10. Because P6 was contributing volitionally, despite the increase in stimulation, she showed no sign of fatigue or decrease in torque production.
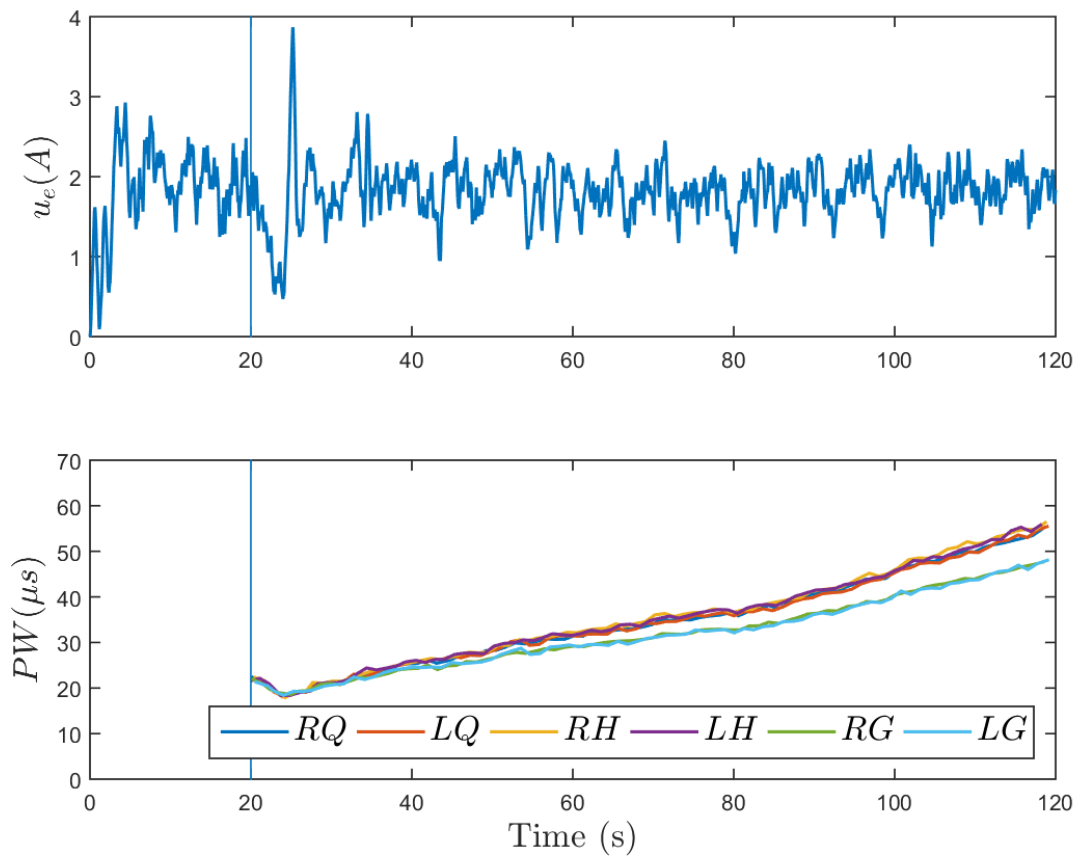
Figure 4-10. P6D: (Top) Control effort sent to motor (Bottom) Control effort sent to rider's right (R) and left (L) quadriceps (Q), hamstring (H), and gluteal (G), respectively. Stimulation was saturated at 60 μs for rider comfort.

Although P7 had Parkinson's disease, he had ample muscle tone and strength due to his regular exercise regime. Accordingly, he was able to produce large amounts of torque and the desired interaction torque was varied according to Tables 4-3.

When examining P7's trial with volition (P7D), it can be seen in Figure 4-11 that he is able to quickly track the desired cadence and meet the desired interaction torque. Compared to the counterpart protocol with the medium damping parameter (Protocol B), P7 was able to produce 44% more torque without significantly affecting the performance of the admittance controller. As depicted in Figure 4-12, P7 was able to keep his stimulation levels low by contributing volitionally. Furthermore, it can been seen that the rider is able to offset the current required by the motor to actuate the cycle.

Across all participants undergoing Protocols A-C, the low damping parameter selected for Protocol A resulted in the generation of the least-stiff admitted trajectory. The admitted trajectory was allowed to deviate the most, and consequently, the position/cadence errors were the largest across all protocols; this resulted in high stimulation and in the highest torque production. Comparatively, the highest damping parameter in Protocol C held the admitted trajectory close to the desired, reduced the position/cadence error, and resulted in the lowest torque production. Hence, without modifying the controller structure or gains, the FES cycle can place more or less emphasis on cadence tracking or torque production. Allowing riders to contribute volitionally (if possible) further increased the torque production, especially when the desired interaction torque was set to a high value (e.g., 2.0 Nm). Accordingly, volition does not destabilize the controllers, nor compromise their performance, and should be encouraged whenever possible.

4.4 Concluding Remarks

In this chapter, two new controllers are developed for the FES cycle to accomplish simultaneous cadence and admittance tracking. The controllers are designed to overcome challenges of Chapter 3; namely, selecting the appropriate desired torque
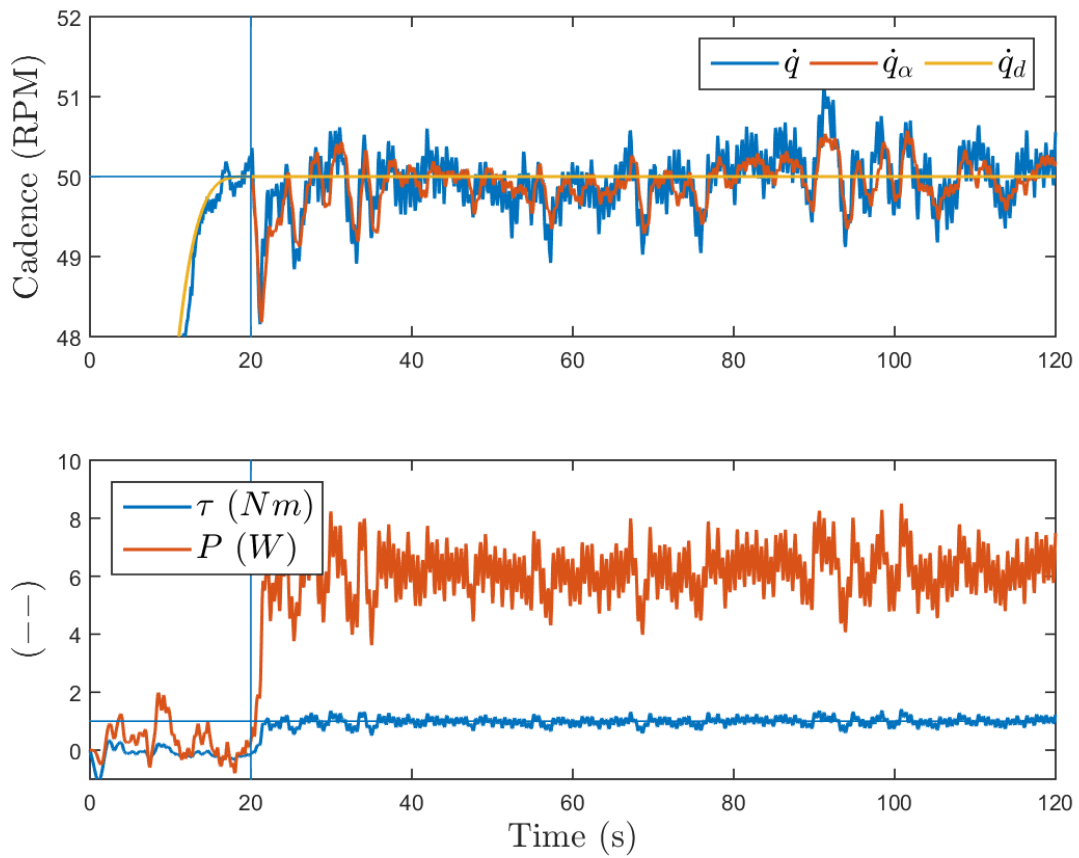
Figure 4-11. P7D: (Top) Measured ($\dot{q}$), admitted ($\dot{q}_a$), and desired cadences ($\dot{q}_d$); (Bottom) Measured torque (τ) and estimated power (P) produced by the rider.
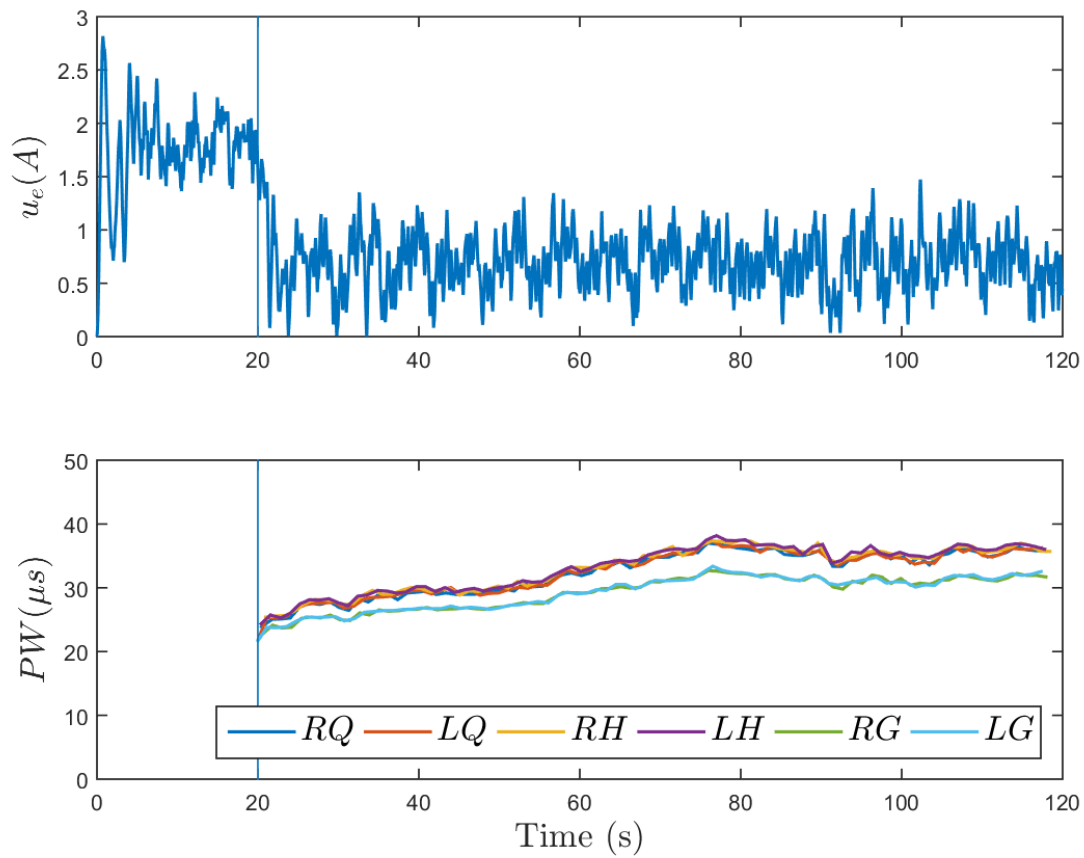
Figure 4-12. P7D: (Top) Control effort sent to motor (Bottom) Control effort sent to rider's right (R) and left (L) quadriceps (Q), hamstring (H), and gluteal (G), respectively. Stimulation was saturated at 120 μs for rider comfort.

trajectory for direct torque tracking. Compared to Chapter 3, the admittance controller implemented on the cycle's motor is capable of indirect torque tracking, accomplished by injecting artificial desired dynamics between the rider and the cycle. Consequently, the rider's muscles are now electrically stimulated using a cadence controller to actuate the cycle. Using the admittance controller, the cycle assumes an assist-as-needed control paradigm and assists the rider is maintaining a desired cadence if the FES is unable to elicit muscle contractions powerful enough to overcome the passive torques of the combined cycle-rider system. Correspondingly, the admittance controller resists the rider if volitional pedaling exceeds the desired cadence. Experiments conducted on three able-bodied participants and four participants with NDs demonstrate controller efficacy and practicality. The experiments also investigated the effect of selecting various admittance parameters and show that a compliant cycle is not only desirable for rider safety, but also for torque/power production. Results indicate the admittance controller is a promising rehabilitation strategy to simultaneously elicit torque from the rider's muscles while introducing a degree of compliance to the system.

To improve upon the controller developed in this chapter, Chapter 5 seeks to add adaptation to the admittance controller while simultaneously measuring and addressing rider asymmetries.

CHAPTER 5
SPLIT-CRANK FUNCTIONAL ELECTRICAL STIMULATION CYCLING: AN ADAPTING ADMITTING REHABILITATION ROBOT

This chapter is developed to promote rehabilitation in individuals with asymmetric movement disorders, specifically hemiparesis. Closed-loop adaptive admittance controllers are implemented on the decoupled motors of the split-crank FES cycle, introduced in Chapter 2, while the rider is electrically stimulated with a robust cadence controller. Compared to past literature and previous work on admittance control of FES cycling (cf. [107, 110, 111]), this chapter provides the first instance of adaptive admittance control applied to a split-crank FES cycle with results on participants possessing NDs. Specifically, compared to the precursory work in [107, 110, 111], the theoretical development in this chapter focuses on adaptive admittance control that adjusts in real-time to the user capabilities. Furthermore, by instrumenting the FES cycle with sensors on each side, the cycle is now able to measure the performance of each rider's right and left leg, allowing for an estimate of asymmetries.

Because few results exist in terms of split-crank cycling, open questions remain regarding how to best design the desired trajectories and select the appropriate admittance parameters. Although the development of this chapter is agnostic to the desired trajectories, various trajectories are hypothesized to have different clinical implications for people with movement disorders [81]. Without loss of generality, the admitted trajectory was selected to average the capabilities of the rider's legs measured by the split-crank FES cycle; that is, torque feedback is implemented on each side of the cycle and averaged, such that the more capable leg experiences resistance and the less capable leg experiences assistance to achieve the same cadence while preserving cycling symmetry. A closed-loop robust cadence controller is subsequently designed to implement FES on the large muscle groups of the rider's legs (quadriceps, hamstrings, gluteals) and maintain the desired cadence. To ensure rider safety, the combined closed-loop cycle-rider system is proven to be energetically dissipative (i.e., stable and

passive). A Lyapunov-based passivity analysis is used to prove the developed cadence controller is passive. A second Lyapunov-based analysis is provided to prove global asymptotic admittance tracking. The two controllers work in tandem to cooperatively pedal the split-crank FES cycle while promoting rehabilitation outcomes using a hybrid exoskeleton. Experiments were conducted on one able-bodied participant, one participant with spina bifida, one participant with post-stroke right-sided hemiparesis, and one participant with Parkinson's disease with and without controller adaptation. An additional experiment was conducted on the participant with Parkinson's to evaluate the effect of adding rider volition to the experiment. Results demonstrate an average admittance tracking error of -0.13±1.77 RPM with adaptation and -0.03±4.05 RPM without adaptation. The split-crank FES cycle successfully admits to the rider, preserves rider safety, and offers a promising robotic rehabilitation strategy for individuals affected by movement disorders.

5.1   Control Development

In the following section, two controllers are developed for one side of the FES cycle, a cadence controller for the rider's muscles and an admittance controller for the cycle's motor; without loss generality, an identical analysis can be repeated for each side of the cycle. To facilitate the following development, the following property is introduced:

Property 5.1. The dynamic equation of 2–8 can be linearly parameterized in terms of M, V, G, and b_c.

5.1.1   Robust Cadence Control

The subsequently presented cadence controller assumes the same form as the result in [67]. However, because a new objective is presented in this work (i.e., admittance tracking), a new stability analysis is required. For notational brevity, all functional dependencies are hereafter suppressed unless required for clarity of exposition. As in [67], the cycle's cadence is regulated using the rider's muscles in the FES regions and the tracking objective is quantified by $e \: : \: \mathbb{R}_{\geq 0} \to \mathbb{R}$ and $r \: : \: \mathbb{R}_{\geq 0} \to \mathbb{R}$, each defined

as

$$e \triangleq q_d - q, \tag{5–1}$$

$$r \triangleq \dot{e} + \alpha e, \tag{5–2}$$

where $q_d : \mathbb{R}_{\geq 0} \to \mathbb{R}$ denotes the desired position, designed to be sufficiently smooth (i.e., $q_d, \dot{q}_d, \ddot{q}_d \in \mathcal{L}_\infty$), and $\alpha \in \mathbb{R}_{>0}$ denotes a constant control gain. The open-loop cadence error system is obtained by taking the derivative of (5–2), multiplying by M, adding and subtracting e, and substituting (2–8), (5–1), and (5–2) to yield

$$M\dot{r} = \chi - B_M u_M - \tau_e - Vr - e, \tag{5–3}$$

where the lumped auxiliary signal $\chi : \mathbb{R}^2 \times \mathbb{R}_{\geq 0} \to \mathbb{R}$ is defined as $\chi \triangleq M(\ddot{q}_d + \alpha r - \alpha^2 e) + V(\dot{q}_d + \alpha e) + G + P + b_c(\dot{q}_d - r + \alpha e) + d + e$ and bounded by Properties 2.1-2.6 as $|\chi| \leq c_1 + c_2 \|z\| + c_3 \|z\|^2$, where c_1, c_2 $c_3 \in \mathbb{R}_{>0}$ are known constants, and the error vector $z \in \mathbb{R}^2$ is defined as $z \triangleq [e, r]^T$. Based on (5–3) and the subsequent stability analysis, the cadence controller is designed as [67]

$$u_M \triangleq \frac{1}{B_{\underline{M}}}\left(k_1 r + \left(k_2 + k_3\|z\| + k_4\|z\|^2\right)\mathsf{sgn}(r)\right), \tag{5–4}$$

where $k_i \in \mathbb{R}_{>0}$ $\forall i = 1, 2, ...,4$ denote constant control gains and $B_{\underline{M}}$ is introduced in Property 2.8. Substituting (5–4) into (5–3) yields the closed-loop cadence error system

$$M\dot{r} = \chi - \tau_e - Vr - e - \frac{B_M}{B_{\underline{M}}}\left(k_1 r + \left(k_2 + k_3\|z\| + k_4\|z\|^2\right)\mathsf{sgn}(r)\right). \tag{5–5}$$

5.1.2 Adaptive Admittance Control

While the rider's muscles regulate cadence, an admittance filter is employed to generate the admitted trajectory, given by

$$\tau - \tau_d \triangleq M_d\ddot{q}_a + B_d\dot{q}_a, \tag{5–6}$$

where τ_d : $\mathbb{R}_{\geq 0} \to \mathbb{R}$ denotes the desired bounded interaction torque, and τ : $\mathbb{R}_{\geq 0} \to \mathbb{R}$ denotes the bounded measurable interaction torque between the cycle and rider (i.e., $\tau \in \mathcal{L}_\infty$) [44, 56]. The filter's parameters, represented by the desired inertial and damping constants M_d, $B_d \in \mathbb{R}_{>0}$, respectively, are selected such that the transfer function of (5–6) is passive [63, Lemma 6.4] (i.e., q_a, $\dot{q}_a$ $\ddot{q}_a \in \mathcal{L}_\infty$); where q_a, $\dot{q}_a$, $\ddot{q}_a$: $\mathbb{R}_{\geq 0} \to \mathbb{R}$ denote the generated admitted position, velocity, and acceleration, respectively.

The primary goal of the admittance controller is to promote rider safety by injecting dynamics of the form in (5–6) that link the admitted trajectory to the desired trajectory. Therefore, while tracking a desired cadence, the most influential admittance parameter is the damping coefficient, B_d. Because damping is proportional to velocity or cadence, increasing the damping coefficient results in a less compliant admitted cadence trajectory and allows for less deviation from the desired cadence trajectory. A less compliant admitted cadence trajectory has repercussions that cascade through the cadence controller, such as reducing the cadence error and over time, position error (i.e., the integral of the cadence error), resulting in less rider stimulation. Consequently, the cadence controller requires more time to accumulate enough position/cadence error to yield sufficiently high stimulation to produce positive torque about the crankshaft. This effect can be compensated for by increasing the position gain in (5–2), which increases the emphasis on the position error inside the cadence controller in (5–4).

Moreover, the admitted cadence trajectory can be made more volatile by decreasing the desired inertia coefficient, M_d. Decreasing the inertia is analogous to removing mass from the system in that admitted trajectory is more susceptible to change. By selectively modifying the admittance parameters, the robot tracks an admitted cadence trajectory linked to the desired cadence trajectory through different dynamic relations of the form in (5–6). The admitted trajectory only evolves if there exists a nonzero value on the left side of (5–6); therefore, if the rider is able to generate the desired interaction

torque, the robot will not assist the rider in maintaining the desired cadence trajectory. Only if the rider falls short of the desired interaction torque does the assist-as-needed control paradigm take effect. Conversely, if the rider exceeds the desired interaction torque (such as is possible in volitional pedaling), the cycle will accelerate and enter a resist-as-needed paradigm to challenge the rider.

To track the admitted trajectory, an inner-loop position controller is designed to regulate the admittance error system, quantified by $\xi : \mathbb{R}_{\geq 0} \to \mathbb{R}$ and $\psi : \mathbb{R}_{\geq 0} \to \mathbb{R}$, and defined as

$$\xi \triangleq \Xi + q_d - q, \tag{5–7}$$

$$\psi \triangleq \dot{\xi} + \beta \xi, \tag{5–8}$$

where $\Xi : \mathbb{R} \to \mathcal{Q}$ represents a customizable continuously differentiable admitted position trajectory generated using the admittance filter in (5–6) (i.e., $\Xi = f(q_a)$), and $\beta \in \mathbb{R}_{>0}$ denotes a constant control gain. Although the admitted trajectory is generated on-line, it determines whether or not the pedals of the cycle act as if they are coupled or decoupled. That is, if both sides share the same admitted trajectory, symmetry is preserved, the pedals will appear to be coupled, and the two sides of the cycle will operate at the same cadence. Otherwise, each side will have a unique admitted trajectory, symmetry will be broken, the pedals will be uncoupled, and the two sides will operate at their own independent cadence. The motivation behind such a design is to establish a framework for which numerous trajectories can be investigated to best promote rehabilitation outcomes without modifying the developed controller. The open-loop admittance error system is generated by taking the time derivative of (5–8), multiplying by M, adding and subtracting ξ, and substituting (2–8), (5–7), and (5–8) to yield

$$M\dot{\psi} \;=\; Y\theta + \Upsilon - \tau_m - B_e u_e - \xi - V\psi, \tag{5-9}$$

$$Y\theta \;\triangleq\; M\left(\ddot{\Xi} + \ddot{q}_d + \beta\psi - \beta^2\xi\right) + V\left(\dot{\Xi} + \dot{q}_d + \beta\xi\right) + G + b_c\left(\dot{\Xi} + \dot{q}_d - \psi + \beta\xi\right), \tag{5-10}$$

where $Y \;:\; \mathbb{R}^2 \times \mathbb{R}_{\geq 0} \rightarrow \mathbb{R}^{1\times 8}$ denotes a computable regression matrix and by Property 5.1 is linear in the parameters; and $\theta \in \mathbb{R}^{8\times 1}$ denotes a matrix of constant system parameters. The lumped auxiliary signal $\Upsilon \;:\; \mathcal{Q} \times \mathbb{R} \times \mathbb{R}_{\geq 0} \rightarrow \mathbb{R}$ is defined as $\Upsilon \triangleq P + d + \xi$ and is bounded by Properties 2.1-2.6 as $|\Upsilon| \leq c_4 + c_5||\phi||$, where $c_4, \; c_5 \in \mathbb{R}_{>0}$ are known constants, and the error vectors $\phi \in \mathbb{R}^3$ and $\zeta \in \mathbb{R}^2$ are defined as $\phi \triangleq \left[\zeta^T, \; \dot{\Xi}\right]^T$ and $\zeta \triangleq [\xi, \; \psi]^T$, respectively. Based on (5–9) and the subsequent stability analysis, the admittance controller is designed as

$$u_e \;\triangleq\; \frac{1}{B_e}\left[Y\hat{\theta} + k_5\psi + (k_6 + k_7\,\|\phi\| + k_8\,|u_M|)\,\mathsf{sgn}\,(\psi)\right], \tag{5-11}$$

where $k_i \in \mathbb{R}_{>0} \;\forall i = 5, \; 6, \; ... \;, 8$ denote constant control gains, and $\hat{\theta} \;:\; \mathbb{R}_{\geq 0} \rightarrow \mathbb{R}^{8\times 1}$ denotes an estimate of the constant system parameters. Based on the subsequent stability analysis, the estimates for the system parameters in (5–10) are generated on-line according to

$$\dot{\hat{\theta}} \;\triangleq\; \mathsf{proj}\left(\Gamma Y^T \psi\right), \tag{5-12}$$

where $\Gamma \in \mathbb{R}^{8\times 8}$ denotes a constant positive definite learning gain, and proj$(\cdot)$ denotes a projection algorithm operator [119, Section 4.4]. Substituting (5–11) into (5–9) yields the closed-loop admittance error system

$$M\dot{\psi} \;=\; \Upsilon - \tau_m - V\psi - \xi + Y\tilde{\theta} - k_5\psi - \left[(k_6 + k_7\,\|\phi\| + k_8\,|u_M|)\,\mathsf{sgn}\,(\psi)\right]. \tag{5-13}$$

5.2 Stability Analysis

To facilitate the following theorems, let $W_L \; : \; \mathbb{R}^2 \rightarrow \mathbb{R}$ denote a continuously differentiable, positive definite storage function defined as

$$W_L \;\triangleq\; \frac{1}{2}Mr^2 + \frac{1}{2}e^2, \tag{5–14}$$

and let $V_L \; : \; \mathbb{R}^{10} \rightarrow \mathbb{R}$ denote a continuously differentiable, positive definite Lyapunov function candidate defined as

$$V_L \;\triangleq\; \frac{1}{2}M\psi^2 + \frac{1}{2}\xi^2 + \frac{1}{2}\tilde{\theta}^T\Gamma^{-1}\tilde{\theta}. \tag{5–15}$$

Theorem 5.1. *Given the closed-loop cadence error system in (5–5), when $q \in \mathcal{Q}_{FES}$, the cadence controller is passive from input $|\tau_e|$ to output $|r|$, $\forall t$, provided the following constant gain conditions are satisfied: $k_2 \geq c_1,\ k_3 \geq c_2,\ k_4 \geq c_3$, where $c_1,\ c_2,$ and c_3 are the bounding constants on χ in (5–3).*

Proof. Let $z \; : \; \mathbb{R}_{\geq 0} \rightarrow \mathbb{R}^2$ for $t \in [t_0,\ \infty)$ be a Filippov solution to the differential inclusion $\dot{z} \in K[h](z)$, where $K[\cdot]$ is defined as in [120], and where $h \; : \; \mathbb{R}^2 \rightarrow \mathbb{R}^2$ is defined as $h \triangleq \begin{bmatrix} \dot{e}, & \dot{r} \end{bmatrix}^T$. Because of the discontinuity in the muscle controller in (5–4), the time derivative of W_L exists almost everywhere (a.e.) (i.e., for almost all $t \in [t_0,\ \infty)$), and $\dot{W}_L(z) \overset{\text{a.e.}}{\in} \dot{\tilde{W}}_L(z)$, where $\dot{\tilde{W}}_L$ is the generalized time derivative of W_L along the Filippov trajectories of $\dot{z} = h(z)$ [121]. Using the calculus of $K[\cdot]$ from [121], and substituting (5–2) and (5–5) into $\dot{\tilde{W}}_L$ yields

$$\begin{aligned}
\dot{\tilde{W}}_L \;\subseteq\; &-\alpha e^2 + r\chi + \left(\frac{1}{2}\dot{M} - V\right)r^2 - \sum_{m \in \mathcal{M}} \frac{K\left[B_m\sigma_m\right]}{B_{\underline{M}}}\Big(k_1 r^2 + \\
&\left(k_2 + k_3\,\|z\| + k_4\,\|z\|^2\right)K\left[\text{sgn}(r)\right]r\Big) - r\tau_e, \tag{5–16}
\end{aligned}$$

where $K\left[B_m\sigma_m\right] \triangleq \{0,\ B_m\}$. For $q \in \mathcal{Q}_M$, $\sum_{m \in \mathcal{M}} K\left[B_m\sigma_m\right]$ is nonzero and may be bounded by Property 2.8 as $B_{\underline{M}}$, which is continuous. Hence, by Properties 2.1-2.7, and since $\dot{W}_L(z) \overset{\text{a.e.}}{\in} \dot{\tilde{W}}_L(z)$, (5–16) can be bounded as

$$\dot{W}_L \overset{\text{a.e.}}{\leq} -\alpha e^2 - k_1 r^2 - \lambda_1 |r| - \lambda_2 |r| \, \|z\| - \lambda_3 |r| \, \|z\|^2 + |r| \, |\tau_e|, \qquad (5\text{--}17)$$

where $\lambda_1, \ \lambda_2, \ \lambda_3 \in \mathbb{R}$ are defined as $\lambda_1 \triangleq k_2 - c_1$, $\lambda_2 \triangleq k_3 - c_2$, and $\lambda_3 \triangleq k_4 - c_3$. Provided the gain conditions in Theorem 5.1 are satisfied, $\lambda_1, \ \lambda_2, \ \lambda_3 \geq 0$; thus, (5–17) can be bounded further as

$$\dot{W}_L \overset{\text{a.e.}}{\leq} -\alpha e^2 - k_1 r^2 + |r| \, |\tau_e|. \qquad (5\text{--}18)$$

Because the interaction torque is bounded, from the perspective of the rider, the physically applied motor torque is similarly bounded [44, 56]. Hence, by [63, Definition 6.3] the cadence error system is output strictly passive with input $|\tau_e|$, output $|r|$, and storage function W_L, and the cadence controller is bounded (i.e., $u_M \in \mathcal{L}_\infty$). $\qquad \square$

Remark 5.1. Although the above analysis does not include volitional contribution from the rider, a common assumption in human-robot interaction is that the human is naturally passive [10]. If the rider volitionally contributes, the cadence controller and rider would act in parallel. Because passive systems in parallel remain passive [63], volitional contributions would not affect $|r|$ being output strictly passive with respect to $|\tau_e|$. Hence, the rider is able to volitionally contribute towards the tracking objective without destabilizing the cadence error system.

Theorem 5.2. *Given the closed-loop error system in (5–13) and the admittance relationship in (5–6), the admittance controller is proven to globally asymptotically regulate the error in the sense that $\zeta \triangleq \begin{bmatrix} \xi, & \psi \end{bmatrix}^T \to 0$ as $t \to \infty$, provided the following constant gain conditions are satisfied: $k_6 \geq c_4, \ k_7 \geq c_5, \ k_8 \geq B_{\overline{M}}$, where c_4 and c_5 are the bounding constants on Υ in (5–9), and $B_{\overline{M}}$ was introduced in Property 2.8.*

Proof. Using an argument similar to the proof for Theorem 5.1, the time derivative of (5–15) can be bounded above using (5–8), (5–13), and Properties 2.1-2.7, and 2.8 as

$$\dot{V}_L \overset{\text{a.e.}}{\leq} -\beta \xi^2 - k_5 \psi^2 - |\psi| \left(\lambda_4 + \lambda_5 \|\phi\| + \lambda_6 |u_M| \right), \qquad (5\text{--}19)$$

where $\lambda_4,\ \lambda_5,\ \lambda_6 \in \mathbb{R}$ are defined as $\lambda_4 \triangleq k_6 - c_4$, $\lambda_5 \triangleq k_7 - c_5$, and $\lambda_6 \triangleq k_8 - B_{\overline{M}}$. Provided the gain conditions listed in Theorem 5.2 are satisfied, $\lambda_4,\ \lambda_5,\ \lambda_6 \geq 0$, thus (5–19) can be upper bounded as

$$\dot{V}_L \overset{\text{a.e.}}{\leq} -\beta\xi^2 - k_5\psi^2. \tag{5–20}$$

Hence, (5–15) is a common Lyapunov function across both the FES and KDZ regions. Subsequently, [135] can be invoked, along with the radially unboundedness of (5–15), to show $|\xi|,\ |\psi|,\ \|\zeta\| \to 0$ as $t \to \infty$. Since $V_L > 0$ and $\dot{V}_L \overset{\text{a.e.}}{\leq} 0$, $V_L \in \mathcal{L}_\infty$, hence, $\xi,\ \psi,\ \tilde{\theta} \in \mathcal{L}_\infty$, which implies $\dot{q},\ \hat{\theta} \in \mathcal{L}_\infty$. Since (5–6) is passive, $\dot{q}_a,\ \ddot{q}_a \in \mathcal{L}_\infty$, which implies $Y,\ \|\phi\| \in \mathcal{L}_\infty$. Finally, because $u_M \in \mathcal{L}_\infty$ by Theorem 5.1, $u_e \in \mathcal{L}_\infty$. $\qquad\square$

5.3 Experiments

5.3.1 Experimental Testbed

The experimental testbed used in this chapter is the split-crank FES cycle, introduced in Chapter 2.

5.3.2 Experimental Methods

Experiments were conducted on one able-bodied male participant, aged 26 years old (P1), one male participant with spina bifida, aged 25 years old (P2), one female participant with post-stroke right-sided hemiparesis, aged 50 years old (P3), and one male participant with Parkinson's disease, aged 64 years old (P4). P2 has spina bifida (L5-S1) with an Arnold Chiari malformation and regularly participates in physical therapy; he uses ankle-foot orthoses and a wheelchair, and is familiar with FES. P3 had her stroke in 2014 and is community ambulatory without aid; she has regained some function in her right leg though this was her first experience with FES cycling. P4 was diagnosed with Parkinson's in 1997 and regularly participates in physical therapy and exercise; although he had noticeable tremor in both arms, his right arm had larger magnitude. Two primary protocols were conducted, Protocol A

which implemented the controllers in (5–4) and (5–11), and Protocol B which also implemented the controllers in (5–4) and (5–11), but with the adaptive feedforward component disabled (i.e., $\Gamma = 0$). Participants 1-4 completed both Protocols A and B in random order, with P1 receiving stimulation only on the quadriceps muscle group for proof of concept, and P2-P4 receiving stimulation on the quadriceps, hamstrings, and gluteals muscle groups. To investigate the effect of adding volition, P4 was asked to repeat Protocol A with volition, denoted by Protocol C. Each protocol had a total duration of 180 seconds, with the first 20 seconds consisting of a smooth motor-only ramp to the desired cadence of 50 RPM. After the initial ramp, the controllers in (5–4) and (5–11) were switched on and errors were recorded. For all protocols except Protocol C, the participants were blind to the desired trajectories for the duration of the experiment. The experimental protocols were approved by the Institutional Review Board at the University of Florida (IRB201600881). For all experiments, the admittance parameters in (5–6) were selected as $B_d = 1 \frac{Nm \cdot s}{rad}$, $M_d = 2 \frac{Nm \cdot s^2}{rad}$, $\tau_d = 0.5$ Nm for P1, $\tau_d = 0.2$ Nm for P2, $\tau_d = 0.3$ Nm for P3, and $\tau_d = 0.2$ Nm for P4. The controller gains in (5–2), (5–4), (5–8), (5–11), and (5–12) were selected as $k_1 \in [3.0, \ 5.5]$, $k_2 = k_3 = k_4 = 0.1$, $k_5 \in [5.0, \ 10.0]$, $k_6 = k_7 = k_8 = k_9 = 0.001$, $\alpha \in [2.0, \ 3.5]$, $\beta \in [0.1, \ 0.2]$, and $\Gamma = 0.1 \cdot \text{diag} \left(3.15, \ 3.15, \ 1.05, \ 2.10, \ 5.25, \ 5.25, \ 1.05, \ 0.63 \right)$.

The admitted trajectory in the error system in (5–7) and (5–8) was generated using $\Xi \triangleq \frac{1}{2} \left(q_{a,L} + q_{a,R} \right)$, where $q_{a,x} \ : \ \mathbb{R}_{\geq 0} \to \mathbb{R}$, $\forall x \in \mathcal{X} \triangleq \{L, \ R\}$ represent the trajectories generated using the admittance filter in (5–6) for the left and right side of the cycle, respectively. The motivation behind the admitted trajectory being an average of the two sides is to synchronize the positions and cadences of each side so the natural coordination of the legs is preserved. This trajectory strikes a dynamic balance between the capabilities of both legs instead of holding the legs to a standard which they may be incapable of reaching (e.g., having a non-dominant leg track the trajectory generated from a dominant leg); instead the trajectory is set to the average capabilities of the

legs, such that the more capable leg experiences resistance and the less capable leg experiences assistance. However, many different trajectories could be selected, with potential clinical differences. For example, the results in [81] suggest that lower cadences may be optimal for strength training, but higher cadences may be best for power training.

5.3.3 Results and Discussion

For the following sections, let participants and protocols be referred to by their respective number and letter; for example, Participant 1 running Protocol B would be referred to as P1B. Numerical results for Protocols A and B are displayed in Table 5-1 with details on the average and standard deviation of the measured cadence, admitted cadence, admitted cadence tracking error, motor control input, and measured torque for each leg. As shown in Table 5-1, the average cadences for each leg (i.e., $\dot{q}_x$, $\forall x \in \mathcal{X}$) were similar with adaptation enabled and disabled. However, with adaptation, the standard deviation of the admitted tracking error was reduced by an average of 75% for P1, 19% for P2, 47% for P3, and 50% for P4. Adaptation resulted in a reduction in the average motor control effort by 15% for P1, 3% for P2, 4% for P3, and 15% for P4.

Table 5-1. Experimental results, reported as average±standard deviation

Partic.	Protocol	$\dot{q}_L$ (RPM)*	$\dot{q}_R$ (RPM)*	$\dot{q}_\alpha$ (RPM)†	$\dot{\xi}_L$ (RPM)	$\dot{\xi}_R$ (RPM)	$u_{e,L}$ (A)	$u_{e,R}$ (A)	τ_L (Nm)	τ_R (Nm)
1	A	49.03±1.73	48.92±1.16	48.80±0.84	-0.23±1.64	-0.13±0.94	-2.42±4.64	1.98±4.69	0.20±3.70	0.15±3.51
	B	47.70±4.90	47.63±5.18	47.58±0.91	-0.13±5.33	-0.05±4.67	-2.59±4.89	2.55±5.35	0.00±3.68	-0.27±3.60
2	A	49.00±1.60	48.98±1.52	48.89±0.09	-0.11±1.60	-0.10±1.53	-2.32±2.73	2.09±2.97	-0.13±1.54	-0.05±1.60
	B	48.63±2.06	48.58±1.78	48.60±0.39	-0.03±1.87	0.30±1.97	-2.38±2.13	2.15±2.63	-0.19±1.55	-0.08±1.55
3	A	48.87±1.40	48.82±1.31	48.74±0.27	-0.13±1.40	-0.09±1.26	-1.97±2.94	2.20±3.01	0.22±2.33	-0.09±2.20
	B	48.50±2.75	48.46±2.43	48.43±0.37	-0.08±2.73	-0.03±2.39	-1.99±3.12	2.37±3.25	0.17±2.33	-0.20±1.95
4	A	49.91±1.46	49.81±2.41	49.72±0.84	-0.19±1.52	-0.09±2.16	-1.91±3.77	2.35±5.15	0.17±2.56	0.07±4.04
	B	49.65±3.68	49.53±4.02	49.51±0.86	-0.14±3.65	-0.03±3.81	-2.21±4.08	2.59±5.03	-0.03±2.49	-0.17±4.10
	C	50.26±1.73	50.16±2.70	49.94±0.83	-0.20±1.87	-0.10±2.40	-1.46±4.11	2.10±5.43	0.36±2.70	0.66±4.37
Mean‡	A	49.20±1.79	49.13±1.93	49.03±0.70	-0.16±1.78	-0.10±1.77	-2.15±4.15	2.15±4.70	0.11±3.05	0.02±3.46
	B	48.62±4.05	48.55±4.16	48.53±0.78	-0.09±4.19	0.04±3.91	-2.29±4.27	2.41±4.87	-0.01±3.03	-0.18±3.46

*At steady state, the average cadence error is given as $\dot{e}_x = 50 - \dot{q}_x, \ \forall x \in \mathcal{X}$.

†$\dot{q}_\alpha \ : \ \mathbb{R}_{\geq 0} \to \mathbb{R}$ denotes the average admitted cadence given as $\dot{q}_\alpha \triangleq \dot{q}_d + \frac{1}{2} (\dot{q}_{a,L} + \dot{q}_{a,R})$, identical for both legs.

‡Protocol C was not included in calculating the mean.

Graphical results for P1-P4 running Protocol A are provided in Figures 5-1-5-10. Figures 5-1, 5-3, 5-5, and 5-7 depict the cadence tracking results along with the root-mean-square (RMS) (windowed at 0.5 seconds) values of $\dot{\xi}$ and $\dot{e}$ for P1A, P2A, P3A, and P4A, respectively. Figures 5-2, 5-4, 5-6, and 5-8 illustrate the control inputs to the cycle's motors and rider's muscle groups for P1A, P2A, P3A, and P4A, respectively. For visual clarity, a half-second moving average filter was applied to all plots displaying measured cadences and motor control inputs (i.e, $\dot{q}_L$, $\dot{q}_R$, u_e). To directly compare results with and without adaptation, Figures 5-9 and 5-10 are included for P4B, which display the cadence tracking results and control inputs, respectively. To examine the effects of the rider volitionally pedaling alongside the admittance and cadence controllers, Figures 5-11 and 5-12 display P4C, which is Protocol A with added volition.

Across all participants, adding adaptation to the admittance controller resulted in significant improvement in the cadence tracking performance in terms of the average cadence error and standard deviation. While adding adaptation increased the average admittance cadence error to -0.13 RPM from -0.02 RPM without adaptation, it reduced the standard deviation of the admitted cadence error from 4.05 RPM without adaptation to 1.78 RPM with adaptation. Reducing the standard deviation of the measured cadence results in smoother cycling performance and more comfortable stimulation for the rider. By examining the results of P1, the effects of adaptation are evident; in Figure 5-1 the RMS value of $\dot{\xi}$ decreases steadily for the first 20 seconds after controller activation. Additionally, as the stimulation input increases, the rider produces more torque and is able to contribute more towards the cadence tracking objective (compare Figures 5-1 and 5-2). Furthermore, as the admittance controller adapts and the rider produces more torque, the motor control effort is notably reduced through the experiment, as shown in Figure 5-2. As the experiment progresses and the rider requires more stimulation to produce torque about the crank, due to the rider's comfort threshold, the stimulation input is saturated. To avoid this case of actuator saturation, the desired torque trajectory
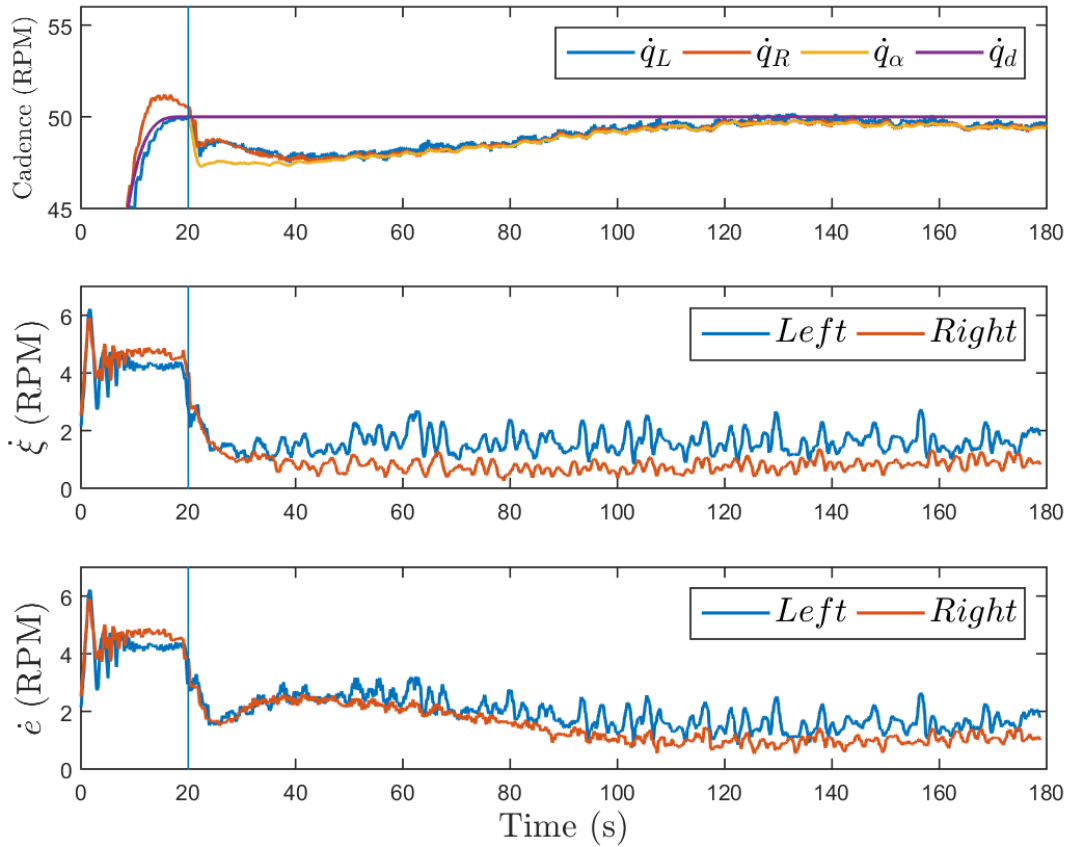
Figure 5-1. P1A (Top) The measured cadence for the left ($\dot{q}_L$) and right ($\dot{q}_R$) leg, admitted cadence ($\dot{q}_a$), and desired cadence ($\dot{q}_d$); (Middle) RMS error of $\dot{\xi}$ for the left and right legs; and (Bottom) RMS error of $\dot{e}$ for the left and right legs. Vertical lines represent the time of controller activation.
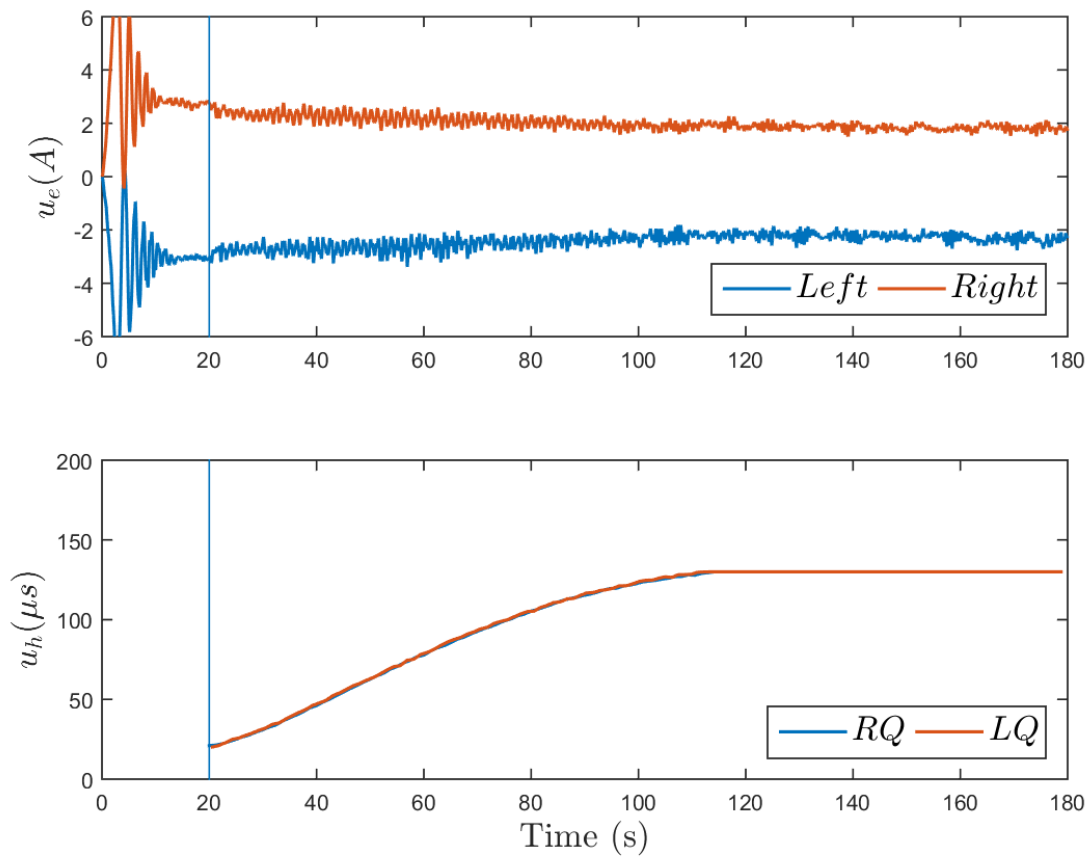
Figure 5-2. P1A (Top) Control inputs to left and right motors and (Bottom) control inputs to the rider's quadriceps femoris muscle groups for the left and right legs. The stimulation input was saturated at 130μs for rider comfort.
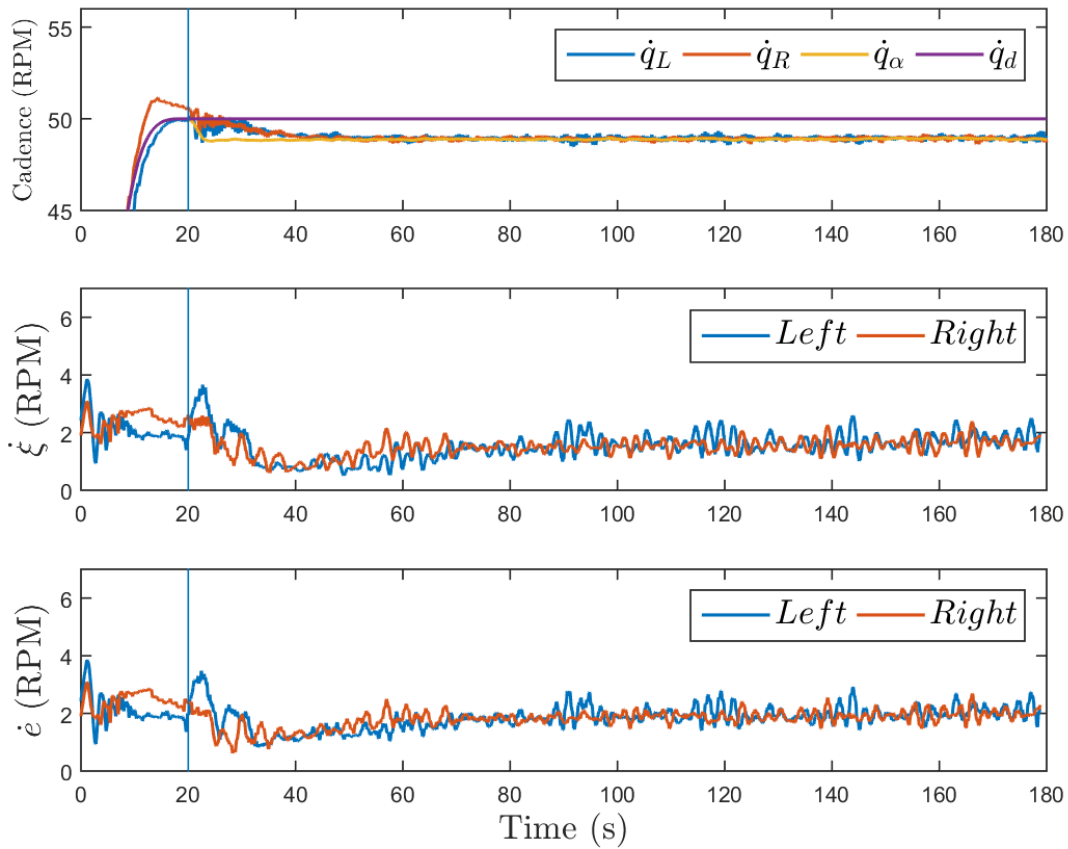
Figure 5-3. P2A (Top) The measured cadence for the left ($\dot{q}_L$) and right ($\dot{q}_R$) leg, admitted cadence ($\dot{q}_a$), and desired cadence ($\dot{q}_d$); (Middle) RMS error of $\dot{\xi}$ for the left and right legs; and (Bottom) RMS error of $\dot{e}$ for the left and right legs.
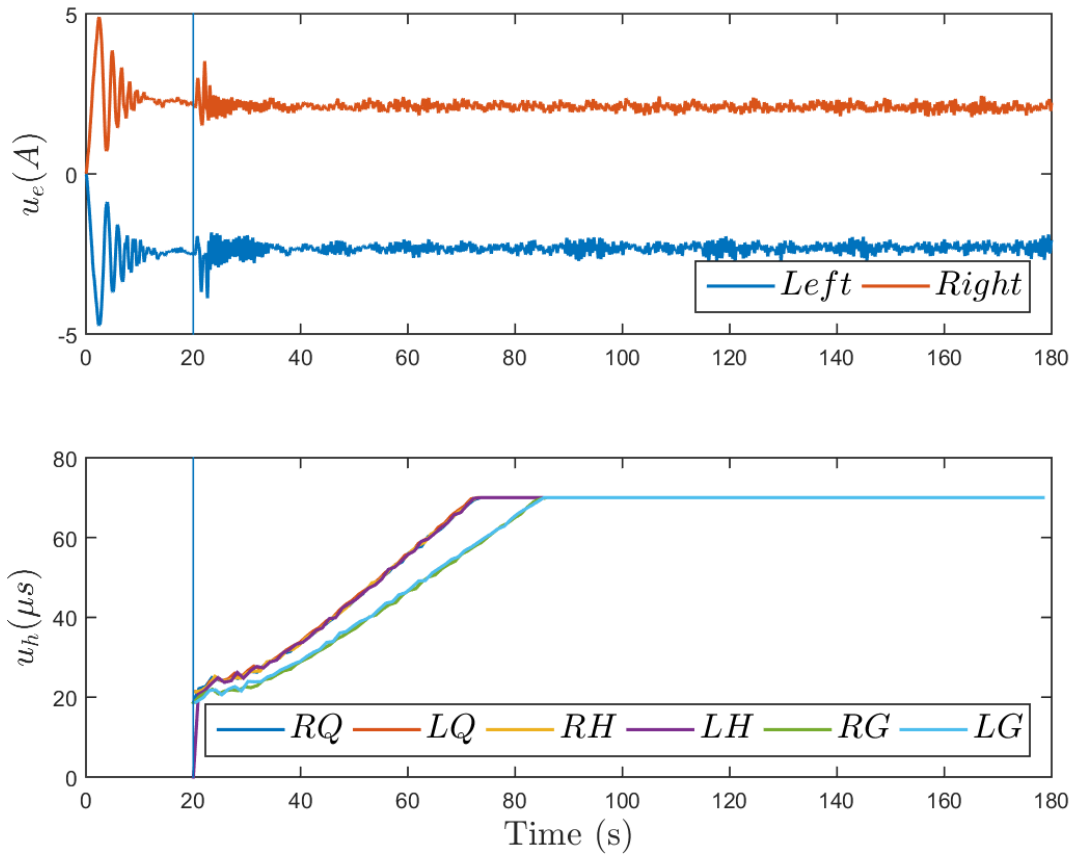
Figure 5-4. P2A (Top) Control inputs to left and right motors and (Bottom) control inputs to the rider's right (R) and left (L) quadriceps (Q), hamstring (H), and gluteal (G) muscle groups. The stimulation input was saturated at 65μs for rider comfort.
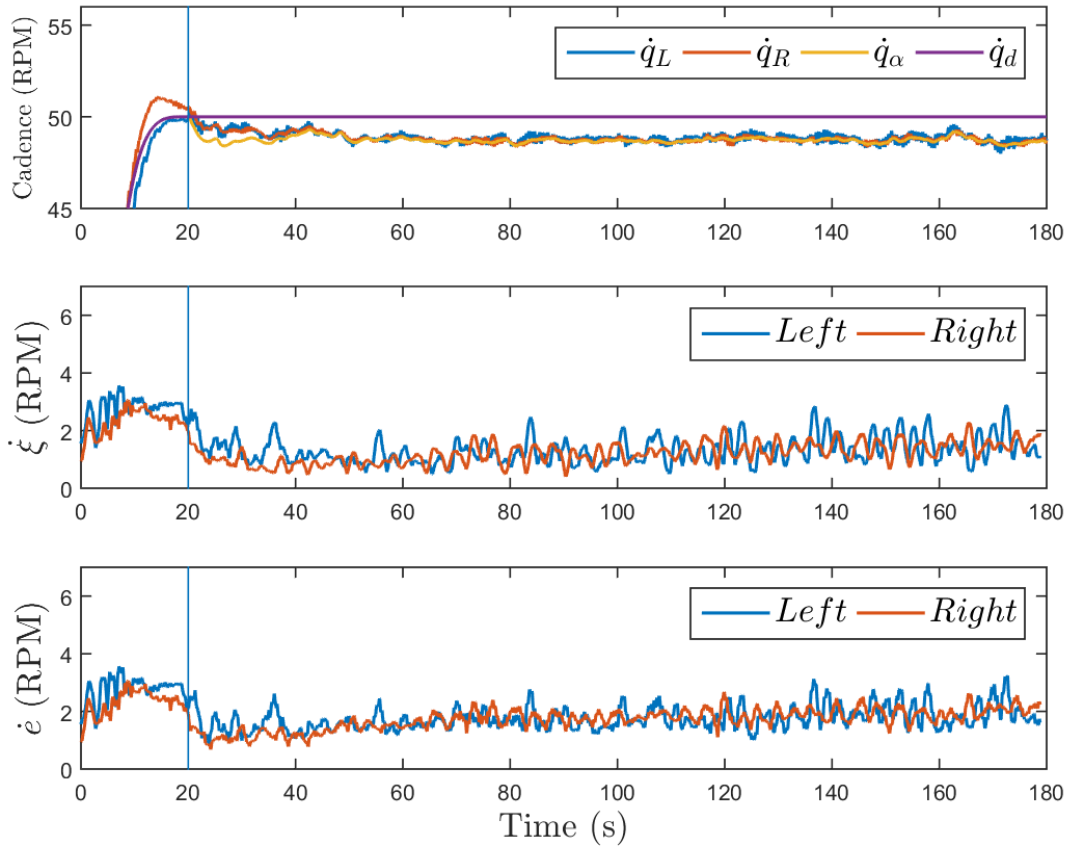
Figure 5-5. P3A (Top) The measured cadence for the left ($\dot{q}_L$) and right ($\dot{q}_R$) leg, admitted cadence ($\dot{q}_a$), and desired cadence ($\dot{q}_d$); (Middle) RMS error of $\dot{\xi}$ for the left and right legs; and (Bottom) RMS error of $\dot{e}$ for the left and right legs.
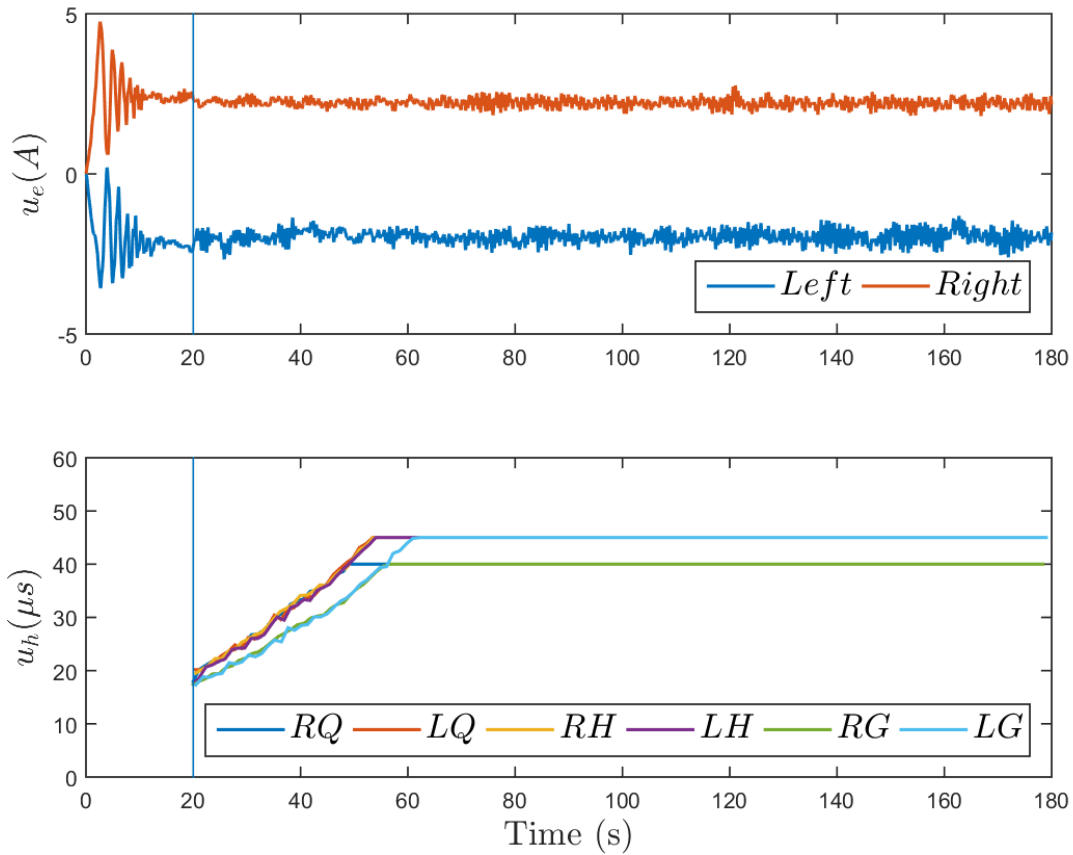
Figure 5-6. P3A (Top) Control inputs to left and right motors and (Bottom) control inputs to the rider's right (R) and left (L) quadriceps (Q), hamstring (H), and gluteal (G) muscle groups. The stimulation input was saturated at 40μs for the right hamstring and gluteal and 45 μs for all other muscle groups.
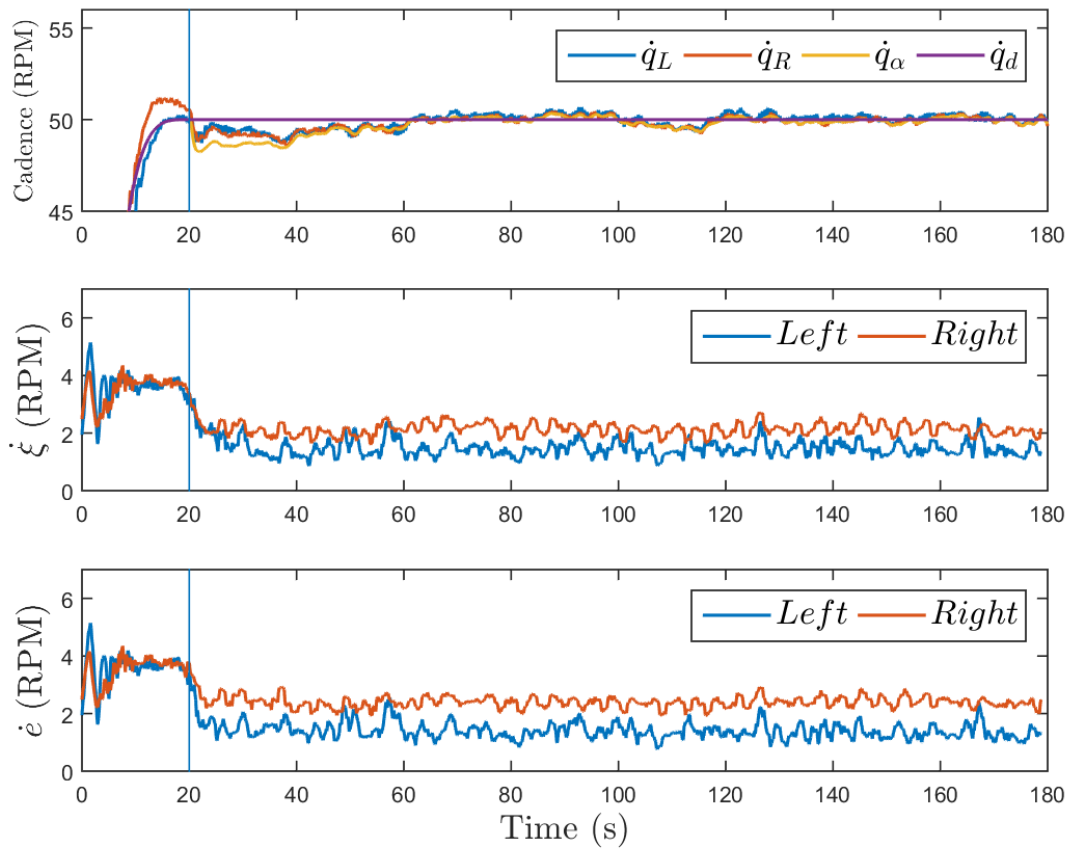
Figure 5-7. P4A (Top) The measured cadence for the left ($\dot{q}_L$) and right ($\dot{q}_R$) leg, admitted cadence ($\dot{q}_a$), and desired cadence ($\dot{q}_d$); (Middle) RMS error of $\dot{\xi}$ for the left and right legs; and (Bottom) RMS error of $\dot{e}$ for the left and right legs.
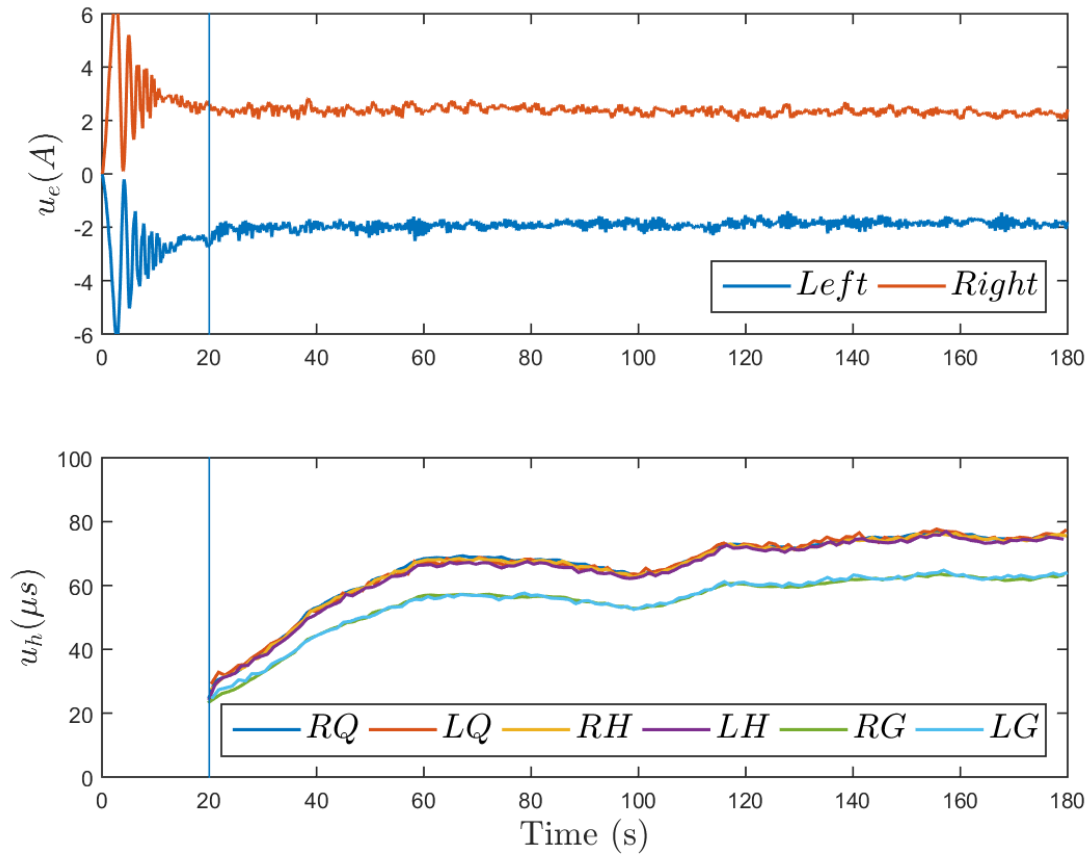
Figure 5-8. P4A (Top) Control inputs to left and right motors and (Bottom) control inputs to the rider's right (R) and left (L) quadriceps (Q), hamstring (H), and gluteal (G) muscle groups. The stimulation input was saturated at 100μs for rider comfort.
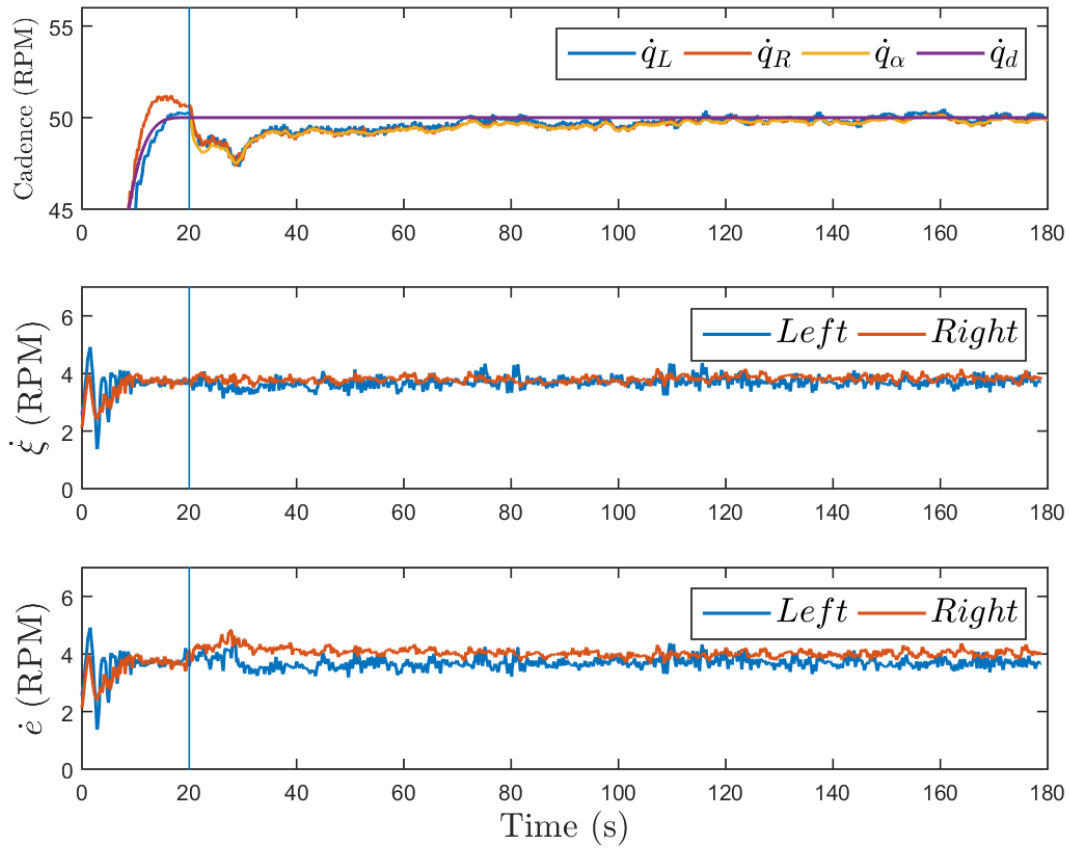
Figure 5-9. P4B (Top) The measured cadence for the left ($\dot{q}_L$) and right ($\dot{q}_R$) leg, admitted cadence ($\dot{q}_a$), and desired cadence ($\dot{q}_d$); (Middle) RMS error of $\dot{\xi}$ for the left and right legs; and (Bottom) RMS error of $\dot{e}$ for the left and right legs.
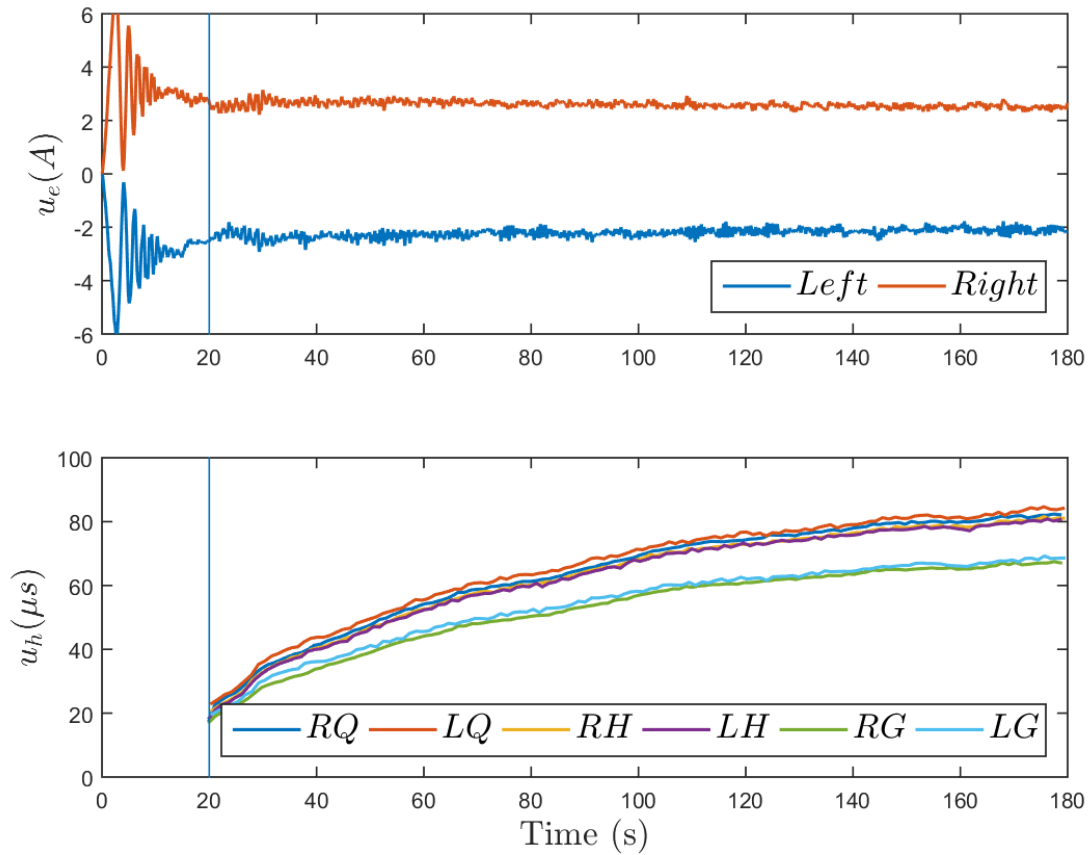
Figure 5-10. P4B (Top) Control inputs to left and right motors and (Bottom) control inputs to the rider's right (R) and left (L) quadriceps (Q), hamstring (H), and gluteal (G) muscle groups. The stimulation input was saturated at 100μs for rider comfort.
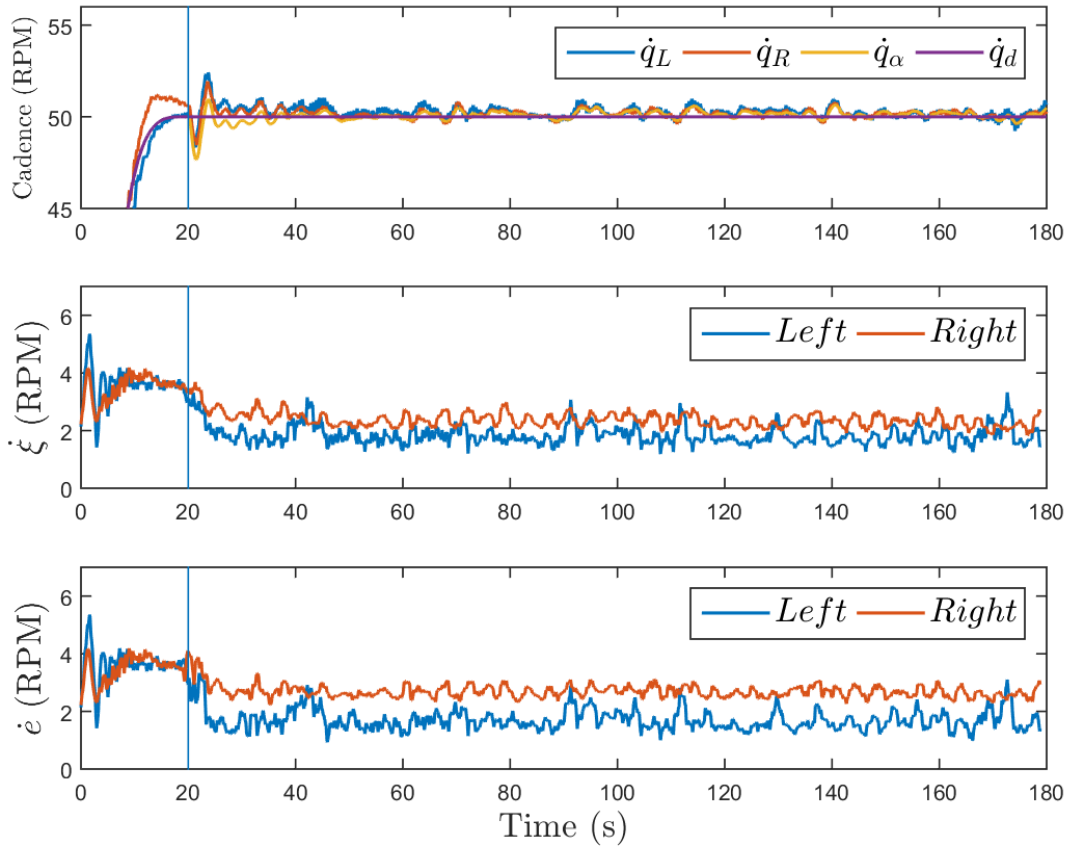
Figure 5-11. P4C (Top) The measured cadence for the left ($\dot{q}_L$) and right ($\dot{q}_R$) leg, admitted cadence ($\dot{q}_a$), and desired cadence ($\dot{q}_d$); (Middle) RMS error of $\dot{\xi}$ for the left and right legs; and (Bottom) RMS error of $\dot{e}$ for the left and right legs.
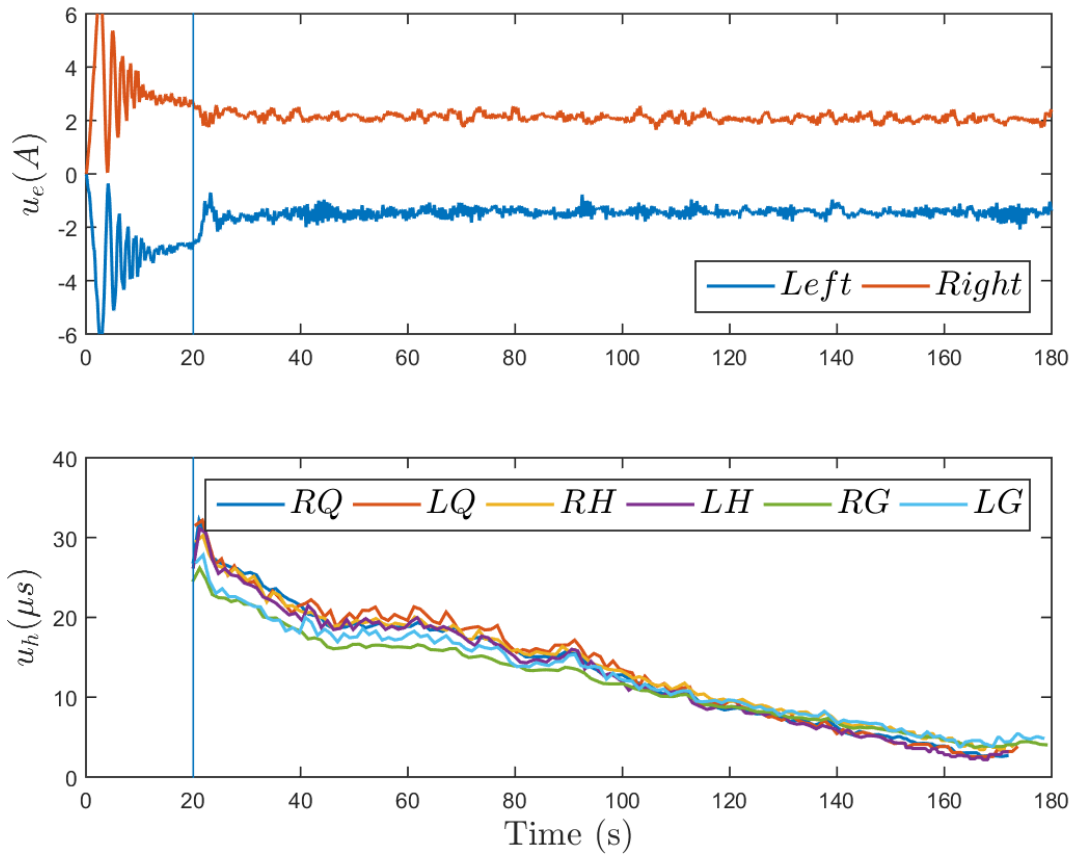
Figure 5-12. P4C (Top) Control inputs to left and right motors and (Bottom) control inputs to the rider's right (R) and left (L) quadriceps (Q), hamstring (H), and gluteal (G) muscle groups. The stimulation input was saturated at 100μs for rider comfort.

can be reduced to lessen the amount of interaction torque between the cycle and the rider, or the position gain αcan be reduced to prevent the rapid accumulation of the position error term in the auxiliary error system denoted by r. Actuator saturation results in the rider not being able to achieve the desired cadence, but due to the admittance controller on the cycle's motor, the rider is assisted in maintaining a nonzero cadence.

When comparing P2 to P1, it is noted P2 had a lower stimulation limit and experienced fatigue at a quicker rate, despite all muscle groups being stimulated. The low stimulation limit made the experiments of P2A and P2B appear very similar in nature (i.e., with and without adaptation), except the adaptation resulted in smoother cadence tracking/performance. Due to adaptation of the motor controller, it can be seen in Figure 5-3 that the RMS value of $\dot{\xi}$ was reduced over the course of the experiment, despite only a subtle reduction in the motor control effort as depicted in Figure 5-4. Because P2's stimulation was saturated early in the experiment, he was unable to achieve the desired cadence at the desired interaction torque. However, because the admittance controller held the admitted cadence trajectory near the desired cadence trajectory, the robot assisted the rider in maintaining his cadence. This exemplifies the assist-as-needed control paradigm. Without the admittance controller, the rider would have been unable to maintain cycle motion. Because the cadence controller is passive and the admittance controller demonstrates asymptotic tracking, the FES-cycle exemplifies stable performance through the remaining portion of the experiment. Although P2 has spina bifida, the cycle detected no notable asymmetries in performance.

P3 presented a strong sensitivity to stimulation, and thus, the amount of stimulation that could be applied (and hence torque contribution) was kept to a minimum. Like P2, P3's stimulation was saturated early in the experiment, however, the cycle was still able to adapt and asymptotically track the admittance error system. According to Table 5-1, her unimpaired leg (left) generated more torque than her impaired leg (right) and both legs demonstrated improved tracking performance with adaptation enabled.

131

Figure 5-5 depicts cadence tracking performance and Figure 5-6 depicts the control efforts for P3A. Despite the fact that P3's stimulation was saturated early in experiments, it allowed for the most powerful contractions to be elicited from the stimulation, and consequently, the best tracking possible. From a rehabilitation perspective, however, there exist outstanding questions as to best balance stimulation levels with functional improvements.

To directly examine the effects of adding adaptation to the admittance controller, Figures 5-7 and 5-8 display the tracking results and control inputs with adaptation enabled for P4 and Figures 5-9 and 5-10 display the tracking results and control inputs with adaptation disabled for P4. By directly comparing Figure 5-7 to 5-9, it can be seen that immediately after controller activation, the RMS admittance and cadence tracking errors decayed to nearly half their pre-activation values when adaptation was enabled. Although the adaptation only occurs on the robot, because the robot and the rider are physically coupled, improved performance from the admittance controller yielded improved performance from the cadence controller. One controller is able to bolster the capabilities of the other, provided they are coupled. This effect is significant because of the challenges when adding adaptation to the cadence controller due to the unknown, nonlinear muscle control effectiveness; hence, adaptation can be added to the robot's controller to improve performance of the cadence controller applied to the rider's muscles. Because P4 did not reach his stimulation limit in either protocol (see Figures 5-8 and 5-10), this indicates he was able to produce the desired interaction torque and align the admitted cadence trajectory with the desired cadence trajectory (shown in Figures 5-7 to 5-9).

To compare the effect of adding rider volition alongside the admittance and cadence controllers, Protocol C was run on P4. As evidenced by the reduction in tracking errors (as seen previously in Figure 5-7), the admittance controller was able to adapt alongside the rider. As displayed by Table 5-1, however, the controllers outperformed at tracking

the desired trajectories than the rider was able to with volition while monitoring his performance. In contrast, the rider was able to generate a larger interaction torque when volition was included. Because the rider was able to track the desired cadence trajectory accurately and quickly (i.e., the stimulation did not require error accumulation to ramp up), the rider's stimulation was kept well below his saturation threshold. According to Table 5-1, P4 surpassed the desired interaction torque, and consequently, the cycle accelerated (while resisting the rider). Furthermore, because the rider was able to reduce the position and cadence errors, the rider's stimulation was withdrawn (see Figure 5-12). Hence, it is shown that if the rider is able to regulate the errors with volition, stimulation is not necessary.

It is important to note that the saturation of the stimulation input (i.e., the cadence controller) does not compromise the performance of the cycle. Regardless of saturation, the admittance controller applied to the cycle's motors asymptotically tracks the admittance error system for all time. Because of the admittance filter, if the rider's muscles are unable to produce the desired interaction torque per the applied stimulation, the cycle decelerates to accommodate the rider and enters the assist-as-needed modality. By manipulating the desired interaction torque and the parameters in (5–6), the cycle's performance can be drastically changed; the interested reader can refer to [111] for additional details. Whether the participant was able-bodied (P1), had a ND with no asymmetry (P2/P4), or had a ND with asymmetry (P3), the combined cadence-admittance controllers applied to the split-crank FES-cycle illustrated stable performance with adaptation improving the tracking results and reducing oscillations (i.e., the standard deviation). The split-crank FES-cycle offers a novel method to treat and manage movement disorders, with particular emphasis on asymmetries or hemiparesis, while preserving rider safety.

5.4 Concluding Remarks

This chapter seeks to improve upon the controllers presented in Chapter 4 by adding adaptation to the admittance controller implemented on the cycle's motor. Additionally, to accommodate for asymmetric rider capabilities (as in post-stroke hemiparesis), the cycle's crank is severed and the cycle's pedals are decoupled. Consequently, the cycle is instrumented with an additional motor, encoder, powermeter, and chain to establish feedback and control authority on both sides of the cycle. The muscles of each leg of the rider are tasked with maintaining the cycle's cadence on their respective sides and each motor is controlled using a separate admittance controller. Using a passivity-based stability analysis, it is shown that rider volition does not destabilize the error systems. When implemented, the admitted trajectory is generated online by averaging the output torques between the two sides such that the pedals are kept at an offset of 180 degrees, maintaining the natural symmetry of cycling. If the rider demonstrates hemiparesis, the stronger leg will experience resistance and the weaker leg will experience assistance such that the two pedals are held in phase. Experiments are conducted on one able-bodied participant and three participants with neuromuscular disorders to compare the effect of adding adaptation to the cycle. Results indicate significant improvement in various performance metrics with the use of adaptation. Specifically, with adaptation, the cadence error was reduced by 41%, the cadence standard deviation was reduced by 57%, the control input to the motors was reduced by 9%, and the pedal phase error was reduced by 41% to an average difference of 174°. Compared to other works on split-crank cycling (cf. [92,93,136]), this chapter develops a combined stable cadence/admittance controller to simultaneously actuate the FES cycle using the cycle's electric motor and torque arising from the rider's muscles elicited by FES. Furthermore, using the developed adaptive admittance controller on a split-crank FES cycle allows for the implementation of highly customizable rehabilitation strategies to target and address rider asymmetries.

CHAPTER 6
CYCLING WITH FUNCTIONAL ELECTRICAL STIMULATION AND NEUROADAPTIVE ADMITTANCE CONTROL

This chapter is designed to improve upon the adaptive admittance controller developed in Chapter 5. The controller is modified with the addition of a neural network to estimate the control effectiveness of the rider's muscles and more accurately track the admitted trajectory. While the neural network is shaped according to the anticipated rider output torque curve, the admittance controller employs a gradient adaptive feedforward term. As in Chapter 5, the rider's muscles are assigned to regulate the cycle's cadence. A stability analysis is conducted and proves the admittance controller globally asymptotically regulates the admittance error system and the cadence controller is passive with respect to the motor. Merging a passive muscle stimulation controller with an asymptotically stable adapting NN admittance controller allows for accurate control of the motorized FES cycle while preserving rider comfort and safety. The designed controller is validated through experiments conducted on one able-bodied participant and four participant with NDs (spina bifida, spinal cord injury, Parkinson's disease, and drug-induced Parkinsonism). Experiments indicate the proposed controller offers improved performance with the feedforward adaptive compensation terms when compared to the same feedback only controller in three of the five participants. The average admittance cadence error is -0.07 ± 1.10 RPM with adaptation and -0.10 ± 1.18 RPM without adaptation.

6.1   Control Development

In the following section, two controllers are developed, a robust sliding-mode cadence controller for the rider's muscles and an adaptive neural network admittance controller for the cycle's motor.

6.1.1   Robust Cadence Control

Although the cadence controller has the same form as in [67], a new stability analysis is required (see Section 6.2) because a new objective is presented (i.e.,

admittance tracking). For clarity, the cadence tracking errors and the controller are presented here. The cycle's cadence is regulated using the rider's muscles in the FES regions and quantified by the tracking errors $e : \mathbb{R}_{\geq 0} \to \mathbb{R}$ and $r : \mathbb{R}_{\geq 0} \to \mathbb{R}$, each defined as

$$e \triangleq q_d - q, \tag{6–1}$$

$$r \triangleq \dot{e} + \alpha e, \tag{6–2}$$

where $q_d : \mathbb{R}_{\geq 0} \to \mathbb{R}$ denotes the desired position, designed to be sufficiently smooth (i.e., $q_d, \dot{q}_d, \ddot{q}_d \in \mathcal{L}_\infty$), and $\alpha \in \mathbb{R}_{>0}$ denotes a selectable constant control gain. The open-loop cadence error system is obtained by taking the derivative of (6–2), multiplying by M, adding and subtracting e, and substituting (2–8), (2–9), (6–1), and (6–2) to yield[1]

$$M\dot{r} = \chi_1 - B_M u_M - \tau_e - Cr - e, \tag{6–3}$$

where the lumped auxiliary signal $\chi_1 : \mathbb{R}^2 \times \mathbb{R}_{\geq 0} \to \mathbb{R}$ is defined as $\chi_1 \triangleq M(\ddot{q}_d + \alpha r - \alpha^2 e) + C(\dot{q}_d + \alpha e) + G + P + b_c(\dot{q}_d - r + \alpha e) + d + e$ and bounded by Properties 2.1-2.6 as $|\chi_1| \leq c_1 + c_2 \|z\| + c_3 \|z\|^2$, where $c_1, c_2\ c_3 \in \mathbb{R}_{>0}$ are known constants, and the error vector $z \in \mathbb{R}^2$ is defined as $z \triangleq [e\ r]^T$. Based on (6–3) and the subsequent stability analysis, the cadence controller is designed as

$$u_M = \frac{1}{B_{\underline{M}}}\left(k_1 r + \left(k_2 + k_3 \|z\| + k_4 \|z\|^2\right)\mathsf{sgn}(r)\right), \tag{6–4}$$

where $k_i \in \mathbb{R}_{>0}\ \forall i = 1,\ 2,\ 3,\ 4$ denote constant control gains and $B_{\underline{M}}$ is introduced in Property 2.8. Substituting (6–4) into (6–3) yields the closed-loop cadence error system

---

[1] To facilitate the following development, let $V(q, \dot{q})$ be redefined as $C(q, \dot{q})$, (i.e., $C(q, \dot{q}) \triangleq V(q, \dot{q})$).

$$M\dot{r} \;=\; \chi_1 - \tau_e - Cr - e - \frac{B_M}{B_{\underline{M}}}\Big(k_1 r + \Big(k_2 + k_3\,\|z\| + k_4\,\|z\|^2\Big)\mathsf{sgn}(r)\Big). \qquad (6\text{--}5)$$

6.1.2 Neuroadaptive Admittance Control

While the rider's muscles regulate cadence, an interaction torque error is introduced, quantified by $e_\tau\; :\; \mathbb{R}_{\geq 0} \to \mathbb{R}$, and defined as

$$e_\tau \triangleq \tau - \tau_d, \qquad (6\text{--}6)$$

where $\tau_d\; :\; \mathbb{R}_{\geq 0} \to \mathbb{R}$ denotes the desired bounded interaction torque and $\tau\; :\; \mathbb{R}_{\geq 0} \to \mathbb{R}$ denotes the bounded measurable interaction torque between the cycle and rider (i.e., $\tau \in \mathcal{L}_\infty$) [56, 132]. By implementing an admittance filter, the interaction torque error can be transformed into an admittance error (i.e., a modified position and cadence error), which can be regulated using an inner-loop position controller. The admittance filter is given by

$$e_\tau \triangleq M_d \ddot{q}_a + B_d \dot{q}_a + K_d q_a, \qquad (6\text{--}7)$$

where $M_d,\; B_d,\; K_d \in \mathbb{R}_{>0}$ denote constant filter parameters, selected such that the transfer function of (6–7) is passive (i.e., $q_a,\; \dot{q}_a,\; \ddot{q}_a \in \mathcal{L}_\infty$) [63, Lemma 6.4]; and $q_a,\; \dot{q}_a,\; \ddot{q}_a\; :\; \mathbb{R}_{\geq 0} \to \mathbb{R}$ denote the generated admitted position, velocity, and acceleration, respectively. To track the admitted trajectory, an adaptive inner-loop position controller is designed to regulate the admittance error system, quantified by $\xi\; :\; \mathbb{R}_{\geq 0} \to \mathbb{R}$ and $\psi\; :\; \mathbb{R}_{\geq 0} \to \mathbb{R}$, and defined as

$$\xi \;\triangleq\; q_a + q_d - q, \qquad (6\text{--}8)$$

$$\psi \;\triangleq\; \dot{\xi} + \beta\xi, \qquad (6\text{--}9)$$

where $\beta \in \mathbb{R}_{>0}$ denotes a constant control gain. The open-loop admittance error system is generated by taking the time derivative of (6–9), multiplying by M, adding and subtracting ξ, and substituting (2–8), (6–8), and (6–9) to yield

$$M\dot{\psi} = Y\theta + d + P - C\psi - B_M u_M - B_e u_e, \tag{6-10}$$

$$Y\theta \triangleq M\left(\ddot{q}_a + \ddot{q}_d + \beta\psi - \beta^2\xi\right) + C\left(\dot{q}_a + \dot{q}_d + \beta\xi\right) + G + b_c\left(\dot{q}_a + \dot{q}_d - \psi + \beta\xi\right),$$
$$\tag{6-11}$$

where $Y : \mathbb{R}^2 \times \mathbb{R}_{\geq 0} \to \mathbb{R}^{1\times 7}$ denotes a computable regression matrix (LP by Property 5.1), and $\theta \in \mathbb{R}^{7\times 1}$ denotes a matrix of constant system parameters. To facilitate the subsequent analysis, (6–10) is further modified by adding and subtracting ξ and $f_m u_M$, yielding

$$M\dot{\psi} = Y\theta + \chi_2 - \xi - C\psi - B_e u_e + (S - f_m) u_M, \tag{6-12}$$

where $f_m \triangleq B_M\left(\sin^2\left(q_d + q_a\right), \dot{q}_d + \dot{q}_a\right)$. The $\sin^2\left(\cdot\right)$ function is utilized to supply a bounded input to the NN, as well as shape the input to match the positive torque contribution of both legs. The auxiliary function $\chi_2 : \mathcal{Q} \times \mathbb{R} \times \mathbb{R}_{\geq 0} \to \mathbb{R}$ is defined as $\chi_2 \triangleq P + \xi + d$, and bounded by Properties 2.4 and 2.6 as $|\chi_2| \leq c_4 + c_5 \|\phi\|$, where $c_4,\ c_5 \in \mathbb{R}_{>0}$ are known constants, and the error vectors $\phi \in \mathbb{R}^3$, $\zeta \in \mathbb{R}^2$ are defined as $\phi \triangleq \left[\zeta^T \ \dot{q}_a\right]^T$ and $\zeta \triangleq \left[\xi \ \psi\right]^T$. The auxiliary function $S : \mathbb{R}^2 \to \mathbb{R}$ in (6–12) is defined as $S \triangleq f_m - B_m$ and can be bounded using the Mean Value Theorem [137] and Property 2.8 as $|S| \leq c_6 + c_7 \|\zeta\|$, where $c_6,\ c_7 \in \mathbb{R}_{>0}$ are known constants. Knowing $q_d,\ \dot{q}_d,\ q_a,\ \dot{q}_a \in \mathcal{L}_\infty$, let $\mathbb{S}$ be a compact simply connected set of $\mathbb{R}^3$ with map $f_m : \mathbb{S} \to \mathbb{R}$, where f_m is continuous. Then, there exist weights and thresholds such that the function $f_m(x_d)$ can be represented by a neural network as [138, 139]

$$f_m = W^T \rho\left(V^T x_d\right) + \epsilon\left(x_d\right), \tag{6-13}$$

where $x_d \triangleq \begin{bmatrix} 1 & \sin^2\left(q_d + q_a\right) & \dot{q}_d + \dot{q}_a \end{bmatrix}^T \in \mathbb{S}$, $V \in \mathbb{R}^{3\times L}$ and $W \in \mathbb{R}^{(L+1)\times 1}$ are bounded constant ideal weight matrices of the neural network, and L is the number of neurons in

the hidden layer. The function $\rho \; : \; \mathbb{R}^L \to \mathbb{R}^{L+1}$ is defined as $\rho \triangleq \begin{bmatrix} 1 & \rho_1 & \rho_2 & ... & \rho_L \end{bmatrix}^T$, where $\rho_i, \; \forall i = \{1, \; 2, \; ..., \; L\}$ represents the activation function for each neuron, and the function reconstruction error is denoted by $\epsilon \; : \; \mathbb{S} \to \mathbb{R}$.

Assumption 6.1. By [114] and Property 2.8, B_m is continuous and analytic on a compact set except at known locations of discontinuities (i.e., σ_m transitions at known locations based on a present muscle activation strategy). Accordingly, based on the design of the discrete switching signals in (2–7), B_m is right-continuous with finite jumps at known locations. Following a development similar to [139, Theorem 3.1.5], sigmoidal jump approximation functions can be employed within the neural network to estimate the jumps. For simplicity, within the current development, the jumps are approximated by continuous functions and combined within the structure of the activation function ρ and the error is captured within ϵ in (6–13).

Since the weights W and V are unknown, an approximated version of (6–13) is generated as

$$\hat{f}_m \triangleq \hat{W}^T \rho \left(\hat{V}^T x_d \right), \tag{6–14}$$

where $\hat{V} \; : \; \mathbb{R}_{\geq 0} \to \mathbb{R}^{3 \times L}$ and $\hat{W} \in : \; \mathbb{R}_{\geq 0} \to \mathbb{R}^{(L+1) \times 1}$ are the estimates of V and W, respectively. To facilitate the following development, let the notation $\tilde{(\cdot)} \triangleq (\cdot) - \hat{(\cdot)}$ denote estimation errors, then $\rho \left(V^T x_d \right)$ may be approximated at $\rho \left(\hat{V}^T x_d \right)$ using a Taylor series expansion as

$$\rho \left(V^T x_d \right) = \hat{\rho} + \hat{\rho}' \tilde{V}^T x_d + \mathcal{O}^2, \tag{6–15}$$

where $\hat{\rho} \triangleq \rho \left(\hat{V}^T x_d \right), \; \hat{\rho}' \triangleq \left. \frac{\partial \rho \left(V^T x_d \right)}{\partial V^T x_d} \right|_{\hat{V}^T x_d}$ denotes the partial derivative.

Assumption 6.2. The ideal weights, thresholds, function approximation error of (6–13), and higher order terms of (6–15) are assumed to be bounded.

Based on (6–12) and the subsequent stability analysis, the admittance controller is designed as

$$u_e \triangleq \frac{1}{B_e}\left(Y\hat{\theta} + k_5\psi - \hat{f}_m u_M + \left(k_6 + k_7\left\|\phi\right\| + (k_8 + k_9\left\|\zeta\right\|)\left|u_M\right|\right)\mathsf{sgn}\left(\psi\right)\right), \text{(6–16)}$$

where $k_i\ \forall i\ \in\ \{5,\ 6,\ ...,\ 9\}\ \in\ \mathbb{R}_{>0}$ denote constant control gains; $\left|u_M\right|\ \triangleq$ $\frac{1}{B_M}\left[k_1\left|r\right| + k_2 + k_3\left\|z\right\| + k_4\left\|z\right\|^2\right]$; and $\hat{\theta}\ :\ \mathbb{R}_{\geq 0}\ \to\ \mathbb{R}^{7\times 1}$ denotes an estimate of the constant system parameters. Substituting (6–16) into (6–12), adding and subtracting $\left(W^T\hat{\rho} + \hat{W}^T\hat{\rho}'\tilde{V}^T x_d\right)u_M$, utilizing (6–15), and performing some algebraic manipulation yields the closed-loop admittance error system

$$
\begin{aligned}
M\dot{\psi} &= Y\tilde{\theta} - \xi - C\psi - k_5\psi - \left(k_6 + k_7\left\|\phi\right\| + \left(k_8 + k_9\left\|\zeta\right\|\right)\left|u_M\right|\right)\mathsf{sgn}\left(\psi\right) - \left(\tilde{W}^T\hat{\rho}\right.\\
&\quad \left. + \hat{W}^T\hat{\rho}'\tilde{V}^T x_d - N\right)u_M + \chi_2,
\end{aligned}
\quad\text{(6–17)}
$$

where $\tilde{\theta}\ :\ \mathbb{R}_{\geq 0}\ \to\ \mathbb{R}^{7\times 1}$ denotes the error between the actual and estimated system parameters, and the auxiliary function $N\ :\ \mathbb{R}^3\ \to\ \mathbb{R}$ is defined as

$$N \triangleq S - \epsilon - \tilde{W}^T\hat{\rho}'\tilde{V}^T x_d - W^T\mathcal{O}^2. \quad\text{(6–18)}$$

Based on the subsequent stability analysis, the estimates for the system parameters in (6–11) and the neural network weights in (6–14) are generated on-line as

$$\dot{\hat{\theta}} = \mathsf{proj}\left(\Gamma_1 Y^T\psi\right), \quad\text{(6–19)}$$

$$\dot{\hat{W}} = \mathsf{proj}\left(-\Gamma_2\hat{\rho}u_M\psi\right), \quad\text{(6–20)}$$

$$\dot{\hat{V}} = \mathsf{proj}\left(-\Gamma_3 x_d u_M\psi\hat{W}^T\hat{\rho}'\right), \quad\text{(6–21)}$$

where $\Gamma_1 \in \mathbb{R}^{7\times 7}$, $\Gamma_2 \in \mathbb{R}^{(L+1)\times(L+1)}$, $\Gamma_3 \in \mathbb{R}^{3\times 3}$ denote constant positive definite learning gains.

Property 6.1. By the Mean Value Theorem, Assumption 6.2, and the projection algorithm, $\left|N\right| \leq c_8 + c_7\left\|\zeta\right\|$ for any combination of switching signals, where $c_8 \in \mathbb{R}_{>0}$ is a known constant and c_7 was introduced above.

6.2 Stability Analysis

To facilitate the following theorems, let $V_1 : \mathbb{R}^2 \to \mathbb{R}$ denote a continuously differentiable, positive definite storage function defined as

$$V_1 \triangleq \frac{1}{2}Mr^2 + \frac{1}{2}e^2, \tag{6--22}$$

and let $V_2 : \mathbb{R}^{4L+10} \to \mathbb{R}$ denote a continuously differentiable, positive definite Lyapunov function candidate defined as

$$V_2 \quad \triangleq \quad \frac{1}{2}M\psi^2 \quad + \quad \frac{1}{2}\xi^2 \quad + \quad \frac{1}{2}\tilde{\theta}^T\Gamma_1^{-1}\tilde{\theta} \quad + \quad \frac{1}{2}\left(\tilde{W}^T\Gamma_2^{-1}\tilde{W} + \text{tr}\left(\tilde{V}^T\Gamma_3^{-1}\tilde{V}\right)\right), \tag{6--23}$$

where $\text{tr}(\cdot)$ is the trace of a matrix.

Theorem 6.1. *Given the closed-loop cadence error system in (6–5), when $q \in \mathcal{Q}_{FES}$, the cadence controller is passive from input $|\tau_e|$ to output $|r|$, $\forall t$ provided the following constant gain conditions are satisfied: $k_2 \geq c_1$, $k_3 \geq c_2$, $k_4 \geq c_3$.*

Proof. Let $z : \mathbb{R}_{\geq 0} \to \mathbb{R}^2$ for $t \in [t_0, \infty)$ be a Filippov solution to the differential inclusion $\dot{z} \in K[h_1](z)$, where $K[\cdot]$ is defined as in [120], and $h_1 : \mathbb{R}^2 \to \mathbb{R}^2$ is defined as $h_1 \triangleq \begin{bmatrix} \dot{e} & \dot{r} \end{bmatrix}^T$. Because of the discontinuity in the muscle controller in (6–4), the time derivative of V_1 exists almost everywhere (a.e.) (i.e., for almost all $t \in [t_0, \infty)$), and $\dot{V}_1(z) \overset{\text{a.e.}}{\in} \dot{\tilde{V}}_1(z)$, where $\dot{\tilde{V}}_1$ is the generalized time derivative of V_1 along the Filippov trajectories of $\dot{z} = h_1(z)$ [121]. Using the calculus of $K[\cdot]$ from [121], substituting (6–2) and (6–5) into $\dot{\tilde{V}}_1$ yields

$$\dot{\tilde{V}}_1 \subseteq -\alpha e^2 + r\chi_1 + \left(\frac{1}{2}\dot{M} - C\right)r^2 - \frac{K[B_M]}{B_{\underline{M}}}\left(k_1 r^2 + \left(k_2 + k_3\|z\|\right.\right.$$
$$\left.\left. +k_4\|z\|^2\right)K[\text{sgn}(r)]r\right) - r\tau_e, \tag{6--24}$$

where $K[B_M] \triangleq \{0, B_M\}$. For $q \in \mathcal{Q}_{FES}$, $K[B_M]$ is nonzero and may be bounded by Property 2.8 as $B_{\underline{m}}$, which is continuous. Hence, by Properties 2.7 and 2.8, and since $\dot{V}_1(z) \overset{\text{a.e.}}{\in} \dot{\tilde{V}}_1(z)$, (6–24) can be bounded by

$$\dot{V}_1 \overset{\text{a.e.}}{\leq} -\alpha e^2 + |r|\,|\chi_1| - k_1 r^2 + |r|\,|\tau_e| - \left(k_2 + k_3\,\|z\| + k_4\,\|z\|^2\right)|r|. \tag{6–25}$$

Furthermore, (6–25) can be bounded above using Properties 2.1-2.6 as

$$\dot{V}_1 \overset{\text{a.e.}}{\leq} -\alpha e^2 - k_1 r^2 - \lambda_1\,|r| - \lambda_2\,|r|\,\|z\| - \lambda_3\,|r|\,\|z\|^2 + |r|\,|\tau_e|, \tag{6–26}$$

where $\lambda_1,\ \lambda_2,\ \lambda_3 \in \mathbb{R}$ are defined as $\lambda_1 \triangleq k_2 - c_1$, $\lambda_2 \triangleq k_3 - c_2$, and $\lambda_3 \triangleq k_4 - c_3$ (where $c_1,\ c_2,\ c_3$ represent the bounding constants of $|\chi_1|$). Provided the gain conditions are satisfied, $\lambda_1,\ \lambda_2,\ \lambda_3 \geq 0$; thus, (6–26) can be bounded as

$$\dot{V}_1 \overset{\text{a.e.}}{\leq} -\alpha e^2 - k_1 r^2 + |r|\,|\tau_e|. \tag{6–27}$$

Because the interaction torque is bounded, from the perspective of the rider, the physically applied motor torque is similarly bounded. Hence, by [63, Definition 6.3] the cadence error system is output strictly passive with input $|\tau_e|$, output $|r|$, storage function V_1, and the cadence controller is bounded (i.e., $u_M \in \mathcal{L}_\infty$). $\qquad\square$

Theorem 6.2. *Given the closed-loop error system in (6–17) and the admittance relation in (6–7), the admittance error system is globally asymptotically stable in the sense that $\|\zeta\| \to 0$ as $t \to \infty$, provided the following constant gain conditions are satisfied: $k_6 \geq c_4,\ k_7 \geq c_5,\ k_8 \geq c_7,\ k_9 \geq c_8$.*

Proof. Let $\Omega : \mathbb{R}_{\geq 0} \to \mathbb{R}^{4L+10}$ be a Filippov solution to the differential inclusion $\dot{\Omega} \in K[h_2](\Omega)$, and $h_2 \colon \mathbb{R}^{4L+10} \to \mathbb{R}^{4L+10}$ be defined as $h_2 \triangleq \begin{bmatrix} \dot{\xi} & \dot{\psi} & \dot{\tilde{\theta}}^T & \dot{\tilde{W}}^T & \operatorname{vec}\left(\dot{\tilde{V}}\right)^T \end{bmatrix}^T$, where the operator $\operatorname{vec}(\cdot)$ stacks the columns of a matrix $A \in \mathbb{R}^{m\times n}$ to form a vector $\operatorname{vec}(A) \in \mathbb{R}^{mn}$. Because of the discontinuity in the admittance controller in (6–16), $\dot{V}_2(\Omega) \overset{\text{a.e.}}{\in} \dot{\tilde{V}}_2(\Omega)$ along the Filippov trajectories of $\dot{\Omega} = h_2(\Omega)$. Using a similar argument to that made in the proof of Theorem 6.1, substituting (6–9) and (6–17) into $\dot{\tilde{V}}_2(\Omega)$, and performing cancellations yields

$$\dot{\tilde{V}}_2 \subseteq -\beta\xi^2 + \psi Y\tilde{\theta} + \psi\chi_2 + \left(\frac{1}{2}\dot{M} - C\right)\psi^2 - k_5\psi^2 - \tilde{\theta}^T\Gamma_1^{-1}\dot{\tilde{\theta}} - \left(k_6 + k_7\left\|\phi\right\| + \left(k_8 + k_9||\zeta||\right)\right.$$

$$\left. \cdot|u_M|\right)K[\text{sgn}(\psi)]\psi - \left(\tilde{W}^T\hat{\rho} + \hat{W}^T\hat{\rho}'\tilde{V}^Tx_d - N\right)K\left[u_M\right]\psi$$

$$- \left(\tilde{W}^T\Gamma_2^{-1}\dot{\hat{W}} + \text{tr}\left(\tilde{V}^T\Gamma_3^{-1}\dot{\hat{V}}\right)\right), \tag{6–28}$$

where $K\left[u_M\right] = \frac{1}{B_M}\left(k_1 r + \left(k_2 + k_3\left\|z\right\| + k_4\left\|z\right\|^2\right) \cdot K\left[\text{sgn}(r)\right]\right)$, whose members can be

least upper bounded by the previously defined singleton $|u_M|$ such that $\sup(K\left[u_M\right]) = |u_M|$. Utilizing Properties 2.1-2.8, inserting the update laws in (6–19)-(6–21), and

performing cancellations allows (6–28) to be further upper bounded as

$$\dot{\tilde{V}}_2 \subseteq -\beta\xi^2 - k_5\psi^2 - (\lambda_4 + \lambda_5\left\|\phi\right\|)\left|\psi\right| - (\lambda_6 + \lambda_7||\zeta||)\left|\psi\right||u_M|, \tag{6–29}$$

where $\lambda_i \in \mathbb{R}$, $\forall i \in \{4, 5, 6, 7\}$ are defined as $\lambda_4 \triangleq k_6 - c_4$, $\lambda_5 \triangleq k_7 - c_5$, $\lambda_6 \triangleq k_8 - c_8$,

and $\lambda_7 \triangleq k_9 - c_7$ (where c_4, c_5 represent the bounding constants of $|\chi_2|$, and c_7, c_8

represent the bounding constants of $|N|$). Provided the gain conditions are satisfied,

λ_4, λ_5, λ_6, $\lambda_7 \geq 0$, and since $\dot{V}_2(\Omega) \stackrel{\text{a.e.}}{\in} \dot{\tilde{V}}_2(\Omega)$, (6–29) can be upper bounded in both the

FES and KDZ regions as

$$\dot{V}_2 \stackrel{\text{a.e.}}{\leq} -\beta\xi^2 - k_5\psi^2. \tag{6–30}$$

Hence, (6–23) has a negative semi-definite derivative across both the FES and KDZ

regions. Subsequently, [135] can be invoked, along with the radially unboundedness of

(6–23), to show $|\xi|$, $|\psi|$, $\left\|\zeta\right\| \to 0$ as $t \to \infty$. Since $V_2 > 0$ and $\dot{V}_2 \stackrel{\text{a.e.}}{\leq} 0$, $V_2 \in \mathcal{L}_\infty$. Hence,

ξ, ψ, $\tilde{\theta} \in \mathcal{L}_\infty$, which implies $\dot{q}$, $\hat{\theta} \in \mathcal{L}_\infty$. Since (6–7) is passive, $\dot{q}_a$, $\ddot{q}_a \in \mathcal{L}_\infty$, which

implies Y, $\left\|\phi\right\|$, $x_d \in \mathcal{L}_\infty$. By (6–20), (6–21), and $x_d \in \mathcal{L}_\infty$, $\hat{f}_m \in \mathcal{L}_\infty$. Finally, because

$u_M \in \mathcal{L}_\infty$ by Theorem 6.1, $u_e \in \mathcal{L}_\infty$. □

6.3 Experiments

6.3.1 Experimental Testbed

The experimental testbed used in this chapter is introduced in Chapter 2.

6.3.2 Experimental Methods

Experiments were conducted on one able-bodied male participant (P1) aged 26, one male participant with spina bifida (L5-S1, Arnold Chiari Malformation) (P2) aged 25, one female participant with a complete spinal cord injury (AIS A, T8-T9) (P3) aged 26, one male participant with Parkinson's disease (P4) aged 64, and one male participant with drug-induced Parkinsonism (P5) aged 52. P2 is familiar with FES, regularly participates in physical and occupational therapy, and uses a wheelchair part-time; he is community ambulatory with ankle-foot orthoses. P3 suffered her spinal cord injury ten years prior, uses a wheelchair full-time, and also has previous experience with FES. P4 is highly active, participating in recreational activities including swimming and boxing, and is familiar with FES. P5 had no previous exposure to FES and reported low activity levels. All participants completed two FES cycling protocols in random order: Protocol A, which ran the controllers in (6–4) and (6–16); and Protocol B, which disabled both the NN feedforward and adaptive feedforward components of (6–16). The purpose of such a design was to isolate the contribution of the feedforward components of the cycle's motor controller. Each protocol had a total duration of 180 seconds, with the first 30 seconds consisting of a smooth motor-only ramp to the desired cadence of 50 RPM using (6–16), i.e., with the admittance controller active. After the initial ramp, the controller in (6–4) was switched on, the rider was stimulated, and steady-state (SS) errors were recorded. For all experiments, the participants were blind to the desired trajectories for the duration of the experiment. The experimental protocols were approved by the Institutional Review Board at the University of Florida. For all experiments, the admittance parameters in (6–6) and (6–7) were selected as $K_d = 0 \frac{Nm}{rad}$, $B_d = 2 \frac{Nm \cdot s}{rad}$, $M_d = 2 \frac{Nm \cdot s^2}{rad}$, and $\tau_d \in [0, \ 0.2] \ Nm$. The controller gains in (6–2), (6–4), (6–9), (6–16), and (6–19)-(6–21) were selected as $k_1 \in [2, \ 6]$, $k_2 = k_3 = k_4 = 0.1$, $k_5 = 4$, $k_6 = k_7 = 0.01$, $k_8 = k_9 = 0.001$, $\alpha \in [1.0, \ 6.0]$, $\beta = 0.1$, $\Gamma_1 = \gamma \cdot \mathsf{diag}\,(0.175, 0.25, 0.125, 0.5, 1.25, 1.25, 0.05)$, $\gamma \in [1, \ 2]$,

$\Gamma_2 = 10^{-6} \cdot \operatorname{diag}(1.5, 1.0, 0.9, 0.75, 0.5, 2.0)$, and $\Gamma_3 = \operatorname{diag}(0.8, 4, 0.8)$. The activation function of the NN was selected as the soft-plus function, $\rho(x) \triangleq \ln(1 + \exp(x))$, and the number of neurons was set to 5 (i.e., $L = 5$). To disable each component of the controller in (6–16) as dictated by the protocol design, the respective learning gains (i.e., Γ_1, Γ_2, and Γ_3) were set to zero. To avoid transient effects from switching the admittance controller in (6–16) on at 30 seconds, it was enabled for all time.

6.3.3 Results and Discussion

Since the cycle's motor tracks an online-generated admittance trajectory, and the rider's muscles track a set cadence trajectory, the achieved cadence is a function of the torque generated by the rider. Thus, if the rider is able to produce the desired amount of interaction torque (through FES), the admittance trajectory will align with the desired cadence trajectory, and both controllers will work in conjunction to pedal the cycle at the desired cadence. If the rider is unable to meet the desired torque (due to stimulation comfort or strength limitations), the achieved cadence will lag the desired cadence. Table 6-1 illustrates this point, which provides details on the average and standard deviation of the measured cadence, admitted cadence, admittance cadence error, current input to the cycle's motor, torque error, and estimated power production by the rider. The average estimated power production is denoted by $\hat{P} : \mathbb{R}_{\geq 0} \to \mathbb{R}$, which is defined as $\hat{P} \triangleq \operatorname{mean}(\dot{q})(\operatorname{mean}(\tau) - \tau_p)$, where $\tau_p : \mathbb{R}_{\geq 0} \to \mathbb{R}$ denotes an estimate of the passive torque required to actuate the combined rider-cycle system at the desired cadence, collected during each trial for 4.8 seconds prior to controller activation (i.e., approximately four crank cycles at 50 RPM).

In the following, the participants and protocols are denoted by their respective number and letter; for example, P1 running Protocol B is referred to as P1B. Numerical results for P1-P5 are provided in Table 6-1, calculated at steady state (i.e., after the initial cadence ramp to 50 RPM). Figure 6-1 displays cadence tracking results, including errors and root-mean-squared (RMS) errors for P1A; for visual clarity, a one second

145

Table 6-1. Experimental results, reported as average $\pm$ standard deviation

Participant	Protocol	$\dot{q}$ (RPM)*	$\dot{q}_\alpha$ (RPM)†	$\dot{\xi}$ (RPM)	$\hat{P}$ (W)
1‡	A	48.84±1.87	-1.24±1.49	-0.08±1.30	3.31±2.79
	B	49.04±1.90	-1.15±1.30	-0.19±1.53	3.22±2.72
2	A	48.14±1.13	-1.95±0.21	-0.10±1.13	0.14±1.09
	B	48.14±1.19	-2.04±0.81	-0.19±1.19	0.24±1.04
3	A	47.56±0.95	-2.52±0.13	-0.08±0.95	-0.14±0.92
	B	47.48±0.96	-2.57±0.13	-0.05±0.97	-0.15±0.88
4	A	49.04±1.36	-0.94±0.77	0.01±1.08	3.70±3.13
	B	48.64±1.43	-1.47±0.68	-0.11±1.27	2.53±2.67
5	A	46.66±1.04	-3.47±0.33	-0.13±1.02	-0.07±1.11
	B	47.15±0.90	-2.85±0.44	0.00±0.81	-0.02±1.06
Mean	A	48.04±1.31	-2.02±0.77	-0.07±1.10	1.38±2.04
Mean	B	48.09±1.32	-2.01±0.77	-0.10±1.18	1.16±1.87

*At SS, the average cadence error is calculated as $\dot{e} = 50 - \dot{q}$.
†$\dot{q}_\alpha : \mathbb{R}_{\geq 0} \to \mathbb{R}$ denotes the average admitted cadence defined as $\dot{q}_\alpha \triangleq \dot{q}_d + \dot{q}_a$.
‡$\tau_d = 0.2$ Nm.

moving average filter was applied. Figure 6-2 displays the control inputs to both the motor and the rider's muscle groups for P1A, and for visual clarity, a half second moving average filter was applied. Figures 6-3 and 6-4 display the evolution of $\hat{\theta}$ and $\hat{f}_m$, respectively, in accordance with the update laws in (6–19)-(6–21).

Prior to the muscle controller in (6–4) being activated, the rider's legs act as a drag on the system, generating negative torque, and therefore decreasing the admitted cadence, as depicted in Figure 6-1. Because only the admitted error system is being regulated at this point, the position error (i.e., e) begins to accumulate; therefore, when the muscle controller in (6–4) is activated, a nonzero stimulation is applied, as displayed in Figure 6-2. Under normal circumstances, this error accumulation would be undesirable; however, because the rider's muscles do not generate torque at low levels of stimulation, this effect becomes desirable to "prime" the muscles for torque generation. By applying low stimulation levels and increasing them over the course of the experiment, torque production is gradually increased and results in a more comfortable experience for the rider. Furthermore, by decreasing the derivative gain (i.e., k_1) on muscle stimulation, sharp increases in stimulation due to system
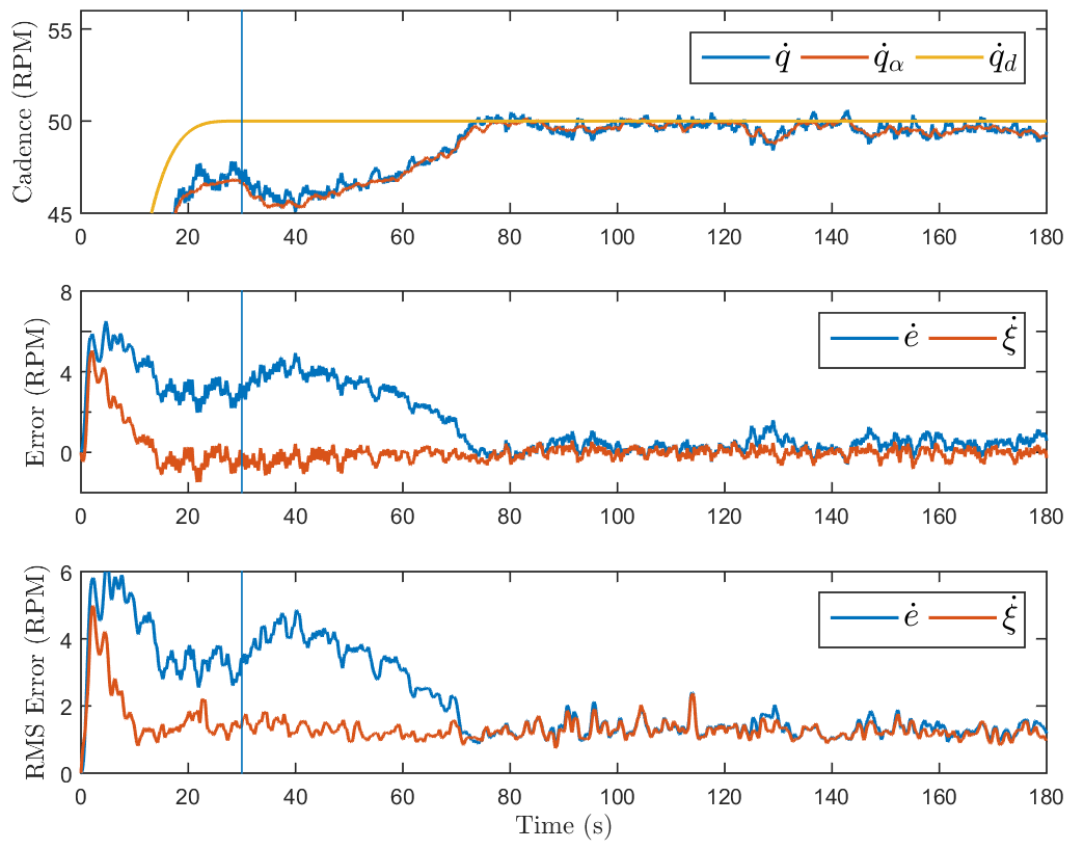
Figure 6-1. P1A: (Top) The actual, admitted, and desired cadence; (Middle) cadence errors; and (Bottom) RMS cadence errors, with the vertical lines representing the time of activation of (6–4).

disturbances are avoided and results in a smoother stimulation pattern. The position gain (i.e., α) on the cadence error system heavily influences the degree to which the stimulation is increased over time; because the primarily tracking objective is concerned with cadence, the position gain acts as an integral-like gain and stimulation increases steadily until the measured cadence aligns with the desired. As the stimulation level increases, the torque from the rider's leg muscles gradually increases to the desired torque (contrast Figures 6-1 and 6-2, at $t \approx 70$ s) and due to the admittance filter in (6–7), the admitted trajectory begins to align with the desired, resulting in less error accumulation (i.e., e) and a less aggressive ramp in the stimulation input. As the muscles begin to fatigue, their cumulative torque production lessens and the admitted trajectory begins to decrease; consequently, the stimulation input increases to maintain torque levels.

As depicted in Figures 6-3 and 6-4, at t=30 s, the update laws for both $\hat{\theta}$ and $\hat{f}_m$ are activated and the estimates begin to evolve. Although the framework for designing the parameter estimates is motivated by the system parameters in the dynamics, there is no guarantee the estimates will approach their true values. Using more advanced forms of learning such as integral concurrent learning [140], however, can be leveraged to ensure parameter convergence with the finite excitation condition. Because the NN is used to estimate the muscle control effectiveness, it continues to evolve over the duration of the experiment as the muscles experience fatigue. Note, the NN estimate in Figure 6-4 begins to increase when the rider's muscles begin generating torque. A single crank cycle view is supplemented in Figure 6-4, to demonstrate the NN emulating the form of a $\sin^2 (\cdot)$ wave, as expected and encouraged per the two FES regions in the crank cycle and by the construction of the NN in (6–13). The estimate of the NN is subsequently multiplied by the stimulation input (6–4) before being added into the control input of the motor. The adaptive and NN feedforward components simultaneously estimate system dynamics, and affect each other over time; therefore, the gains on the adaptive gradient

component were set significantly higher than those of the NN to encourage learning on two different time scales.

To demonstrate the effect of the feedforward components of (6–16), the adaptive gradient and NN components were disabled (i.e., Protocol B). As illustrated by Table 6-1, for P1, using adaptation results in the reduction of the admittance cadence error $\dot{\xi}$ by 58% and the standard deviation of the admittance cadence error by 15%. Despite the reduction in error, the average control inputs to the motor were similar, with similar torque production by the rider.

Subsequently, P2 and P3 completed both protocols, with Figures 6-5 and 6-6 displaying cadence results and control inputs, respectively, from P2A. Because P2 was limited in terms of his ability to generate torque from FES (due to comfort thresholds), the NN estimate of the control effectiveness relating stimulation input to torque output was near zero. However, as illustrated by Table 6-1, adaptation results in the reduction of the admittance cadence error by 48% and the standard deviation of the admittance cadence error by 5%, illustrating the effect of the gradient adaptive component of the controller. P2 was unable to produce the desired amount of torque, hence his measured cadence lagged the desired for the duration of the experiment; however, the admittance error system was closely tracked by the motor controller. Due to the position error accumulating, P2's stimulation steadily increased until it reached his comfort threshold, depicted in Figure 6-6.

P3 was limited in her ability to produce torque elicited from the applied stimulation and consequently relied exclusively on the electric motor to actuate the cycle at a near-constant cadence. Figure 6-7 displays the resulting cadence and error systems for P3A. Unlike P2, however, P3 was limited because of significant muscle atrophy occurring in the ten years since her injury. Because P3 had no sensation below mid-abdomen, the stimulation pulsewidth was allowed to reach the hardware maximum of 500μs, as indicated in Figure 6-8. Despite the high stimulation level, according to Table 6-1, P3
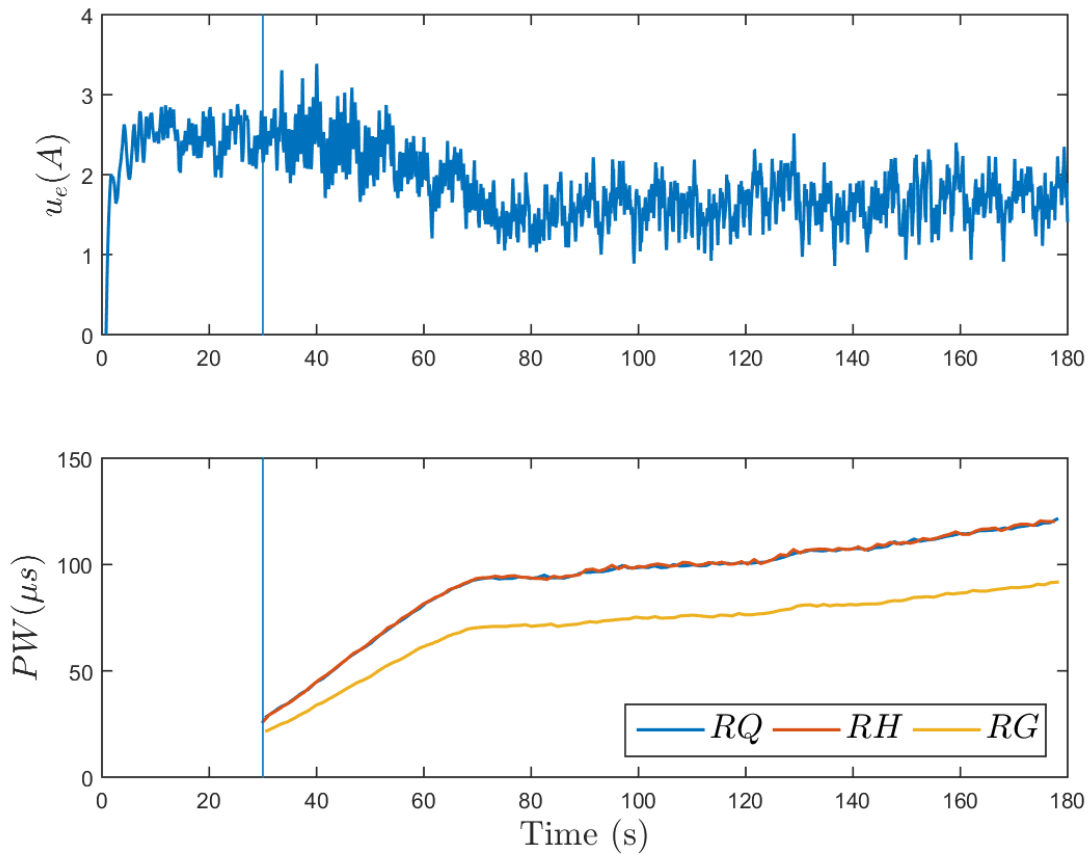
Figure 6-2. P1A: (Top) Control input to the motor and (Bottom) to the rider's quadriceps femoris, hamstrings, and gluteal muscle groups of the right leg. Due to identical muscle gains (i.e., k_m, $\forall m \in \{Q, H\}$) the quadriceps and hamstring control inputs overlap. Although stimulation is applied in a pulsetrain (dependent on the fixed frequency and amplitude, and controller-modulated pulsewidth) it is plotted as the maximum stimulation pulsewidth for each FES region.
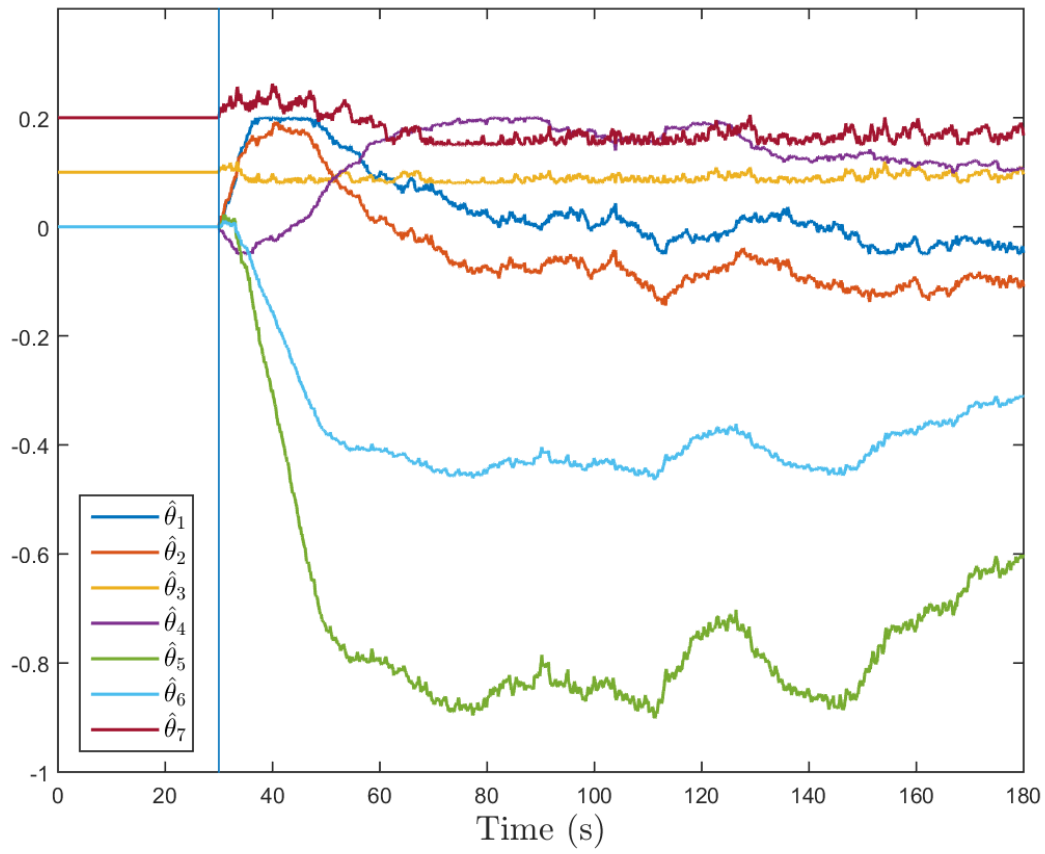
Figure 6-3. P1: Evolution of $\hat{\theta}_i \ \forall i \in \{1, 2, ...,7\}$.
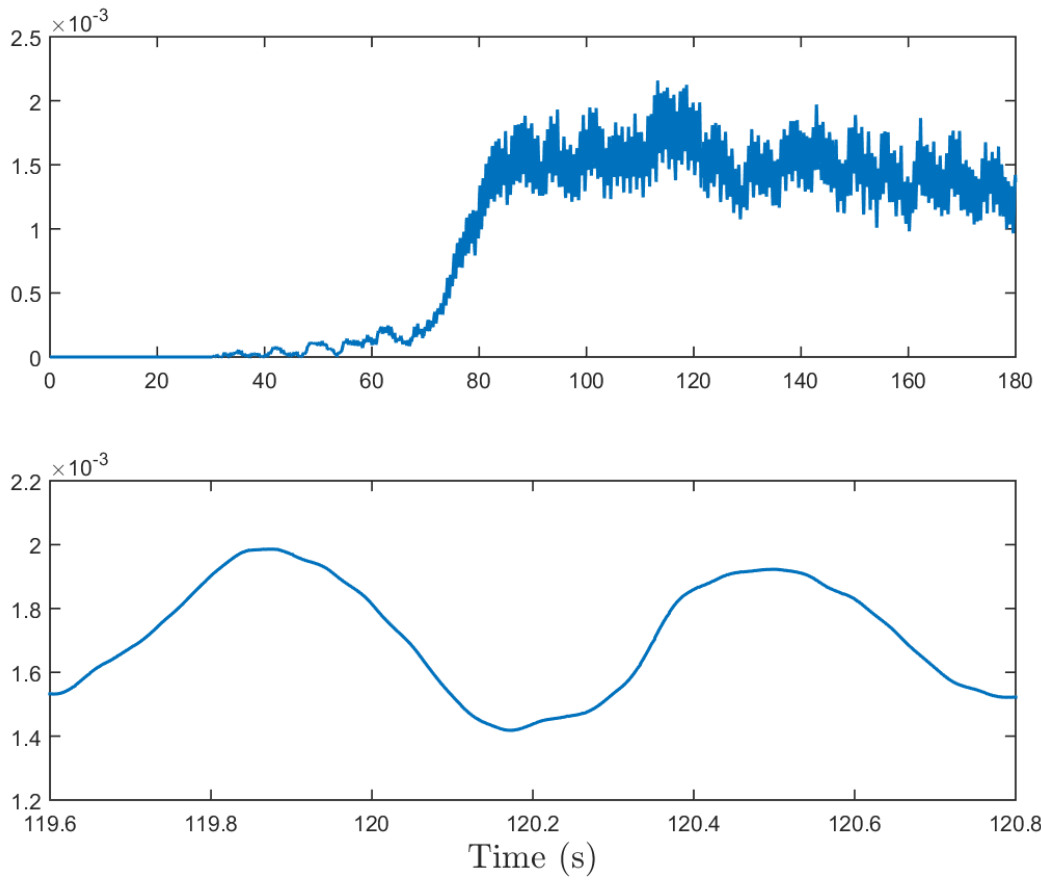
Figure 6-4. P1: (Top) Evolution of $\hat{f}_m$ over the experiment and (Bottom) evolution of $\hat{f}_m$ over one crank cycle.
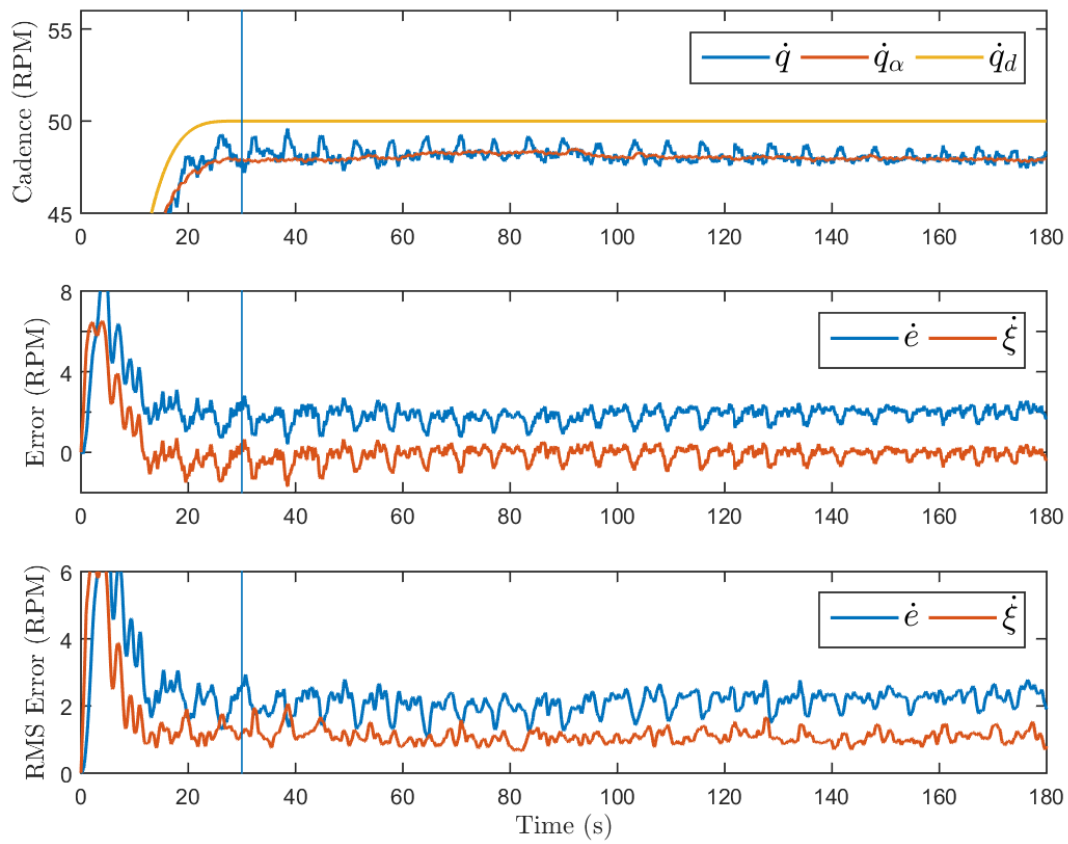
Figure 6-5. P2A: (Top) The actual, admitted, and desired cadence; (Middle) cadence
errors; and (Bottom) RMS cadence errors.
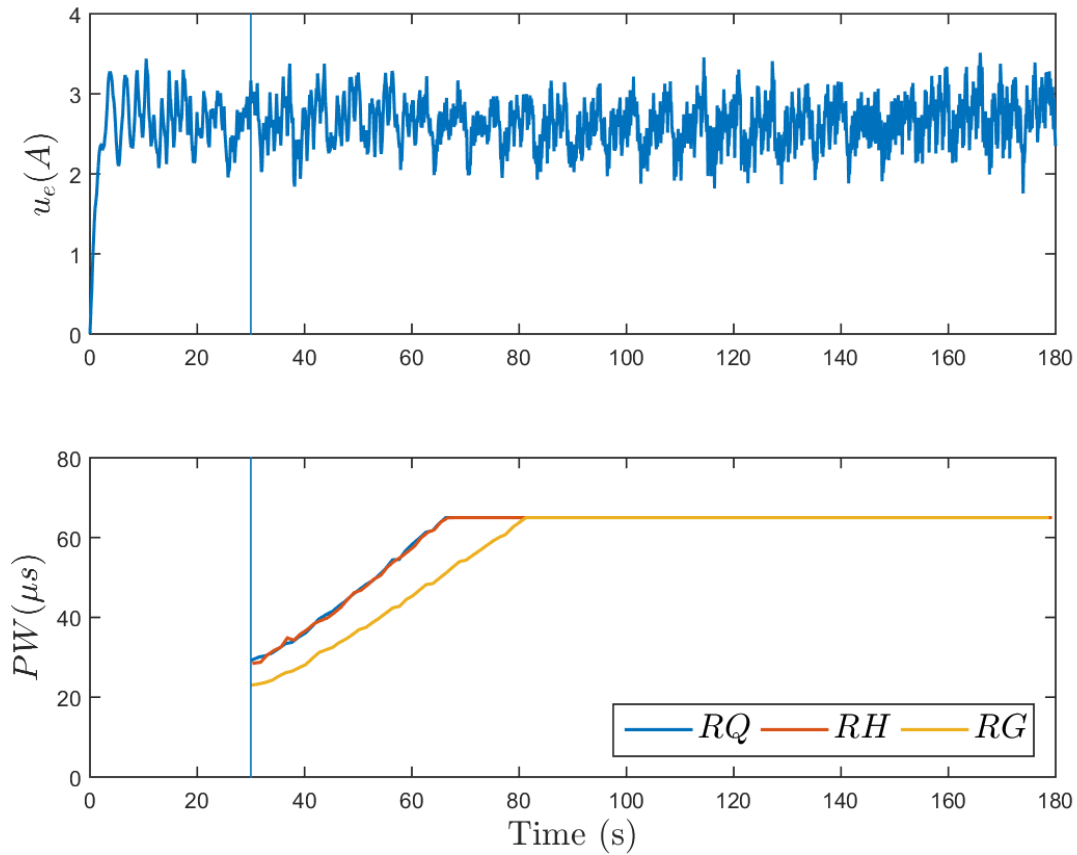
Figure 6-6. P2A: (Top) Control input to the motor and (Bottom) to the rider's muscle groups. Due to identical muscle gains (i.e., k_m, $\forall m \in \{Q, H\}$) the quadriceps and hamstring control inputs overlap. The input to the rider's muscle groups was subject to a saturation limit of 65 μs.
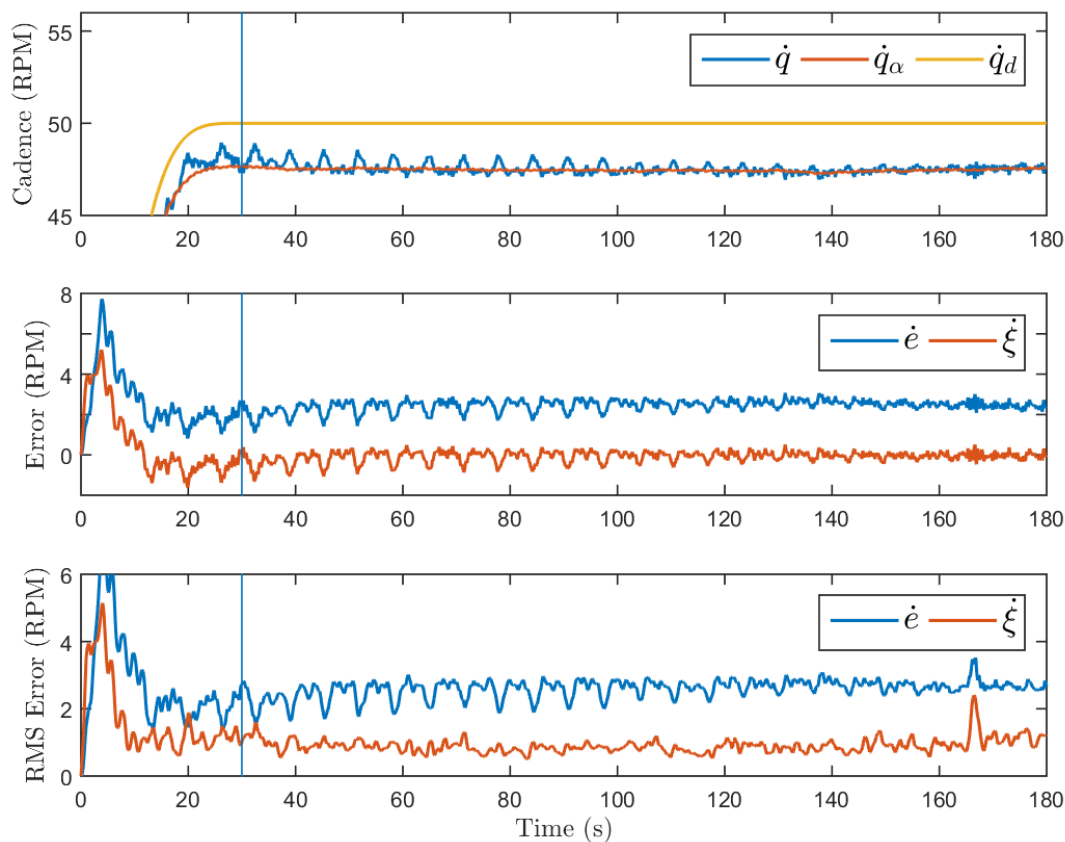
Figure 6-7. P3A: (Top) The actual, admitted, and desired cadence; (Middle) cadence
errors; and (Bottom) RMS cadence errors.

was unable to produce any positive torque about the crank; however, P3 did get the

benefit of a range-of-motion exercise on the FES cycle. Using adaptation on P3 did not

result in any improvement in tracking errors; however, due to time constraints, minimal

gain tuning was conducted.

The experimental results for P4A are depicted in Figures 6-9 and 6-10. As shown

in Figure 6-9, the cycle's measured cadence is above the desired cadence and does

not decrease significantly upon controller activation at t=30 s; by examining the stim-

ulation input plot in Figure 6-10, it is also shown that the stimulation pulsewidth was

approximately 20-30 μs at t=30 s. Although each participant reacts differently to the
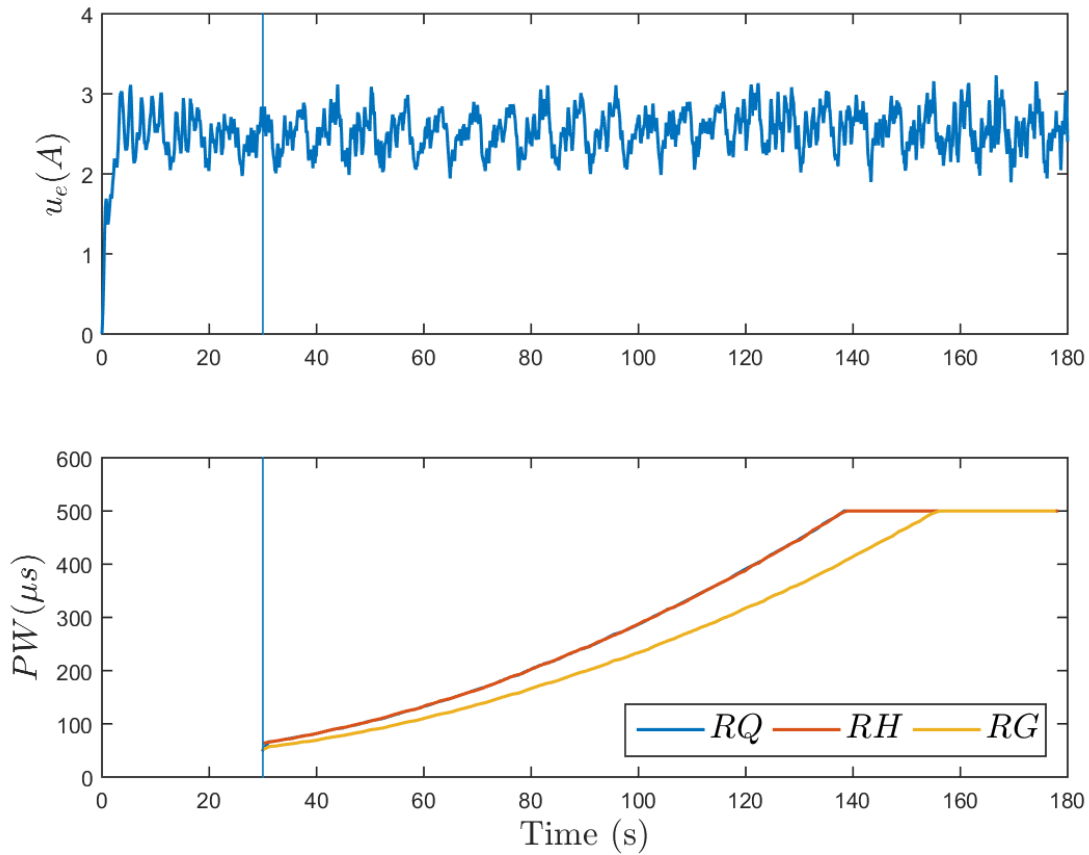
Figure 6-8. P3A: (Top) Control input to the motor and (Bottom) to the rider's muscle groups. Due to identical muscle gains (i.e., k_m, $\forall m \in \{Q, H\}$) the quadriceps and hamstring control inputs overlap. The input to the rider's muscle groups was subject to a saturation limit of 500 μs.

applied stimulation (hence, the uncertain nonlinear control effectiveness B_m), the authors have not previously witnessed visible contractions at these low stimulation levels. Consequently, we have surmised that the participant was volitionally contributing to the cycling task, despite not measuring muscle activity levels with methods such as electromyography. Although the participant was blind to his performance and the desired trajectory, upon controller activation, the applied stimulation can be used as cues to trigger the rider to pedal the cycle, and based on the stimulation intensity, to an appropriate magnitude. As the experiment progressed, however, the stimulation was observed to increase at approximately $t \approx 60$ s, at which point we assume the rider began to relax and withdraw his volitional contributions. When the rider relaxed, the observed cadence decreased and both error systems increased, as shown in Figure 6-9. As the experiment progressed and the stimulation evoked stronger contractions, it began to plateau, indicating that the applied stimulation was sufficient to evoke contractions powerful enough to pedal the cycle and overcome the passive torque required to actuate the rider's limbs. Despite the results of P4 indicating he contributed to the cycling task volitionally, the adaptive admittance controller was able to reduce the admittance error to 0.01 ± 1.08 RPM compared to the non-adaptive case of -0.11 ± 1.27 RPM.

Compared to P2, P3, and P4, P5's neurological condition was unique in that his symptoms (i.e., tremor) were induced through oral medications and resulted in drug-induced Parkinsonism. When P5 participated in the current study, however, he had since changed medications and demonstrated no signs of discernible tremor. The results from P5A are shown in Figures 6-11 and 6-12. Because of P5's low activity levels and sensitivity to stimulation, similar to P2, the applied stimulation was unable to evoke strong muscle contractions. Furthermore, due to participant comfort, the hamstring muscle groups were not stimulated and further limited the available rider torque. P5 was the only participant where adding the adaptation detracted from the
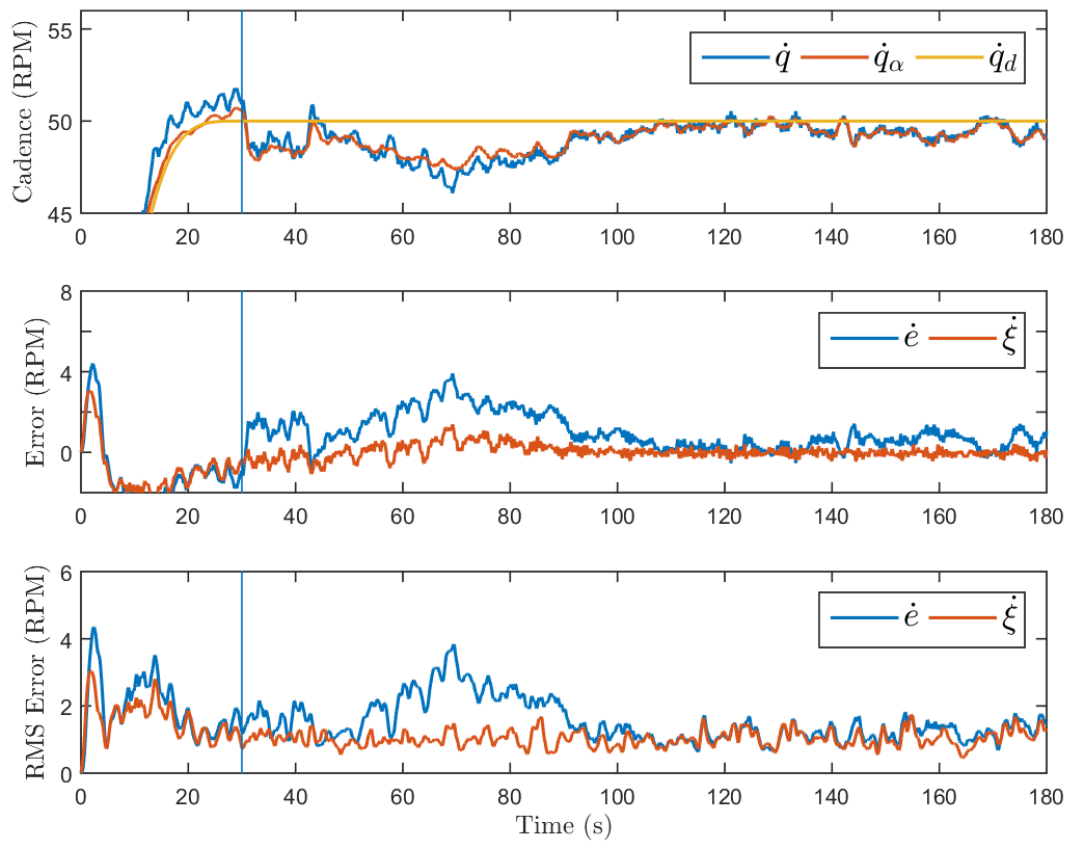
Figure 6-9. P4A: (Top) The actual, admitted, and desired cadence; (Middle) cadence errors; and (Bottom) RMS cadence errors.

158
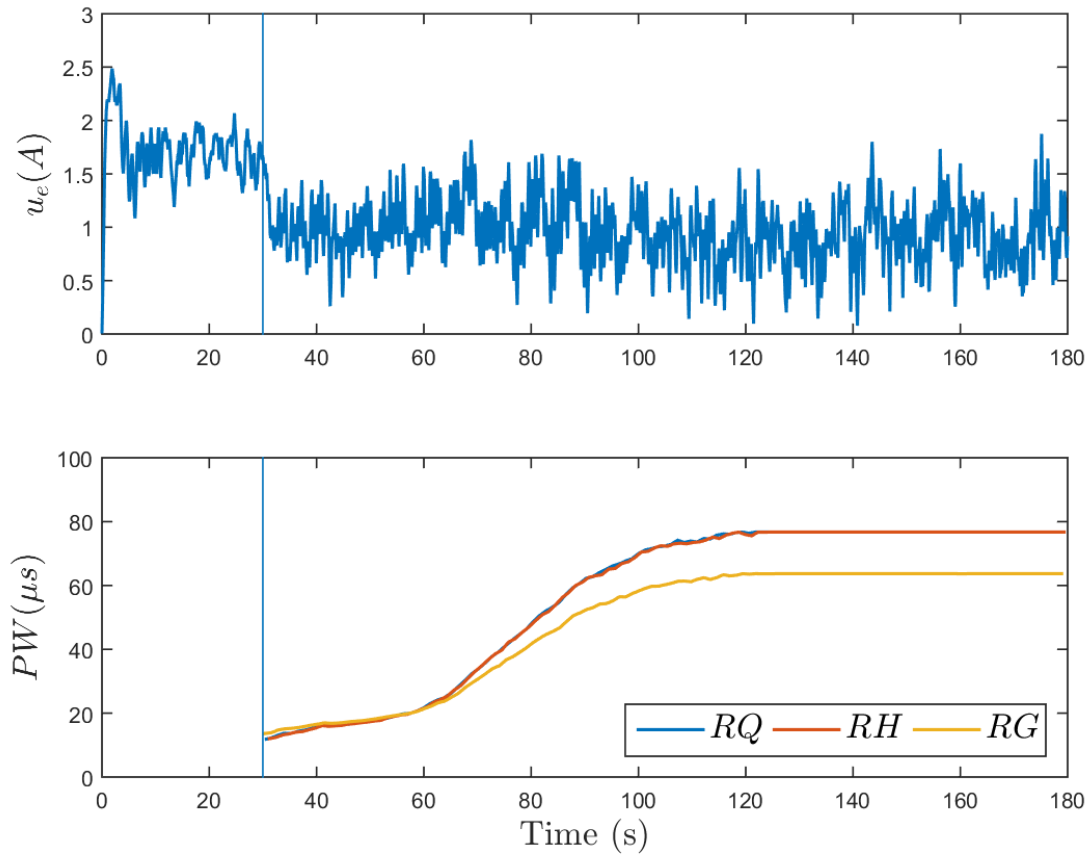
Figure 6-10. P4A: (Top) Control input to the motor and (Bottom) to the rider's muscle groups. Due to identical muscle gains (i.e., $k_m, \ \forall m \in \{Q, H\}$) the quadriceps and hamstring control inputs overlap. The input to the rider's muscle groups was subject to a saturation limit of 77 μs.
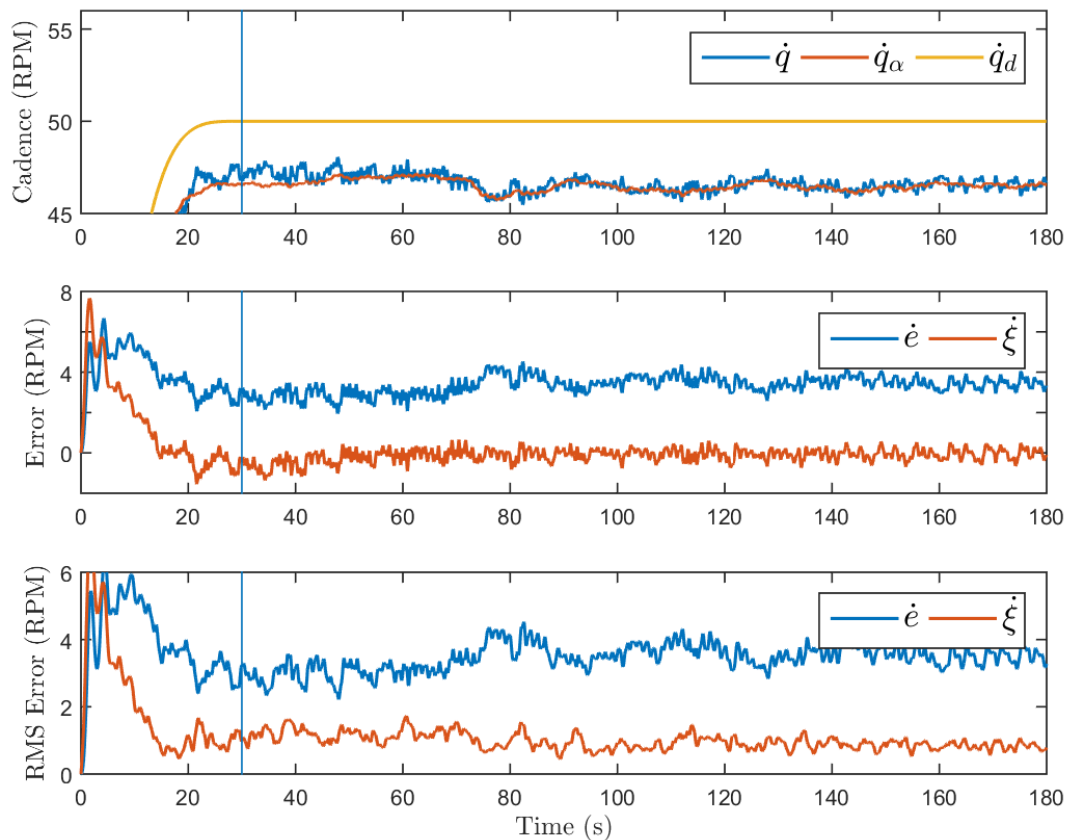
Figure 6-11. P5A: (Top) The actual, admitted, and desired cadence; (Middle) cadence
errors; and (Bottom) RMS cadence errors.

performance of the cycle and increased the admittance error from 0.00±0.81 RPM
without adaptation to -0.13±1.02 RPM with adaptation.

As demonstrated by the tracking results of P1-P5, the FES cycle remained stable
under a wide range of participant capabilities. In three participants (i.e., P1, P2, and
P4) adaptation was able to noticeably improve the tracking performance, whereas in
P5, adaptation detracted from the cycle's performance. Although four of the participants
reached their stimulation threshold, the position gain (i.e., α) could be reduced to
increase the amount of time until saturation. Balancing stimulation levels with fatigue,
comfort, and torque output remains one of the foremost challenging and promising
topics in FES cycling.
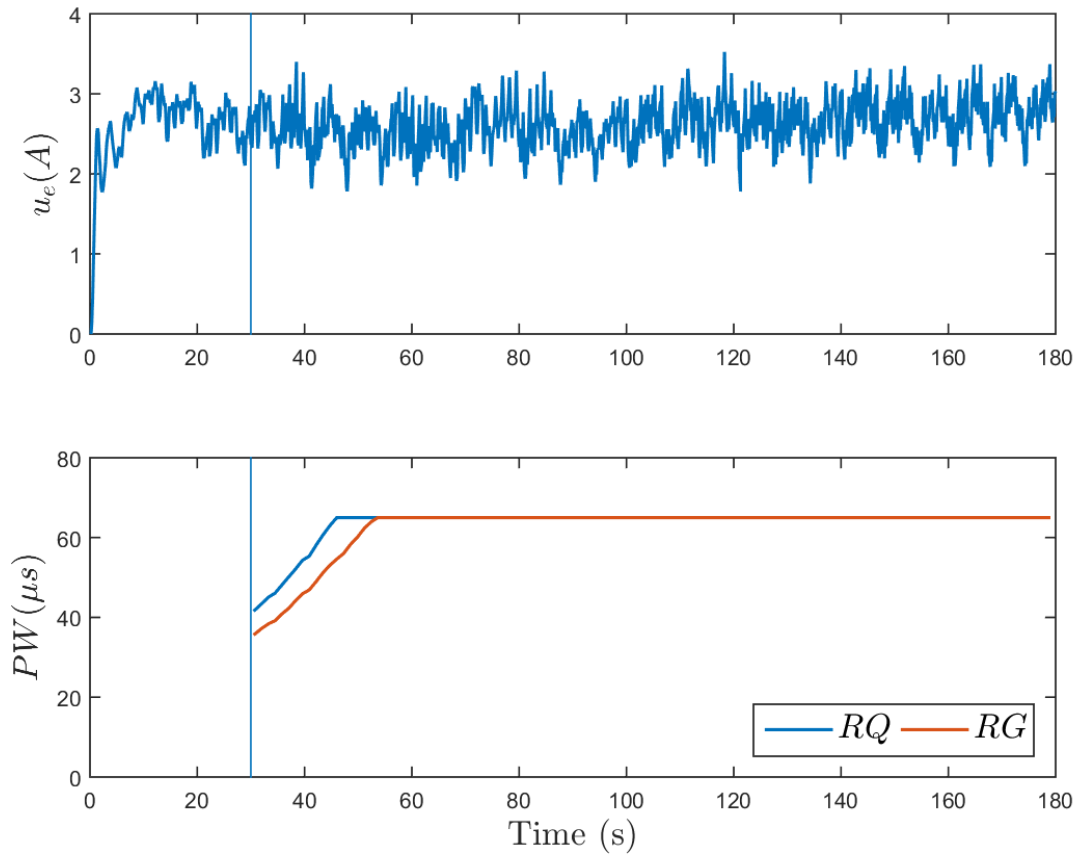
Figure 6-12. P5A: (Top) Control input to the motor and (Bottom) to the rider's muscle groups. Due to participant comfort, the hamstring muscle groups were not stimulated. The input to the rider's muscle groups was subject to a saturation limit of 65 μs.

6.4 Concluding Remarks

This chapter modifies the adaptive admittance controller developed in Chapter 5 with the addition of a neural network designed to estimate the control effectiveness of the rider's muscles and more accurately track the admitted trajectory. While the neural network is shaped according to the anticipated rider output torque curve, the cycle's admittance controller simultaneously employs a gradient adaptive feedforward term to estimate the linear-in-the-parameter dynamics. Experiments are conducted using the single-crank FES cycle on one able-bodied participant and four participants with neuromuscular disorders. Results demonstrate improvements of performance metrics in three of five participants when adaptation is enabled.

CHAPTER 7
CONCLUSIONS

For individuals suffering from neuromuscular disorders (e.g., spinal cord injury, traumatic brain injury, spina bifida, etc.), hybrid exoskeletons offer a number of rehabilitative benefits (e.g., increased muscle mass, range of motion, cardiovascular parameters, etc.). Hybrid exoskeletons combine functional electrical stimulation (FES) with rehabilitation robots to merge the benefits and reduce the drawbacks of the two therapeutic strategies. Because hybrid exoskeletons exhibit uncertain, time-varying, nonlinear, switched system dynamics, appropriate control strategies must be selected to not only ensure safe operation, but simultaneously promote rehabilitation for individuals with neuromuscular disorders. Moreover, because physical human-robot interaction arises from hybrid exoskeletons, a switched systems stability analysis is crucial to ensure desired behavior and prevent injury. In this physical human-robot interaction problem, both the human and the robot are controlled subsystems and require control objectives. To promote rehabilitation, objectives such as position/cadence control, torque/power control, and admittance control have all been proposed and investigated.

Over the course of this dissertation, numerous stabilizing controllers have been developed to safely implement human-machine interaction with an emphasis on rehabilitation robots and hybrid exoskeletons. In Chapter 1, motivation for the use of FES, robots, and hybrid exoskeletons in rehabilitation settings is presented. A survey of the literature on various control techniques for interfacing with these technologies is then introduced, establishing a framework for this dissertation to build upon. Chapter 2 introduces the hybrid exoskeleton used through this dissertation, an FES cycle, along with the corresponding nonlinear, uncertain, time-varying, switched system dynamics. Autonomous state-dependent switching is necessary because multiple muscle groups receive stimulation at different angles throughout the crank cycle to produce positive

torque about the crank and propel the cycle forward. The controllers designed in subsequent chapters are designed to interface with the FES cycle to accomplish various control objectives such as position, cadence, and admittance tracking.

In Chapter 3, an FES cycling controller is developed to track both cadence and instantaneous power. The torque error system uses a running integral to update the torque error in real-time, compared to once per cycle in discretized tracking prevalent in other cycling methods. Using the proposed controller, a Lyapunov-like switched system stability analysis is conducted which guarantees global exponential cadence tracking and uniform ultimate boundedness of the instantaneous power objective. Experiments were conducted on seven able-bodied participants and six participants with NDs to evaluate the performance of the proposed controller. A comparison is then made to two previously developed FES-cycling controllers using experimental results. While the controllers varied in their control authority and their method of tracking torque, all controllers demonstrated the ability to accomplish the dual-objective of cadence and power tracking; however, the developed controller exhibited favorable performance and characteristics. These results indicate that cadence should be controlled by the electric motor for all time (i.e., within the FES and KDZ regions) and power should be tracked instantaneously using the large muscle groups of the legs in the FES regions. The contributions of this chapter include a novel switched-systems stability analysis to prove the stability of the instantaneous torque error system supported by experimental results obtained from individuals with NDs.

In Chapter 4, two new controllers are developed for the FES cycle to accomplish simultaneous cadence and admittance tracking. The controllers are designed to overcome challenges of Chapter 3; namely, selecting the appropriate desired torque trajectory for direct torque tracking. Compared to Chapter 3, the admittance controller implemented on the cycle's motor is capable of indirect torque tracking, accomplished by injecting artificial desired dynamics between the rider and the cycle. Consequently,

the rider's muscles are now electrically stimulated using a cadence controller to actuate the cycle. Using the admittance controller, the cycle assumes an assist-as-needed control paradigm and assists the rider is maintaining a desired cadence if the FES is unable to elicit muscle contractions powerful enough to overcome the passive torques of the combined cycle-rider system. Correspondingly, the admittance controller resists the rider if s/he pedals volitionally and exceeds the desired cadence. Experiments conducted on three able-bodied participants and four participants with NDs demonstrated controller efficacy. The experiments also investigated the effects of selecting various admittance parameters and show that a compliant cycle is not only desirable for rider safety, but also for torque/power production. Results indicate the admittance controller is a promising rehabilitation strategy to simultaneously elicit torque from the rider's muscles while introducing a degree of compliance to the system. The contributions of this chapter include developing the first admittance controller on an FES cycle, along with arguments to select the appropriate admittance structure and parameter values. Furthermore, experiments show that the torque requirement from the exoskeleton can be offset by torque supplemented from FES, allowing for the use of smaller motors and batteries on hybrid exoskeletons.

Chapter 5 seeks to improve upon the controllers presented in Chapter 4 by adding adaptation to the admittance controller implemented on the cycle's motor. Additionally, to accommodate for asymmetric rider capabilities (as in post-stroke hemiparesis), the cycle's crank is severed and the cycle's pedals are decoupled. Consequently, the cycle is instrumented with an additional motor, encoder, powermeter, and chain to establish feedback and control authority on both sides of the cycle. The muscles of each leg of the rider are tasked with maintaining the cycle's cadence on their respective sides and each motor is controlled using a separate admittance controller. Using a passivity-based stability analysis, it is shown that rider volition does not destabilize the error systems. When implemented, the admitted trajectory is generated online by averaging the output

torques between the two sides such that the pedals are kept at an offset of 180 degrees, maintaining the natural symmetry of cycling. If the rider demonstrates hemiparesis, the stronger leg will experience resistance and the weaker leg will experience assistance such that the two pedals are held in phase. Experiments are conducted on one able-bodied participant and three participants with neuromuscular disorders to compare the effect of adding adaptation to the cycle. Results indicate significant improvement in various performance metrics with the use of adaptation. Specifically, with adaptation, the cadence error was reduced by 41%, the cadence standard deviation was reduced by 57%, the control input to the motors was reduced by 9%, and the pedal phase error was reduced by 41% to an average difference of 174°. The contributions of this chapter include developing the first adaptive admittance controller for FES cycles and designing a novel admitted trajectory to balance the contributions of both the rider's legs while simultaneously promoting symmetry training. Furthermore, because of the physical coupling between the rider and the cycle, it has been demonstrated that adding adaptation to the cycle also adds a form of pseudo-adaptation to the rider as well, reducing tracking errors.

In Chapter 6, the adaptive admittance controller developed in Chapter 5 is modified with the addition of a neural network designed to estimate the control effectiveness of the rider's muscles and more accurately track the admitted trajectory. While the neural network is shaped according to the anticipated rider output torque curve, the cycle's admittance controller simultaneously employs a gradient adaptive feedforward term to estimate the linear-in-the-parameter dynamics. Experiments are conducted using the single-crank FES cycle on one able-bodied participant and four participants with neuromuscular disorders. Results demonstrate improvements of performance metrics in three of five participants when adaptation is enabled. The contributions of this chapter include developing a neuroadaptive controller to estimate the rider's muscle control effectiveness.

Supported by experimental evidence, this dissertation provides robust arguments on the development and usage of various nonlinear and adaptive control strategies for physical human-robot interaction on hybrid exoskeletons. Previous chapters include controller development, rigorous switched system stability analyses, and experimental results demonstrating the efficacy of the controllers. While all controllers included a cadence control objective, based on the desire to better accommodate individual and asymmetric NDs, this dissertation has evolved from robust direct torque control on single-crank FES cycles to adaptive admittance control on split-crank FES cycles. Along these lines, an effort has been made to fuse control systems engineering with clinical science and rehabilitation. Due to the collaboration with the Brooks Rehabilitation Hospital in Jacksonville, FL and the Shands Hospital on the University of Florida campus, experiments have been conducted on participants with NDs such as spinal cord injury, traumatic brain injury, hemorrhagic and ischemic stroke, spina bifida, Parkinson's disease, and drug-induced Parkinsonism, validating the controllers across a broad spectrum of NDs.

While FES cycles offer a promising rehabilitation strategy for individuals with NDs, there is ample room for additional research directions. Future works may include more accurately accounting for the electromechanical delay demonstrated by muscles under neuromuscular electrical stimulation, or modifying the desired trajectories online to avoid saturating the muscles with stimulation. Regardless of the selected strategy, clinical trials are necessary to demonstrate the benefits of closed-loop control methods over the open-loop methods prevalently seen in clinical practice today.

REFERENCES

[1] S. E. Wallace and M. L. Kimbarow, *Cognitive Communication Disorders*. Plural Publishing, 2016.

[2] E. J. Benjamin, M. J. Blaha, S. E. Chiuve, M. Cushman, S. R. Das, R. Deo, S. D. de Ferranti, J. Floyd, M. Fornage *et al.*, "Heart disease and stroke statistics - 2017 update," *Circulation*, vol. 135, no. 10, pp. 146–603, 2017.

[3] "Spinal cord injury facts and figures at a glance," *J. Spinal Cord Med.*, 2017.

[4] J. H. Rimmer and J. L. Rowland, "Health promotion for people with disabilities: implications for empowering the person and promoting disability-friendly environments," *Am. J. Lifestyle Med.*, vol. 2, no. 5, pp. 409–420, 2008.

[5] T. Mohr, J. Pødenphant, F. Biering-Sørensen, H. Galbo, G. Thamsborg, and M. Kjær, "Increased bone mineral density after prolonged electrically induced cycle training of paralyzed limbs in spinal cord injured man," *Calcif. Tissue Int.*, vol. 61, no. 1, pp. 22–25, 1997.

[6] M. Bélanger, R. B. Stein, G. D. Wheeler, T. Gordon, and B. Leduc, "Electrical stimulation: can it increase muscle strength and reverse osteopenia in spinal cord injured individuals?" *Arch. Phys. Med. Rehabil.*, vol. 81, no. 8, pp. 1090–1098, 2000.

[7] S. Ferrante, A. Pedrocchi, G. Ferrigno, and F. Molteni, "Cycling induced by functional electrical stimulation improves the muscular strength and the motor control of individuals with post-acute stroke," *Eur. J. Phys. Rehabil. Med.*, vol. 44, no. 2, pp. 159–167, 2008.

[8] M. M. Rodgers, R. M. Glaser, S. F. Figoni, S. P. Hooker, B. N. Ezenwa, S. R. Collins, T. Mathews, A. G. Suryaprasad, and S. C. Gupta, "Musculoskeletal responses of spinal cord injured individuals to functional neuromuscular stimulation-induced knee extension exercise training," *J. Rehabil. Res. Dev.*, vol. 28, no. 4, pp. 19–26, 1991.

[9] S. P. Hooker, S. F. Figoni, M. M. Rodgers, R. M. Glaser, T. Mathews, A. G. Suryaprasad, and S. C. Gupta, "Physiologic effects of electrical stimulation leg cycle exercise training in spinal cord injured persons," *Arch. Phys. Med. Rehabil.*, vol. 73, no. 5, pp. 470–476, 1992.

[10] A. J. del Ama, Á. Gil-Agudo, J. L. Pons, and J. C. Moreno, "Hybrid FES-robot cooperative control of ambulatory gait rehabilitation exoskeleton," *J. Neuroeng. Rehab.*, vol. 11, no. 1, p. 27, 2014.

[11] R. Downey, M. Merad, E. Gonzalez, and W. E. Dixon, "The time-varying nature of electromechanical delay and muscle control effectiveness in response to

stimulation-induced fatigue," *IEEE Trans. Neural Syst. Rehabil. Eng.*, vol. 25, no. 9, pp. 1397–1408, September 2017.

[12] S. Jezernik, R. G. Wassink, and T. Keller, "Sliding mode closed-loop control of FES controlling the shank movement," *IEEE Trans. Biomed. Eng.*, vol. 51, no. 2, pp. 263–272, 2004.

[13] H. I. Krebs, J. J. Palazzolo, L. Dipietro, M. Ferraro, J. Krol, K. Rannekleiv, B. T. Volpe, and N. Hogan, "Rehabilitation robotics: Performance-based progressive robot-assisted therapy," *Auton. Robot.*, vol. 15, no. 1, pp. 7–20, 2003.

[14] H. I. Krebs and B. T. Volpe, "Robotics: A rehabilitation modality," *Curr. Phys. Med. Rehab. Rep.*, vol. 3, no. 4, pp. 243–247, 2015.

[15] L. Marchal-Crespo and D. J. Reinkensmeyer, "Review of control strategies for robotic movement training after neurologic injury," *J. Neuroeng. Rehabil.*, vol. 6, no. 1, 2009.

[16] C. Patten, J. Dozono, S. G. Schmidt, M. E. Jue, and P. S. Lum, "Combined functional task practice and dynamic high intensity resistance training promotes recovery of upper-extremity motor function in post-stroke hemiparesis: A case study," *J. Neuro. Phys. Ther.*, vol. 30, no. 3, pp. 99–115, 2006.

[17] P. S. Lum, C. G. Burgar, P. C. Shor, M. Majmundar, and M. Van der Loos, "Robot-assisted movement training compared with conventional therapy techniques for the rehabilitation of upper-limb motor function after stroke," *Archiv. Phys. Med. Rehabil.*, vol. 83, no. 7, pp. 952–959, 2002.

[18] E. Akdogan and M. A. Adli, "The design and control of a therapeutic exercise robot for lower limb rehabilitation: Physiotherabot," *Mechatron.*, vol. 21, no. 3, pp. 509–522, 2011.

[19] S. Haddadin, A. Albu-Schäffer, and G. Hirzinger, "Safety analysis for a human-friendly manipulator," *Int. J. Soc. Robot.*, vol. 2, no. 3, pp. 235–252, 2010.

[20] H. Lee and N. Hogan, "Essential considerations for design and control of human-interactive robots," in *IEEE Int. Conf. Robot. Autom.*, 2016, pp. 3069–3074.

[21] P. K. Jamwal, S. Hussain, M. H. Ghayesh, and S. V. Rogozina, "Impedance control of an intrinsically compliant parallel ankle rehabilitation robot," *IEEE Trans. Ind. Electron.*, vol. 63, no. 6, pp. 3638–3647, 2016.

[22] H. Taheri, D. J. Reinkensmeyer, and E. T. Wolbrecht, "Model-based assistance-as-needed for robotic movement therapy after stroke," in *IEEE Int. Conf. Eng. Med. Biol. Soc.*   IEEE, 2016, pp. 2124–2127.

[23] E. T. Wolbrecht, V. Chan, D. J. Reinkensmeyer, and J. E. Bobrow, "Optimizing compliant, model-based robotic assistance to promote neurorehabilitation," *IEEE Trans. Neur. Sys. and Rehab. Eng.*, vol. 16, no. 3, pp. 286–297, 2008.

[24] C.-S. Poon, "Sensorimotor learning and information processing by bayesian internal models," in *IEEE Proc. Eng. Med. Biol. Soc.*, vol. 2. IEEE, 2004, pp. 4481–4482.

[25] P. M. Rossini and G. Dal Forno, "Integrated technology for evaluation of brain function and neural plasticity," *Phys. Med. Rehabil. Clin. N. Am.*, vol. 15, no. 1, pp. 263–306, 2004.

[26] A. Weiss, T. Suzuki, J. Bean, and R. A. Fielding, "High intensity strength training improves strength and functional performance after stroke," *Am. J. Phys. Med. Rehabil.*, vol. 79, no. 4, pp. 369–376, 2000.

[27] M. M. Ouellette, N. K. LeBrasseur, J. F. Bean, E. Phillips, J. Stein, W. R. Frontera, and R. A. Fielding, "High-intensity resistance training improves muscle strength, self-reported function, and disability in long-term stroke survivors," *Stroke*, vol. 35, no. 6, pp. 1404–1409, 2004.

[28] S. L. Morris, K. J. Dodd, and M. E. Morris, "Outcomes of progressive resistance strength training following stroke: a systematic review," *Clin. Rehabil.*, vol. 18, no. 1, pp. 27–39, 2004.

[29] J. Stein, H. I. Krebs, W. R. Frontera, S. E. Fasoli, R. Hughes, and N. Hogan, "Comparison of two techniques of robot-aided upper limb exercise training after stroke," *Am. J. Phys. Med. Rehabil.*, vol. 83, no. 9, pp. 720–728, 2004.

[30] M. Lotze, C. Braun, N. Birbaumer, S. Anders, and L. G. Cohen, "Motor learning elicited by voluntary drive," *Brain*, vol. 126, no. 4, pp. 866–872, 2003.

[31] M. A. Perez, B. K. Lungholt, K. Nyborg, and J. B. Nielsen, "Motor skill training induces changes in the excitability of the leg cortical area in healthy humans," *Exp. Brain Res.*, vol. 159, no. 2, pp. 197–205, 2004.

[32] S. Haddadin, A. Albu-Schaffer, A. De Luca, and G. Hirzinger, "Collision detection and reaction: A contribution to safe physical human-robot interaction," in *Proc. IEEE/RSJ Int. Conf. Intell. Robot. Sys. (IROS)*. IEEE, 2008, pp. 3356–3363.

[33] P. A. Lasota, G. F. Rossano, and J. A. Shah, "Toward safe close-proximity human-robot interaction with standard industrial robots," in *Proc. IEEE Int. Conf. Autom. Sci. Eng. (CASE)*. IEEE, 2014, pp. 339–344.

[34] M. Bernhardt, M. Frey, G. Colombo, and R. Riener, "Hybrid force-position control yields cooperative behaviour of the rehabilitation robot lokomat," in *IEEE Int. Conf. Rehabil. Robot.* IEEE, 2005, pp. 536–539.

[35] M.-S. Ju, C.-C. Lin, D.-H. Lin, I.-S. Hwang, and S.-M. Chen, "A rehabilitation robot with force-position hybrid fuzzy controller: hybrid fuzzy control of rehabilitation robot," *IEEE Trans. Neur. Sys. Rehab. Eng.*, vol. 13, no. 3, pp. 349–358, 2005.

[36] S. Okada, T. Sakaki, R. Hirata, Y. Okajima, S. Uchida, and Y. Tomita, "Tem: a therapeutic exercise machine for the lower extremities of spastic patients," *Adv. Robot.*, vol. 14, no. 7, pp. 597–606, 2001.

[37] H. I. Krebs, N. Hogan, M. L. Aisen, and B. T. Volpe, "Robot-aided neurorehabilitation," *IEEE Trans. Rehab. Eng.*, vol. 6, no. 1, pp. 75–87, 1998.

[38] R. Richardson, M. Brown, B. Bhakta, and M. Levesley, "Design and control of a three degree of freedom pneumatic physiotherapy robot," *Robotica*, vol. 21, no. 6, pp. 589–604, 2003.

[39] ——, "Impedance control for a pneumatic robot-based around pole-placement, joint space controllers," *Control Eng. Pract.*, vol. 13, no. 3, pp. 291–303, 2005.

[40] M. L. Aisen, H. I. Krebs, N. Hogan, F. McDowell, and B. T. Volpe, "The effect of robot-assisted therapy and rehabilitative training on motor recovery following stroke," *Archiv. Neuro.*, vol. 54, no. 4, pp. 443–446, 1997.

[41] N. Hogan, "Impedance control: An approach to manipulation: Part I-theory, part II-implementation, part III-applications," *J. Dyn. Sys., Meas., Control*, vol. 107, no. 1, pp. 1–24, Mar. 1985.

[42] J. Zhang and C. C. Cheah, "Passivity and stability of human–robot interaction control for upper-limb rehabilitation robots," *IEEE Trans. Robot.*, vol. 31, no. 2, pp. 233–245, 2015.

[43] I. Ranatunga, F. L. Lewis, D. O. Popa, and S. M. Tousif, "Adaptive admittance control for human–robot interaction using model reference design and adaptive inverse filtering," *IEEE Trans. Control Sys. Tech.*, vol. 25, no. 1, pp. 278–285, 2017.

[44] M. Kimmel and S. Hirche, "Invariance control for safe human–robot interaction in dynamic environments," *IEEE Trans. Robot.*, vol. 33, no. 6, pp. 1327–1342, 2017.

[45] A. U. Pehlivan, D. P. Losey, and M. K. O'Malley, "Minimal assist-as-needed controller for upper limb robotic rehabilitation," *IEEE Trans. Robot.*, vol. 32, no. 1, pp. 113–124, 2016.

[46] J. Zhang and C. C. Cheah, "Passivity and stability of human-robot interaction control for upper-limb rehabilitation robots," *IEEE Trans. on Robot.*, vol. 31, no. 2, pp. 233–245, 2015.

[47] N. Vitiello, T. Lenzi, S. Roccella, S. M. M. De Rossi, E. Cattin, F. Giovacchini, F. Vecchi, and M. C. Carrozza, "Neuroexos: A powered elbow exoskeleton for physical rehabilitation," *IEEE Trans. Robot.*, vol. 29, no. 1, pp. 220–235, 2013.

[48] S. F. Atashzar, I. G. Polushin, and R. V. Patel, "A small-gain approach for nonpassive bilateral telerobotic rehabilitation: Stability analysis and controller synthesis," *IEEE Trans. Robot.*, vol. 33, no. 1, pp. 49–66, 2017.

[49] T. Valency and M. Zacksenhouse, "Accuracy/robustness dilemma in impedance control," *J. Dyn. Syst. Meas. Control*, vol. 125, no. 3, pp. 310–319, 2003.

[50] M. J. Kim, W. Lee, C. Ott, and W. K. Chung, "A passivity-based admittance control design using feedback interconnections," in *Proc. IEEE Int. Conf. Intell. Robot. Syst.* IEEE, 2016, pp. 801–807.

[51] R. Kikuuwe, "A sliding-mode-like position controller for admittance control with bounded actuator force," *IEEE/ASME Trans. Mechatron.*, vol. 19, no. 5, pp. 1489–1500, 2014.

[52] K. Anam and A. A. Al-Jumaily, "Active exoskeleton control systems: State of the art," *Proced. Eng.*, vol. 41, pp. 988–994, 2012.

[53] G. Liu and A. Goldenberg, "Robust hybrid impedance control of robot manipulators," in *Proc. IEEE Int. Conf. Robot. Autom.* IEEE, 1991, pp. 287–292.

[54] W. Yu, J. Rosen, and X. Li, "Pid admittance control for an upper limb exoskeleton," in *Proc. Am. Control Conf.* IEEE, 2011, pp. 1124–1129.

[55] Y. Li, S. Sam Ge, and C. Yang, "Learning impedance control for physical robot–environment interaction," *Int. J. Control*, vol. 85, no. 2, pp. 182–193, 2012.

[56] Y. Li and S. S. Ge, "Impedance learning for robots interacting with unknown environments," *IEEE Trans. Control Sys. Tech.*, vol. 22, no. 4, pp. 1422–1432, 2014.

[57] A. Roy, H. I. Krebs, D. J. Williams, C. T. Bever, L. W. Forrester, R. M. Macko, and N. Hogan, "Robot-aided neurorehabilitation: a novel robot for ankle rehabilitation," *IEEE Trans. Robot.*, vol. 25, no. 3, pp. 569–582, 2009.

[58] Y. Choi, J. Gordon, D. Kim, and N. Schweighofer, "An adaptive automated robotic task-practice system for rehabilitation of arm functions after stroke," *IEEE Trans. Robot.*, vol. 25, no. 3, pp. 556–568, 2009.

[59] A. Alamdari, R. Haghighi, and V. Krovi, "Stiffness modulation in an elastic articulated-cable leg-orthosis emulator: Theory and experiment," *IEEE Trans. Robot.*, no. 99, pp. 1–14, 2018.

[60] S. A. Bowyer and F. R. y Baena, "Dissipative control for physical human–robot interaction," *IEEE Trans. Robot.*, vol. 31, no. 6, pp. 1281–1293, 2015.

[61] A. J. Del-Ama, A. D. Koutsou, J. C. Moreno, A. De-Los-Reyes, Á. Gil-Agudo, and J. L. Pons, "Review of hybrid exoskeletons to restore gait following spinal cord injury," *J. Rehabil. Res. Dev.*, vol. 49, no. 4, pp. 497–514, 2012.

[62] F. Anaya, P. Thangavel, and H. Yu, "Hybrid FES–robotic gait rehabilitation technologies: a review on mechanical design, actuation, and control strategies," *Int. J. Intell. Robot. Appl.*, pp. 1–28, 2018.

[63] H. K. Khalil, *Nonlinear Systems*, 3rd ed.   Upper Saddle River, NJ: Prentice Hall, 2002.

[64] R. Ortega, A. J. V. der Schaft, I. Mareels, and B. Maschke, "Putting energy back in control," *IEEE Control Sys.*, vol. 21, no. 2, pp. 18–33, 2001.

[65] G. Herrnstadt and C. Menon, "Admittance-based voluntary-driven motion with speed-controlled tremor rejection," *IEEE/ASME Trans. Mech.*, vol. 21, no. 4, pp. 2108–2119, 2016.

[66] Q. Wu, X. Wang, B. Chen, and H. Wu, "Development of a minimal-intervention-based admittance control strategy for upper extremity rehabilitation exoskeleton," *IEEE Trans. Syst. Man Cybern: Sys.*, 2017.

[67] M. J. Bellman, R. J. Downey, A. Parikh, and W. E. Dixon, "Automatic control of cycling induced by functional electrical stimulation with electric motor assistance," *IEEE Trans. Autom. Science Eng.*, vol. 14, no. 2, pp. 1225–1234, April 2017.

[68] C.-W. Peng, S.-C. Chen, C.-H. Lai, C.-J. Chen, C.-C. Chen, J. Mizrahi, and Y. Handa, "Review: Clinical benefits of functional electrical stimulation cycling exercise for subjects with central neurological impairments," *J. Med. Biol. Eng.*, vol. 31, pp. 1–11, 2011.

[69] A. T. Harrington, C. G. A. McRae, and S. C. K. Lee, "Evaluation of functional electrical stimulation to assist cycling in four adolescents with spastic cerebral palsy," *J. Pediatr.*, vol. 2012, pp. 1–11, 2012.

[70] L. Griffin, M. Decker, J. Hwang, B. Wang, K. Kitchen, Z. Ding, and J. Ivy, "Functional electrical stimulation cycling improves body composition, metabolic and neural factors in persons with spinal cord injury," *J. Electromyogr. Kinesiol.*, vol. 19, no. 4, pp. 614–622, 2009.

[71] V. R. Edgerton, R. D. de Leon, S. J. Harkema, J. A. Hodgson, N. London, D. J. Reinkensmeyer, R. R. Roy, R. J. Talmadge, N. J. Tillakaratne, W. Timoszyk, and A. Tobin, "Retraining the injured spinal cord," *J. Physiol.*, vol. 533, no. 1, pp. 15–22, 2001.

[72] V. Edgerton and R. R. Roy, "Paralysis recovery in humans and model systems," *Curr. Opin. Neurobiol.*, vol. 12, no. 6, pp. 658–667, 2002.

[73] K. J. Hunt, D. Hosmann, M. Grob, and J. Saengsuwan, "Metabolic efficiency of volitional and electrically stimulated cycling in able-bodied subjects," *Med. Eng. Phys.*, vol. 35, no. 7, pp. 919–925, Jul. 2013.

[74] K. J. Hunt, J. Fang, J. Saengsuwan, M. Grob, and M. Laubacher, "On the efficiency of FES cycling: A framework and systematic review," *Technol. Health Care*, vol. 20, no. 5, pp. 395–422, 2012.

[75] M. Grohler, T. Angeli, T. Eberharter, P. Lugner, W. Mayr, and C. Hofer, "Test bed with force-measuring crank for static and dynamic investigations on cycling by means of functional electrical stimulation," *IEEE Trans. Neural Syst. Rehabil. Eng.*, vol. 9, no. 2, pp. 169–180, 2001.

[76] H. Kawai, M. Bellman, R. Downey, and W. E. Dixon, "Closed-loop position and cadence tracking control for FES-cycling exploiting pedal force direction with antagonistic bi-articular muscles," *IEEE Trans. Control Syst. Tech.*, vol. 27, no. 2, pp. 730–742, Feb. 2019.

[77] R. Berkelmans, "FES cycling," *J. Autom. Control*, vol. 18, no. 2, pp. 73–76, 2008.

[78] L. D. Duffell, N. d. N. Donaldson, and D. J. Newham, "Power output during functional electrically stimulated cycling in trained spinal cord injured people," *Neuromod. Technol. Neural Interface*, vol. 13, no. 1, pp. 50–57, 2010.

[79] L. D. Duffell, N. d. N. Donaldson, T. A. Perkins, D. N. Rushton, K. J. Hunt, T. H. Kakebeeke, and D. J. Newham, "Long-term intensive electrically stimulated cycling by spinal cord–injured people: Effect on muscle properties and their relation to power output," *Muscle Nerve*, vol. 38, no. 4, pp. 1304–1311, 2008.

[80] A. J. van Soest, M. Gföhler, and L. Casius, "Consequences of ankle joint fixation on FES cycling power output: a simulation study." *Med. Sci. Sports Exerc.*, vol. 37, no. 5, pp. 797–806, 2005.

[81] C. Fornusek and G. M. Davis, "Maximizing muscle force via low-cadence functional electrical stimulation cycling," *J. Rehabil. Med.*, vol. 36, pp. 232–237, 2004.

[82] J. Szecsi, A. Straube, and C. Fornusek, "Comparison of the pedalling performance induced by magnetic and electrical stimulation cycle ergometry in able-bodied subjects," *Med. Eng. Phys.*, vol. 36, no. 4, pp. 484–489, 2014.

[83] J. Szecsi, P. Krause, S. Krafczyk, T. Brandt, and A. Straube, "Functional output improvement in FES cycling by means of forced smooth pedaling," *Med. Sci. Sports Exerc.*, vol. 39, no. 5, pp. 764–780, May 2007.

[84] K. J. Hunt, B. Stone, N.-O. Negård, T. Schauer, M. H. Fraser, A. J. Cathcart, C. Ferrario, S. A. Ward, and S. Grant, "Control strategies for integration of electric motor assist and functional electrical stimulation in paraplegic cycling: Utility for exercise testing and mobile cycling," *IEEE Trans. Neural Syst. Rehabil. Eng.*, vol. 12, no. 1, pp. 89–101, Mar. 2004.

[85] A. Farhoud and A. Erfanian, "Fully automatic control of paraplegic FES pedaling using higher-order sliding mode and fuzzy logic control," *IEEE Trans. Neural Syst. Rehabil. Eng.*, vol. 22, no. 3, pp. 533–542, 2014.

[86] C. Cousin, V. H. Duenas, C. Rouse, and W. E. Dixon, "Motorized functional electrical stimulation for torque and cadence tracking: A switched Lyapunov approach," in *Proc. IEEE Conf. Decis. Control*, 2017, pp. 5900–5905.

[87] M. Bellman, "Control of cycling induced by functional electrical stimulation: A switched systems theory approach," Ph.D. dissertation, University of Florida, 2015.

[88] E. Ambrosini, S. Ferrante, T. Schauer, G. Ferrigno, F. Molteni, and A. Pedrocchi, "Design of a symmetry controller for cycling induced by electrical stimulation: preliminary results on post-acute stroke patients," *Artif. Organs*, vol. 34, no. 8, pp. 663–667, Aug. 2010.

[89] V. H. Duenas, C. Cousin, V. Ghanbari, and W. E. Dixon, "Passivity-based learning control for torque and cadence tracking in functional electrical stimulation (FES) induced cycling," in *Proc. Am. Control Conf.*, 2018, pp. 3726–3731.

[90] C. Fornusek, G. M. Davis, P. J. Sinclair, and B. Milthorpe, "Development of an isokinetic functional electrical stimulation cycle ergometer," *Nueromodulation*, vol. 7, no. 1, pp. 56–64, 2004.

[91] E. Ambrosini, S. Ferrante, G. Ferrigno, F. Molteni, and A. Pedrocchi, "Cycling induced by electrical stimulation improves muscle activation and symmetry during pedaling in hemiparetic patients," *IEEE Trans. Neural Syst. Rehabil. Eng.*, vol. 20, no. 3, pp. 320–330, May 2012.

[92] M. Van der Loos, L. Worthen-Chaudhari, and D. Schwandt, "A split-crank bicycle ergometer uses servomotors to provide programmable pedal forces for studies in human biomechanics," *IEEE Trans. Neural Syst. Rehabil. Eng.*, vol. 18, no. 4, pp. 445–52, April 2010.

[93] L. Ting, S. Kautz, D. Brown, and F. Zajac, "Contralateral movement and extensor force generation alter flexion phase muscle coordination in pedaling," *J. Neurophysiol.*, vol. 83, no. 6, pp. 3351–65, Jun 2000.

[94] S. J. Elmer, J. McDaniel, and J. C. Martin, "Biomechanics of counterweighted one-legged cycling," *J. Appl. Biomech.*, vol. 32, no. 1, pp. 78–85, 2016.

[95] T. C. Bulea, C. J. Stanley, and D. L. Damiano, "Part 2: Adaptation of gait kinematics in unilateral cerebral palsy demonstrates preserved independent neural control of each limb," *Front. Human Neurosci.*, vol. 11, p. 50, 2017.

[96] D. S. Reisman, A. J. Bastian, and S. M. Morton, "Neurophysiologic and rehabilitation insights from the split-belt and other locomotor adaptation paradigms," *Phys. Ther.*, vol. 90, no. 2, pp. 187–195, 2010.

[97] A. L. Penko, J. R. Hirsch, C. Voelcker-Rehage, P. E. Martin, G. Blackburn, and J. L. Alberts, "Asymmetrical pedaling patterns in parkinson's disease patients," *Clin. Biomech.*, vol. 29, no. 10, pp. 1089–1094, 2014.

[98] D. Liberzon, *Switching in Systems and Control.* Birkhauser, 2003.

[99] K. J. Hunt, C. Ferrario, S. Grant, B. Stone, A. N. McLean, M. H. Fraser, and D. B. Allan, "Comparison of stimulation patterns for FES-cycling using measures of oxygen cost and stimulation cost," *Med. Eng. Phys.*, vol. 28, no. 7, pp. 710–718, Sep. 2006.

[100] P. F. Li, Z. G. Hou, F. Zhang, Y. Chen, X. Xie, M. Tan, and H. Wang, "Adaptive neural network control of fes cycling," in *Int. Conf. on Bioinformatics and Biomedical Eng.* IEEE, Jun. 2010, pp. 1–4.

[101] J. Szecsi, A. Straube, and C. Fornusek, "A biomechanical cause of low power production during fes cycling of subjects with SCI," *J. Neurorehabil. Eng.*, vol. 11, no. 1, p. 123, 2014.

[102] M. J. Bellman, T. H. Cheng, R. J. Downey, C. J. Hass, and W. E. Dixon, "Switched control of cadence during stationary cycling induced by functional electrical stimulation," *IEEE Trans. Neural Syst. Rehabil. Eng.*, vol. 24, no. 12, pp. 1373–1383, 2016.

[103] W. E. Dixon and M. Bellman, "Cycling induced by functional electrical stimulation: A control systems perspective," *ASME Dyn. Syst. & Control Mag.*, vol. 4, no. 3, pp. 3–7, Sept 2016.

[104] V. H. Duenas, C. A. Cousin, C. Rouse, E. J. Fox, and W. E. Dixon, "Distributed repetitive learning control for cooperative cadence tracking in functional electrical stimulation cycling," *IEEE Trans. Cybern.*, to appear.

[105] V. H. Duenas, C. A. Cousin, A. Parikh, P. Freeborn, E. J. Fox, and W. E. Dixon, "Motorized and functional electrical stimulation induced cycling via switched repetitive learning control," *IEEE Trans. Control Syst. Tech.*, to appear.

[106] C. Cousin, P. Deptula, C. Rouse, and W. E. Dixon, "Cycling with functional electrical stimulation and adaptive neural network admittance control," in *Proc. Am. Control Conf.*, 2019.

[107] C. Cousin, V. H. Duenas, C. Rouse, and W. E. Dixon, "Cadence and admittance control of a motorized functional electrical stimulation cycle," in *Proc. IEEE Conf. Decis. Control*, Dec. 2018, pp. 6470–6475.

[108] V. Ghanbari, V. H. Duenas, P. J. Antsaklis, and W. E. Dixon, "Passivity-based iterative learning control for cycling induced by functional electrical stimulation with electric motor assistance," *IEEE Trans. Control Sys. Tech.*, to appear.

[109] V. Duenas, C. A. Cousin, C. Rouse, and W. E. Dixon, "Extremum seeking control for power tracking via functional electrical stimulation," in *Proc. IFAC Conf. Cyber. Phys. Hum. Syst.*, 2018, pp. 164–169.

[110] C. Cousin, V. H. Duenas, C. Rouse, and W. E. Dixon, "Stable cadence tracking of admitting functional electrical stimulation cycle," in *Proc. ASME Dyn. Syst. Control Conf.*, 2018.

[111] C. A. Cousin, V. Duenas, C. Rouse, and W. E. Dixon, "Admittance control of motorized functional electrical stimulation cycle," in *Proc. IFAC Conf. Cyber. Phys. Hum. Syst.*, 2018, pp. 328–333.

[112] V. Duenas, C. Cousin, A. Parikh, and W. E. Dixon, "Functional electrical stimulation induced cycling using repetitive learning control," in *Proc. IEEE Conf. Decis. Control*, 2016.

[113] E. S. Idsø, T. Johansen, and K. J. Hunt, "Finding the metabolically optimal stimulation pattern for FES-cycling," in *Proc. Conf. of the Int. Funct. Electrical Stimulation Soc.*, Bournemouth, UK, Sep. 2004.

[114] N. Sharma, K. Stegath, C. M. Gregory, and W. E. Dixon, "Nonlinear neuromuscular electrical stimulation tracking control of a human limb," *IEEE Trans. Neural Syst. Rehabil. Eng.*, vol. 17, no. 6, pp. 576–584, Jun. 2009.

[115] M. J. Bellman, T.-H. Cheng, R. Downey, and W. E. Dixon, "Cadence control of stationary cycling induced by switched functional electrical stimulation control," in *Proc. IEEE Conf. Decis. Control*, 2014.

[116] M. J. Bellman, T.-H. Cheng, R. J. Downey, and W. E. Dixon, "Stationary cycling induced by switched functional electrical stimulation control," in *Proc. Am. Control Conf.*, 2014, pp. 4802–4809.

[117] D. B. Popović, "Advances in functional electrical stimulation," *J Electromyogr Kinesiol*, vol. 24, no. 6, pp. 795–802, Dec. 2014.

[118] M. Ferrarin, F. Palazzo, R. Riener, and J. Quintern, "Model-based control of FES-induced single joint movements," *IEEE Trans. Neural Syst. Rehabil. Eng.*, vol. 9, no. 3, pp. 245–257, Sep. 2001.

[119] W. E. Dixon, A. Behal, D. M. Dawson, and S. Nagarkatti, *Nonlinear Control of Engineering Systems: A Lyapunov-Based Approach*.   Birkhauser: Boston, 2003.

[120] A. F. Filippov, "Differential equations with discontinuous right-hand side," in *Fifteen papers on differential equations*, ser. American Mathematical Society Translations - Series 2.   American Mathematical Society, 1964, vol. 42, pp. 199–231.

[121] B. E. Paden and S. S. Sastry, "A calculus for computing Filippov's differential inclusion with application to the variable structure control of robot manipulators," *IEEE Trans. Circuits Syst.*, vol. 34, no. 1, pp. 73–82, Jan. 1987.

[122] M. O. Ibitoye, N. A. Hamzaid, N. Hasnan, A. K. A. Wahab, and G. M. Davis, "Strategies for rapid muscle fatigue reduction during fes exercise in individuals with spinal cord injury: A systematic review," *Plos One*, 2016.

[123] N. Stefanovic, M. Ding, and L. Pavel, "An application of L2 nonlinear control and gain scheduling to erbium doped fiber amplifiers," *Control Eng. Pract.*, vol. 15, pp. 1107–1117, 2007.

[124] T. Fujinaka, Y. Kishida, M. Yoshioka, and S. Omatu, "Stabilization of double inverted pendulum with self-tuning neuro-PID," in *Proc. IEEE-INNS-ENNS Int. Joint Conf. Neural Netw.*, vol. 4, 24–27 July 2000, pp. 345–348.

[125] F. Nagata, K. Kuribayashi, K. Kiguchi, and K. Watanabe, "Simulation of fine gain tuning using genetic algorithms for model-based robotic servo controllers," in *Proc. Int. Sym. Comput. Intell. Robot. Autom.*, 20-23 June 2007, pp. 196–201.

[126] N. J. Killingsworth and M. Krstic, "PID tuning using extremum seeking: online, model-free performance optimization," *IEEE Control Syst. Mag.*, vol. 26, no. 1, pp. 70–79, 2006.

[127] R. Kelly, V. Santibanez, and A. Loria, *Control of Robot Manipulators in Joint Space*. Springer, 2005.

[128] R. J. Downey, T.-H. Cheng, M. J. Bellman, and W. E. Dixon, "Closed-loop asynchronous electrical stimulation prolongs functional movements in the lower body," *IEEE Trans. Neural Syst. Rehabil. Eng.*, vol. 23, no. 6, pp. 1117–1127, 2015.

[129] R. J. Downey, M. J. Bellman, H. Kawai, C. M. Gregory, and W. E. Dixon, "Comparing the induced muscle fatigue between asynchronous and synchronous electrical stimulation in able-bodied and spinal cord injured populations," *IEEE Trans. Neural Syst. Rehabil. Eng.*, vol. 23, no. 6, pp. 964–972, 2015.

[130] N. Sharma, N. A. Kirsch, N. A. Alibeji, and W. E. Dixon, "A nonlinear control method to compensate for muscle fatigue during neuromuscular electrical stimulation," *Front. Robot. AI*, vol. 4, p. 68, Dcember 2017.

[131] S. Obuz, J. R. Klotz, R. Kamalapurkar, and W. E. Dixon, "Unknown time-varying input delay compensation for uncertain nonlinear systems," *Automatica*, vol. 76, pp. 222–229, February 2017.

[132] K. P. Tee, R. Yan, and H. Li, "Adaptive admittance control of a robot manipulator under task space constraint," in *IEEE Int. Conf. Robot. Autom.* IEEE, 2010, pp. 5181–5186.

[133] C. Rouse, C. Cousin, V. H. Duenas, and W. E. Dixon, "Cadence tracking for switched FES cycling combined with voluntary pedaling and motor resistance," in *Proc. Am. Control Conf.*, 2018, pp. 4558–4563.

[134] M. Laubacher, E. A. Aksoez, A. K. Brust, M. Baumberger, R. Riener, S. Binder-Macleod, and K. J. Hunt, "Stimulation of paralysed quadriceps muscles with sequentially and spatially distributed electrodes during dynamic knee extension," *J. Neuroeng. Rehab.*, vol. 16, no. 1, p. 5, 2019.

[135] R. Kamalapurkar, J. A. Rosenfeld, A. Parikh, A. R. Teel, and W. E. Dixon, "Invariance-like results for nonautonomous switched systems," *IEEE Trans. Autom. Control*, vol. 64, no. 2, pp. 614–627, Feb. 2019.

[136] L. Ting, C. C. Raasch, D. Brown, S. Kautz, and F. E. Zajac, "Sensorimotor state of the contralateral leg affects ipsilateral muscle coordination of pedaling," *J. Neurophysiol.*, vol. 80, no. 3, pp. 1341–51, Sep 1998.

[137] A. Behal, W. E. Dixon, B. Xian, and D. M. Dawson, *Lyapunov-Based Control of Robotic Systems*. CRC Press, 2009.

[138] F. L. Lewis, "Nonlinear network structures for feedback control," *Asian J. Control*, vol. 1, no. 4, pp. 205–228, 1999.

[139] F. L. Lewis, R. Selmic, and J. Campos, *Neuro-Fuzzy Control of Industrial Systems with Actuator Nonlinearities*. Philadelphia, PA, USA: Society for Industrial and Applied Mathematics, 2002.

[140] A. Parikh, R. Kamalapurkar, and W. E. Dixon, "Integral concurrent learning: Adaptive control with parameter convergence using finite excitation," *Int J Adapt Control Signal Process*, to appear.

BIOGRAPHICAL SKETCH

Christian A. Cousin was born in August 1992 in Ocala, Florida. He received his B.S. in mechanical engineering with a minor in electrical engineering from the University of Florida in May 2015. Christian joined the Nonlinear Controls and Robotics (NCR) research group to pursue his Ph.D. under the advisement of Dr. Warren E. Dixon in August 2015. After becoming a National Science Foundation Graduate Research Fellow, he received his M.S. degree in mechanical engineering with a minor in both electrical engineering and mathematics from the University of Florida in August 2017. Christian was named the Best Student Researcher of the 2017-2018 academic year by the Department of Mechanical and Aerospace Engineering at the University of Florida. He subsequently received his Ph.D. in mechanical engineering from the University of Florida in May 2019. His research interests include switched systems, neuromuscular electrical stimulation, rehabilitation robotics, and Lyapunov-based nonlinear and adaptive control techniques.